

THE JOURNAL OF
PHYSICAL
CHEMISTRY

Volume 74

AUGUST—DECEMBER 1970

PAGES 3029—4696

BRYCE CRAWFORD, JR., *Editor*

STEPHEN PRAGER, *Associate Editor*

ROBERT W. CARR, JR., FREDERIC A. VAN CATLEDGE, *Assistant Editors*

EDITORIAL BOARD

A. O. ALLEN
R. BERSOHN
S. BRUNAUER
M. FIXMAN
H. S. FRANK
G. J. HILLS
J. R. HUIZENGA

M. KASHA
W. J. KAUZMANN
W. R. KRIGBAUM
R. A. MARCUS
W. J. MOORE
B. S. RABINOVITCH
H. REISS

S. A. RICE
R. E. RICHARDS
F. S. ROWLAND
R. L. SCOTT
R. SEIFERT
S. I. WEISSMAN

CHARLES R. BERTSCH, *Manager, Editorial Production*

AMERICAN CHEMICAL SOCIETY, PUBLICATIONS DIVISION

RICHARD L. KENYON
Director

JOSEPH H. KUNEY
Director of Business Operations
Director of Publications Research

DAVID E. GUSHEE
Publication Manager, Journals

THE JOURNAL OF PHYSICAL CHEMISTRY

Volume 74, Number 16 August 6, 1970

The Photoperoxidation of Unsaturated Organic Molecules. VI. The Inhibited Reaction	B. E. Algar and B. Stevens	3029
Some Novel Observations Concerning the Thermal Decomposition of 2,4,6-Trinitrotoluene	Joseph C. Dacons, Horst G. Adolph, and Mortimer J. Kamlet	3035
Bonding in Dye Aggregates. Energetics of the Dimerization of Aqueous Cobalt(II)-4,4',4'',4'''-Tetrasulphthalocyanine Ion	Z. A. Schelly, D. J. Harward, P. Hemmes, and E. M. Eyring	3040
The γ Radiolysis of 2-Propanol. V. Oxidation by Carbon Tetrachloride	Cecelia Radlowski and Warren V. Sherman	3043
Yields of the Lowest Triplet and Excited Singlet States in γ Radiolysis of Liquid Benzene	Robert R. Hentz and Lewis M. Perkey	3047
The Yield of Radiation-Induced Ionization in Condensed Organic Systems	Tadamasa Shida	3055
Free-Radical Intermediates in the Reaction of the Hydroxyl Radical with Amino Acid Derivatives and Related Compounds.	Hitoshi Taniguchi, Hiroyuki Hatano, Hideo Hasegawa, and Tetsuo Maruyama	3063
Radiolysis Transients in Viscous Liquids. Biphenyl in Liquid Paraffin	J. Fuller, N. Peteleski, D. Ruppel, and M. Tomlinson	3066
A Far-Infrared Study of the Reaction of Phosphorus Oxychloride Vapor with Ferric Chloride	Eugene P. Scheide and George G. Guilbault	3074
Consecutive and Competing Metastable Ion Transitions in the Mass Spectra of Monochlorophenols and Monobromophenols	James C. Tou	3076
Derivation and Interpretation of the Spectrum of the Dimer of Acridine Orange Hydrochloride, Dilute Aqueous Solution, and Oriented Film Studies	T. Kurucsev and Ulrich P. Strauss	3081
On an Empirical Correlation between Nuclear Conformation and Certain Fluorescence and Absorption Characteristics of Aromatic Compounds.	Isadore B. Berlman	3085
Geminate Retention from Nuclear Isomeric Transition and Radiative Neutron Capture in Carbon Tetrabromide-Ethanol Solutions	Gerald P. Gennaro and Kenneth E. Collins	3094
The Molecular Composition of Liquid Sulfur	Robert E. Harris	3102
Relative Cation Mobilities in Silver Bromide-Potassium Bromide Melts	Richard W. Laity and Albert S. Tenney	3112
New Compounds Consisting of Sodium <i>p</i> -Toluenesulfonate, Water, and a Polar Benzenoid Nonelectrolyte	Joseph Steigman, Richard DeJasi, and Judah Lando	3117
On the Mechanism of Charging and Discharging Ionic Double Layers at Electrodes	Chaim Yarnitzky and Fred C. Anson	3123
The Vaporization Thermodynamics of Samarium Oxide Fluoride.	Dale E. Work and Harry A. Eick	3130
Polymorphism of the Crystalline Methylchloromethane Compounds. III. A Differential Scanning Calorimetric Study.	Lawrence Silver and Reuben Rudman	3134

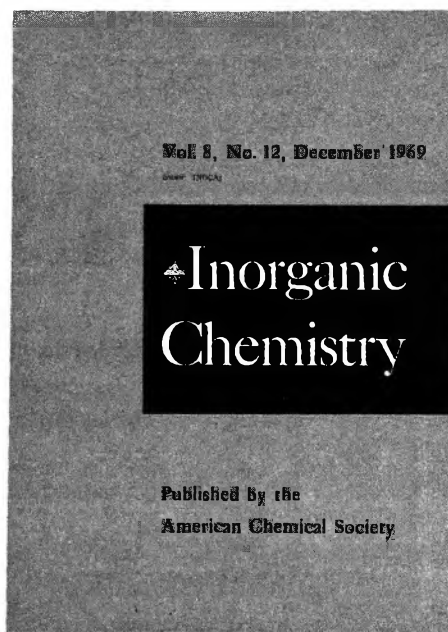
Inorganic Chemistry is the one...

that publishes both experimental and theoretical fundamental studies in *all phases of inorganic chemistry*.

These studies include synthesis and properties of new compounds, quantitative studies regarding structure, and thermodynamics and kinetics of inorganic reactions. Articles may range from the borders of organic chemistry to the borders of theoretical physics . . . giving you a broad expanse of authoritative information.

Besides the 35 or more papers presented in each monthly issue, you'll also profit from the shorter *Notes* and the *Correspondence* sections, that provide an informal medium of exchange for scientific views and ideas.

Inorganic Chemistry is the one . . . to order right now for your own professional interests. Simply complete and return the form below.



American Chemical Society / 1155 Sixteenth Street, N.W., Washington, D.C. 20036

Please enter my subscription to **Inorganic Chemistry** at the rates checked below:

ACS Members: U.S. \$14 Canada, PUAS \$17 Other Nations \$17.50

Nonmembers: U.S. \$28 Canada, PUAS \$31 Other Nations \$31.50

Bill me Bill employer Payment enclosed (Payable to American Chemical Society)

Name _____ Title _____

Employer _____

Address: Home Business _____

City _____ State/Country _____ Zip _____

Nature of employer's business? Manufacturing or processing Academic Government
 Other _____

(Please indicate)

Note: Subscriptions at ACS Member Rates are for personal use only.

I am an ACS member I am not an ACS member

Payment must be made in U.S. currency, by international money order, UNESCO coupons, U.S. bank draft; or order through your book dealer.

PDA

NOTES

- Catalytic Polarographic Current of a Metal Complex. IX. The Effect of Lithium Hexafluorophosphate Supporting Electrolyte on the Nickel(II)-*o*-Phenylenediamine System . . . **Hubert C. MacDonald, Jr., and Harry B. Mark, Jr.** 3140
- The Empirical Shielding Parameter *Q* and Trisubstituted Benzenes. **G. Socrates** 3141
- Free-Radical Intermediates in the Reaction of the Hydroxyl Radical with Nitrogen Heterocyclic Compounds **Hitoshi Taniguchi** 3143

COMMUNICATIONS TO THE EDITOR

- Prediction on the Mass Spectra of Normal Alkanes with the Molecular Orbital Theory **Mitsuo Saito, Iwao Fujita, and Kozo Hirota** 3147
- A Kinetic Study of Monochlorocarbene Insertion into Silicon-Hydrogen Bonds **Y.-N. Tang, S. H. Daniel, and N.-B. Wong** 3148

AUTHOR INDEX

- | | | | | |
|----------------------|------------------------|--------------------------------|----------------------|------------------------------|
| Adolph, H. G., 3035 | Eyring, E. M., 3040 | Hirota, K., 3147 | Peteleski, N., 3066 | Stevens, B., 3029 |
| Algar, B. E., 3029 | Fujita, I., 3147 | Kamlet, M. J., 3035 | Radlowski, C., 3043 | Strauss, U. P., 3081 |
| Anson, F. C., 3123 | Fuller, J., 3066 | Kurucsev, T., 3081 | Rudman, R., 3134 | Tang, Y.-N., 3148 |
| Berlman, I. B., 3085 | Gennaro, G. P., 3094 | Laity, R. W., 3112 | Ruppel, D., 3066 | Taniguchi, H., 3063,
3143 |
| Collins, K. E., 3094 | Guilbault, G. G., 3074 | Lando, J., 3117 | Saito, M., 3147 | Tenney, A. S., 3112 |
| Dacons, J. C., 3035 | Harris, R. E., 3102 | MacDonald, H. C., Jr.,
3140 | Scheide, E. P., 3074 | Tomlinson, M., 3066 |
| Daniel, S. H., 3148 | Harward, D. J., 3040 | Mark, H. B., Jr., 3140 | Shelly, Z. A., 3040 | Tou, J. C., 3076 |
| DeIasi, R., 3117 | Hasegawa, H., 3063 | Maruyama, T., 3063 | Sherman, W. V., 3043 | Wong, N.-B., 3148 |
| Eick, H. A., 3130 | Hatano, H., 3063 | Perkey, L. M., 3047 | Shida, T., 3055 | Work, D. E., 3130 |
| | Hemmes, P., 3040 | | Silver, L., 3134 | Yarnitzky, C., 3123 |
| | Hentz, R. R., 3047 | | Socrates, G., 3141 | |
| | | | Steigman, J., 3117 | |

THE JOURNAL OF PHYSICAL CHEMISTRY

Registered in U. S. Patent Office © Copyright, 1970, by the American Chemical Society

VOLUME 74, NUMBER 16 AUGUST 6, 1970

The Photoperoxidation of Unsaturated Organic Molecules.

VI. The Inhibited Reaction

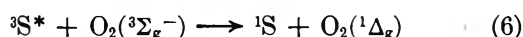
by B. E. Algar and B. Stevens¹

Department of Chemistry, The University, Sheffield, England (Received January 28, 1970)

The inhibition of photosensitized peroxidation is described in terms of the quenching of one or more of the electronically excited intermediates involved. Examples are given of inhibition by azulene quenching of the sensitizer singlet state (rubrene), by azulene quenching of sensitizer singlet and triplet states (9,10-dimethylanthracene (DMA) and 9,10-dimethyl-1,2-benzanthracene), and by olefin quenching of $O_2(^1\Delta_g)$ by competitive addition. From the ratio of azulene and oxygen quenching constants for the sensitizer triplet states it is concluded that oxygen quenching of triplet states has a lower encounter probability than (diffusion-limited) oxygen quenching of singlet states by a spin statistical factor of $1/9$. The marked azulene inhibition of DMA autoperoxidation illustrates the essential role of the sensitizer triplet state which, in view of the virtual absence of intersystem crossing in DMA, must be generated by oxygen quenching of the singlet state.

Introduction

Recent evidence² supports the role of $O_2(^1\Delta_g)$ as the active intermediate in the photosensitized addition of molecular oxygen to an unsaturated hydrocarbon substrate M. The dependence of the overall quantum yield γ_{MO_2} on concentration of dissolved oxygen is consistent^{3,4} with a mechanism in which the processes



are predominantly responsible for oxygen quenching of excited singlet and triplet states $^1S^*$ and $^3S^*$ of the sensitizer S.^{5,6} Accordingly, the simplest reaction sequence shown in Figure 1 allows γ_{MO_2} to be expressed as the product of (a) the sensitizer triplet-state formation efficiency given by

$$\phi_T = (k_2 + k_4[O_2]) / (k_1 + k_2 + k_3 + k_4[O_2])$$

(b) the yield of $O_2(^1\Delta_g)$ from the sensitizer triplet state defined as

$$\phi_\Delta = k_6[O_2] / (k_5 + k_6[O_2])$$

and (c) the $O_2(^1\Delta_g)$ -substrate addition probability expressed as

$$\phi_M = k_7[M] / (k_7[M] + k_8)$$

A reduction in the overall quantum yield

$$\gamma_{MO_2} = \phi_T \phi_\Delta \phi_M$$

by the addition of an inhibitor Q should therefore reflect a decrease in one or more of the quantities ϕ_T , ϕ_Δ , and ϕ_M due to quenching of at least one of the electronically excited intermediates $^1S^*$, $^3S^*$, and $O_2(^1\Delta_g)$ discussed in turn below.

Quenching of the sensitizer singlet state by the energy-transfer process



(1) Address inquiries to this author at the Department of Chemistry, University of South Florida, Tampa, Fla. 33620.

(2) Cf. C. S. Foote, *Accounts Chem. Res.*, **1**, 104 (1968).

(3) Part II: B. Stevens and B. E. Algar, *J. Phys. Chem.*, **72**, 3468 (1968).

(4) Part IV: B. Stevens and B. E. Algar, *ibid.*, **73**, 1711 (1969).

(5) If process 6 produces $O_2(^1\Sigma_g^+)$ in any of the systems studied this must undergo quantitative relaxation to $O_2(^1\Delta_g)$.⁴

(6) Part V: B. E. Algar and B. Stevens, submitted for publication.

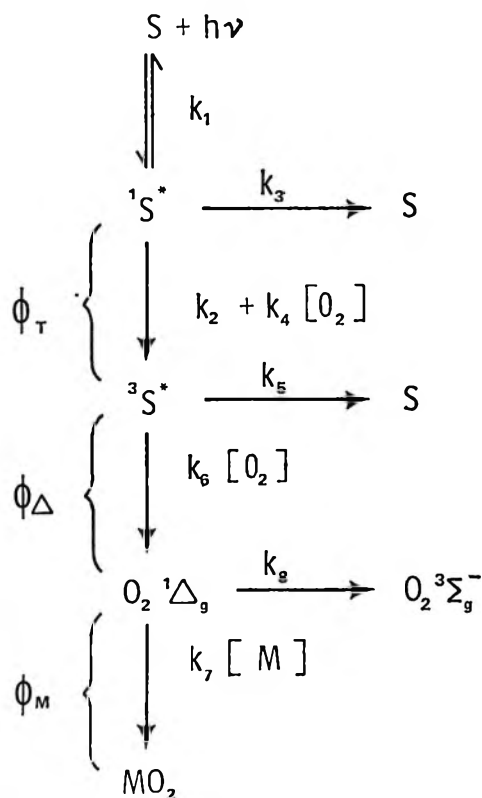


Figure 1. Probable reaction sequence for photoperoxidation of substrate M in presence of sensitizer S.

reduces both the sensitizer fluorescence yield from F to F_Q and the triplet-state formation efficiency from ϕ_T to ϕ_T^Q where

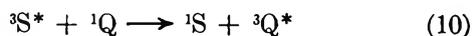
$$F/F_Q = \phi_T/\phi_T^Q = \frac{1 + k_9[Q]/(k_1 + k_2 + k_3 + k_4[O_2])}{1 + k_{11}[Q]/(k_7[M] + k_8)} \quad (\text{I})$$

If the quenching product ${}^1Q^*$ takes no further part in the overall reaction and the simultaneous quenching of ${}^3S^*$ or $O_2({}^1\Delta_g)$ is inoperative, the reduction in quantum yield from γ_{MO_2} to $\gamma_{MO_2}^Q$ given by

$$\gamma_{MO_2}/\gamma_{MO_2}^Q = \phi_T/\phi_T^Q \quad (\text{II})$$

should parallel the reduction in sensitizer fluorescence yield.

The additional transfer of energy from the sensitizer triplet state



lowers the $O_2({}^1\Delta_g)$ yield from ϕ_Δ to ϕ_Δ^Q where

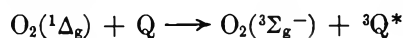
$$\phi_\Delta/\phi_\Delta^Q = 1 + k_{10}[Q]/(k_5 + k_6[O_2])$$

and further reduces the overall photoperoxidation yield in accordance with eq III if the unimolecular relaxation

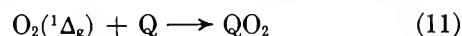
$$\gamma_{MO_2}/\gamma_{MO_2}^Q = \phi_T\phi_\Delta/\phi_T^Q\phi_\Delta^Q = \left(\frac{F}{F_Q}\right)\left\{1 + k_{10}[Q]/(k_5 + k_6[O_2])\right\} \quad (\text{III})$$

of ${}^3Q^*$ effectively competes with the oxygen quenching of this species.

The inhibition of photoperoxidation by energy transfer from $O_2({}^1\Delta_g)$ in the process



requires that the inhibitor triplet state lies below 8000 cm^{-1} and to date has been reported only for $Q = \beta$ -carotene.⁷ The more general quenching process 11, involves a competitive addition of $O_2({}^1\Delta_g)$ to olefins,



dienes, and certain aromatic hydrocarbons which reduces the quantum yield of substrate peroxidation according to eq IV in the absence of transfer from ${}^1S^*$

$$\gamma_{MO_2}/\gamma_{MO_2}^Q = \phi_M/\phi_M^Q = \frac{1 + k_{11}[Q]/(k_7[M] + k_8)}{1 + k_{11}[Q]/(k_7[M] + k_8)} \quad (\text{IV})$$

and ${}^3S^*$ (processes 9 and 10). Of the quenching processes detailed only (11) leads to consumption of the quenching species with a quantum yield of

$$\gamma_{QO_2}^M = \phi_T\phi_\Delta\phi_Q = \phi_T\phi_\Delta k_{11}[Q]/(k_8 + k_7[M] + k_{11}[Q])$$

Simultaneous measurements of $\gamma_{MO_2}^Q$ and $\gamma_{QO_2}^M$ related by

$$\gamma_{MO_2}^Q/\gamma_{QO_2}^M = k_7[M]/k_{11}[Q] \quad (\text{V})$$

therefore provide direct estimates of the relative reactivities k_7/k_{11} of M and Q toward $O_2({}^1\Delta_g)$ addition.

This communication reports the inhibition of auto-oxidation of the substrates listed in Table I by azulene quenching of sensitizer singlet and triplet states (processes 9 and 10) and by competitive addition of $O_2({}^1\Delta_g)$ to several olefinic and aromatic hydrocarbons (process 11). The use of azulene is dictated by the relatively rapid relaxation of its lowest excited singlet and triplet states⁸ which must be responsible for its inefficient sensitization of this type of reaction⁴ and which ensures that these in turn do not act as additional sources of $O_2({}^1\Delta_g)$ at the prevailing oxygen concentrations.

Experimental Section

The sources and methods of purification of azulene and the aromatic hydrocarbon sensitizers have been described previously;⁹ the olefins supplied by K & K Laboratories Inc., England, were used without further treatment.

To minimize the effects of light absorption by azulene, fluorescence quenching data were obtained as sensitizer fluorescence decay constants⁹ as a function of azulene concentration in nitrogen-purged solutions; the determination of photoperoxidation quantum yields has been described in part II of this series.³

(7) C. S. Foote and R. W. Denny, *J. Amer. Chem. Soc.*, **90**, 6233 (1968).

(8) P. M. Rentzepis, *Chem. Phys. Lett.*, **3**, 717 (1969).

(9) Part I: B. Stevens and B. E. Algar, *J. Phys. Chem.*, **72**, 2582 (1968).

Table I: Spectroscopic and Kinetic Data

	DMA	DMBA	Rubrene	Azulene
$E(^1S^*)$, cm^{-1}	25,000	26,100	18,900	14,400 ($^1Q^*$)
$E(^3S^*)$, cm^{-1}	$\sim 14,700^a$	15,500 ^b	$< 10,250^c$	10,500 ($^3Q^*$) ^d
k_4 , $M^{-1} \text{sec}^{-1}$	3.15×10^{10}	2.76×10^{10}	1.18×10^{10}	...
τ_{F^0} , nsec	13.9	24.4	16.7	...
k_9 , $M^{-1} \text{sec}^{-1}$	1.1×10^{10}	0.83×10^{10}	5.1×10^{10}	...
k_{10}/k_8	2.5 ± 0.3	3.3 ± 0.4
k_6 , $M^{-1} \text{sec}^{-1}$	4.0×10^9	3.0×10^9
k_6/k_4	$\sim 1/8$	$1/9$

^a Cf. C. A. Parker, "Photoluminescence of Solutions," Elsevier, Amsterdam, 1968, p 315. ^b M. Moodie and C. Reid, *J. Chem. Phys.*, **22**, 252 (1954). ^c Assumed to lie below triplet state of naphthalene. ^d Reference 8. ^e Reference 9. ^f With $k_{10} = k_d$ (eq VI).

All measurements refer to solutions in benzene (Hopkins and Williams Analar reagent) at 25°.

Results and Discussion

(1) *Azulene Quenching of Sensitizer Fluorescence.* The lowest excited singlet states of 9,10-dimethylanthracene (DMA), 9,10-dimethyl-1,2-benzanthracene (DMBA), and rubrene should be susceptible to quenching by energy transfer (process 9) to produce the azulene 1L_b state ($^1Q^*$) at 14,400 cm^{-1} (Table I). The appropriate fluorescence quenching data are displayed in Figure 2 according to the relationship

$$\tau_{F^0}/\tau_{F^Q} = 1 + k_9[Q]\tau_{F^0} \quad (\text{VI})$$

where $1/\tau_{F^0} = k_1 + k_2 - k_3$ is the fluorescence decay constant of the sensitizer in the absence of quenching species. For DMA and DMBA the values of k_9 obtained from the slopes of the data lines in Figure 2 and listed in Table I are in good agreement with the diffusion-limited value

$$k_d = 8RT/3000\eta = 1.0 \times 10^{10} M^{-1} \text{sec}^{-1} \quad (\text{VII})$$

for benzene as solvent at 25°; however the substantial overlap of the rubrene fluorescence and azulene ($^1L_b \leftarrow ^1A$) absorption spectra may promote a resonance energy transfer in this system characterized by a significantly larger rate constant.¹⁰

In the presence of dissolved oxygen (during photoperoxidation) the azulene quenching of sensitizer fluorescence is estimated from expression VIII using previously measured values⁹ for $k_{O_2} = k_4$ (Table I).

$$F/F_Q = 1 + k_9[Q]\tau_{F^0}/(1 + k_{O_2}[O_2]\tau_{F^0}) \quad (\text{VIII})$$

(2) *Photoperoxidation Inhibition by Azulene Quenching of the Sensitizer Singlet State.* According to the relative disposition of energy levels listed in Table I, azulene quenching of the rubrene triplet state should be inefficient and any inhibition of rubrene autoperoxidation should reflect a quenching of the rubrene singlet state only. This is quantitatively confirmed by the data $\gamma_{MO_2^Q}([Q])$ plotted in accordance with eq I in Figure 3 for the concentrations of dissolved oxygen quoted; the broken lines describe the azulene quenching

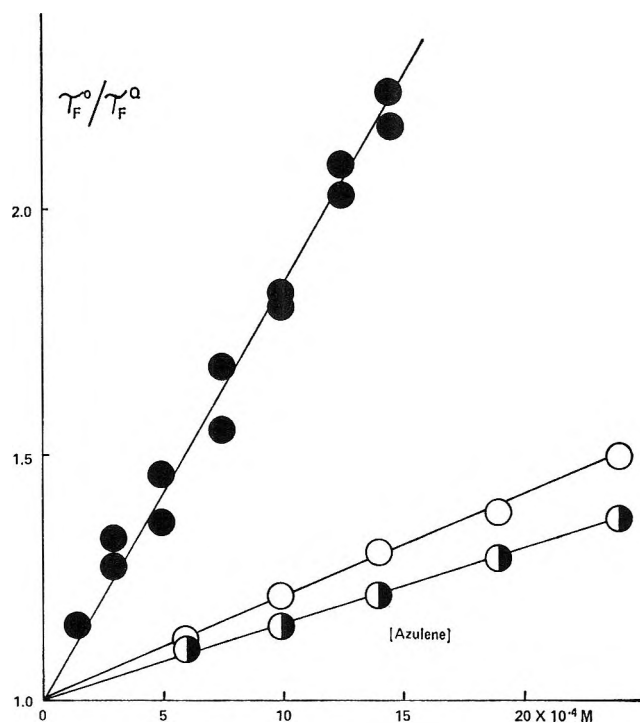


Figure 2. Azulene quenching of sensitizer fluorescence in nitrogen-purged benzene at 25°: ●, rubrene ($5 \times 10^{-5} M$); ○, DMBA ($6 \times 10^{-5} M$); ◐, DMA ($5 \times 10^{-5} M$).

of rubrene fluorescence $F/F_Q([Q])$ computed from eq VIII for the appropriate oxygen concentration.

The parallel reduction in quantum yields of rubrene fluorescence and autoperoxidation by azulene (Figure 3) also supports the assumption that the electronically excited singlet state of azulene ($^1Q^*$) does not further contribute to the overall photochemical process and places an upper limit of $\sim 10,500 \text{ cm}^{-1}$ on the triplet-state energy of rubrene.

(3) *Photoperoxidation Inhibition by Azulene Quenching of the Sensitizer Triplet State.* Both the excited singlet and triplet states of DMA and DMBA are expected to undergo energy transfer to azulene according to the spectroscopic data in Table I, in which case

(10) Cf. Th. Förster, *Discuss. Faraday Soc.*, **27**, 7 (1959).

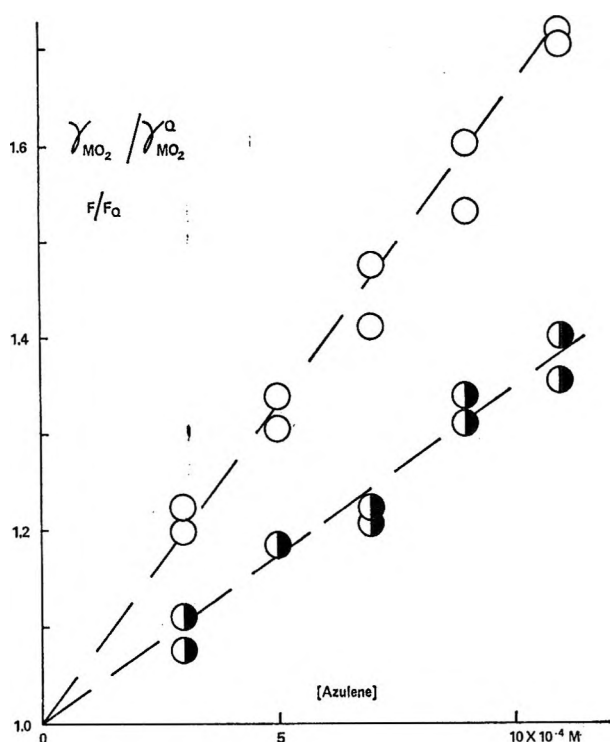


Figure 3. Azulene inhibition of rubrene autoperoxidation plotted in accordance with eq I and II: \circ , $[O_2] = 1.5 \times 10^{-3} M$; \bullet , $[O_2] = 7.3 \times 10^{-3} M$. Dashed lines denote azulene quenching of rubrene fluorescence computed from eq VIII.

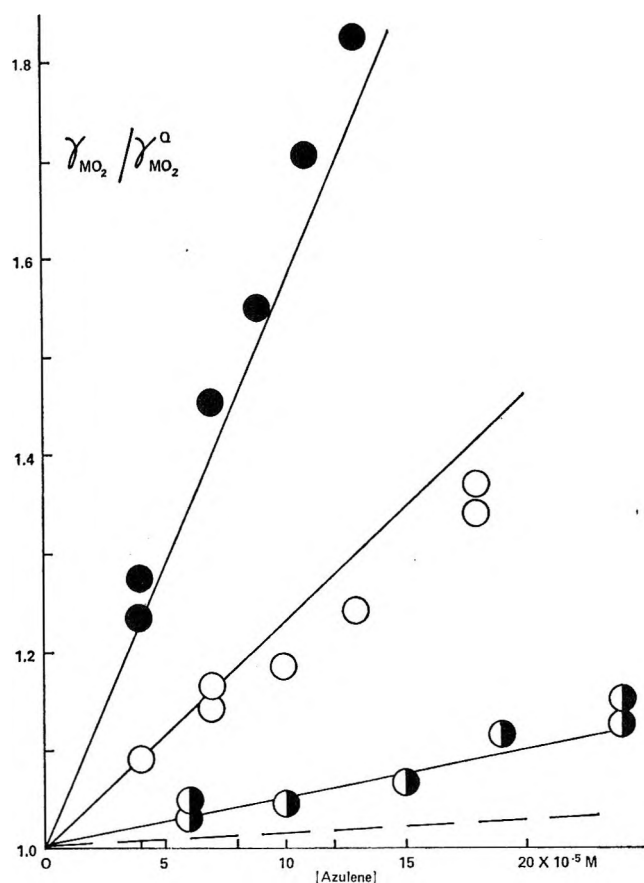


Figure 5. Azulene inhibition of DMBA autoperoxidation plotted in accordance with eq III: \bullet , $[O_2] = 6 \times 10^{-4} M$; \circ , $[O_2] = 1.5 \times 10^{-3} M$; \bullet , $[O_2] = 7.3 \times 10^{-3} M$. Dashed line denotes maximum azulene quenching of DMBA fluorescence computed from eq VIII with $[O_2] = 6 \times 10^{-4} M$. Solid lines from eq III using parameters listed in Table I.

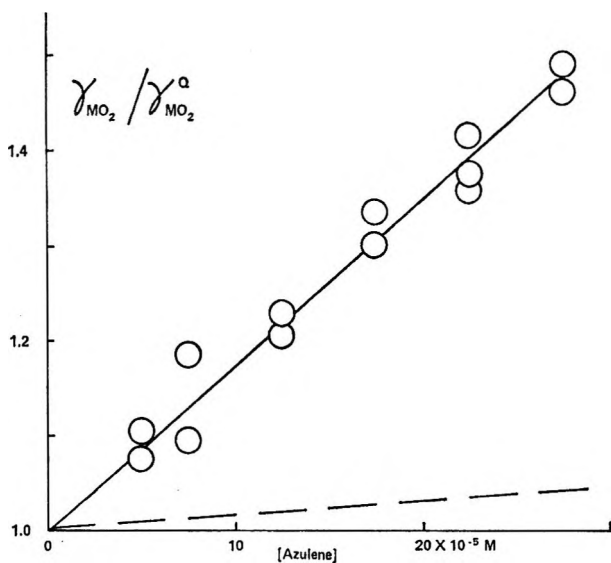


Figure 4. Azulene inhibition of DMA autoperoxidation plotted in accordance with eq III; $[O_2] = 1.5 \times 10^{-3} M$. Dashed line denotes azulene quenching of DMA fluorescence computed from eq VIII.

eq III should describe the azulene inhibition of the autoperoxidation ($S = M$) of these compounds.

The experimental data $\gamma_{MO_2}/\gamma_{MO_2}^0([Q])$ are presented for DMA and DMBA in Figures 4 and 5, respectively, where the broken lines represent extrapola-

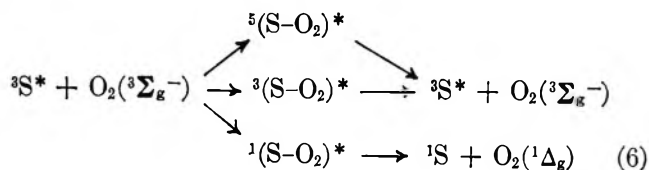
tions of the sensitizer fluorescence quenching data $F/F_Q([Q])$ obtained at higher azulene concentrations and corrected for oxygen quenching of the sensitizer fluorescence (eq VIII). Clearly the azulene inhibition of photoperoxidation in these systems must be attributed to its simultaneous quenching of both the excited singlet and triplet states of DMA and DMBA (processes 9 and 10) as predicted.

For DMBA in benzene it has been shown³ that $k_6/k_5 \approx 2.2 \times 10^5 M^{-1}$ or $k_5 \ll k_6[O_2]$ at the lowest oxygen concentration used here (Figure 5); if it may be assumed that the DMA triplet state is also effectively quenched by dissolved oxygen, the slopes of the data lines $\gamma_{MO_2}/\gamma_{MO_2}^0([Q])$ in Figures 4 and 5 are given by $Fk_{10}/F_Qk_6[O_2]$ (eq III) from which the corresponding values of k_{10}/k_6 are listed in Table I. Since the energy-transfer process 10 is expected^{11,12} to be diffusion limited (as in the anthracene–azulene system in ben-

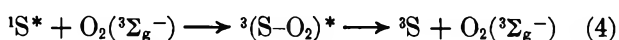
(11) The relatively short lifetime of the azulene triplet state⁸ should eliminate reversible transfer as an effective process.¹²

(12) B. Stevens and M. S. Walker, *Proc. Chem. Soc.*, 26, 109 (1964).

zene¹³ and hexane¹⁴), the use of eq VII for k_{10} provides values for k_8 listed in Table I which are an order of magnitude lower than the measured rate constants k_1 for oxygen quenching of the corresponding singlet state; this is consistent with spin statistical factors of $1/3$ for the energy-transfer sequence



and of unity for the oxygen-induced intersystem crossing process



where ${}^i(\text{S-O}_2)^*$ denotes a sensitizer-oxygen complex of i -fold degeneracy.

(4) *Photoperoxidation Inhibition by Competitive Addition (Quenching) of $\text{O}_2(\text{}^1\Delta_g)$.* In the presence of 1-methylcyclopentene (MCP), 1-methylcyclohexene (MCH), and 2,3-dimethylbut-2-ene (TME) at the concentrations stated, the quantum yields of auto-oxidation of DMA, DMBA, naphthacene, and rubrene are reduced by the factors listed in Table II.

Table II: Inhibition of Autooxidation by Olefins Expressed as $\gamma_{\text{MO}_2^Q}/\gamma_{\text{MO}_2}$ under Stated Conditions

Q	M			
	DMA ($2.0 \times 10^{-4} M$)	DMBA ($2.6 \times 10^{-4} M$)	Naphthacene ($5.0 \times 10^{-4} M$)	Rubrene ($2.0 \times 10^{-4} M$)
1-Methylcyclohexene ($1.0 M$)	5.55	7.00	6.75	5.25
1-Methylcyclopentene ($0.1 M$)	4.44	5.60	5.60	4.50
2,3-Dimethylbut-2-ene ($2 \times 10^{-3} M$)	2.54	2.21	2.21	2.61

The fluorescence of these compounds is not quenched by the olefins under these conditions and it is assumed that energy transfer in the triplet manifold (process 10) is energetically prohibited in order to interpret this inhibition in terms of $\text{O}_2(\text{}^1\Delta_g)$ quenching (process 11) described by eq IV. The use of previously reported⁴ values for k_7/k_8 (Table III) provides the $\text{O}_2(\text{}^1\Delta_g)$ quenching constants k_{11}/k_8 listed in Table III.

The addition of DMA and DMBA also reduces the autooxidation quantum yields of naphthacene and rubrene excited by the Hg line at 436 nm to which these additives are transparent. In the absence of energy transfer (Table I) from sensitizer to additive (processes 9 and 10), this inhibition is also attributed to the quenching of $\text{O}_2(\text{}^1\Delta_g)$ by competitive addition to DMA and DMBA (process 11). The simultaneous

measurement of the inhibitor peroxidation quantum yield $\gamma_{\text{QO}_2^M}$ in these systems, obtained by periodically monitoring its optical density at 366 nm, provides the quantum yield ratios $\gamma_{\text{MO}_2^Q}/\gamma_{\text{QO}_2^M}$ listed in Table IV which are converted by eq V to the relative $\text{O}_2(\text{}^1\Delta_g)$ addition reactivities k_7/k_{11} tabulated in parentheses. These are in excellent agreement with the ratios $(k_7/k_8)/(k_{11}/k_8)$ of $\text{O}_2(\text{}^1\Delta_g)$ addition constants measured independently for each of the four compounds and listed in Table III together with previously reported⁴ values obtained with perylene and anthanthrene as sensitizers.

Within an estimated uncertainty of $\pm 30\%$ the inhibitor quenching constants k_{11}/k_8 and substrate addition constants k_7/k_8 for $\text{O}_2(\text{}^1\Delta_g)$ listed in Table III are independent of sensitizer as expected for a common reaction intermediate $\text{O}_2(\text{}^1\Delta_g)$. Similar findings have been reported by Wilson¹⁵ and by Kopecky and Reich,¹⁶ whose relative reactivity data are in fair agreement (except for DMA¹⁵) with those reported here (Table V). However the absolute olefin- $\text{O}_2(\text{}^1\Delta_g)$ addition reactivities computed² as $\beta = k_8/k_{11}$ from the data in Table II on the assumption that process 1 is solely responsible for inhibition are some 3–5 times less than the corresponding values obtained by Foote and coworkers^{2,17} from rates of product formation in a methanol-*t*-butyl alcohol solvent (Table V); this discrepancy exceeds the combined limits of error ($\pm 30\%$ in each case) and a factor of 40% due to the change in solvent and may reflect a contribution to inhibition by physical quenching of $\text{O}_2(\text{}^1\Delta_g)$ (or ${}^3\text{S}^*$) by these olefins. It should also be noted that the olefin β values are obtained from eq IV using previously measured values of $\beta = k_8/k_7$ for the substrates M listed in Table II, which in at least one case (rubrene) is lower than the value reported by Bowen and Tanner¹⁸ by a factor of ~ 4 ; however, use of this higher β value for rubrene leads to an increase in the computed olefin β values of less than 20% and simultaneous examination of olefin inhibition effects and hydroperoxidation rates under identical conditions would be desirable to resolve this discrepancy.

The wide range of $\text{O}_2(\text{}^1\Delta_g)$ addition reactivities (Table V) previously noted by Foote and coworkers^{2,17} must originate in the variation of k_7 (or k_{11}) for different $\text{O}_2(\text{}^1\Delta_g)$ acceptors which is not solely attributable to steric effects (*cf.* MCP and MCH, naphthacene and rubrene). In terms of the more detailed reaction sequence

(13) A. A. Lamola, W. G. Herkstroeter, J. C. Dalton, and G. S. Hammond, *J. Chem. Phys.*, **42**, 1715 (1965).

(14) W. R. Ware, *ibid.*, **37**, 932 (1962).

(15) T. Wilson, *J. Amer. Chem. Soc.*, **88**, 2898 (1966).

(16) K. R. Kopecky and H. J. Reich, *Can. J. Chem.*, **43**, 2265 (1965).

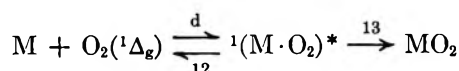
(17) R. Higgins, C. S. Foote, and H. Cheng, *Advances in Chemistry Series*, No. 77, American Chemical Society, Washington, D.C., 1968, p 102.

(18) E. J. Bowen and D. W. Tanner, *Trans. Faraday Soc.*, **51**, 475 (1955).

Table III: $O_2(^1\Delta_g)$ Quenching Constants (k_{11}/k_8) (M^{-1}) for Olefin Inhibitors and $O_2(^1\Delta_g)$ Addition Constants (k_7/k_8) (M^{-1}) for Aromatic Substrates in Benzene at 25°

Inhibitor or substrate	Sensitizer					
	DMA	DMBA	Naphthacene	Rubrene	Perylene	Anthanthrene
MCH ^{a,d}	7.6	8.2	7.2	6.8
MCP ^{b,d}	57	63	57	56
Naphthacene ^e	600 ^f
TME ^{c,d}	1300	830	800	1400
DMBA ^e	...	1400 ^f	1400	1200	1400 ^g	1400 ^g
Rubrene ^e	3300 ^f
DMA ^e	3300 ^f	...	3300	3300	3300 ^g	3300 ^g

^a 1-Methylcyclohexene. ^b 1-Methylcyclopentene. ^c 2,3-Dimethylbut-2-ene. ^d (k_{11}/k_8) (M^{-1}) from inhibition of sensitizer auto-oxidation. ^e (k_7/k_8) (M^{-1}) from substrate disappearance. ^f Autoperoxidation. ^g From ref 4.



with

$$k_7 \text{ (or } k_{11}) = k_d k_{13} / (k_{12} + k_{13})$$

the overall reactivity is essentially determined by the relative rates of dissociative $O_2(^1\Delta_g)$ regeneration (process 12) and peroxide formation (process 13) by the encounter complex ${}^1(M \cdot O_2)^*$. Thus Koch¹⁹ has shown that for reactive acceptors ($k_{13} \gg k_{12}$) the temperature coefficient of reactivity parallels the temperature

Table IV: Relative Photoperoxidation Quantum Yields $\gamma_{MO_2^2}/\gamma_{QO_2^M}$ of Sensitizer M and Inhibitor Q in Air-Saturated Benzene at 25°^a

Q	M	
	Naphthacene ($3.3 \times 10^{-4} M$)	Rubrene ($4.0 \times 10^{-4} M$)
DMA ($2.5 \times 10^{-4} M$)	0.24 (0.18)	1.6 (1.0)
DMBA ($1.0 \times 10^{-4} M$)	1.5 (0.46)	10.6 (2.8)

^a Relative addition efficiencies k_7/k_{11} given in parentheses are from eq V.

Table V: $O_2(^1\Delta_g)$ Quenching and Addition Reactivities^a

Inhibitor or substrate ^b	$\beta(M)^c$	$\beta(M)^2$	Relative reactivity ^d			
			This work	Ref 17 ^e	Ref 15 ^f	Ref 16 ^g
MCH	0.13	0.67	0.007	0.002	...	0.008
MCP	0.017	0.05	0.05	0.05	...	0.07
Naphthacene	0.0017	...	0.5
TME	0.0009	0.0027	(1.0)	(1.0)	(1.0)	(1.0)
DMBA	0.0007	...	1.3
Rubrene	0.0003	...	3.0	...	2.25	...
DMA	0.0003	...	3.0	...	1.0	...

^a Expressed as $\beta = k_8/k_7$ or k_8/k_{11} .² ^b Abbreviations as in Table III. ^c Reciprocal of average values of k_7/k_8 or k_{11}/k_8 listed in Table III; solvent is benzene. ^d Based on value of 1.0 for TME. ^e In methanol-*t*-butyl alcohol (50:50) mixture. ^f In pyridine. ^g In methanol.

dependence of the diffusion-limited rate constant, k_d , whereas the activation energy of process 13 contributes to the observed temperature dependence of reactivity when this is reaction limited ($k_{13} \ll k_{12}$).

Conclusions

1. The inhibition of photoperoxidation may be described quantitatively in terms of a physical or chemical quenching of one or more of the electronically excited intermediates ${}^1S^*$, ${}^3S^*$, and $O_2(^1\Delta_g)$, and provides an indirect confirmation of this reaction sequence.

2. The marked inhibition of DMA autoperoxidation by azulene substantiates the essential intermediary role of the triplet state which, in the virtual absence of intersystem crossing in DMA ($\gamma_F \simeq 1.0$) must be produced by oxygen quenching of the singlet state (process 4) in a yield-limiting process.⁴

3. Oxygen quenching of the sensitizer triplet state, necessary to produce $O_2(^1\Delta_g)$, is attended by an encounter probability close to the spin statistical factor of $1/9$ for triplet-triplet annihilation generating two singlet states; this confirms (6) as the major quenching process⁴ insofar as competitive quenching of the triplet state by catalyzed intersystem crossing, ${}^3S^* + O_2(^3\Sigma_g^-) \rightarrow {}^1S + O_2(^3\Sigma_g^-)$, might be expected to increase the encounter quenching probability to a limiting spin statistical factor of $1/3$.

4. In the absence of energy transfer to azulene from the rubrene triplet state, the energy E_T of the latter is within the range $10,500 \geq E_T > 8000 \text{ cm}^{-1}$.

5. The inhibited reaction yield is determined by four bimolecular quenching processes (4, 6, 9, and 10) with different rate constants in the order k_9 (resonance transfer to azulene from rubrene ${}^1S^*$) $> k_{11}$ (diffusion-limited oxygen quenching of ${}^1S^*$) $> k_{10}$ (diffusion-limited azulene quenching of ${}^3S^*$) $> k_6$ (spin-limited oxygen quenching of ${}^3S^*$).

Acknowledgment. B. E. A. is grateful for the award of a maintenance grant from the Science Research Council of Great Britain.

(19) E. Koch, *Tetrahedron*, **24**, 6295 (1968).

Some Novel Observations Concerning the Thermal Decomposition of 2,4,6-Trinitrotoluene

by Joseph C. Dacons, Horst G. Adolph, and Mortimer J. Kamlet

Advanced Chemistry Division, U. S. Naval Ordnance Laboratory, White Oak, Silver Spring, Maryland 20910
(Received January 22, 1970)

Samples of TNT were partially decomposed (ca. 10–25%) by heating for 16-hr periods at 200°. The complex decomposition product mixtures were shown by column chromatography to contain at least 25 discrete species as well as large amounts of a telomeric or polymeric material of indefinite composition ("explosive coke"). Sharply melting samples of seven of the decomposition products were isolated; three of these were identified as 4,6-dinitroanthranil, 2,4,6-trinitrobenzaldehyde, and 2,4,6-trinitrobenzyl alcohol. The absence in our decomposition residues of 1,3,5-trinitrobenzene, a decomposition product found by other workers, is demonstrated. Possible implications of these findings regarding reported activation parameters for TNT thermal decompositions are discussed.

Introduction

The thermal decomposition of 2,4,6-trinitrotoluene has been a subject of recurring interest for almost 50 years. Several investigators^{1,2} have addressed themselves to the isolation and identification of intermediate products with a view toward elucidation of a stepwise decomposition mechanism; a more frequent approach^{3–8} has involved the determination of apparent activation parameters for the overall process by comparison of time-to-explosion or gas evaluation data at a number of temperatures. Wide discrepancies between reported results of the latter types, determined over different temperature spans and under differing degrees of confinement (*e.g.*, activation energies ranging from 14 to 43.4 kcal/mol),^{3–8} demonstrate that the process is far from well understood.

The significant and unresolved differences notwithstanding, however, differing sets of the reported activation parameters have recently been used as the bases for extended temperature range extrapolations to calculate reaction zone widths and induction times in the shock initiation of liquid TNT (estimated shock temperature ca. 880°).^{9,10}

In the present paper we attempt to shed some light on the processes involved in the isothermal decomposition of TNT at 200°. Although the work reported here was carried out a number of years ago without the benefit of tlc, nmr, and other of the more recent analytical techniques, some of our results are of interest in that they differ significantly from the findings of other workers. They also demonstrate clearly the complexity and dependence of the thermal decomposition of TNT on reaction conditions and environmental factors as well as the pitfalls inherent in extended temperature range rate extrapolations.

Experimental Section

The mixtures of decomposition products used in the present study were obtained by heating TNT samples under air¹¹ as follows. In each of ten 9-in. Pyrex test tubes was placed 15 g of TNT (purified by several recrystallizations from acetone); the tubes were loosely fitted with glass stoppers to permit the escape of evolved gases and placed in a heating block which had been preheated to 200°. The block was of an insulated aluminum type, bored so as to accommodate each tube in its own compartment. The temperature was maintained at 200 ± 1° using a Brown potentiometer, Model 113CIPS-10, as a controller-recorder. The tops of the tubes protruded ca. 2.5 in. from the block, and small amounts of material which evaporated from the molten mass were condensed on the upper parts of the tubes or on the stoppers. At the end of the standard 16-hr period, the block was allowed to cool to 80° (4–5 hr required) and the samples were removed.

- (1) R. N. Rogers, *Anal. Chem.*, **39**, 730 (1967).
- (2) G. K. Adams, P. R. Rowland, and L. A. Wiseman, Ministry of Supply Report A. C. 3982, Great Britain, 1943.
- (3) A. J. B. Robertson, *Trans. Faraday Soc.*, **44**, 977 (1948).
- (4) J. Zinn and R. N. Rogers, *J. Phys. Chem.*, **66**, 2646 (1962).
- (5) M. A. Cook and M. T. Abegg, *Ind. Eng. Chem.*, **48**, 1090 (1956).
- (6) R. Robertson, *J. Chem. Soc.*, **119**, 1 (1921).
- (7) T. Urbanski and S. Rychter, *C. R. Acad. Sci.*, **208**, 900 (1939).
- (8) J. Wenograd, *Trans. Faraday Soc.*, **57**, 1612 (1961).
- (9) J. W. Enig and F. J. Petrone, *Phys. Fluids*, **9**, 398 (1966).
- (10) C. L. Mader, "A Study of the One-Dimensional Time-Dependent Reaction Zone of Nitromethane and Liquid TNT," Report LA-3297, Los Alamos Scientific Laboratory, Los Alamos, N. M., 1965; *Phys. Fluids*, **6**, 375 (1963).
- (11) Control experiments where the decomposition was carried out under nitrogen did not show distinguishable differences from decompositions under air.

The combined decomposition residues from 150 g of TNT were digested in 1500 ml of boiling benzene for 30 min and filtered hot, and the insoluble material on the filter was washed with a further 1000 ml of boiling benzene. An insoluble residue consisting of varying amounts (almost nil to 18 g) of brown powdery material which did not melt at 360° was recovered (fraction C). This product ("explosive coke") burned with intumescence when ignited in a flame, leaving an abundance of carbon.

The filtrate, containing the soluble fraction, was concentrated under reduced pressure and used in subsequent chromatography.

Materials for Chromatography. All chromatographic tubes were of the tapered type. Chromatographic grade Silica (G. Frederic Smith Chemical Co., Columbus, Ohio) was ground in a ball mill for 5 hr and used without screening. Silicic acid was Mallinckrodt, Analytical Grade, 100-mesh powder. Celite 535 was obtained from Johns-Manville Products Co.

Preliminary Resolution of Benzene-Soluble Fractions. The soluble products from 250 g of TNT in 1250 ml of benzene were fractionated on five 70 × 270-mm columns of ground silica-Celite (5:1). Each column was pretreated with benzene and a 250-ml aliquot of the solution was introduced. The column was then washed with 1600 ml of benzene, 1200 ml of benzene-methanol (9:1, v/v), 1500 ml of benzene-methanol (1:1, v/v), and finally 1000 ml of acetone. The effluents from each solvent were taken as separate fractions, corresponding fractions were combined, and the solids in each were recovered by evaporation under reduced pressure. Fractions 1-4 yielded 188, 17, 14, and 7 g of solids, respectively. The first fraction (fraction A) was nearly pure TNT, mp 78-81°. The chromatography of the intermediate fractions (combined, fraction B) is described in the next section. The final acetone fraction was combined with the benzene-insoluble material. Subsequent attempts to resolve the latter complex mixture of "explosive coke" components were not successful.

Chromatography of Intermediate Fractions. Fraction 2 from the preliminary separation was rechromatographed on eight 48 × 230-mm columns of silicic acid-Celite (5:1). Approximately 2.1-g quantities of the residue, dissolved in 30-ml portions of chloroform, were introduced on the columns after pretreatment with 50 ml of *n*-hexane and developed with 900 ml of *n*-hexane-benzene (3:1). Although two zones were visible without streaking, the columns were extracted from the tubes and streaked with alcoholic sodium hydroxide to define the limits of the zones more clearly. The zones were cut from the columns; the corresponding zones were combined eluted with benzene-methanol (20:1) and, on evaporation of the solvent, yielded approximately equal quantities of solids. The amounts were not accurately determined. An additional 8.8 g of TNT was recovered from the combined effluents.

By rechromatographing zone 1, using a similar procedure, 2.5 g of 4,6-dinitroanthranil (**1**), mp and mmp 125-126° with authentic sample,¹² was recovered along with traces of TNT. Zone 2, on similar treatment, yielded 1.1 g of 2,4,6-trinitrobenzaldehyde (**2**), mp and mmp 118-119° with authentic sample,¹³ and 200 mg of a compound, **6**, which on crystallization from benzene-*n*-hexane formed very fine tan needles, mp 225-227°. The identity of **6** has not been established, but the elemental analyses (Table I) indicate that it is a reduction product of TNT.

Fraction 3 from the preliminary separation was dissolved in 30 ml of dioxane and the solution was diluted with 130 ml of benzene. It was then chromatographed on two 70 × 270 mm columns of ground silica-Celite (5:1). Each column was pretreated with 100 ml of benzene, 80 ml of the solution was introduced, and the column was developed with 2200 ml of benzene-methanol (200:1), 4800 ml of benzene-methanol (100:1), and 4000 ml of benzene-methanol (75:1). The resulting chromatograms showed two zones before and after streaking with alcoholic sodium hydroxide. The zones were cut from the columns and like zones were combined and eluted with acetone. On evaporation of the solvents, the recovery of materials was as follows: effluents, 2.1 g; zones 1, 3.6 g; zones 2, 7.0 g.

The effluent fraction was rechromatographed on silicic acid-Celite (5:1), using benzene-*n*-hexane solutions as developers. This resulted in the isolation of 1.4 g of **1**, 0.3 g of **2**, and 0.1 g of a compound, **5**, which formed white prisms, mp 132-133°, from benzene-hexane. The identity of **5** has not been established; analyses (Table I) indicate that it is an oxidation product of TNT.

Several attempts to isolate pure compounds from zone 1 were unsuccessful. It appeared to be a highly complex mixture. When zone 2 was rechromatographed on silicic acid-Celite (5:1), using benzene-hexane solutions as developers, 0.33 g of 2,4,6-trinitrobenzyl alcohol (**4**), mp and mmp 102-103° with authentic sample,¹⁴ and 0.32 g of a compound, **7**, mp 221-222°, were isolated. The latter crystallized as straw-colored needles from benzene-hexane; analyses (Table I) indicate that it is a reduction product of TNT.

When the original benzene-soluble fraction was chromatographed on ground silica-Celite, using 800 ml of benzene-ethanol (100:1) as developer, two zones appeared near the bottom of the chromatogram. On rechromatographing the effluent from this trial on the same adsorbent, using 1500 ml of benzene-methanol, a complex chromatogram showing 11 poorly defined zones was produced. Extensive efforts to isolate pure products from these zones resulted in the recovery of

(12) J. S. Splitter and M. Calvin, *J. Org. Chem.*, **20**, 1086 (1955).

(13) "Beilsteins Handbuch," Vol. VII, p 265.

(14) "Beilsteins Handbuch," Vol. VI, 1st Suppl., p 224.

1, 2, and a compound, 3, mp 217–218°, which the analyses (Table I) indicated to be a reduction product of TNT. Attempts to obtain pure materials from the zones in the initial chromatogram were not successful; the use of silica–Celite columns was therefore discontinued.

Results and Discussion

As standard reaction conditions for the decomposition of TNT, a reaction temperature of 200° and a 16-hr reaction time appeared most appropriate. At lower temperatures, the reaction was too slow; samples heated to 150 and 180° for 70-hr periods, for example, showed only slight decomposition as indicated by melting point depressions of 1 and 3°, respectively, with only minor darkening of the resolidified mass in the latter instance.

At 200° intense darkening of the melt indicated a more rapid reaction. If not intercepted, this went over to an autocatalytic process which generally resulted in autoignition in about 37–39 hr. At 210° the spontaneous self-ignition stage was usually reached in 14–16 hr, but occasionally in appreciably shorter periods.

The process seemed highly susceptible to minor variations in procedure and to adventitious catalysis. The amount of TNT consumed in the decompositions varied from 10 to 25% and the relative proportions of the primary decomposition products varied over a two- to threefold range from run to run (*vide infra*). Further, for no known reason, several samples reached the self-burning stage before the standard 16-hr reaction period had been completed (*i.e.*, more than twice as rapidly as the norm).

Initial small-scale separations resulted in three main fractions: (A) 75–90% of unreacted TNT; (B) benzene-soluble decomposition products, probably of intermediate molecular weights (*i.e.*, 200–500) in amounts representing 5–10% of the starting TNT; (C) benzene-insoluble decomposition products, probably telomeric or polymeric (*i.e.*, molecular weights >500) in amounts ranging from essentially nil to 13 wt % of starting material (or 60% of consumed TNT). Taken with the fact that total weight losses attributable to evolved gases amounted to no more than several per cent when as much as 25% of the starting TNT had been consumed, the relative quantities and gross properties of these fractions, particularly fraction C, gave strong preliminary insights into the nature of the TNT thermal decomposition process.

Fraction C, a brown intractable powder (“explosive coke”), which did not melt below 300° and burned with intumescence when ignited by a flame leaving an abundance of soot, showed strong characteristic absorption near 1600 cm⁻¹ in the infrared spectrum, indicating that it contained unreacted aromatic nitro groups and hence was still a reasonably energetic material. In appearance and properties it closely resembled a tolu-

ene-insoluble fraction described by Adams, Rowland, and Wiseman,² who reported that their material was reasonably soluble in molten TNT, acted as a strong decomposition catalyst, and showed an elemental analysis corresponding roughly to the empirical formula C₆H₃N₂O_{3.75}.

Implications Regarding Kinetic Studies and Activation Parameters. These and findings to be published subsequently from this laboratory point up a major difference between thermal decompositions of polynitro-, nitroxy- and nitroazaaliphatic and -alicyclic explosives, on the one hand, and polynitroaromatic explosives on the other. Compounds of the former types, *e.g.*, HMX (1,3,5,7-tetranitro-1,3,5,7-tetraazacyclooctane),¹⁵ generally decompose directly to relatively low molecular weight species, primarily gaseous, with little intermediate buildup of decomposition products in the condensed phase. For explosives of these types, determinations of evolved gases in thermal decompositions may represent fair measures of extents of reaction; we have no basis to question published kinetics by the gas evolution method in such cases.

In marked contrast with the above, however, TNT and a large number of polynitroaromatic compounds^{16,17} generate relatively small amounts of gaseous products during their early decomposition stages¹⁷ but instead go over to intermediate molecular weight decomposition products which self-condense to “explosive cokes” prior to ignition or detonation. Hoffsommer¹⁷ has also demonstrated that, for most materials which go over to “explosive cokes,” ratios of moles of gas evolved to moles of starting explosive consumed may vary over a five- to tenfold range depending on the extent of decomposition and the reaction temperature.

Hence, activation parameters for thermal decompositions of polynitroaromatic compounds, determined in the 200–420° range,^{3–6} seem to us to be subject to serious question. Data deriving from time-to-explosion studies are suspect on the basis that the phenomena leading to explosion are likely to be governed by the properties and reactivity of the “explosive coke” rather than by primary processes involving the TNT. Data from gas evolution studies are equally uncertain inasmuch as they are likely to reflect strong inaccuracies arising from differing ratios of gas evolved to explosive consumed at different temperatures.

We therefore suggest that the use of such Arrhenius-type parameters for the mathematical treatment of

(15) B. Suryanarayana, R. J. Graybush, and J. Autera, *Chem. Ind. (London)*, 2177 (1967); “Proceedings of the 36th International Congress on Industrial Chemistry, Brussels, 1967,” Vol. III, 1967, p 647.

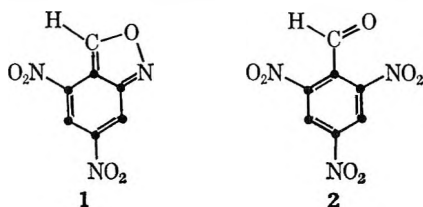
(16) Including *sym*-trinitrobenzene, picramide, 2,2',4,4',6,6'-hexanitrobiphenyl and its 3-amino and 3,3'-diamino derivatives, 1,3-diamino-2,4,6-trinitrobenzene, 2,2',4,4',6,6'-hexanitroazobenzene, and 2,2',2'',4,4',4'',6,6',6''-nonanitro-*m*-terphenyl.¹⁷

(17) J. C. Hoffsommer, “Thermal Stability of Polynitroaromatic Amines,” Report NOLTR 65-227, U. S. Naval Ordnance Laboratory, Silver Spring, Md., Feb 16, 1966.

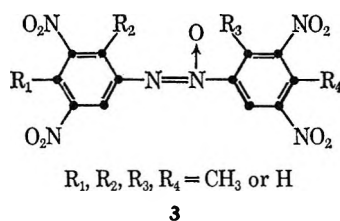
shock initiation phenomena at much higher temperatures^{9,10} and for other extended temperature range extrapolations appears to be unwarranted. Further information regarding the strong dependence of the course and mechanism of TNT thermal decomposition on relatively minor changes in reaction conditions and temperatures, discussed in greater detail below, reinforces this view.

Isolation and Identification of Decomposition Products. Preliminary attempts to resolve fraction B by column chromatography showed that, even in its early stages, the TNT thermal decomposition was of a highly complex nature. Striking the various columns with alcoholic alkali disclosed the existence of *more than 25 distinct zones*, each probably attributable to a unique monomeric (single aromatic nucleus) or dimeric (two aromatic nuclei joined) molecular species deriving from TNT. Two of these products were seen to be present in significant quantities; the others, in minor amounts only.

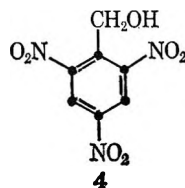
Repeated rechromatographing of the benzene-soluble fraction from 10 to 15 combined 15-g decomposition batches on silica-Celite, followed by fractional crystallization, resulted in the isolation of sharply melting samples of the two major components of the mixture, together with one of the lesser products. The first of the major decomposition products, mp 125–126°, was identified as 4,6-dinitroanthranil (**1**) by comparison (infrared spectrum and mixture melting point) with an independently prepared authentic sample.¹² Elemental analyses of the second major component, mp 118–119°, corresponded well with calculated values for 2,4,6-trinitrobenzaldehyde (**2**); this identity was also confirmed by comparison with an authentic sample.¹³ In these and the subsequent trials at separation (*vide infra*), the amounts of **1** accounted for between 7 and 20% of the consumed TNT and those of **2** for 4–10%.



The minor component **3**, amber crystals, mp 217–218° dec, was isolated in only one instance and in milligram quantities. Elemental analyses, melting point, and solubility properties suggested that it was a dimeric reduction product of TNT, containing a bridging azo or azoxy linkage

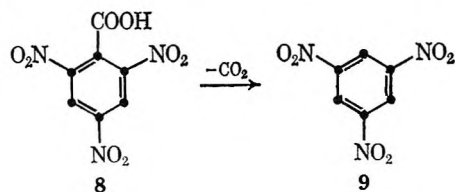
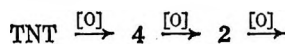


Subsequent chromatography on silicic acid-Celite led to the isolation of four additional minor decomposition products (but never again of **3**). No one of these additional products accounted for as much as 1% of the consumed TNT.



One of these compounds obtained from the further trials was readily characterized as 2,4,6-trinitrobenzyl alcohol (**4**), mp 102–103°, by comparison with an authentic sample.¹⁴ Insufficient quantities of the other products were available for full characterization, but elemental analyses and solubility properties indicated that **5**, mp 132–134°, was also an oxidation product of TNT, and that **6** and **7**, mp 225–227 and 221–222°, respectively, were dimeric reduction products with structures analogous to **3**. The results of the various trials at separation and data serving toward product identification are summarized in Table I.

Nonappearance of Trinitrobenzene among Decomposition Products. Of at least as much interest as those decomposition products which we succeeded in isolating was one compound which failed to appear. Formally (but not necessarily in terms of mechanism), **4** and **2** are successive stepwise oxidation products of TNT. The logical sequential steps are to 2,4,6-trinitrobenzoic acid (**8**) and, since the latter compound is known to undergo ready decarboxylation at advanced temperatures, to 1,3,5-trinitrobenzene (TNB, **9**). TNB has been shown to be quite stable at temperatures as high as 280–300°.¹⁷



To ascertain where TNB would appear in our resolution schemes, mixtures of TNB with TNT and 4,6-dinitroanthranil (**1**) were chromatographed on silicic acid-Celite columns with benzene-*n*-hexane as developer. The TNB appeared as a discrete zone between TNT and **1**. Since, in our standard separations, **1** was the first of the decomposition products behind unreacted TNT, with a sizable interzone, TNB should have been easily detectable if present in our residues. Despite an exhaustive search, however, we were in no instance able to observe even traces of this material.

Our findings in these respects differ markedly from results by Rogers,¹ who recently described some pro-

Table I: Decomposition Products of TNT

Product	Recovery, ^a wt %	Mp, °C	Elemental analyses, ^{b,c} %		
			C	H	N
Unconsumed TNT	75-90	78-81
4,6-Dinitroanthranil (1) ^d	2-4	125-126	40.4 40.0 (40.2)	1.86 1.75 (1.43)	21.0 20.8 (20.1)
2,4,6-Trinitrobenzaldehyde (2)	1-2	118-119	35.1 35.0 (34.9)	1.42 1.39 (1.25)	17.6 17.5 (17.5)
Reduction product 3 ^e	<0.1	217-218 dec	42.1	3.11	23.2
2,4,6-Trinitrobenzyl alcohol (4)	~0.2	102-103	35.4 34.5 (34.6)	2.73 2.69 (2.06)	17.0 17.2 (17.3)
Oxidation product 5	~0.04	132-134	35.3 36.0	1.09 1.18	16.4
Reduction product 6 ^e	~0.2	225-227	40.8 41.0	2.38 2.68	21.8 22.1
Reduction product 7 ^e	~0.1	221-222	41.9	1.79	22.8
"Explosive coke"	0-13	>360	41.6 ...	2.44 ...	22.7 ...

^a Based on starting TNT. ^b Elemental analyses of high-melting organic explosives are frequently poor because of the tendency of such compounds to decompose vigorously in the combustion tube. ^c Calculated values are in parentheses. ^d Molecular weight (X-ray) Found, 204. ^e *Anal.* Calcd for C₁₄H₁₀N₆O₉: C, 41.4; H, 2.47; N, 20.7.

grammed temperature pyrolyses of TNT (*ca.* 11° temperature rise/min from ambient temperatures to 300°), with separation and identification of products by thin layer chromatography. Rogers' reactions were conducted under a gas carrier stream; intermediate products were swept out prior to significant further reaction. No mention was made of polymeric material or "explosive coke" as a significant pyrolysis product.¹

Whereas we isolated neither **8** nor TNB from our decompositions at 200° and definitely confirmed the absence of the latter, Rogers identified **8** as a minor product (which appeared at temperatures between 175 and 225°) and TNB as the principal decomposition product appearing between 233 and 285°. Further, our preliminary report¹⁸ that **2** was a major product at 200° prompted Rogers to an intensive search for this species. Although he was able to identify trace amounts from the pyrolysis of some TNT-containing compositions, *2,4,6-trinitrobenzaldehyde never appeared under Rogers' conditions from pyrolysis of pure TNT.* In both Rogers' experiments and our own, **1** and **4** were observed in comparable amounts.

We can draw no firm conclusions from the differing findings regarding **8** since, from its position on Rogers' chromatograms, it may have been that minor amounts of 2,4,6-trinitrobenzoic acid were present in our decomposition residues but were lost with the "explosive coke" in our fraction C, nor is it conclusive from Rogers' description that small amounts of higher molecular weight materials (corresponding to **3**, **6**, and **7**, and our "explosive coke") were not also present in the tlc spot which he attributed solely to **8**.

The sharply contrasting findings regarding TNB and **2** do not seem subject to question, however, inasmuch as both species have been shown to be isolable and identifiable by both Rogers' techniques and our own. Here, the conflicting observations appear to signal an important change in TNT thermal decomposition pathways with changing reaction medium and/or changing time-temperature history over a relatively narrow temperature span.

A number of rationales may be advanced to account for this change in decomposition mechanism. (a) A sharp temperature threshold between our 200° and Rogers' 233° might arise from a very high activation energy in the TNB-forming reaction. This would require that the rate-determining step(s) in TNB formation differ markedly from that (those) in the TNT-consuming reactions. (b) Extraneous decomposition products, present in our mixtures but swept out of those of Rogers by his carrier gas stream, may react preferentially with **2** to form products other than TNB or otherwise inhibit the conversion of **2** to **8** and TNB. (c) TNB, although extremely thermally stable *per se*, may have undergone further rapid reactions with products present in our residues but swept out of those of Rogers. (d) Adventitious catalysis by a trace impurity, present in Rogers' TNT but absent in ours, may have led to rapid conversion of **2** to TNB. (e) The polymeric "explosive coke," present in significant amounts in our mixtures but not given time to form in

(18) J. C. Dacons, M. K. Kamlet, and D. V. Sickman, "Thermal Decomposition of TNT," Report NavOrd 6831, U. S. Naval Ordnance Laboratory, May 1, 1960.

those of Rogers, may have affected the course of the decomposition either by selective catalysis or through gross properties of the reaction medium.

Further observations which suggest that the properties of the medium and the nature of the coproducts play important roles by both increasing and decreasing reactivities of the various species are as follows. A 4-g sample of pure **2** was found to ignite spontaneously in less than 30 min at 200°; the amounts recovered from our residues require, however, that this aldehyde survives appreciably longer in the presence of its coproducts. On the other hand, **2** does seem to catalyze reactions of other species; 0.5 g of **2**, when admixed

with 2 g of TNT, caused extensive decomposition of the latter after only 1 hr at 200°.

Any one of the phenomena mentioned above could markedly influence relative times-to-explosion or gas evolution rates. Taken in combination, they provide strong reinforcement to our views regarding the discrepancies and uncertainties in published activation parameters.

Acknowledgments. The authors are indebted to Dr. Darrell V. Sickman for useful discussions. The work was carried out under U. S. Naval Ordnance Laboratory Foundational Research Task FR-44.

Bonding in Dye Aggregates. Energetics of the Dimerization of Aqueous Cobalt(II)-4,4',4'',4'''-Tetrasulfophthalocyanine Ion

by Z. A. Schelly, D. J. Harward, P. Hemmes, and E. M. Eyring

Department of Chemistry, University of Utah, Salt Lake City, Utah 84112 (Received April 3, 1970)

The thermodynamic functions ΔH° , ΔG° , and ΔS° , as well as the activation parameters of the dimerization $2M \xrightleftharpoons[ok_{-1}]{ok_1} D$ of aqueous Co(II)-4,4',4'',4'''-tetrasulfophthalocyanine ion (Co(II)-TSPC) were calculated using concentration-jump relaxation kinetic and equilibrium photometric data obtained at 38, 48, and 58°. The radius of the activated complex r^\ddagger and the binding energy between the constituents in the dimer were calculated. The nature of binding forces and effect of the dielectric constant of the medium are discussed.

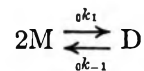
Introduction

In a recent paper¹ we reported on the kinetics of the dimerization of Co(II)-TSPC in aqueous solution at 58°. In the present work we focus on the energetics of this association equilibrium thus elucidating the reaction mechanism and the nature of binding forces between the constituents in the dimer.

This kinetic-thermodynamic approach should supplement the substantial spectroscopic-thermodynamic effort² which has been made to explain the forces in aggregates of charged or neutral dye molecules in general. The results show again the abilities of relaxation kinetic techniques to reveal intimate details of fast association processes.³

Based on the temperature dependence of the thermodynamic equilibrium constant K and the forward and reverse ionic strength independent rate constants ok_1 and ok_{-1} , respectively, we show below the results of a calculation of the standard molar reaction enthalpy ΔH° , molar free energy change ΔG°_{331} , and entropy of

aggregation ΔS°_{331} of the reaction as well as the activa-



tion parameters $\Delta H_{\pm 1}^\ddagger$, $\Delta G_{\pm 1}^\ddagger$, and $\Delta S_{\pm 1}^\ddagger$, for the forward (1) and reverse (-1) reactions, respectively. The important effect of the dielectric constant of the solvent on the rate constants and the nature of the bonding in the dimer are discussed.

Experimental Section

We have supplemented our previous concentration-jump relaxation kinetic and equilibrium photometric

(1) Z. A. Schelly, R. D. Farina, and E. M. Eyring, *J. Phys. Chem.*, **74**, 617 (1970).

(2) On the nature of bonding in dye aggregates, cf. K. K. Rohatgi and G. S. Singhal, *J. Phys. Chem.*, **70**, 1695 (1966), and references cited therein.

(3) M. Eigen and L. DeMaeyer in A. Weissberger's "Techniques of Organic Chemistry," Vol. VIII, Part II, Interscience Publishers, New York, N. Y., 1963, p 895 ff; E. F. Caldin, "Fast Reactions in Solution," Wiley, New York, N. Y., 1964.

Table I: Rate Constants, Equilibrium Constants, and the Dielectric Constant of Water at Different Temperatures

	38°	48°	58°
${}^0k_1, M^{-1} \text{ sec}^{-1}$	$16.0 \pm 0.5 \times 10^2$	$13.3 \pm 0.3 \times 10^2$	$5.36 \pm 0.15 \times 10^2$
${}^0k_{-1}, \text{ sec}^{-1}$	$2.6 \pm 0.1 \times 10^{-3}$	$3.0 \pm 0.1 \times 10^{-3}$	$2.8 \pm 0.1 \times 10^{-3}$
K_{opt}, M^{-1}	$8.0 \pm 0.5 \times 10^6$	$4.7 \pm 0.1 \times 10^6$	$2.05 \pm 0.05 \times 10^6$
$K_{\text{kin}} = {}^0k_1/{}^0k_{-1}, M^{-1}$	$6.17 \pm 0.43 \times 10^6$	$4.55 \pm 0.25 \times 10^6$	$1.92 \pm 0.12 \times 10^6$
Temp, °K	311.15	321.15	331.15
$D_{\text{H}_2\text{O}}$	73.96	70.68	67.38
$D_{\text{H}_2\text{O}} \times T, \text{ °K}$	2.3×10^4	2.27×10^4	2.23×10^4

^a Photometrically determined thermodynamic equilibrium constant.

Table II: Thermodynamic Functions and Activation Parameters for Forward (1) and Reverse (-1) Reaction, Respectively. (Energies Are Given in kcal/mol, and Entropies in eu)

	${}_1E_a = -12.6 \pm 0.63$	$-{}_1E_a = 0 \pm 0.66$	
$\Delta H^\circ = -14 \pm 0.9$	$\Delta H_1^\ddagger = -13.3 \pm 0.63$	$\Delta H_{-1}^\ddagger = -0.66 \pm 0.66$	$\Delta H_1^\ddagger - \Delta H_{-1}^\ddagger = -12.64 \pm 1.29$
$\Delta G^\circ_{331} = -8 \pm 0.02$	$\Delta G_1^\ddagger_{331} = 15.3 \pm 1.3$	$\Delta G_{-1}^\ddagger_{331} = 23.3 \pm 1.3$	$\Delta G_1^\ddagger - \Delta G_{-1}^\ddagger = -8 \pm 2.6$
$\Delta S^\circ_{331} = -18 \pm 3$	$\Delta S_1^\ddagger_{331} = 86.2 \pm 2$	$\Delta S_{-1}^\ddagger_{331} = -72.4 \pm 2$	$\Delta S_1^\ddagger - \Delta S_{-1}^\ddagger = -13.8 \pm 4$

work¹ done at 58° with new data obtained at 48 and 38°. An extension of the temperature to a range significantly above 58° is not possible because of formation of bubbles within the stopped-flow apparatus as well as in the spectrophotometer cell. Below 58°, on the other hand, further polymerization (beyond the dimer stage) starts at a lower total concentration $C_T = C_M + 2C_D$ than at 58°. Since we had to restrict our investigations to the monomer-dimer equilibrium, the experiments at 48 and 38° were performed with solutions of $C_T \leq 3 \times 10^{-7} M$. The experimental uncertainty increases, of course, at such high dilution and this is reflected in the lower precision of the data obtained at 48 and 38°.

The experimental procedure¹ and the interpretation of the kinetic data⁴ have already been described.

Results and Discussion

All experimental data and calculated results are collected in Tables I and II. Uncertainties associated with numerical values are given as average deviations from the mean. The kinetically determined equilibrium constants $K_{\text{kin}} = {}^0k_1/{}^0k_{-1}$ are presented as the mean of the extreme values of the quotients. In the calculation of the thermodynamic quantities the standard state of the components is considered to be the state of the pure components in an ideal dilute solution. In this case, if $C_T \rightarrow 0$, then the activities $a_i \rightarrow c_i$, and the change of the standard molar enthalpy of the reaction ΔH° becomes equal to ΔH^∞ (change of the molar enthalpy at infinite dilution) which can be calculated from $d \ln K/dT = \Delta H^\circ/RT^2$. Similarly, $\Delta G^\circ = \Delta G^\infty = -RT \ln K$, and $\Delta G^\circ \equiv \Delta H^\circ - T\Delta S^\circ$.

The Arrhenius activation energy ${}_{\pm 1}E_a$ for the forward or reverse reaction was obtained from the least-square corrected linear plot of $\ln {}^0k_{\pm 1}$ vs. T^{-1} . Since

$E_a = \Delta H^\ddagger + RT$, the entropy of activation can be calculated from the equation

$${}^0k_{\pm 1} = \frac{kT}{h} \exp(-\Delta H_{\pm 1}^\ddagger/RT) \exp(\Delta S_{\pm 1}^\ddagger/R) \quad (1)$$

as given by the transition-state theory. Obviously, since $K = {}^0k_1/{}^0k_{-1}$, then $\Delta H^\circ = \Delta H_1^\ddagger - \Delta H_{-1}^\ddagger$, and $\Delta G^\circ = \Delta G_1^\ddagger - \Delta G_{-1}^\ddagger$ and $\Delta S^\circ = \Delta S_1^\ddagger - \Delta S_{-1}^\ddagger$.

The dimerization reaction is exothermic ($\Delta H = -14$ kcal), and in spite of a decrease in entropy (-18 eu), formation of dimer is favored from an energetic point of view ($\Delta G = -8$ kcal). Since the change in enthalpy includes also the heat of solution of the monomer and dimer, which are not known, ΔH° cannot be interpreted in terms of bond energy or heat of dissociation. The zero activation energy for the dissociation reaction is noteworthy. It indicates that in the course of separation of the constituents of the dimer to a distance corresponding to that in the activated complex, the repelling and binding forces are approximately in balance. Based on a simple electrostatic picture, viewing two point charges of the same sign ($z = -4$) in a continuous medium, the electrical work W_{el} of bringing them together from an infinite distance to a distance of $2r_{\pm}$ by which they are separated in the activated complex is given by Coulomb's law

$$W_{\text{el}} = \frac{z_1 z_2 e_0^2}{D 2r_{\pm}} \quad (2)$$

D is the dielectric constant of the medium and r_{\pm} is the radius of the activated complex in eq 2. A value

(4) Z. A. Schelly, R. D. Farina, and E. M. Eyring, *Monatsh. Chem.*, **101**, 493 (1970).

for r_{\pm} can be obtained from the slope of the $\ln {}_0k_1$ vs. $1/DT$ plot based on the equation⁵

$$\ln {}_0k_1 = \ln k' - \frac{z_+z_+e_0^2}{r_{\pm}kDT} \quad (3)$$

where k' symbolizes the ionic strength independent rate constant in a medium with $D = \infty$. The calculated value for r_{\pm} is 2.51 Å representing a charge separation of ~ 5 Å in the activated complex. Since we are dealing with large planar ions, this distance is equal to the separation of the two parallel monomer planes. Comparing this with values obtained from X-ray measurements on phthalocyanine⁶ and Ni-phthalocyanine⁷ crystals as well as on graphite, where the distances between the planes of the parallel molecules (staggered stacking) are 3.38, 3.38, and 3.41 Å, respectively, one may expect that the separation within the dimer in solution is between 5 and 3.38 Å. In other words, the structure of the dimer in solution resembles that in the crystalline state, and the bonding is accomplished by the overlapping of the extended π -electron clouds of two conjugated systems. Thus, the possibility of hydrogen bonding or "sandwich structure" can be excluded. The bond energy, as indicated earlier, can be calculated from eq 2. Multiplying W_{e1} by N we obtained 16.5 kcal/mol.

The fact that the experimentally determined activation energy for the forward reaction is negative is striking. This, however, can be understood in the following way. Noting that k' in eq 3 is temperature dependent, we may rewrite this equation as

$$\ln {}_0k_1 = \ln k'' - \frac{{}_1E_a'}{RT} - \frac{z_+z_+e_0^2}{r_{\pm}kDT} \quad (4)$$

where k'' is the forward rate constant at $D = T = \infty$, and ${}_1E_a'$ is the activation energy of the association at $D = \infty$. Infinite dielectric constant, however, means that charges do not "see" one another; consequently there is no repulsion between the similarly charged reacting ions. In this case the activation energy ${}_1E_a'$ is presumably zero or negligibly small and so the dependence of ${}_0k_1$ on D and T is determined by the last term on the right side of eq 4. In water with increasing temperature D goes down faster than T goes up so that the product DT decreases (Table I), resulting in a smaller ${}_0k_1$. Thus the plot of $\ln {}_0k_1$ vs. $1/T$ gives an apparently negative activation energy for the association process.

The effect of the dielectric constant of the medium on the kinetics of the association may partially explain earlier equilibrium observations⁸ that in alcohol or glycerol solution dye aggregation is much weaker than in water.

Acknowledgment. This work has been sponsored by AFOSR (SRC)-OAR, USAF, Grant No. 69-1717-D.

(5) A. A. Frost and R. G. Pearson, "Kinetics and Mechanism," 2nd ed, Wiley, New York, N. Y., 1965, p 145.

(6) J. M. Robertson, *J. Chem. Soc.*, 1195 (1936).

(7) J. M. Robertson and L. Woodward, *ibid.*, 219 (1937).

(8) E. Rabinowitch and L. F. Epstein, *J. Amer. Chem. Soc.*, **63**, 69 (1941); V. L. Levschin and L. V. Krotova, *Opt. Spektrosk.*, **13**, 457 (1962); V. L. Levschin and E. G. Baranova, *J. Chim. Phys. Physicochim. Biol.*, **55**, 869 (1958); K. Bernauer and S. Fallab, *Helv. Chim. Acta*, **44**, 1287 (1961).

The γ Radiolysis of 2-Propanol. V.^{1a} Oxidation by Carbon Tetrachloride

by Cecelia Radlowski^{1b} and Warren V. Sherman

Department of Physical Science, Chicago State College, Chicago, Illinois 60621 (Received January 21, 1970)

Dilute solutions of carbon tetrachloride in 2-propanol have been subjected to ⁶⁰Co γ irradiation. Reduction of the solute to chloroform and hydrogen chloride was observed with the concomitant oxidation of the solvent to acetone in accord with the stoichiometry: $\text{CCl}_4 + (\text{CH}_3)_2\text{CHOH} \rightarrow \text{CHCl}_3 + \text{HCl} + (\text{CH}_3)_2\text{CO}$. The 100-eV yields were independent of initial carbon tetrachloride concentration in the range 1×10^{-2} to $2 \times 10^{-1} M$ but showed a first-order dependence on 2-propanol concentration when the system was diluted with 2-methyl-2-propanol. A chain mechanism is indicated by the magnitude of $G(\text{products})$; inhibition by O_2 is consistent with free radical intermediates being involved. The observed dose-rate dependence is in accord with free radical chain carriers undergoing second-order termination. The data are consistent with the chain propagation steps, $\dot{\text{C}}\text{Cl}_3 + (\text{CH}_3)_2\text{CHOH} \rightarrow \text{CHCl}_3 + (\text{CH}_3)_2\dot{\text{C}}\text{OH}$ (3) and $(\text{CH}_3)_2\dot{\text{C}}\text{OH} + \text{CCl}_4 \rightarrow (\text{CH}_3)_2\text{CO} + \text{HCl} + \text{CCl}_3$ (4), with $k_3 = 3 M^{-1} \text{sec}^{-1}$ and $k_3 < k_4$.

The original motivation for an examination of the radiation chemistry of 2-propanol solutions of carbon tetrachloride was to gain further information concerning the scope of the recently reported¹⁻⁵ radical-initiated chain oxidation of primary and secondary aliphatic alcohols which occurs under alkaline conditions. It was thought that carbon tetrachloride would fulfill the criteria set^{1,5} for compounds that would enter into electron transfer with the ionized form of the α -hydroxymethyl radical (generated by free radical attack on the alcohol solvent) and thus effect a chain oxidation reaction analogous to that obtained with alkyl and aryl monobromides and monoiodides.

It has long been known⁶ that carbon tetrachloride undergoes *slow* decomposition in basic alcoholic solution. In the present work it was found that 2-propanol solutions containing 0.1 *M* carbon tetrachloride and 0.1 *M* potassium hydroxide could be stored for several days without the occurrence of a significant amount of chemistry. However, on deaerating (flushing with nitrogen or pumping on a vacuum line), a relatively rapid reaction set in.⁷ Because of this instability of O_2 -free alkaline carbon tetrachloride solutions a quantitative study of their radiation chemistry was not attempted.

Preliminary experiments on the radiolysis of neutral solutions of carbon tetrachloride, however, indicated some interesting chemistry, and hence study of the system was continued. Some time ago, Hannerz,⁸ in search of a potential γ -ray dosimetry system involving the production of acid in proportion to absorbed dose, briefly surveyed the radiolysis of 50 vol % mixtures of carbon tetrachloride with primary and secondary alcohols. Although the very large 100-eV yields of hydrochloric acid observed are an asset for such a chemical dosimeter, Hannerz concluded that "insufficient stability to impurities preclude an extended use of these systems for dosimetric purposes." In the present study the data for dilute deaerated solutions of

carbon tetrachloride in 2-propanol show that although certain criteria for a sensitive chemical dosimeter are met (large 100-eV yields, direct proportionality of yield to exposure time when subjected to constant radiation intensities, yield reproducibility), observation of a dependence of yield-dose upon radiation intensity is not consistent with the requirements of a useful dosimeter. In connection with the present study, the earlier work of Minder⁹ on the radiolysis of polychlorinated hydrocarbons in alcohols should be cited.

Experimental Section

Materials. 2-Propanol (Baker Spectrophotometric reagent) was used as received; the only impurity detected by glc analysis was acetone ($<10^{-4} M$). Carbon tetrachloride (Eastman Spectrograde), 1-propanol (Allied chemical, B & A), and 2-methyl-2-propanol (Eastman) were used as received. The nitrogen used for deoxygenation was Airco prepurified.

(1) (a) Part IV in this series: W. V. Sherman, *J. Amer. Chem. Soc.*, **90**, 6773 (1968). (b) This paper is taken in part from the thesis submitted by C. R. in partial fulfillment of the requirements for the B.S. degree at Chicago State College, 1969.

(2) W. V. Sherman, *J. Amer. Chem. Soc.*, **89**, 1302 (1967).

(3) W. V. Sherman, *J. Phys. Chem.*, **71**, 1695 (1967).

(4) W. V. Sherman, *ibid.*, **71**, 4245 (1967).

(5) W. V. Sherman, *ibid.*, **72**, 2287 (1968).

(6) J. V. Nef, *Justus Leigibis Ann. Chem.*, **308**, 329 (1899).

(7) Products identified were carbon monoxide and acetone, and a loss of basicity occurred. Rate of loss of hydroxide was equal to the rate of formation of acetone, and both were constant with time. The time required for 50% disappearance of OH^- was approximately 5 hr with the solution stored in a sealed tube at room temperature. The nature of the products and the effect of O_2 indicate that the decomposition of CCl_4 is probably *via* a dihalocarbene (see J. Hine, "Divalent Carbon," Ronald Press, N. Y., 1964). During the preparation of this paper, evidence has been published that CCl_4 undergoes solvolysis to dichlorocarbene in several alcohol solutions in the presence of potassium hydroxide (C. Y. Myers, A. M. Malte, and W. S. Matthews, *J. Amer. Chem. Soc.*, **91**, 7510 (1969)).

(8) K. Hannerz, *Research*, **9**, S1 (1956).

(9) W. Minder and H. Heydrich, *Discuss. Faraday Soc.*, **12**, 305 (1952).

Procedure. Aliquots (5 ml) of freshly prepared solutions were irradiated in 16-mm Pyrex test tubes fitted with a rubber septum. Deoxygenation (or oxygenation) was performed by flushing the solution for 1 hr with nitrogen (or oxygen) which had been presaturated with solution vapor. Entrance and exit of the flushing gas was *via* hypodermic needles which pierced the septum. (As a check for the effectiveness of deoxygenation by nitrogen flushing, a number of solutions were degassed on a vacuum line by the freeze-pump-thaw method; the two methods of sample preparation led to identical yields.) Irradiation was carried out in the Argonne A-063 cobalt chamber in which the samples could be arranged radially around a central rod of cobalt. The radiation intensity received by the sample was varied by change of distance from the source. At 9 cm from the source the dose rate received by Fricke dosimeter solutions was 1.10×10^{18} eV ml⁻¹ min⁻¹. At this position the dose rate in 2-propanol, calculated by correcting for electron density, was 8.40×10^{17} eV ml⁻¹ min⁻¹. After irradiation, the solution was analyzed for HCl by titration with 0.01 M sodium hydroxide (phenolphthalein), and for CHCl₃, CH₂Cl₂, and acetone by gas chromatography (Hewlett-Packard Model 5750 with flame-ionization detector).

Results

1. *Solutions of Carbon Tetrachloride in 2-Propanol.* The principal liquid phase products identified in the radiolysis of deoxygenated solutions were hydrochloric acid, chloroform, and acetone. For 0.1 M solutions the yields of all three products showed a linear dependence on radiation dose up to yields corresponding to almost 100% conversion of the initial carbon tetrachloride to hydrochloric acid and chloroform (Figure 1). From the slopes of the plots, $G(\text{HCl}) = G(\text{CHCl}_3) = G(\text{acetone}) = 2.7 \times 10^2$ molecules/100 eV. Essentially identical yield-dose plots were obtained for solutions initially containing 0.02, 0.05, and 0.2 M carbon tetrachloride.

A break in the yield-dose curve was noted for all four solutions at doses corresponding to approximately 100% reduction of the initial concentration of carbon tetrachloride. At higher doses although [HCl] and [acetone] increased progressively with dose, chloroform was consumed. A new product, methylene chloride, was identified, but the yields were too small to account completely for the loss of chloroform.

A linear yield-dose plot was observed for oxygen-saturated solutions up to the highest dose used (1.0×10^{20} eV ml⁻¹); $G(\text{HCl}) = G(\text{acetone}) = 22$ (chloroform was not determined in this experiment). A more complex behavior was noted with air-equilibrated solutions. Although very little reaction took place on the absorption of doses up to $\sim 5 \times 10^{18}$ eV ml⁻¹, very rapid reaction set in on absorption of further radiation

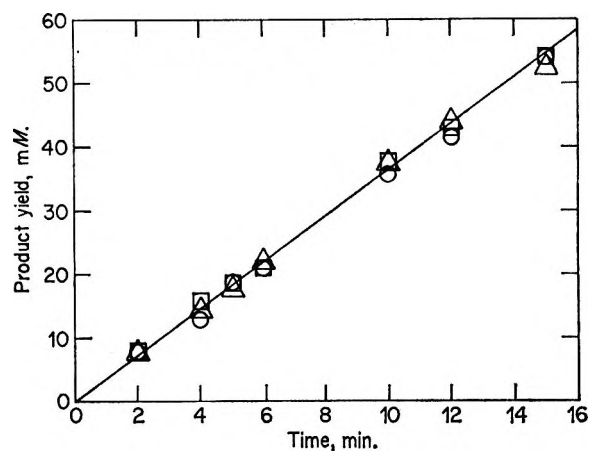


Figure 1. Product yields as a function of dose from deaerated 0.1 M CCl₄ in 2-propanol, dose rate, 8.4×10^{17} eV ml⁻¹ min⁻¹. (□, HCl; Δ, acetone; ○, CHCl₃.)

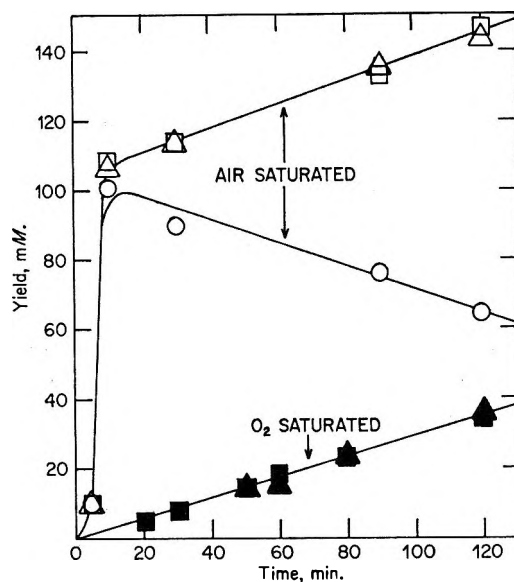


Figure 2. Product yields as a function of dose from air saturated and oxygen saturated 0.1 M CCl₄ in 2-propanol. Dose rate, 8.4×10^{17} eV ml⁻¹ min⁻¹. (Air-saturated: □, HCl, Δ, acetone; ○, CHCl₃. O₂-saturated: ■, HCl; ▲, acetone.)

so that by a dose of $\sim 8 \times 10^{18}$ eV ml⁻¹ approximately 100% conversion of carbon tetrachloride was observable (Figure 2). The exact dose at which the onset of this rapid reaction took place was not reproducible.

The dependence of yield on dose rate was investigated over the range 1.53×10^{18} to 5.65×10^{16} eV ml⁻¹ min⁻¹. The 100-eV yields were found to decrease with increasing dose rate and for all three products measured conform to the relationship $G(\text{product}) \propto (\text{dose rate})^{-0.5}$ (see Figure 3).

2. *Solutions of Carbon Tetrachloride in 1-Propanol and in 2-Methyl-2-Propanol.* As with the CCl₄-2-propanol system, HCl yields from deoxygenated 1-propanol and 2-methyl-2-propanol solutions showed initially a linear dependence on dose (Figure 4). From the

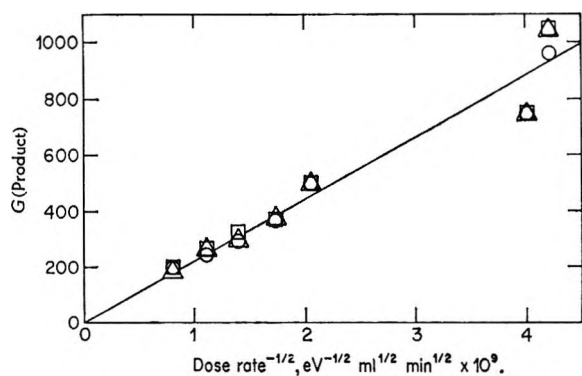


Figure 3. Product yields as a function of $(\text{dose rate})^{-1/2}$ from deaerated 0.1 M CCl_4 in 2-propanol (total dose such that final [product] = 10–50 mM). (\square , HCl; Δ , acetone; \circ , CHCl_3).

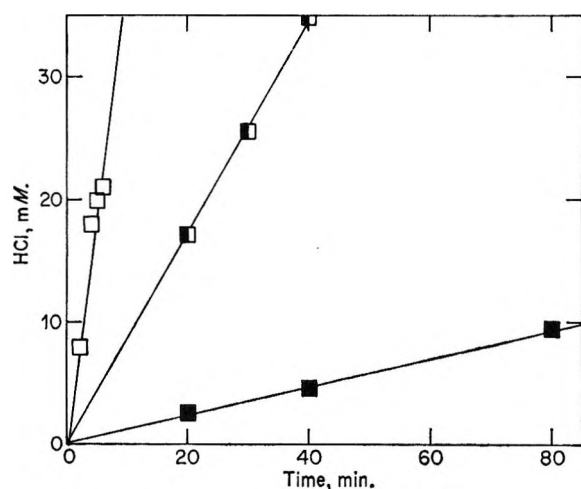


Figure 4. HCl yields as a function of dose from 0.1 M CCl_4 in 1-propanol and in 2-methyl-2-propanol (2-propanol data are also included). Dose rates: 1-propanol, 8.6×10^{17} eV $\text{ml}^{-1} \text{min}^{-1}$; 2-methyl-2-propanol, 9.0×10^{17} eV $\text{ml}^{-1} \text{min}^{-1}$. (\square , 2-propanol, \blacksquare , 1-propanol, \blacksquare , 2-methyl-2-propanol.)

slopes of the yield-dose plots, the HCl yields from 1-propanol and 2-methyl-2-propanol were 62 and 7.7 molecules/100 eV, respectively. Data on the effect of added 2-propanol on the radiolysis of 0.1 M CCl_4 in 2-methyl-2-propanol were obtained; a progressive increase of $G(\text{HCl})$ with initial [2-propanol] was noted (Figure 5).

Discussion

The chemical change in γ -irradiated dilute solutions of carbon tetrachloride in 2-propanol may be described as the oxidation of one molecule of 2-propanol to acetone and the concomitant reduction of one molecule of carbon tetrachloride to chloroform



The magnitude of the product yields in anaerobic solutions at all carbon tetrachloride concentrations and all radiation doses and dose rates studied indicates

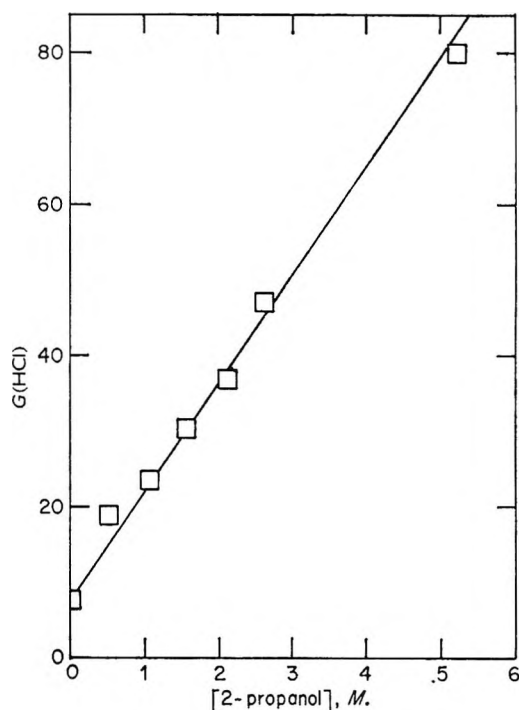


Figure 5. HCl yields as a function of 2-propanol concentration from solutions of 0.1 M CCl_4 in 2-methyl-2-propanol.

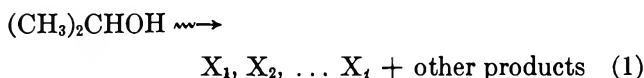
that a chain process is operative. The 100-eV product yields were independent of the initial concentration of carbon tetrachloride up to a total yield corresponding to close to 100% conversion of carbon tetrachloride to chloroform. From the preceding, and the fact that initial $G(\text{products})$ were identical for solutions initially containing 0.05, 0.1, and 0.2 M carbon tetrachloride, it may be concluded that (a) the chain reaction does not involve carbon tetrachloride in the rate-determining step, and (b) carbon tetrachloride present in the system at concentrations down to approximately 10^{-2} M scavenges all radiolytic species capable of initiating the observed chain reaction.

If carbon tetrachloride is not involved in the rate-determining step then the only other compound in the system, namely the solvent, must be. This was confirmed in the experiments in which 2-propanol was replaced progressively with 2-methyl-2-propanol (Figure 5). The hydrochloric acid yield from carbon tetrachloride in pure 2-methyl-2-propanol indicates that this solvent does not participate in a chain reaction and is therefore a suitable "inert" solvent for determination of the reaction order with respect to 2-propanol. The linear dependence of $G(\text{HCl})$ on [2-propanol] indicates that the rate-determining step involves one molecule of 2-propanol. The only datum that deviates significantly from the best straight line is that for carbon tetrachloride in pure 2-propanol. The simplest explanation for this is that reactive intermediates capable of initiating the chain (free radicals such as alcohol-minus-H radical, e_{sol}^- , $\text{H}\cdot$) are produced in

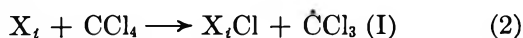
higher yields (or with longer lifetimes) in 2-propanol than in 2-methyl-2-propanol. Using benzoquinone and ferric chloride as probes for free radicals, Adams, Baxendale, and Sedgwick¹⁰ obtained $G = 6.7$ and 4.5 radicals/100 eV for 2-propanol and 2-methyl-2-propanol solutions, respectively. The radiolytic yield of chain-initiating radicals in mixtures of the two alcohols, however, may be assumed to be constant and equal to that from neat 2-methyl-2-propanol since any primary ionization in 2-propanol would be rapidly transferred to 2-methyl-2-propanol owing to the expected lower ionization potential of the latter.¹¹ Subsequent neutralization leading to radical formation would then involve solely cations derived from 2-methyl-2-propanol.

The sequence, reactions 1-5, is consistent with the data for O_2 -free solutions of CCl_4 in 2-propanol.

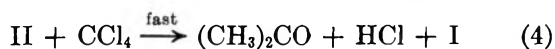
Initiation.



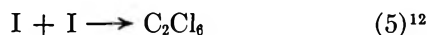
where X_t is any species (organic radical, e_{solv}^- , $H\cdot$) that can undergo reaction 2.



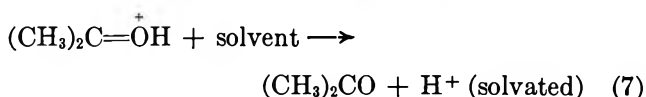
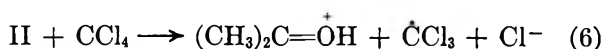
Propagation.



Termination.



The interesting reactions in the above sequence are propagation steps 3 and 4. These steps were proposed by Razuvaev, Moryganov, and Volkova¹³ to explain the chain reaction they observed between carbon tetrachloride and 2-propanol initiated by free radicals produced by the thermolysis of dissolved benzoyl peroxide. They considered (4) to be a two-step process via 2-chloro-2-propanol formed by abstraction of a chlorine atom by II from carbon tetrachloride. Based on the evidence that carbon tetrachloride undergoes dissociative electron transfer with ionized dimethylhydroxymethyl radicals,^{2,14} it would seem more likely that (4) involves initial electron transfer from dimethylhydroxymethyl radicals to carbon tetrachloride (6) followed by proton transfer (7)



Assuming that under steady irradiation (dose rate, I) constant concentrations of intermediates X_t , I, and II are established then analysis of 1-5 gives:

$$G(HCl) = G(CHCl_3) = G(\text{acetone}) =$$

$$10k_3[2\text{-propanol}] \left\{ \frac{G(X_t)}{k_5 I} \right\}^{1/2} \quad (A)$$

The predicted linear dependence of $G(\text{products})$ on $I^{-1/2}$ is in agreement with the experimental data (Figure 3). From Figure 3, $dG(HCl)/d(I^{-1/2}) = 1.9 \times 10^9$ molecules $eV^{-1/2} ml^{-1/2} min^{-1/2}$. Substituting $[2\text{-propanol}] = 13 M$ and $k_5 = 1 \times 10^8 M^{-1} sec^{-1}$,¹⁵ then $k_3(G(X_t))^{1/2} = 1.3 \times 10^{-24} l. sec^{-1} eV^{-1/2} molecules^{-1/2}$. If it is assumed that $G(X_t)$ is similar to the radical yield scavangeable by ferric chloride,¹⁰ then $k_3 = 2.9 M^{-1} sec^{-1}$.

From the linear dependence of $G(HCl)$ on 2-propanol concentrations in 2-methyl-2-propanol solutions $dG(HCl)/d[2\text{-propanol}] = 2.4 \times 10^{-25} l. eV^{-1}$. Substitution into (A) (putting $k_5 = 1 \times 10^8 M^{-1} sec^{-1}$ and $I = 9.00 \times 10^{17} eV ml^{-1} min^{-1}$) gives $k_3 G(X_t)^{1/2} = 1.2 \times 10^{-24} l. sec^{-1} eV^{-1/2} molecules^{-1/2}$. If $G(X_t)$ for 2-methyl-2-propanol solutions is taken as 4.5 molecules/100 eV¹⁰ then $k_3 = 3.4 M^{-1} sec^{-1}$, in good agreement with the value obtained above.

At high doses yields of HCl and acetone were observed to exceed that expected for 100% reduction of carbon tetrachloride to chloroform. This is due to the reactivity of chloroform in irradiated 2-propanol. In a study of the radiation chemistry of chloroform solutions¹⁶ it was found that this solute undergoes chain reduction (mainly to hydrogen chloride and methylene chloride) with the concomitant oxidation of the solvent to acetone ($G(HCl) = G(\text{acetone}) = 45$ molecules/100 eV at $8.4 \times 10^{17} eV ml^{-1} min^{-1}$).

The magnitude of $G(\text{products})$ in the radiolysis of carbon tetrachloride in 1-propanol is indicative of a chain reaction. In this solvent the rate-determining step involves homolysis of a primary carbinol C-H. The lower yields observed in this system are consistent with this process being ~ 4 kcal less favorable than that involving the secondary alcohol and therefore less able to compete with the chain termination reaction 5.

The effect of dissolved molecular oxygen on the radiolysis of carbon tetrachloride in 2-propanol is interesting. In view of its low concentration ($7 \times 10^{-3} M$

(10) G. E. Adams, J. H. Baxendale, and R. D. Sedgwick, *J. Phys. Chem.*, **63**, 854 (1959).

(11) Values for ionization potentials in the liquid phase are not available. However, in a review of gas-phase IP values (K. Watanabe, T. Nakayama, and J. Mottl, *J. Quant. Spectrosc. Radiat. Transfer*, **2**, 369 (1962)) it may be noted that IP decreases as the molecular weight and carbon-chain branching of the monohydric alcohols decreases. The same trend may be expected for liquids.

(12) Radical-radical termination reactions involving X_t and II are considered kinetically unimportant since at the CCl_4 concentrations used $G(\text{products})$ are independent of $[CCl_4]$.

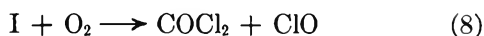
(13) G. A. Razuvaev, B. N. Moryganov, and A. S. Volkova, *J. Gen. Chem. U.S.S.R.*, **25**, 463 (1955), and preceding papers.

(14) W. V. Sherman, *J. Amer. Chem. Soc.*, **90**, 6773 (1968).

(15) J. M. Tedder and J. C. Walton in *Progr. React. Kinet.*, **4**, 37 (1967).

(16) W. V. Sherman, to be published.

for O₂-saturated solutions¹⁷), O₂ will not compete significantly with carbon tetrachloride for X₁. However, as a consequence of the low rate constant for reaction 3, it would be expected to scavenge most trichloromethyl radicals according to the highly exothermic reaction



However, in the absence of more extensive data on oxygenated solutions, an analysis of the complex behavior illustrated in Figure 2 is not warranted in the present discussion.

Acknowledgments. This work was supported in part by a grant from the Petroleum Research Fund administered by the American Chemical Society, and in part by a grant from the Committee on Organized Research of Chicago State College. We are grateful to Dr. E. J. Hart of Argonne National Laboratory for the use of the ⁶⁰Co facility in the Chemistry Division.

(17) "International Critical Tables," Vol. III. Although a determination of the solubility of O₂ in 2-propanol is not cited, its solubility in the lower aliphatic alcohols is relatively insensitive to structure. An average Bensen absorption coefficient, $\alpha = 0.16$ is assumed for 2-propanol.

Yields of the Lowest Triplet and Excited Singlet States in γ Radiolysis of Liquid Benzene

by Robert R. Hentz and Lewis M. Perkey

Department of Chemistry and the Radiation Laboratory,¹ University of Notre Dame, Notre Dame, Indiana 46556
(Received April 1, 1970)

The γ radiolysis of benzene solutions of 3,5-cycloheptadienone (CHDO) was studied for determination of the yield ¹G of lowest excited singlets of benzene and the yield ³G of lowest triplets of benzene that do not have the lowest excited singlet as a precursor. By study of the photochemistry of CHDO in various solutions, it was shown that (1) singlet excitation yields CO and hexatriene, with ¹ ϕ (HT) = 0.44, but no isomer and (2) triplet excitation yields the isomer bicyclo[3.2.0]hept-6-en-3-one, with ³ ϕ (ISO) = 0.16, but no CO or HT. Study of the quenching of benzene fluorescence (excited with 2537-Å light) by CHDO, *trans*-stilbene, and *trans*-octene-2 gave the following values for the product ¹ $\tau \cdot k$ of lifetime and specific rate of quenching of the lowest excited singlet of benzene: ¹ $\tau \cdot k$ (CHDO) = $4.8 \times 10^2 M^{-1}$, ¹ $\tau \cdot k$ (*trans*-stilbene) = $1.29 \times 10^3 M^{-1}$, and ¹ $\tau \cdot k$ (*trans*-octene-2) = $2.5 M^{-1}$. A value of $\chi = 0.58$ was determined for intersystem crossing efficiency of the lowest excited singlet of benzene by comparison of the photosensitized isomerization of *trans*-octene-2 in benzene with that in acetone. From results of the photoexcitation experiments and measurements of *G*(HT) and *G*(ISO) in γ radiolysis of benzene solutions of CHDO ($\leq 0.05 M$), values of ¹G = 1.45 and ³G = 4.0 are obtained. Such values, with the photoexcitation results, are found to be in accord with results of a reexamination of radiation-induced isomerization of *trans*-stilbene ($\leq 0.1 M$) in benzene. Assuming a diffusion-controlled ³ $k \approx 10^{10} M^{-1} sec^{-1}$ for triplet transfer from benzene to CHDO and *trans*-stilbene, ³ $\tau \approx 7$ nsec is estimated for the benzene triplet lifetime from ³ $\tau \cdot k$ (CHDO) = $76 M^{-1}$ and ³ $\tau \cdot k$ (*trans*-stilbene) = $61 M^{-1}$.

Introduction

The yields and behavior of solute excited states in radiolysis of benzene solutions has been a subject of considerable recent interest.² However, a lack of consensus is evident with regard to the precise mechanism of formation of solute excited states and the yields of precursors.³⁻¹¹ Of particular importance are values for the yields of the lowest triplet and excited singlet states of benzene in radiolysis of the liquid and a value for the intersystem crossing efficiency with which the lowest excited singlet state converts to the triplet state. A careful determination of such values by some unequivocal method is essential.

Schuster, Sckolnick, and Lee¹² have reported that photoexcitation of 3,5-cycloheptadienone (CHDO) in

(1) The Radiation Laboratory of the University of Notre Dame is operated under contract with the U. S. Atomic Energy Commission. This is AEC Document No. COO-38-719.

(2) Reference to all papers devoted to the subject would require an extensive bibliography; instead, reference is made throughout this paper to papers that are particularly relevant or illustrative.

(3) R. R. Hentz, D. B. Peterson, S. B. Srivastava, H. F. Barzynski, and M. Burton, *J. Phys. Chem.*, **70**, 2362 (1966).

(4) R. R. Hentz and H. G. Altmeiler, *ibid.*, **74**, 2646 (1970).

(5) R. A. Caldwell, D. G. Whitten, and G. S. Hammond, *J. Amer. Chem. Soc.*, **88**, 2659 (1966).

(6) G. S. Hammond, R. A. Caldwell, J. M. King, H. Kristinsson, and D. G. Whitten, *Photochem. Photobiol.*, **7**, 695 (1968).

various solvents gives only CO and hexatriene (HT) whereas triplet sensitization with acetone or benzophenone gives only bicyclo[3.2.0]hept-6-en-3-one (ISO). The authors conclude that excited singlets of CHDO give CO and HT but no triplets and that triplets of CHDO rearrange to form ISO. Such behavior is just that required for unequivocal determination with a single solute of the radiolytic yields of the lowest triplet and excited singlet states of benzene. Consequently, after a study of the photochemistry of CHDO with the determination of quantum yields, we have examined the radiolysis of benzene solutions of CHDO. For determination of the intersystem crossing efficiency of the lowest excited singlet of benzene, the photosensitized isomerization of *trans*-octene-2 was investigated. In addition, radiation-induced isomerization of *trans*-stilbene in benzene has been reexamined carefully for comparison with results of the CHDO and octene-2 studies.

Experimental Section

Procedures. The general procedure for preparation of degassed samples has been described.^{3,13} Solutions sensitive to light were prepared in dim light using Pyrex low actinic volumetric flasks which are opaque to wavelengths less than 5000 Å. Solutions containing CHDO were degassed immediately after preparation and were kept at 77°K except during irradiation and analysis. Solutions of *trans*-stilbene were prepared by measurement with a calibrated syringe of appropriate volumes of 0.500 *M trans*-stilbene in benzene into cells which then were attached to a vacuum line and the benzene was evaporated. The cells were sealed after addition of 5 ml of benzene (previously degassed to less than 10⁻⁶ Torr over the solid at 77°K) from a buret on the vacuum line. Care was taken at all times to minimize exposure of solutions to light by wrapping cells in aluminum foil and working in dim light. Concentrations calculated from weight of stilbene and volume of benzene were in excellent agreement with those determined by gas chromatographic analysis.

Cells used in the radiolysis, photolysis, and luminescence work have been described.⁴ Those used in the benzene sensitization experiments were equipped with magnetically driven stirrers. All photochemical experiments were performed with degassed 3-ml samples and with simultaneous ferrioxalate actinometry¹⁴ on a "merry-go-round" device; bar magnets were located around the outside in such a way as to produce 5 to 10 rotations of a cell stirrer per revolution. Several actinometry solutions were exposed for shorter periods at regular intervals during the period of exposure of a set of samples. The measured intensities, which never changed by more than 10% over the course of a sample photolysis, were averaged.

The lamp and filter systems used for photolysis at 3130 Å and 3660 Å have been described.⁴ A solution

of 100 g NiSO₄·6H₂O, 50 g CoSO₄·7H₂O, and 0.03 g 2,7-dimethyl-3,6-diazacyclohepta-1,6-diene perchlorate in 300 ml of water was used to isolate the 2537-Å line from a Hanovia 88A-45 low-pressure lamp. Absorption spectrophotometry and luminescence measurements have been described.⁴ In all measurements of the quenching of benzene fluorescence, the conditions used were such that there was negligible absorption of either the incident light or the measured fluorescent light by the quencher.

All γ irradiations were performed with degassed 5-ml samples at room temperature in a ⁶⁰Co source. Dose rates to the Fricke dosimeter solution, based on $G(\text{Fe}^{3+}) = 15.6$, were near 2.0×10^{18} eV ml⁻¹ min⁻¹ over the course of the work. Dose to a particular solution was calculated by correction for the decay of ⁶⁰Co and for the electron density relative to that of the dosimeter.

Analyses. Collection and measurement of gas products has been described.¹³ Gas products were analyzed with a Consolidated 21-103A mass spectrometer. A Beckman GC-5 gas chromatograph with dual flame-ionization detectors was used for analysis of all solutions. Peak areas were measured with a disk integrator (Disk Instruments, Inc.) when possible. At low solute concentrations, owing to base-line drift, it was necessary to measure peak areas with an Ott planimeter.

Determination of CHDO and ISO was accomplished by on-column injection using a 1/8 in. \times 6-ft column of 5% Ucon 1715 oil on 60-80 mesh Chromosorb G; the column was operated at 70° with a helium flow rate of 20 ml min⁻¹. With bromobenzene as internal standard, the following retention times were obtained: benzene, 1.1 min; bromobenzene, 8.5 min; ISO, 11.8 min; CHDO, 13.3 min. For hexatriene analysis, a 1/8 in. \times 10-ft column of 5% β,β' -oxydipropionitrile on 60-80 mesh Chromosorb G was operated at 25° with a helium flow rate of 20 ml min⁻¹. Retention times were: *trans*-octene-2 (internal standard), 3.8 min; *trans*-hexatriene, 6.1 min; *cis*-hexatriene, 7.1 min; benzene, 12.5 min. Benzene solutions of *cis*- and *trans*-stilbene were analyzed with hexadecane as internal standard on a 1/8 in. \times 12-ft column of 2% silicone gum rubber on 60-80 mesh Chromosorb G at 160°. Separation

(7) P. Skarstad, R. Ma, and S. Lipsky, *Mol. Cryst.*, **4**, 3 (1968).

(8) R. B. Cundall and W. Tippet, *Advances in Chemistry Series*, No. 82, American Chemical Society, Washington, D. C., 1968, p 387.

(9) E. Fischer, H. P. Lehmann, and G. Stein, *J. Chem. Phys.*, **45**, 3905 (1966).

(10) R. Cooper and J. K. Thomas, *ibid.*, **48**, 5097 (1968).

(11) E. J. Land and A. J. Swallow, *Trans. Faraday Soc.*, **64**, 1247 (1968).

(12) D. I. Schuster, B. R. Skolnick, and F. H. Lee, *J. Amer. Chem. Soc.*, **90**, 1300 (1968).

(13) R. R. Hentz and W. V. Sherman, *J. Phys. Chem.*, **72**, 2635 (1968).

(14) C. G. Hatchard and C. A. Parker, *Proc. Roy. Soc., Ser. A*, **235**, 518 (1956).

tion of the octene-2 isomers in benzene (with heptane as internal standard) was accomplished with two columns operated in series at 25° with a helium flow rate of 20 ml min⁻¹. The 1/8 in. × 6-ft columns were packed with 80–100 mesh Variport 30 which supported 20% β,β'-oxydipropionitrile in the first column and a 20% liquid phase of 33% AgNO₃ in diethylene glycol in the second.

Materials. All distillations were performed with a Nester–Faust spinning-band column. Purification procedures for benzene (Fisher Certified) and cyclohexane (Fisher Spectranalyzed) have been described.^{3,4} Acetone (Fisher Certified) was purified by distillation. Scintillation grade *trans*-stilbene of Matheson Coleman and Bell was recrystallized from cyclohexane four times. The only impurity detectable by gas chromatography was less than 0.01% *cis*-stilbene. Benzophenone of J. T. Baker Chemical Co. was zone refined; no impurities were detectable by gas chromatography. Vacuum distillation of 1,3,5-hexatriene (K and K Laboratories) gave a mixture of the *cis* and *trans* isomers, ~99 wt % pure, with a uv absorption spectrum identical with reported spectra.¹⁵ The *trans*-octene-2 (Aldrich Reagent Grade) contained less than 0.01% *cis* impurity and was used as received.

Tropone (1,3,5-cycloheptatrienone) was prepared from cycloheptatriene by the procedure of Radlick.¹⁶ The product was a pale yellow liquid boiling at 90° and 4 Torr; gas chromatography indicated a purity of ~90%. The tropone was reduced to CHDO with LiAlH₄, as described by Schuster, *et al.*¹² Distillation of the reaction mixture at 5 Torr gave a colorless liquid which boiled at 50° and was identified as CHDO by comparison of its infrared and uv spectra with published spectra.¹⁷ Gas chromatography showed a number of impurities amounting to ~8% of the CHDO. This impure CHDO was stored under vacuum in a sealed tube at 77°K.

Portions of the impure CHDO were purified, as needed for experiments, on a Wilkens Autoprep 700. A 3/8 in. × 12-ft column of 10% diglycerol on 45–60 mesh Chromosorb P was used with a helium flow rate of 1 l. min⁻¹; temperatures of column, injection port, and detector were 60°, 80°, and 100°, respectively. The uv absorption spectrum of the purified CHDO in cyclohexane is shown in Figure 1. The purified CHDO was stored on a vacuum line at 77°K.

Even in the absence of air, neat CHDO became pale yellow after about 1 hr at room temperature. Decomposition was slower in dilute solutions. Gas chromatographic analysis showed no change in a 0.1 M benzene solution after 3 hr; however, the solution turned yellow overnight. Partially decomposed CHDO was restored to its original purity, as shown by gas chromatographic analysis, by bulb-to-bulb distillation on the vacuum line. The dark yellow, waxy residue from such a distillation would not come off the chromatog-

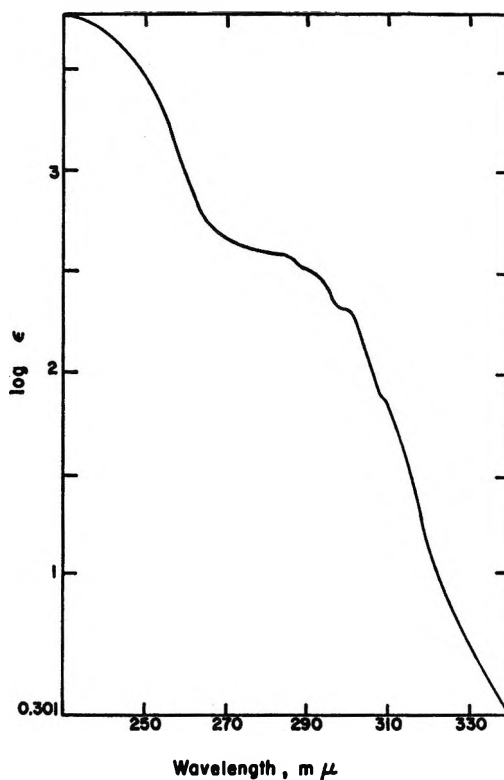


Figure 1. Absorption spectrum of 3,5-cycloheptadienone in cyclohexane; ϵ is the decadic extinction coefficient in units of $M^{-1} \text{ cm}^{-1}$.

raphy column even at 120°. Storage of CHDO at 77°K prevented decomposition.

Results

Photoexcitation of CHDO Solutions. In preliminary experiments, for confirmation of the results of Schuster *et al.*,¹² solutions were prepared from the "impure" CHDO and photolyses were carried to high conversions of CHDO to facilitate detection of minor products. Quantum yields measured in such experiments do not represent initial yields for pure CHDO at the specified concentration.

Two benzene solutions with 0.05 M "impure" CHDO and two with 0.10 M "impure" CHDO were photolyzed at 3130 Å to ~50% conversion of the CHDO. Average values of measured quantum yields¹⁸ with average deviations were $\Phi(\text{HT}) = 0.39 \pm 0.01$, $\Phi(\text{CO}) = 0.37 \pm 0.02$, and $\Phi(-\text{CHDO}) = 0.49 \pm 0.04$. No other products could be detected.

(15) G. F. Woods and L. H. Schwartzman, *J. Amer. Chem. Soc.*, **70**, 3394 (1948); J. C. H. Hwa, P. L. de Benneville, and H. J. Sims, *ibid.*, **82**, 2537 (1960).

(16) P. Radlick, *J. Org. Chem.*, **29**, 960 (1964).

(17) J. Meinwald, S. L. Emerman, N. C. Yang, and G. Büchi, *J. Amer. Chem. Soc.*, **77**, 4401 (1955); W. E. Parham, R. W. Soeder, J. R. Throckmorton, K. Kuncel, and R. M. Dodson, *ibid.*, **87**, 321 (1965); W. E. Parham, R. W. Soeder, and R. M. Dodson, *ibid.*, **84**, 1755 (1962).

(18) Measured and primary quantum yields are denoted by Φ and ϕ , respectively; in radiolyses, the symbol G denotes a yield in molecules per 100 eV absorbed by the system.

Seven acetone solutions of "impure" CHDO at concentrations in the range 5–50 mM were photolyzed at 3130 Å to conversions of 20–50%. $\Phi(\text{ISO}) = 0.141 \pm 0.004$ and $\Phi(-\text{CHDO}) = 0.19 \pm 0.01$ were obtained as averages of all measured values, which showed no dependence on concentration or conversion over the specified ranges. $\Phi(\text{HT})$ increased from 0.0006 to 0.014 as CHDO concentration increased from 5 mM to 50 mM. No other products could be detected. For each acetone solution, $\Phi(\text{HT})$ was smaller than the value calculated solely from $\phi(\text{HT}) \approx 0.4$ and the fraction of absorbed quanta that are absorbed by CHDO. For example, with $\epsilon(\text{CHDO}) = 56 \text{ M}^{-1} \text{ cm}^{-1}$ and $\epsilon(\text{acetone}) = 1.85 \text{ M}^{-1} \text{ cm}^{-1}$ at 3130 Å, CHDO absorbs 10% of all quanta absorbed by a 50 mM solution and, therefrom, $\Phi(\text{HT}) = 0.04$ is calculated as compared with the measured $\Phi(\text{HT}) = 0.014$. Apparently, acetone quenches excited singlets of CHDO.

In agreement with the work of Schuster, *et al.*,¹² results obtained in the preliminary experiments with benzene and acetone solutions of "impure" CHDO show that excited singlets of CHDO yield CO and HT but no ISO whereas triplets excited by acetone sensitization yield ISO but no CO or HT. The purified CHDO was used in all subsequent experiments.

Cyclohexane solutions of CHDO and 0.1 M benzophenone were photolyzed with 3660-Å light, which is absorbed only by the benzophenone ($\epsilon 80 \text{ M}^{-1} \text{ cm}^{-1}$). The only detectable product was ISO; results are presented in Table I. The results for 19 mM and 38 mM solutions indicate attainment of a limiting yield of $\Phi(\text{ISO}) = 0.159 \pm 0.002$.

Table I: Benzophenone^a-Sensitized Isomerization of CHDO in Cyclohexane at 3660 Å

[CHDO], mM	$\Phi(\text{ISO})$	% conv ^b	[CHDO], mM	$\Phi(\text{ISO})$	% conv ^b
4.62	0.119	14	19.0	0.159	17
4.62	0.113	33	38.0	0.157	8
6.6	0.128	17	38.0	0.157	7
6.6	0.127	34	38.0	0.157	20
9.4	0.142	16	38.0	0.163	23
19.0	0.163	11			

^a 0.1 M. ^b Measured per cent conversion of CHDO.

Benzene solutions of CHDO were photolyzed at 2537 Å. The results are presented in Figure 2 in the form of a plot of $\Phi(\text{HT})^{-1}$ vs. $[\text{CHDO}]^{-1}$. Yields of ISO were too small for accurate measurement. Only 4% of the absorbed light was absorbed by CHDO at the highest concentration used (41.5 mM). The solutions were stirred during photolysis to prevent a disproportionate decrease in CHDO concentration in the small volume within which essentially all light absorption occurred. A *ca.* fourfold change in intensity,

accomplished with neutral density filters, had no effect on values of $\Phi(\text{HT})$. For CHDO concentrations greater than 10 mM, CHDO conversions (calculated from the concentration of HT produced) were in the range 0.3–1.6%; for concentrations less than 10 mM, conversions were in the range 2–12%. Within such ranges, no effect of per cent conversion on $\Phi(\text{HT})$ was detectable.

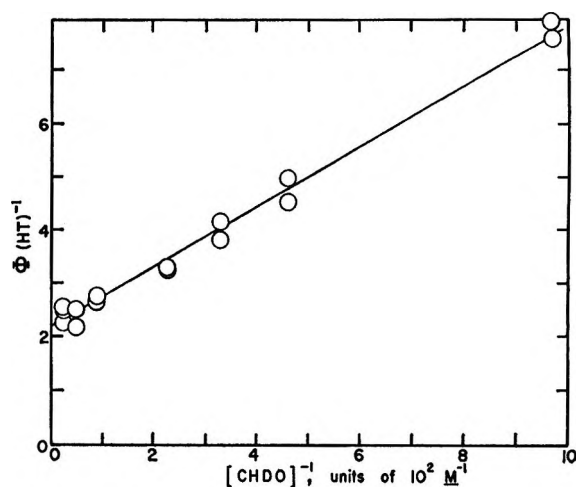


Figure 2. Concentration dependence of the hexatriene quantum yield in 2537-Å photolysis of benzene solutions of CHDO.

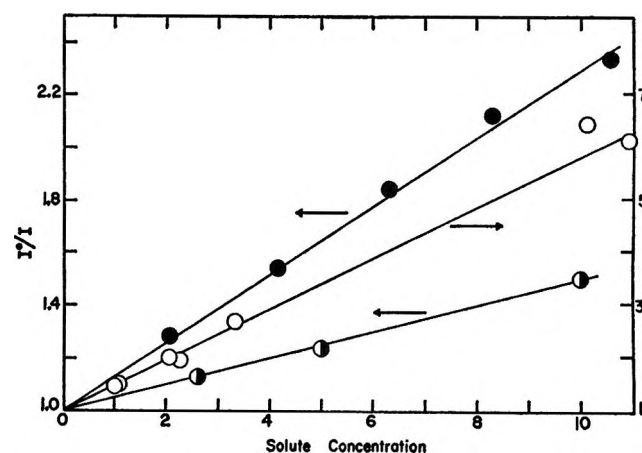


Figure 3. Stern-Volmer plots for quenching of benzene fluorescence, I , by solutes: O, [CHDO] in units of 10^{-3} M ; ●, [trans-stilbene] in units of 10^{-4} M ; ◐, [trans-octene-2] in units of 0.02 M.

accomplished with neutral density filters, had no effect on values of $\Phi(\text{HT})$. For CHDO concentrations greater than 10 mM, CHDO conversions (calculated from the concentration of HT produced) were in the range 0.3–1.6%; for concentrations less than 10 mM, conversions were in the range 2–12%. Within such ranges, no effect of per cent conversion on $\Phi(\text{HT})$ was detectable.

Benzene solutions of CHDO were excited at 2537 Å and benzene fluorescence was measured at 3100 Å. Figure 3 shows a Stern-Volmer plot for the quenching of benzene fluorescence, I , by CHDO. Slope of such a plot gives the product of specific rate of quenching, 1k , and lifetime, ${}^1\tau$, for the lowest excited singlet of benzene. A value of ${}^1k{}^1\tau = 4.8 \times 10^2 \text{ M}^{-1}$ is obtained from Figure 3.

Photoexcitation of Stilbene Solutions. Benzene solutions of trans-stilbene were excited at 2537 Å and benzene fluorescence was measured at 2900 Å (at which

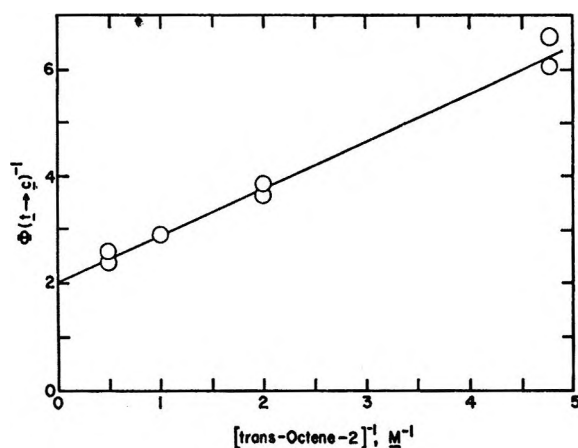


Figure 4. Concentration dependence of the quantum yield in acetone-sensitized isomerization of *trans*-octene-2 at 3130 Å.

trans-stilbene does not fluoresce). The results are presented in Figure 3 as a Stern-Volmer plot the slope of which gives ${}^1k^1\tau = 1.29 \times 10^3 M^{-1}$ for quenching of benzene fluorescence by *trans*-stilbene.

Six stirred samples of 0.054 *M* *trans*-stilbene in benzene were photolyzed at 2537 Å to about 1% conversion of the *trans*-stilbene. Stilbene absorbed about 8% of the light that was absorbed by the solution. An average value of $\Phi(t \rightarrow c) = 0.46 \pm 0.03$ was obtained. Such a value (note that 0.054 *M* *trans*-stilbene quenches ~99% of the excited singlets of benzene) should correspond to the primary isomerization yield for singlet excitation of *trans*-stilbene.

Photoexcitation of Octene Solutions. Photosensitized isomerization of *trans*-octene-2 was studied in acetone at 3130 Å and in benzene at 2537 Å. Light was absorbed only by the solvents, and conversions of *trans* to *cis* never exceeded 1%. Results for acetone solutions are presented in Figure 4 in the form of a plot of $\Phi(t \rightarrow c)^{-1}$ vs. $[trans\text{-octene-2}]^{-1}$; a limiting yield of $\Phi(t \rightarrow c) = 0.48$ is obtained from the intercept. Results for benzene solutions are presented in Table II.

Table II: Benzene-Sensitized Isomerization of *trans*-Octene-2 at 2537 Å

[Octene], mM	$\Phi(t \rightarrow c)$	[Octene], mM	$\Phi(t \rightarrow c)$
5.9	0.023	52.1	0.110
5.9	0.026	52.1	0.128
8.9	0.037	99	0.154
8.9	0.039	99	0.144
23.2	0.080	200	0.147
23.2	0.078		

Benzene solutions of *trans*-octene-2 were excited at 2537 Å and benzene fluorescence was measured at 3000 Å. The results are presented in Figure 3 as a

Stern-Volmer plot the slope of which gives ${}^1k^1\tau = 2.5 M^{-1}$ for quenching of benzene fluorescence by *trans*-octene-2.

Radiolysis of Benzene Solutions of CHDO. Results obtained in γ radiolysis of benzene solutions of CHDO are shown in Table III. Only CHDO at the initial

Table III: Radiolysis of Benzene Solutions of CHDO

[CHDO], mM	<i>G</i> (ISO)	<i>G</i> (HT)	<i>G</i>
1.11	0.059	0.175	1.14
1.35	0.061	0.214	1.23
2.04	0.104	0.276	1.27
2.25	0.108	0.297	1.30
3.34	0.132	0.344	1.27
5.00	0.215	0.457	1.47
7.08	0.254	0.500	1.47
10.1	0.267	0.500	1.37
10.9	0.305	0.522	1.41
20.1	0.389	0.580	1.45
50.8	0.464	0.650	1.54

concentration was found in unirradiated controls. In units of 10^{13} eV ml⁻¹, doses used were 1.10, 2.05, and 3.22. Values of *G*(ISO) were independent of dose at all concentrations and, therefore, the average values given in Table III represent initial yields. For 20.1 mM and 50.8 mM CHDO, values of *G*(HT) also were independent of dose and the average values are given in Table III.

However, at CHDO concentrations less than 20.1 mM a significant decrease in *G*(HT) was observed with increase in dose. For example, at 7.08 mM CHDO, *G*(HT) obtained at the highest dose was 14% lower than that obtained at the lowest dose. Therefore, for the best possible approximation to initial yields, values of *G*(HT) given in Table III are those for the lowest dose at concentrations less than 20.1 mM.

Radiolysis of Benzene Solutions of Stilbene. Results obtained in γ radiolysis of benzene solutions of *trans*-stilbene are shown in Table IV. No *cis*-stilbene was

Table IV: Radiation-Induced Isomerization of *trans*-Stilbene, S_t, in Benzene

[S _t], mM	<i>G</i> (t → c)	[S _t], mM	<i>G</i> (t → c)
2.00	0.77	20.0	1.95
5.00	1.16	50.0	2.39
10.0	1.61	100	2.70

detectable in unirradiated controls. In units of 10^{19} eV ml⁻¹, doses used were 0.63, 1.26, and 1.89. Yields were independent of dose and, therefore, the average values given in Table IV represent initial yields.

Discussion

Photochemistry of CHDO. The work of Schuster, *et al.*,¹² provides strong evidence for their conclusion that singlet excitation of CHDO yields HT and CO and no intersystem crossing to the triplet state whereas triplet excitation of CHDO yields ISO. Our results support that conclusion and give primary quantum yields for the products.

With information presently available, an accurate assignment of the energy of the lowest excited singlet of CHDO is not possible; however, a reasonable estimate is obtainable from the uv absorption spectrum in Figure 1. Schuster, *et al.*,¹² observed a shoulder at 352.5 m μ (ϵ 5.90 M^{-1} cm $^{-1}$) and a maximum at 372.5 m μ (ϵ 4.75 M^{-1} cm $^{-1}$) in the spectrum of their CHDO and associated such absorptions with the $n \rightarrow \pi^*$ transition of the carbonyl group. The absorption spectrum of "impure" CHDO prepared by the same technique for use in the present work also had a shoulder at 352 m μ (ϵ 3 M^{-1} cm $^{-1}$) and a peak at 372 m μ (ϵ 2 M^{-1} cm $^{-1}$). However, with ethanol as solvent the absorptions at 352 m μ and 372 m μ did not undergo the blue shift characteristic of $n \rightarrow \pi^*$ transitions while the broad peak at 280 m μ (*cf.* Figure 1) was obscured by the tail of the $\pi \rightarrow \pi^*$ transition (λ_{\max} 220 m μ). Furthermore, purification of the CHDO by gas chromatography eliminated the absorptions at 352 m μ and 372 m μ . Consequently, an impurity in CHDO must be responsible for such absorptions. The uv spectrum of purified CHDO in Figure 1 suggests that the broad absorption peak at 280 m μ corresponds to the $n \rightarrow \pi^*$ transition which, therefore, has an energy close to that for the same transition in acetone—namely, ~ 86 kcal mol $^{-1}$ above the ground state.¹⁹ The quenching of excited singlets of CHDO by acetone (noted in the acetone sensitization experiments) also suggests that the excitation energy of CHDO is close to and perhaps somewhat above that of acetone.

With a singlet excitation energy of ~ 86 kcal mol $^{-1}$ for CHDO, transfer of singlet excitation from benzophenone (singlet excitation energy²⁰ = 74 kcal mol $^{-1}$) cannot be important in the study of benzophenone-sensitized isomerization of CHDO. Therefore, the formation of ISO in such experiments (*cf.* Table I) is plausibly attributed to transfer of triplet excitation from benzophenone to CHDO. Thus (as noted by Schuster, *et al.*)¹² the 69 kcal mol $^{-1}$ triplet energy of benzophenone²⁰ is an upper limit for the triplet energy of CHDO. Because the intersystem crossing efficiency is unity in benzophenone,²¹ the limiting yield of $\Phi(\text{ISO}) = 0.16$ corresponds to a primary yield of ${}^3\phi(\text{ISO}) = 0.16$ from the triplet state of CHDO.

Results shown in Figure 2 for the benzene-sensitized decomposition of CHDO provide a value for the primary quantum yield of HT, ${}^1\phi(\text{HT})$, from the excited singlet state of CHDO. Furthermore, the conditions of such experiments correspond to those for determination

of the radiolytic yield of lowest excited singlets of benzene. Results of the benzene-sensitization experiments should conform to eq I. Thus, from the slope

$$\Phi(\text{HT})^{-1} = {}^1\phi(\text{HT})^{-1}\{1 + ({}^1k^1\tau[\text{CHDO}])^{-1}\} \quad (\text{I})$$

and intercept of the line in Figure 2, ${}^1\phi(\text{HT}) = 0.44$ and ${}^1k^1\tau = 4.0 \times 10^2 M^{-1}$ are obtained.

The value of ${}^1k^1\tau = 4.0 \times 10^2 M^{-1}$ should correspond to ${}^1k^1\tau = 4.8 \times 10^2 M^{-1}$ obtained from the quenching of benzene fluorescence by CHDO (*cf.* Figure 3). Such values are in reasonably good agreement considering the accuracy with which $\Phi(\text{HT})$ can be measured at the lower concentrations of CHDO. For example, for each concentration of CHDO in Figure 2, a value of ${}^1\phi(\text{HT})$ can be calculated from eq I with ${}^1k^1\tau = 4.8 \times 10^2 M^{-1}$ and the measured $\Phi(\text{HT})$. After rejection of the result for the lowest concentration in Figure 2, the average of all such values with the average deviation is ${}^1\phi(\text{HT}) = 0.43 \pm 0.01$. Thus, results of the quenching experiments are consistent with the photochemical data. Use of ${}^1\tau = 27$ nsec^{22a} in ${}^1k^1\tau = 4.8 \times 10^2 M^{-1}$ gives ${}^1k = 1.8 \times 10^{10} M^{-1} \text{ sec}^{-1}$ as the phenomenological specific rate of excitation transfer from the quasiequilibrium mixture of monomer and excimer excited singlet states of benzene.^{22b}

The negligible yields of ISO obtained in benzene-sensitization experiments are attributable to ${}^1k^1\tau$ being about sixfold greater than ${}^3k^3\tau$ (evaluated subsequently) for transfer of triplet excitation from benzene to CHDO. Thus, at CHDO concentrations at which the efficiency of triplet transfer becomes appreciable, production of benzene triplets is inefficient owing to quenching of the excited-singlet precursors.

Intersystem Crossing Efficiency of Benzene. The intersystem crossing efficiency, χ , of the lowest excited singlet of benzene is determined from results for the photosensitized isomerization of *trans*-octene-2 in acetone and benzene. Because the intersystem crossing efficiency is unity in acetone,¹⁹ the acetone-sensitized limiting yield of $\Phi(t \rightarrow c) = 0.48$ (obtained from the intercept in Figure 4) corresponds to a primary yield of ${}^3\phi(t \rightarrow c) = 0.48$ for triplet excitation of *trans*-octene-2. Such a value agrees well with that of ${}^3\phi(t \rightarrow c) = 0.50$ determined by Golub, *et al.*,²³ from a photostationary isomer ratio of unity obtained by photosensitization in liquid benzene.

(19) R. F. Borkman and D. R. Kearns, *J. Chem. Phys.*, **44**, 945 (1966).

(20) J. G. Calvert and J. N. Pitts, Jr., "Photochemistry," Wiley, New York, N. Y., 1966, p 297.

(21) A. A. Lamola and G. S. Hammond, *J. Chem. Phys.*, **43**, 2129 (1965).

(22) P. K. Ludwig and C. D. Amata, *ibid.*, **49**, 326, 333 (1968).

(23) M. A. Golub, C. L. Stephens, and J. L. Brash, *ibid.*, **45**, 1503 (1966).

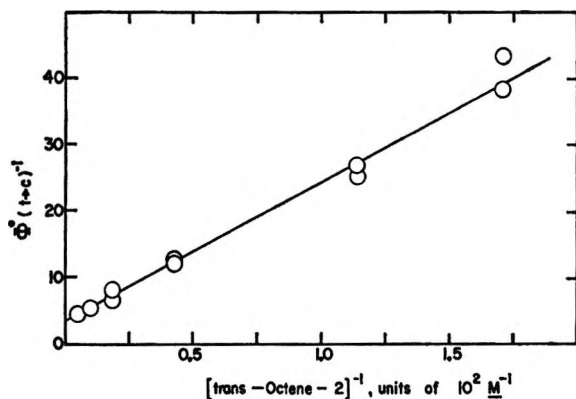


Figure 5. Concentration dependence of the "corrected" quantum yield (cf. eq III) in benzene-sensitized isomerization of *trans*-octene-2 at 2537 Å.

Though olefins do quench excited singlets of aromatics, Hammond and coworkers²⁴ have shown that no isomerization of the olefin occurs as a consequence of such quenching. Therefore, results for the benzene-sensitized isomerization should conform to eq II, in which $[O_t]$ denotes concentration of *trans*-octene-2

$$\Phi(t \rightarrow c) = {}^3\phi(t \rightarrow c)\{{}^3k^3\tau[O_t]/(1 + {}^3k^3\tau[O_t])\}\{\chi/(1 + {}^1k^1\tau[O_t])\} \quad (\text{II})$$

and ${}^3k^3\tau$ is the product of specific rate of excitation transfer (in this case to *trans*-octene-2) and lifetime for the triplet state of benzene. The quantity $(1 + {}^1k^1\tau[O_t])$ corresponds to I°/I in Figure 3 for octene quenching of benzene fluorescence. With the appropriate substitutions eq III is obtained.

$$\Phi^{\circ}(t \rightarrow c) \equiv \Phi(t \rightarrow c)I^{\circ}/I = 0.48\chi{}^3k^3\tau[O_t]/(1 + {}^3k^3\tau[O_t]) \quad (\text{III})$$

For each concentration of *trans*-octene-2 in Table II, a value of $\Phi^{\circ}(t \rightarrow c)$ can be calculated by multiplication of $\Phi(t \rightarrow c)$ and I°/I (ordinate of the line for octene quenching in Figure 3) for that concentration. A plot of the reciprocal of $\Phi^{\circ}(t \rightarrow c)$ vs. $[O_t]^{-1}$ is presented in Figure 5. From the slope and intercept of that plot, in accordance with eq III, ${}^3k^3\tau = 18 M^{-1}$ and $\chi = 0.58$ are obtained.

Radiolysis of Benzene Solutions of CHDO. In radiolysis of benzene solutions, solute concentrations below 0.1 *M* have little effect on those processes that in neat benzene determine the ultimate yields of (1) lowest excited singlets and (2) lowest triplets that do not have the lowest excited singlet as a precursor.⁴ Consequently, such yields can be related to measured yields of products from particular excited states of solutes at concentrations below 0.1 *M*. Thus, eq IV gives

$$G(\text{HT}) = {}^1G^1\phi(\text{HT}){}^1k^1\tau[\text{CHDO}]/(1 + {}^1k^1\tau[\text{CHDO}]) \quad (\text{IV})$$

the relationship between yield of the lowest excited singlet of benzene, 1G , and $G(\text{HT})$ from radiolysis of benzene solutions of CHDO (cf. Table III). With ${}^1k^1\tau = 4.8 \times 10^2 M^{-1}$ (from quenching of benzene fluorescence by CHDO) and ${}^1\phi(\text{HT}) = 0.44$, values of 1G shown in Table III are calculated from eq IV for each concentration of CHDO. For $[\text{CHDO}] \geq 5 \text{ mM}$, such values are in good agreement and give an average value with average deviation of ${}^1G = 1.45 \pm 0.04$. The lower values of 1G for $[\text{CHDO}] < 5 \text{ mM}$ are attributed to $G(\text{HT})$ being a poor approximation to the initial yield owing to the appreciable dose effect at such low concentrations.

Results in Table III for $G(\text{ISO})$ in radiolysis of benzene solutions of CHDO should conform to eq V, in

$$G(\text{ISO}) = {}^3\phi(\text{ISO})\{{}^3k^3\tau[\text{CHDO}]/(1 + {}^3k^3\tau[\text{CHDO}])\}\{{}^3G + {}^1G\chi/(1 + {}^1k^1\tau[\text{CHDO}])\} \quad (\text{V})$$

which 3G denotes the yield of lowest triplets of benzene which do not have the lowest excited singlet as a precursor. The second term in the second set of brackets represents the contribution of lowest excited singlets to the benzene triplet yield. That contribution should be small at all concentrations used for the same reason that very little ISO was formed in 2537-Å photolysis of benzene solutions of CHDO. As a first approximation, the excited-singlet contribution in eq V can be ignored and, thereby, ${}^3k^3\tau = 80 M^{-1}$ is obtained from the slope and intercept of a plot of $G(\text{ISO})^{-1}$ vs. $[\text{CHDO}]^{-1}$. With ${}^3k^3\tau = 80 M^{-1}$, ${}^3\phi(\text{ISO}) = 0.16$, ${}^1G = 1.45$, $\chi = 0.58$, and ${}^1k^1\tau = 4.8 \times 10^2 M^{-1}$ in eq V, the contribution of lowest excited singlets to $G(\text{ISO})$ can be calculated for each concentration of CHDO. Values obtained for that contribution, denoted by ${}^1G(\text{ISO})$, are indeed small (varying from 0.007 at 1.11 mM, through a maximum of 0.010 in the range 3.3–10.9 mM, to 0.005 at 50.8 mM). Subtraction of such values for ${}^1G(\text{ISO})$ from $G(\text{ISO})$ gives, as indicated in eq VI, the contribution of 3G . A plot of the reciprocal of

$${}^3G(\text{ISO}) \equiv G(\text{ISO}) - {}^1G(\text{ISO}) = 0.16{}^3G{}^3k^3\tau[\text{CHDO}]/(1 + {}^3k^3\tau[\text{CHDO}]) \quad (\text{VI})$$

${}^3G(\text{ISO})$ vs. $[\text{CHDO}]^{-1}$ is presented in Figure 6. From the slope and intercept of that plot, in accordance with eq VI, ${}^3k^3\tau = 76 M^{-1}$ and ${}^3G = 4.0$ are obtained.

Radiolysis of Benzene Solutions of Stilbene. In radiolysis of benzene solutions of *trans*-stilbene at concentrations less than $\sim 0.1 M$, there are three distinct paths through which isomerization of the solute is accomplished. One path involves triplet transfer to stilbene from benzene triplets which do not have the lowest excited singlet as a precursor; the contribution

(24) L. M. Stephenson, D. G. Whitten, and G. S. Hammond, "Chemistry of Ionization and Excitation," G. R. A. Johnson and G. Scholes, Ed., Taylor and Francis, London, 1967, p 35; S. Murov and G. S. Hammond, *J. Phys. Chem.*, **72**, 3797 (1968).

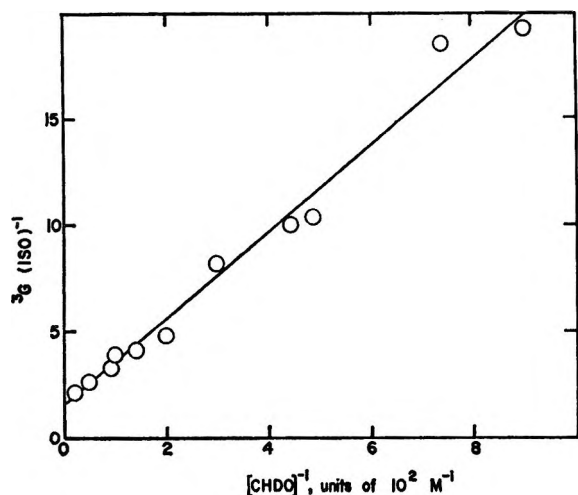


Figure 6. Plot of the reciprocal of ${}^3G(\text{ISO})$, defined in eq VI, vs. $[\text{CHDO}]^{-1}$.

to $G(t \rightarrow c)$ via this path is denoted by G_1 and is given by eq VII, in which $[S_t]$ denotes concentration of *trans*-stilbene and ${}^3\phi(t \rightarrow c)$ denotes the primary isomerization yield for triplet excitation of *trans*-stilbene.

$$G_1 = {}^3\phi(t \rightarrow c) {}^3G {}^3k {}^3\tau [S_t] / (1 + {}^3k {}^3\tau [S_t]) \quad (\text{VII})$$

A second path also involves triplet transfer to stilbene but from benzene triplets which are formed by intersystem crossing from the lowest excited singlet of benzene; the contribution to $G(t \rightarrow c)$ via this path is denoted by G_2 and is given by eq VIII. The third path involves transfer of singlet excitation to stilbene

$$G_2 = {}^3\phi(t \rightarrow c) {}^1G \left\{ {}^3k {}^3\tau [S_t] / (1 + {}^3k {}^3\tau [S_t]) \right\} \times \left\{ \chi / (1 + {}^1k {}^1\tau [S_t]) \right\} \quad (\text{VIII})$$

from the lowest excited singlets of benzene; the contribution to $G(t \rightarrow c)$ via this path is denoted by G_3 and is given by eq IX, in which ${}^1\phi(t \rightarrow c)$ denotes the pri-

$$G_3 = {}^1\phi(t \rightarrow c) {}^1G {}^1k {}^1\tau [S_t] / (1 + {}^1k {}^1\tau [S_t]) \quad (\text{IX})$$

mary isomerization yield for singlet excitation of *trans*-stilbene.

For *trans*-stilbene as acceptor, ${}^1k {}^1\tau = 1.29 \times 10^3 M^{-1}$. Consequently, G_2 is expected to be small compared to G_1 at all solute concentrations in Table IV. For each concentration in Table IV, a value of G_3 can be calculated from eq IX with ${}^1G = 1.45$ and ${}^1\phi(t \rightarrow c) = 0.48$. The latter value is the average of our ${}^1\phi(t \rightarrow c) = 0.46 \pm 0.03$ (from 2537-Å excitation of 0.054 *M* benzene solutions) and ${}^1\phi(t \rightarrow c) = 0.50$ of Malkin and Fischer²⁵ (obtained by 3130-Å excitation of *trans*-stilbene in an alkane solvent). By neglect of G_2 and subtraction of calculated values of G_3 from values of $G(t \rightarrow c)$ in Table IV, values of G_1 are obtained for each concentration of *trans*-stilbene. For such values, a plot of G_1^{-1} vs. $[S_t]^{-1}$ is presented in Figure 7. From the slope and intercept of that plot, in accordance with eq VII, ${}^3k {}^3\tau = 61 M^{-1}$ and ${}^3\phi(t \rightarrow c) {}^3G = 2.3$ are ob-

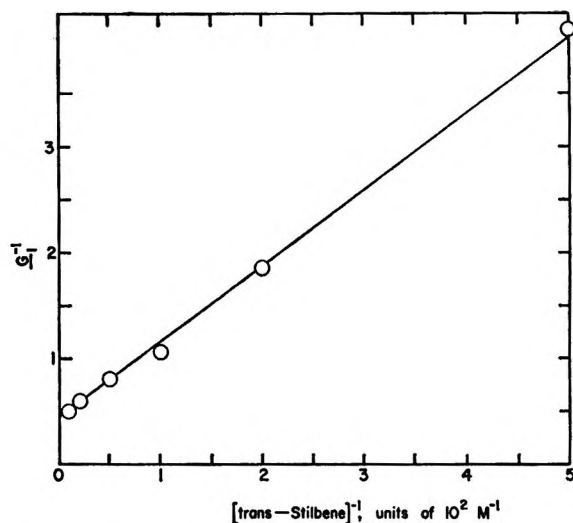


Figure 7. Plot of G_1^{-1} (cf. eq VII) vs. $[\text{trans-stilbene}]^{-1}$.

tained. Use of ${}^3\phi(t \rightarrow c) = 0.55^{26}$ gives ${}^3G = 4.2$. For such values, G_2 is indeed small compared to G_1 at all concentrations of *trans*-stilbene in Table IV, the largest value of G_2/G_1 being 0.06 at 2 *mM* *trans*-stilbene.

Comparisons and Conclusions. Cundall and Tippett²⁷ have reported a value of $\chi = 0.57$ for liquid benzene. Such a value agrees well with $\chi = 0.58$ obtained in the present work. Cundall and Tippett²⁷ report a total fluorescence quantum yield of 0.02 and conclude, therefore, that the quantum yield of internal conversion is 0.41.

Our value of ${}^1G = 1.45$ is in good agreement with ${}^1G = 1.55$ obtained by Lipsky and coworkers⁷ in a study of *p*-terphenyl luminescence from ${}^{14}\text{C}$ β -particle irradiation of benzene solutions. Hammond and coworkers⁶ have obtained a much larger value of ${}^1G = 3.4$ from γ -induced decomposition of tetramethyloxetane in benzene containing 0.4 *M* biphenyl. Such a result may be attributable to the presence of additional and alternative paths for solute excitation at the relatively large biphenyl concentration (cf. ref 4).

The values of ${}^3G = 4.0$ obtained with CHDO and ${}^3G = 4.2$ obtained with *trans*-stilbene agree well with each other and with ${}^3G = 4.1$ from study of the radiation-induced isomerization of *trans*-1,2-diphenylpropene in benzene.⁴ As shown in the diphenylpropene paper,⁴ it is possible to interpret much of the published work on radiation-induced isomerizations in benzene in terms of ${}^3G = 4.1$, ${}^1G = 1.5$, and $\chi = 0.60$. Assuming a diffusion-controlled ${}^3k \approx 10^{10} M^{-1} \text{sec}^{-1}$ for triplet transfer from benzene to CHDO and *trans*-stilbene, ${}^3\tau \approx 7$ nsec is estimated for the benzene triplet lifetime from ${}^3k {}^3\tau = 61 M^{-1}$ and ${}^3k {}^3\tau = 76 M^{-1}$ for *trans*-stilbene and CHDO, respectively, as triplet acceptors.

(25) S. Malkin and E. Fischer, *J. Phys. Chem.*, **68**, 1153 (1964).

(26) H. A. Hammond, D. E. DeMeyer, and J. L. R. Williams, *J. Amer. Chem. Soc.*, **91**, 5180 (1969).

(27) R. B. Cundall and W. Tippett, *Trans. Faraday Soc.*, **66**, 350 (1970).

The Yield of Radiation-Induced Ionization in Condensed Organic Systems

by Tadamasu Shida

The Institute of Physical and Chemical Research, Yamatomachi, Kibaadachi-gun, Saitama Prefecture, Japan
(Received March 26, 1970)

The yield of ionization in γ -irradiated amorphous organic solids at 77°K was determined using alkyl disulfides as charge scavengers. The disulfide anion produced on scavenging electrons was measured by optical absorption spectroscopy for a number of solutions in various solvents, covering the complete range of concentration from pure solvent to pure disulfide. The yield of the anion showed a linear dependence on the electron fraction of disulfide in the solution. Based on the known oscillator strength of the Wurster's ion and the yield of scavengeable electrons in irradiated methyltetrahydrofuran the G values of ionization in pure amyl disulfide as well as in pure solvents were determined to be ~ 1 to ~ 3 . It is proposed that the observed yields may correspond to the total ionization in the amorphous solids and that the W value may not have relevance to the ionization in solids.

Introduction

Considerable interest in radiation chemistry is currently being focused on quantitative measurement of ionization in liquids and solids. Since the W value, the average energy required to form an ion pair, is established only for gases and vapors, application of any such value to condensed matter must be justified. Although most investigators avoid indicating the yield of total ionization for condensed matter, some have presented substantial data. For example, Jha and Freeman have deduced a G value of total ionization (the reciprocal of W referred to the energy of 100 eV absorbed) of 4.6 for liquid methanol by measuring $G(N_2)$ of N_2O solutions in methanol.¹ Warman, *et al.*, suggested 3.9 for liquid cyclohexane on the basis of an empirical kinetic analysis.² These results indicate comparatively little difference in the energy required to produce an ion pair in the gas and liquid phases. Buchanan and Williams, on the other hand, have estimated a total yield of 2.6 ion pairs per 100 eV for liquid cyclohexane from the $G(HD)$ of C_2H_5OD in $c-C_6H_{12}$. They, however, concluded that a substantial fraction of ion pairs escape scavenging under any experimental conditions.³

For frozen amorphous solids, ionization can be manifested by charge scavengers which produce optically measurable ion radicals. Compared with liquid systems, less complication arises in correlating the ionization of the matrix with the observed yield of ions of scavengers. However, since the solubility of additives in the low-temperature solid solution is usually limited, uncertainty remains whether the additive has scavenged all the electrons including those which recombine geminately. If a scavenger is capable of forming a transparent glass in the pure state at 77°K, it can form glasses of any concentration when mixed with a compatible glass-forming solvent, thereby solving the problem of solubility. *n*-Amyl disulfide meets the requirement; it scavenges electrons efficiently and the anion produced absorbs strongly in a convenient part

of the spectral region ($\lambda_{max} \cong 420$ nm).^{4,5} It has a high miscibility with a number of organic liquids and forms a clear glass at 77°K in the pure state and in the admixture. Besides, the irradiated disulfide exhibits the absorption bands of not only the anion but also the cation-radical ($\lambda_{max} \cong 780$ nm).⁵ The simultaneous appearance of both bands provides information on the fate of both electron and positive hole.

In this work the yields of disulfide ions were measured for a number of solutions covering the complete range of concentration. The behavior of the disulfide anion and cation in irradiated pure disulfide indicates either that geminate recombination in this system is negligible or that the recombination cannot be revealed by the scavenger technique. The yield of the disulfide anion in the solution exhibited a linear dependence on the electron fraction of disulfide in the binary mixture. By extrapolation the ionization yields in the pure solvents were determined as $G = \sim 1-3$. They are significantly smaller than $G = \sim 4$ which is expected on the basis of W values. It is shown that such low G values of ionization are generally observed for amorphous solids, and the implication of the yields is discussed.

Experimental Section

Di-*n*-amyl and di-*t*-butyl disulfides both from K and K Laboratories, Inc., were purified by distillation under reduced pressure. The disulfides were mixed with a number of organic solvents which were appropriately purified. The solvents which were chosen are chemically inert toward electrons and form glassy

(1) K. N. Jha and G. R. Freeman, *J. Chem. Phys.*, **48**, 5480 (1968).

(2) J. M. Warman, K. D. Asmus, and R. H. Schuler, *J. Phys. Chem.*, **73**, 931 (1969).

(3) J. W. Buchanan and F. Williams, *J. Chem. Phys.*, **44**, 4377 (1966).

(4) J. Wendenburg, H. Mockel, A. Granzow, and A. Henglein, *Z. Naturforsch. A*, **21**, 632 (1966).

(5) T. Shida, *J. Phys. Chem.*, **72**, 2597 (1968).

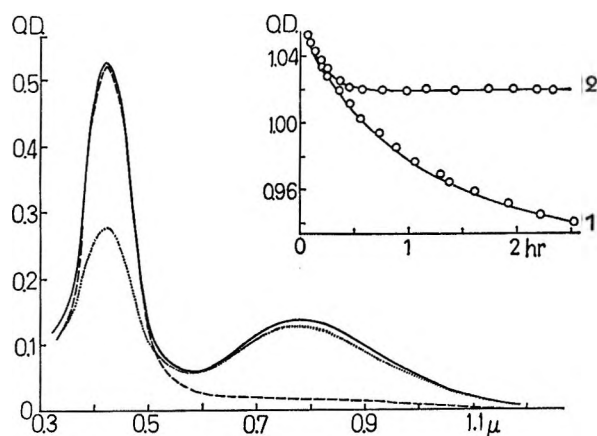


Figure 1. Absorption spectra of λ -irradiated *n*-amyl disulfide at 77°K with and without charge scavengers: solid curve, pure deaerated disulfide; the bands at 420 and 780 nm are due to the disulfide anion and cation, respectively;⁵ dotted curve, disulfide containing 17 wt % of CCl_4 ; broken curve, disulfide containing 30 wt % of triethylamine; dose; 6.90×10^{18} eV/g for all the samples. Inset: thermal decay curves for the disulfide anion in γ -irradiated deaerated *n*-amyl disulfide at low temperatures; curve 1, irradiated at 77°K to the dose of 1.38×10^{19} CV/g and kept at the same temperature; curve 2, similar to 1 but the ambient temperature was lowered from 77°K to 63°K at about 15 min.

solids at 77°K. The concentration of disulfide was varied as widely as possible within the glass-forming range. Since *n*-amyl disulfide in the pure state is glassy at 77°K, its solutions with a glass-forming solvent covered the whole range of composition. Although pure *t*-butyl disulfide polycrystallized, solutions containing this disulfide also formed glasses over a wide concentration range (up to ca. 60 wt % of disulfide).

The absorption spectrum of the glassy solid was measured at 77°K in a thin silica cell (1.50 mm thick) before and after γ irradiation. The irradiation was carried out using a 12,000-Ci ^{60}Co source at the dose rate of $\sim 2 \times 10^{18}$ eV/g min for about 3 min. Dissolved oxygen did not cause an appreciable effect on the results except for dilute solutions of disulfide concentration less than ~ 10 mM. Spectra such as shown in Figure 1 were obtained by reading the difference of absorptions before and after irradiation. Care was exercised to reproduce the cell positioning between the two measurements. A Cary 14 RI spectrophotometer was set so as to allow us to measure the absorption of irradiated samples within less than 4 min. The yield of products was linearly dependent on the radiation dose up to the level of about 10^{19} eV/g. Absorptions in disulfide-rich solutions showed a slow isothermal decay even at 77°K in the dark. For such samples a few irradiations and optical measurements were made at about 63°K with liquid nitrogen at reduced pressure. In the calculation of G values, the density of samples at 77°K was necessary because the absorbed energy was assumed to be proportional to the weight of sample

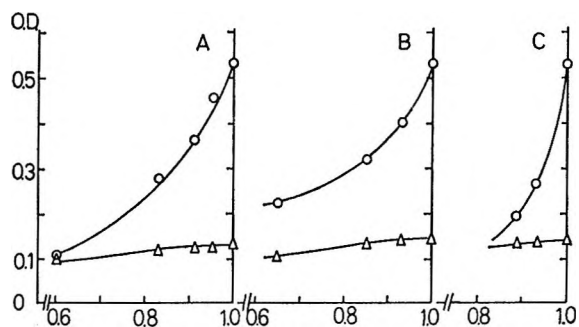


Figure 2. Optical densities of disulfide ions in *n*-amyl disulfide containing electron scavengers: A, CCl_4 , B, CHCl_3 , C, CS_2 , dose; 6.90×10^{18} eV/g for all the samples; circles and triangles are for disulfide anion and cation, respectively. Abscissa represents the weight fraction of disulfide.

while the optical density is related to the concentration per unit volume. Thus, for example, the density of *n*-amyl disulfide at 77°K, 1.045, was obtained from the density at 24.0° (0.922) and the volume contraction of 11.83%.

Results

As reported before,⁵ γ irradiation of pure *n*-amyl disulfide at 77°K produced two absorption bands at 420 and 780 nm which have been ascribed to the anion and cation radicals of disulfide (Figure 1). At 77°K the intensity of absorption gradually decreased as shown in the inset of Figure 1. The decay ceased upon lowering the temperature to 63°K. The anion yield of samples irradiated and measured at 63°K was only a few per cent higher than that of samples irradiated at 77°K and measured at 4 min after the irradiation. Thus the extrapolated yield in the inset is regarded as the "initial" yield of the anion at 77°K. Since all the optical measurements were finished within 4–6 min after the irradiation, the decrement from the "initial" yield could be corrected to reduce the error to an insignificant degree. All the yields of ions plotted in the figures were obtained by extrapolation.

The absorption bands of anion and cation were efficiently suppressed by the addition of electron and hole scavengers, respectively. Figure 2 and the dotted curve in Figure 1 show that carbon tetrachloride and carbon disulfide decrease the disulfide anion. Similarly, Figure 3 and the broken curve in Figure 1 illustrate that amines such as tetramethyl-*p*-phenylenediamine (TMPD) and triethylamine (TEA) decrease the disulfide cation. It is noted that the decrease in the disulfide anion does not accompany the increase in the disulfide cation, and vice versa.

Both bands of the anion and cation also appear for dilute solutions of disulfide in various matrices where electrons and/or positive holes produced on ionization of the matrix migrate to the disulfide.⁵ Figure 4 shows the dependence of the yield of disulfide ions on the weight fraction of disulfide in various solvents represen-

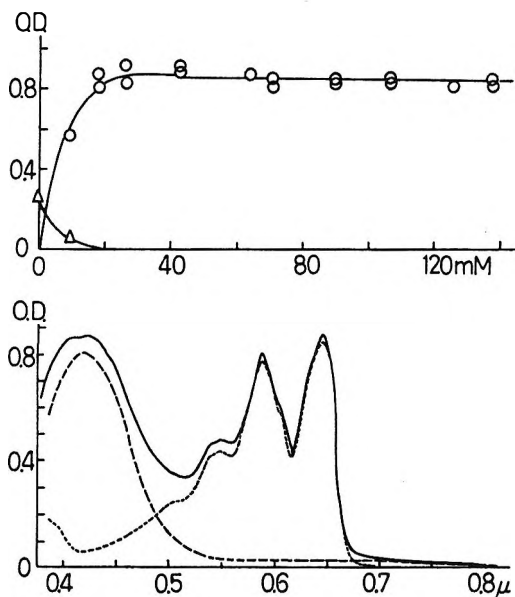


Figure 3. TMPD cation in γ -irradiated TMPD in *n*-amyl disulfide. Upper, dependence of optical densities of TMPD cation at λ_{max} 643 nm (O) and of disulfide cation at λ_{max} 780 nm (Δ) upon the concentration of TMPD. The OD's were read from such spectra as shown in the lower part of the figure; dose; 1.24×10^{19} eV/g for all the samples; lower, absorption spectrum of γ -irradiated *n*-amyl disulfide containing 27 mM TMPD. The observed solid curve can be decomposed into two components in broken curve. The component at 400–700 nm agrees with the absorption spectrum of TMPD cation observed for uv-photolyzed solutions of TMPD in *n*-amyl disulfide at 77°K. The other component is identified with the absorption due to the disulfide anion (*cf.* Figure 1). Note that the absorption of disulfide cation at about 780 nm is absent.

tative of those compiled in Table I. It is seen that the yield of disulfide anion is linear against the weight fraction, whether the disulfide is *n*-amyl or *t*-butyl. Apparently both disulfides have the same efficiency of charge scavenging. [Impure disulfides supplied from a commercial source gave lower yields of disulfide anion which differed from one disulfide to the other. Contamination with alkyl halides, the possible raw materials might be responsible for lowering the yield (see the discussion). There was a slight difference in the λ_{max} of the anion band between *n*-amyl (420 nm) and *t*-butyl (425 ~ 430 nm) disulfides.⁵] The linearity was not noticeably distorted when the total electron fraction was used instead of the weight fraction. The yield of disulfide cation, on the other hand, exhibited several types of dependence; hydrocarbons gave convex curves while ethers and alcohols showed sigmoid curves. Amines depressed the yield of disulfide cation at small concentrations.

Table I: The *G* Values of Ionization in γ -Irradiated Organic Substances at 77°K as Determined from the Yield of Disulfide Anion

Aliphatic hydrocarbons		Alcohols	
3-Methylpentane	2.10	Ethanol	2.35
Methylcyclohexane	2.10	1-Propanol	2.35
2-Methylpentene-1	1.70	2-Propanol	2.35
Methylcyclohexene-1	1.75	Pentanol-1	2.35
4-Vinylcyclohexene-1	1.15	Pentanol-2	2.35
Pentyne-1	1.30	Allyl alcohol	0.80
Aromatic hydrocarbons		Amines	
Benzene	1.40	2-Methylamino-	2.60
Toluene	1.40	ethanol	2.35
Ethylbenzene	1.40	2-Dimethylamino-	2.75
Tetralin	1.45	ethanol	2.55
		1,2-Propanediamine	2.55
		N-Dimethylamino-	
		propylamine	3.20
		Triethylamine	2.00
		Ethers and ester	
Methyltetrahydro-	2.55		
furan ^a		<i>sec</i> -Butylamine	2.10
Isoamyl ether	2.20	Isobutylamine	2.25
Vinylethyl ether	1.65	<i>n</i> -Amylamine	2.00
Diallyl ether	1.00	Allylamine	2.10
Tetrahydrofurfuryl	2.40	Diallylamine	1.45
alcohol		Triallylamine	1.25
Ethyl- <i>n</i> -butyrate	1.75	Benzylamine	1.45
		Chloride	
<i>sec</i> -Butyl chloride ^b	3.25		

^a Cited from our previous work¹² for the standardization in the present work. See text. ^b See Appendix.

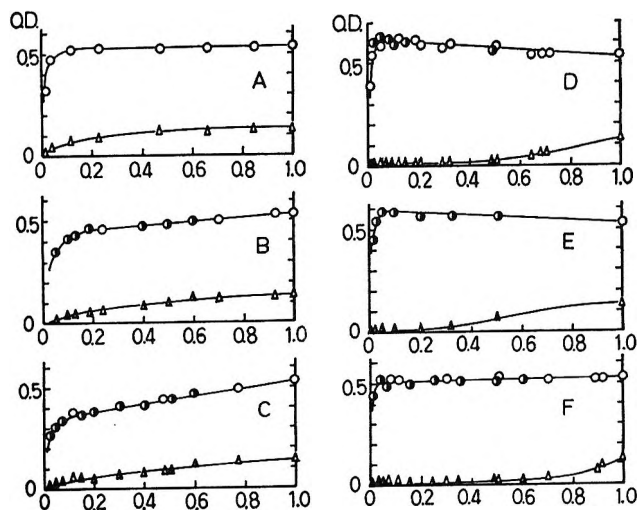
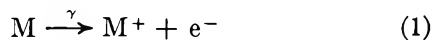


Figure 4. The yields of disulfide anion and cation for γ -irradiated binary solutions of disulfide in various solvents at 77°K: ordinate, optical densities for both anion (O, *n*-amyl, ⊙, *t*-butyl) and cation (Δ , *n*-amyl, \blacktriangle , *t*-butyl); abscissa, weight fraction of the disulfides; dose, 6.90×10^{18} eV/g for all the samples. Key to the solvents; A, methylcyclohexane; B, methylcyclohexene-1; C, ethylbenzene; D, methyltetrahydrofuran; E, pentanol-1; F, triethylamine.

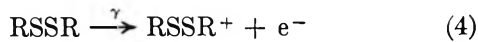
Results and Discussion

The Yield of Ionization in Pure Disulfide. It has been shown that γ irradiation of disulfide solutions in rigid matrices, M, induces the following reactions.^{4,5}





Both bands appear in irradiated pure amyl disulfide also, indicating that the following reactions have replaced reactions 1-3.



An esr study of the same system indicates that the fragmentation of the ions is negligible in the low-temperature medium.⁶ The slow isothermal decay of the anion (the inset of Figure 1) is regarded as indicating that the disulfide matrix at 77°K is not rigid enough to prevent the slow movement of the ions leading to charge neutralization. The effect of lowering the temperature to 63°K indicates that the disappearance of ions involves mass movements and not any electronic transfer such as electron tunnelings from the anion or charge migration of positive holes. Similar temperature effects on the isothermal decay of trapped electron have been observed for irradiated alkane glasses.⁷

Since the yield of disulfide ions in pure disulfide diminishes markedly in the presence of charge scavengers (Figures 1-3), electrons and holes produced by reaction 4 seem to migrate extensively before they are immobilized as the ion-radicals. Resonant positive hole migration has been proposed for several irradiated glassy solids,^{8,9} and the same mechanism may be operative for amyl disulfide also. As for electron migration, similar examples are not known since most matrices so far studied are chemically inert to electrons, but a resonant process is also possible depending on the interaction between the two states before and after one jump of an electron (see also the Appendix). Attention should be paid to the fact that scavenging electrons by CCl_4 and CS_2 does not increase the yield of disulfide cation, nor does the scavenging of holes by TEA enhance the yield of disulfide anion. This suggests that during the migration electrons and holes do not encounter each other to any significant extent. Otherwise, one would expect an increase in the yield of one ion upon scavenging the charge of opposite sign. To account for such independent behavior of the ions two explanations are conceivable. (A) In pure disulfide electrons and holes are completely separated and no charge recombination takes place owing to the diffusibility of both charges and the potentiality of the disulfide matrix for stabilizing both as the ion radicals. That is to say, the observed yields of ions are identified with the yields of the total ionization of the system. (B) A certain fraction of electrons and holes in pure disulfide recombine geminately. When one of the charge species is trapped by the scavenger, the counter charge invariably neutralizes the scavenger ions so that the same fraction of charge pairs annihilate as in

the pure disulfide. Only those charges that escape the pairwise recombination exhibit the observed effect of scavengers. These postulates will be examined comparatively in the following.

Whether all the charges in pure disulfide are separated or not, the yield of net ionization is obtained by measuring the disulfide ions. Since the extinction coefficients of the ions are not known, they are measured indirectly by the following two methods.

(1) Figure 3 indicates that all the positive holes which would give the disulfide cation produce TMPD cations at the TMPD concentrations above $\sim 20 \text{ mM}$. The latter ions can be quantitatively determined using the known oscillator strength of the visible band at 400 to 700 nm. (The oscillator strength, $f = 0.2015$, was obtained by recording the absorption spectrum of the Wurster's ion in aqueous solution at 24° and normalizing to the extinction coefficient of $12,470 \pm 60$ at $\lambda_{\text{max}} 565 \text{ nm}$ determined by Albrecht and Simpson.¹⁰ The extinction coefficient of the ion varied not only with temperature but also with the solvent. For example, ϵ at $\lambda_{\text{max}} 633 \sim 643 \text{ nm}$ was 1.337×10^4 , 1.640×10^4 , and 2.047×10^4 in *n*-amyl disulfide, *sec*-butyl chloride, and 3-methylpentane¹¹ at 77°K, respectively. The G value of 1.94 was obtained with the ϵ of 1.337×10^4 .) The limiting optical density, 0.84, of the TMPD cation at $\lambda_{\text{max}} 643 \text{ nm}$ gives the yield of scavenged positive holes as $G = 1.94$. (2) As will be discussed in detail in the next section, the yield of disulfide anion in methyl-tetrahydrofuran (MTHF) is linearly dependent on the disulfide concentration (Figure 4D). If the yield extrapolated to pure MTHF corresponds to the total scavengable electron yield in pure MTHF which has been determined as $G = 2.55$ for aromatic hydrocarbons in MTHF,¹² the extrapolation to pure disulfide gives $G(\text{disulfide anion}) = 2.1$.

Although the two methods are independent, they point to the same G value of about 2. We regard that the discrepancy is not serious considering the rather lengthy procedures of deriving the values. (Truby estimated by esr the yield of disulfide anion in irradiated pure amyl disulfide as $G = 2.4$.^{6b} Although his estimation is crude, it is in fair proximity to the G value above.)

In all probability the W value of the disulfide vapor will fall in the "normal" range of 23 \sim 25 eV/ion

(6) (a) F. K. Truby, *J. Chem. Phys.*, **40**, 2768 (1964); (b) F. K. Truby, D. C. Wallace, and J. E. Hesse, *ibid.*, **42**, 3845 (1965).

(7) J. B. Gallivan and W. H. Hamill, *ibid.*, **44**, 1279 (1966).

(8) W. H. Hamill, "Radical Ions," E. T. Kaiser and L. Kevan, Ed., Wiley-Interscience, New York, N. Y., 1968, p 321.

(9) T. Shida, *J. Phys. Chem.*, **72**, 723 (1968).

(10) A. C. Albrecht and W. T. Simpson, *J. Amer. Chem. Soc.*, **77**, 4454 (1955).

(11) W. C. Meyer and A. C. Albrecht, *J. Phys. Chem.*, **66**, 1168 (1962).

(12) T. Shida, *ibid.*, **73**, 4311 (1969).

pair.¹³ Therefore, if the value is also meaningful in the amorphous disulfide at 77°K, the yield of total ionization in the solid should be $G \cong 4$, roughly double the observed yield of ionization. If, according to postulate A, the observed yield corresponds to the total ionization, it must be concluded that the efficiency of ionization in the solid is lower than in the vapor and that the W value is not relevant to the ionization in the solid. If, to the contrary, the W value is valid in the solid, postulate B is invoked with the understanding that about half of the total ion pairs are not revealed by the scavenger technique.

The Yield of Ionization in Various Solvents. That the observed yield of ionization in pure disulfide is rather small would be of little significance if it was merely a peculiarity of the disulfide system. In this section it will be shown that similar low yields of ionization are observed for a number of organic amorphous solids at 77°K.

The linear yield of disulfide anion shown in Figure 4 is most straightforwardly interpreted in terms of the additivity of ionization in the binary mixtures. Then the yields of ionization in pure solvents can be obtained by extrapolation to the pure solvent. Table I lists the G values obtained by the relation, $G = G_{\text{RSSR}} \times (\text{OD}/\text{OD}_{\text{RSSR}})$ where $G_{\text{RSSR}} = 2.1$, $\text{OD}_{\text{RSSR}} = 0.53$, and OD is the optical density of disulfide anion extrapolated to the pure solvent. The G values fall in the range of ~ 1 –3. Therefore, not only disulfide but also a variety of organic substances have G values smaller than ~ 4 to be expected on the basis of the W value.

The total scavengeable yield of ionization in condensed phases is a rather vague quantity depending upon the scavenger and the state of aggregation, temperature, and so forth. Enhancement of scavenger concentration to ensure the complete scavenging often results in charge recombination *via* hole conduction through scavenger molecules. (Professor Hamill pointed out to the author that a single benzene molecule in 3-methylpentane matrices traps both electrons and holes and the yield of C_6H_6^+ in 3-MP is a maximum at $\sim 1\%$. At higher concentrations of benzene, however, the hole migrates from C_6H_6^+ by hopping and pure C_6H_6 conducts both electrons and holes.) Some electrons may return to positive ions before they are fully thermalized. In order to scavenge such energetic electrons, scavengers must have a wide spectrum of reaction cross section *vs.* the energy of electron. (For the water system recombination by epithermal electrons was not considered in the Samuel–Magee theory.¹⁴ In other cases such recombination may be possible, the excess energy being dissipated by predissociation of “superexcited” molecules.)¹⁵ Thus, highly correlated charge pairs, which may be envisaged as a Wannier type exciton, may be revealed by one scavenger but may not by the other.

Notwithstanding the limitation of the scavenger method we are tempted to associate the apparent simplicity and regularity of the experimental data with some general cause. Postulate A, in comparison with B, is unfamiliar and may be difficult to accept. Nevertheless, the assumption that the observed yield of ionization corresponds to the total ionization in the solids appears to be compatible with the results for the following reasons. (1) Two prominent features of the experimental results, *i.e.*, the absence of “protecting” effect of scavengers on the counter charge in disulfide-rich solutions and the linearity of $G(\text{RSSR}^-)$ observed for so many solutions, are more simply explained in terms of postulate A than B. Under postulate B we have to assume that each compound has a characteristic fraction of geminate recombination and that the fraction is not affected in solutions of all constitutions. (2) A survey of the reported yields of scavengeable electrons in irradiated glasses shows that they fall in the range of $G = 2$ –3.^{12,16–19} In all these experiments the yield was measured optically as the scavenger anion. Although the concentration of scavenger does not exceed ~ 100 mM, all the data indicate that the yield will not reach $G \sim 4$ at ultimate scavenger concentrations. ESR studies on MTHF and aqueous glasses at 77°K also show comparable yields of $G = 2.5$ –3.²⁰ The proximity of these values to those in Table I is taken as support for our postulate that the observed yield of ionization is an ultimate quantity independent of the scavenger employed. In this context the agreement of the ultimate $G(\text{TMPD}^+)$ in TMPD–disulfide solutions and the $G(\text{RSSR}^-)$ in disulfide–MTHF solutions is consistent.

(3) That the $G(\text{total ionization})$ is different in gases and solids is theoretically permissible; although the excitation spectrum for most organic substances may not change appreciably upon condensation, the apportionment of the absorbed energy among direct ioniza-

(13) (a) R. Cooper and R. M. Mooring, *Aust. J. Chem.*, **21**, 2417 (1968); (b) C. E. Klots, “Fundamental Processes in Radiation Chemistry,” P. Ausloos, Ed., Wiley-Interscience, New York, N. Y., 1968, p 7.

(14) A. H. Samuel and J. L. Magee, *J. Chem. Phys.*, **21**, 1080 (1953).

(15) (a) R. L. Platzman, “Radiation Research,” G. Silini, Ed., North Holland, Amsterdam, 1967, p 20; (b) W. A. Chupka and J. Berkowitz, *J. Chem. Phys.*, **47**, 2921 (1967); **51**, 2341, 4244 (1969); (c) R. S. Berry, *ibid.*, **45**, 1228 (1966).

(16) M. R. Ronayne, J. P. Guarino, and W. H. Hamill, *J. Amer. Chem. Soc.*, **84**, 4230 (1962).

(17) J. A. Ward and W. H. Hamill, *ibid.*, **87**, 1853 (1965).

(18) (a) F. S. Dainton, G. A. Salmon, and J. Teply, *Proc. Roy. Soc. Ser. A*, **286**, 27 (1965); (b) F. S. Dainton and G. A. Salmon, *ibid.*, **285**, 319 (1965); (c) F. S. Dainton, G. A. Salmon, and P. Wardman, *ibid.*, **313**, 1 (1969); (d) F. S. Dainton, G. A. Salmon, and C. Sonntag, *ibid.*, **313**, 31 (1969).

(19) T. Shida and W. H. Hamill, *J. Chem. Phys.*, **44**, 2369, 4372 (1966).

(20) (a) D. R. Smith and J. J. Pieroni, *Can. J. Chem.*, **43**, 2141 (1965); (b) J. H. Baxendale and M. A. J. Rodgers, *Trans. Faraday Soc.*, **63**, 2004 (1967); (c) B. G. Ershov and A. K. Pikaev, *Advances in Chemistry Series*, No. 81, American Chemical Society, Washington, D. C., 1968, p 1.

tion, autoionization, and predissociation may be subject to the effect of aggregation.¹⁵ If most ionizations are caused *via* superexcited states as Platzman suggested,¹⁵ and if the aggregation enhances the rate of predissociation at the expense of autoionization, one could expect a lower yield of ionization in solids. Moreover, in deference to recent work on ionization of benzene in rigid matrices, ionization in solids may well be quite different from that in gases.²¹ (4) Although the recent measurements of W for liquid argon show practically no difference between the gas and liquid phases,²² the results may not be relevant to the ionization of polyatomic molecules where predissociation can interfere ionization contrary to the rare gas atom.

The above argument is admittedly not strong enough to preclude the conventional presumption that the W value is transferable to condensed matter^{1,2,23} and should be regarded as tentative. However, even if the W value is valid in solids, it may have little practical significance insofar as a certain fraction of charge pairs are unobservable under most of the experimental conditions.

Whether the yields in Table I are those of the total ionization or not, we note that they reflect the chemical character of each substance more distinctly than the W value. For example, alkenes, alkynes, and aromatic hydrocarbons have lower G values than alkanes. It is interesting to note that the yields for aromatic hydrocarbons are not vanishingly small although ionic processes in these hydrocarbons are not necessarily apparent from product analysis or pulse radiolytic experiments. The lowering effect of the double bond and the aromatic ring is also seen in other classes of compounds such as ethers, alcohol, and amine. While the saturated alcohols have more or less similar G values, those of amines are more diversified but the general tendency seems to be that the polar functional groups, $-O-$, OH , NH_2 , enhance the yield of ionization.

The Yield of Disulfide Cation. The convex or sigmoid curves of the yield of disulfide cation for disulfide-rich solutions in hydrocarbons, ethers, and alcohols indicate that more cations are formed than expected from the direct ionization of disulfide. Hole migration from solvent to disulfide is the most plausible explanation because the ionization potential of all the solvents showing this type of curve is higher than that of the disulfides.²⁴ The negative deviation of the cation yield observed at low concentrations of disulfide in alcohols and ethers is explained as follows; in this concentration range cations of the solvents should undergo protonation in competition with positive charge transfer and the supply of the charge from the solvent cation to disulfide would be inefficient.^{9,9} One might still expect the cation yield equal to the amount of ionization originating in disulfide, but this assumes implicitly that the disulfide cation is produced in the ground electronic state. If the nascent cation has enough excess energy

to ionize the surrounding alcohol or ether, and if the ionized solvent then stabilizes the positive charge by the protonation reaction, the yield of disulfide cation will be depressed as is observed.

The concave curves of the cation yield in the amine solutions are attributed to the migration of positive hole of disulfide to the amine whose ionization potential is less than that of disulfide.

Remarks on The Yield of Ionization in Liquids. In view of the general difference between liquids at ordinary temperatures and solid solutions at 77°K, we may not carry our conclusion too far, but there are indications that the ionization yields in liquids also are smaller than $G \cong 4$. Williams's result that the G for the total observable ionization in liquid cyclohexane is 2.6³ seems to be congruous with our conclusion. The apparently conflicting result of $G(\text{total ionization}) = 4.6$ for methanol¹ might be attributed to the fact that nitrous oxide liberates nitrogen not only with electron but also with excited molecules²⁵ (in this particular case superexcited methanol molecules to be predissociated). In a recent work, Arai, *et al.*, showed that the yield of solvated electron in pure methanol increases upon the addition of various inorganic salts and attains a saturation value, about 1.7 times that in the pure methanol, at the solute concentrations of 1 to 3 *M*. The increment was attributed to the protecting effect of the salts scavenging positive species in the spur.²⁸ The yield, $G(e_s^-) = 1.0 \pm 0.3$, originally reported for pure methanol^{18c,27} was derived on the basis of $\epsilon_{405\text{nm}} = 58,000$ of the biphenyl anion.²⁸ However, this extinction coefficient seems to be erroneously high in the light of the recent value of 4.0×10^4 .^{12,29} When we adopt the new extinction coefficient, the $G(e_s^-)$ for pure methanol becomes 1.45 which leads to the saturation yield of solvated electron, $1.45 \times 1.7 \cong 2.5$.

In this context comparative studies of liquid solutions at room temperature using disulfide as a charge scavenger should be interesting. We carried out studies on the disulfide solutions with a pulsed electron beam (2.7 MeV, 100 mA, 1 μsec) from a Van de Graaff generator.

(21) B. Katz, M. Brith, B. Sharf, and J. Jortner, *J. Chem. Phys.*, **50**, 5195 (1969).

(22) (a) D. W. Swan, *Proc. Phys. Soc.*, **85**, 1297 (1965); (b) H. A. Ullmaier, *Phys. Med. Biol.*, **11**, 95 (1966); (c) P. H. Tewari and G. R. Freeman, *J. Chem. Phys.*, **51**, 1276 (1969); (d) N. V. Klassen and W. F. Schmidt, *Can. J. Chem.*, **42**, 4286 (1969).

(23) W. F. Schmidt and A. O. Allen, *J. Phys. Chem.*, **72**, 3730 (1968).

(24) K. Watanabe, T. Nakayama, and J. Mottl, *J. Quant. Spectrosc. Radiat. Transfer*, **2**, 369 (1962).

(25) R. A. Holroyd, *J. Phys. Chem.*, **72**, 759 (1968).

(26) S. Arai, A. Kira, and M. Imamura, *ibid.*, **74**, 2102 (1970).

(27) M. C. Sauer, Jr., S. Arai, and L. M. Dorfman, *J. Chem. Phys.*, **42**, 708 (1965).

(28) S. Ogawa and R. W. Fessenden, Quarterly Report No. 6041, Mellon Institute, Dec 1964, p 10.

(29) (a) J. J. Grodzinski, M. Feld, S. Yang, and M. Szwarc, *J. Phys. Chem.*, **69**, 628 (1965); (b) K. H. J. Buschow, J. Dielman, and G. J. Hoijtink, *J. Chem. Phys.*, **42**, 1993 (1965).

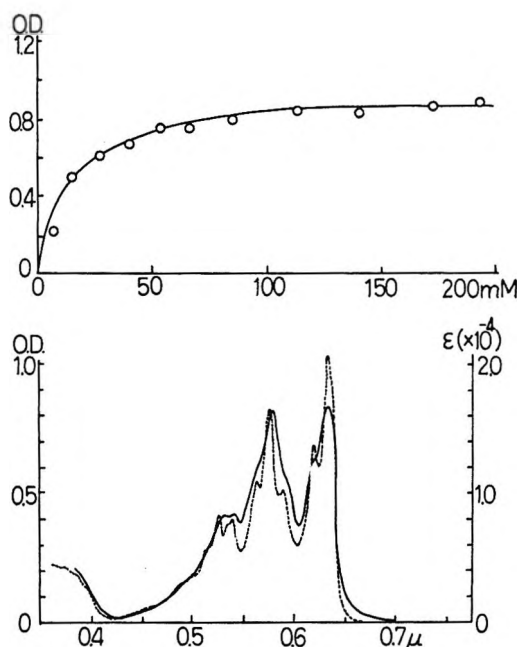


Figure 5. TMPD cation in γ -irradiated TMPD in *sec*-BuCl at 77°K; upper, dependence of optical densities of TMPD cation at λ_{\max} 636 nm upon the concentration of TMPD. The OD's were read from such spectra as shown in the lower part of the figure. The absorption due to the matrix-trapped positive hole at 500–600 nm¹⁸ appeared slightly only for the solution of the lowest concentration. Dose, 1.247×10^{19} eV/g for all the samples; lower, absorption spectrum of γ -irradiated *sec*-BuCl containing 30 mM TMPD (solid curve). The spectrum in broken curve obtained for uv-photolyzed TMPD in 3-MP at 77°K was shown for the comparison of solvent effect upon the spectrum (see also ref 11). Uv-photolyzed solutions in *sec*-BuCl at 77°K produced a spectrum exactly superposable on that of the γ -irradiated solution.

However, we failed to observe any absorption ascribable to disulfide ions for deaerated solutions of *t*-butyl disulfide in ethanol (10 ~ 100 mM). In the visible region no appreciable absorption was detected although the solvated electron was produced abundantly for pure ethanol under the same condition. We consider that the disulfide anion is stable only in the low-temperature rigid matrix. Reactions of the type of $\text{CH}_3\text{SSCH}_3 \rightarrow \text{CH}_3\text{S}\cdot + \text{CH}_3\text{S}^-$ and $\rightarrow \text{CH}_3\text{SH} + \cdot\text{CH}_2\text{S}^-$ ³⁰ may be responsible for the disappearance of both the solvated electron and the disulfide anion in the pulse-irradiated solutions.

Conclusion

In the present work we showed that the measurement of disulfide anion from the disulfide solutions in various solvents provides insight into the yield of ionization in irradiated organic amorphous solids at 77°K. It is proposed that the total observable yield of ionization in the solids is less than ~3 in the *G* unit and that reference to the *W* value for gases is not appropriate. A similar inference was tentatively extended to some of the liquid systems at room temperature.

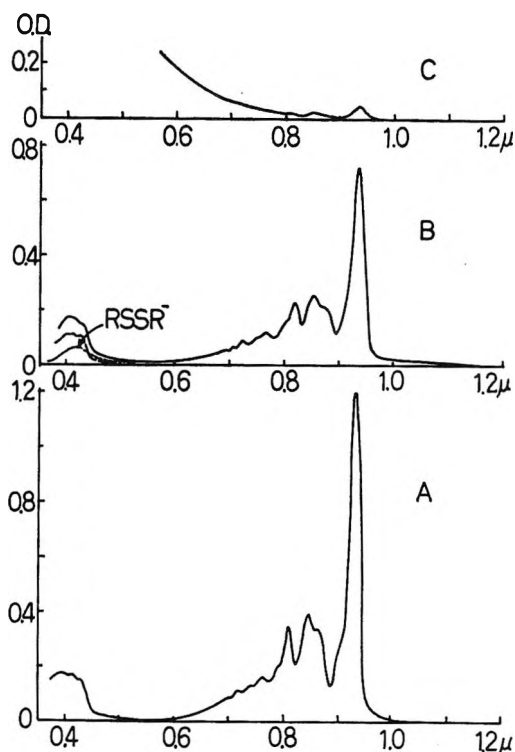


Figure 6. Absorption spectra of *p*-dinitrobenzene anion in γ -irradiated MTHF, A, *n*-amyl disulfide, B, and *sec*-BuCl, C, at 77°K. Concentration of *p*-dinitrobenzene; 25 mM for all the samples; dose, 2.08×10^{18} eV/g for A and B, 2.08×10^{19} eV/g for C. The band at about 420 nm in B is due to the disulfide anion. The tailing absorption at <800 nm in C is due to the matrix-trapped positive hole.¹⁹

Acknowledgment. The author wishes to acknowledge Dr. A. Kira for his assistance in the pulse radiolytic experiment. He is also indebted to Dr. M. Imamura and Professor W. H. Hamill for their reviewing the manuscript and for valuable discussions. He thanks Dr. A. O. Allen for sending two pertinent preprints.

Appendix

The Ionization Yield in Butyl Chloride. All the solvents in Table I are chemically inert toward electrons. (Benzene and other alkylated derivatives have slight affinity for electrons.) It is these solvents that exhibit the linear dependence of $G(\text{RSSR}^-)$ on the electron fraction of disulfide. Electron-reactive solvents such as carbon tetrachloride and butyl chloride give a concave dependence as shown in Figure 2, and the ionization yield cannot be obtained from the *G* value of disulfide anion. Since butyl chloride is a standard matrix for observing the absorption spectrum of cation-radicals of solutes,⁸ establishing the total yield of positive holes in the chloride is needed to obtain the extinction coefficient of absorption bands of solute cations. (For obtaining ϵ 's of solute anions, MTHF is recommended as the matrix since the $G(\text{electron}) = 2.55$ in irradiated MTHF¹² has now acquired more

(30) K. Jaeger and A. Henglein, *Z. Naturforsch. A*, 21, 1251 (1966).

confirmation by the present work.) We applied the TMPD technique used for the disulfide system (Figure 3) to *sec*-butyl chloride (*sec*-BuCl). Essentially the same experiment was carried out in our previous work¹⁹ but the quantitative discussion was not rigorous enough by the standard of the present work. In the previous paper¹⁹ we estimated that the scavengeable positive hole in irradiated *sec*-BuCl was roughly $G = 3$ based on the assumption that the ϵ of TMPD cation at $\lambda_{\max} \cong 630$ nm was equal to 1.93×10^4 reported by Albrecht for 3-methylpentane (3-MP) at 77°K. However, the ϵ was found to vary with the solvent and that in *sec*-BuCl at 77°K was about 80% of that in 3-MP (1.640×10^4 and 2.047×10^4 , respectively). The absorption bands in 3-MP were sharper than in *sec*-BuCl as shown in the inset of Figure 5. Assuming that the limiting optical density of 0.90 in Figure 5 corresponds to the total scavengeable holes, the G value is calculated as 3.25 from the above ϵ and the density of *sec*-BuCl at 77°K, 1.09 g/cm³. As mentioned in the previous paper¹⁹ the linear dependence of $G(\text{TMPD}^+)$ on dose at $[\text{TMPD}] > 30$ mM is indicative of the absence of charge recombination. Thus, the G value obtained is regarded to correspond to the total observable ionization in the chloride glass and is included in Table I.

Lastly, a piece of evidence was obtained to confirm the previous assumption that in the chloride matrix the

ejected electron is rapidly stabilized as Cl^- ,¹⁹ while in the disulfide matrix electrons migrate before they are stabilized as RSSR^- ; *p*-dinitrobenzene is a useful electron scavenger whose anion absorbs in the near-ir region with a remarkable vibrational structure.³¹ Since the ϵ at $\lambda_{\max} \cong 930$ nm is as high as 8.7×10^4 , it detects electrons sensitively when added in matrices as an electron scavenger. Figure 6 shows the absorption bands of *p*-dinitrobenzene anion in irradiated MTHF, *n*-amyl disulfide, and *sec*-BuCl at 77°K. As the concentration of the solute and the radiation dose are the same for the three solutions, the optical density of the anion gives relative yields of electron available to the solute in each matrix. It is seen that very few electrons can reach the solute molecule in *sec*-BuCl. If the OD at $\lambda_{\max} \cong 930$ nm of the solute anion in MTHF corresponds to $G(\text{electron}) = 2.55$, the ratio of OD's in MTHF and in disulfide, 1.2:0.7, gives an approximate G of 1.48 for the solute anion in the disulfide matrix. This amounts to *ca.* 70% of the total electrons in disulfide. The rest of the electrons, of course, become the disulfide anion as shown by the broken curve in Figure 6. The absorption due to disulfide cation seems to underlie that of the solute anion at 500–1100 nm.

(31) T. Shida and S. Iwata, to be published.

Free-Radical Intermediates in the Reaction of the Hydroxyl Radical with Amino Acid Derivatives and Related Compounds¹

by Hitoshi Taniguchi, Hiroyuki Hatano,

Department of Chemistry, Faculty of Science, Kyoto University, Kyoto 606, Japan

Hideo Hasegawa, and Tetsuo Maruyama

Japan Electron Optics Laboratory Company, Akishima, Tokyo 196, Japan (Received February 2, 1970)

Free-radical intermediates in the reaction of the hydroxyl radical with several acetylated amino acids, dipeptides, and related compounds containing peptide groups have been studied by electron spin resonance (esr) spectroscopy using a continuous flow method. The hydroxyl radical was produced chemically in a titanous chloride-hydrogen peroxide system. ESR spectra with sufficient signal-to-noise ratio were obtained from acetylglycine, glycylglycine, acetyllanine, dimethylurea, ethylurea, and urethan (ethyl carbamate). The structure of the radicals and the hyperfine coupling constants are obtained from the analysis of the spectra. It is found that the hydroxyl radical abstracts hydrogen atom preferentially from the C-H bond adjacent to the amide-nitrogen atom. The hyperfine splitting due to the nitrogen nucleus was found to be small and was not observed as resolved peaks in most cases. This is consistent with the results of the spin density calculation by the LCAO-SCF method.

Introduction

Electron spin resonance (esr) studies of unstable free radicals in aqueous solution have been extensively carried out, since Dixon and Norman² applied a flow method to esr spectroscopy. In a previous paper,³ we reported results of our study on the intermediate radicals formed in the reaction of carboxylic acids, amines, and amino acids with the hydroxyl radical generated in a titanous chloride-hydrogen peroxide system, and in the present paper, we extend the study to amino acid derivatives and several substrates containing the peptide groups.

Experimental Section

Experimental procedures for measurements of esr spectra using a continuous flow technique were the same as described previously,³ except for minor modifications.

The esr spectra of intermediate radicals were recorded at room temperature on an X-band spectrometer (JEOL, Model JES-3BS) within 6 to 13 msec after mixing two reactants. Modulation width used for the recording was varied 0.3 to 2 G from one compound to the other. Hyperfine coupling constants were measured using manganous ion as a reference (splitting between the two central peaks, 86.9 G).

The concentration of titanous chloride, hydrogen peroxide, and organic substrates was 0.008 to 0.02 *M*, 0.1 *M*, and 0.5 to 1.0 *M*, respectively. The reactant solutions were acidified to about pH 2 with dilute sulfuric acid.

Glycylglycine and glycyl-DL- α -alanine were purchased from the Institute for Protein Research, Osaka University, Osaka; acetyl-DL- α -alanine was prepared

by the acetylation of DL- α -alanine following the usual method.⁴ Other materials were obtained from commercial sources and used without further purification.

The calculation of π -electron spin density was performed with a KDC-II (HITAC 5020) computer of Kyoto University.⁵

Results and Discussion

Structures and Hyperfine Coupling Constants of the Intermediate Radicals. Most compounds examined gave esr spectra with fairly good signal-to-noise ratio, and some typical spectra are shown in Figures 1 to 4. Glycylalanine, sarcosine, and betaine, on the other hand, showed only weak signals. The structure of the intermediate radicals deduced from the spectra and the hyperfine coupling constants are summarized in Table I. It is found that the hydroxyl radical abstracts hydrogen atom preferentially from the C-H bonds adjacent to the amide nitrogen atoms. In the cases of amines and amino acids, the abstraction did not occur at the C-H bonds adjacent to the protonated amino groups.³

The hyperfine splitting due to the nitrogen nucleus adjacent to the unpaired carbon (C₁)⁶ was found to be

(1) This work was presented at the 22nd Annual Meeting of the Chemical Society of Japan, Tokyo, April 1969.

(2) W. T. Dixon and R. O. C. Norman, *J. Chem. Soc.*, 3119 (1963).

(3) H. Taniguchi, K. Fukui, S. Ohnishi, H. Hatano, H. Hasegawa, and T. Maruyama, *J. Phys. Chem.*, 72, 1926 (1968).

(4) See, for example, J. P. Greenstein and M. Winitz, "Chemistry of the Amino Acids," Vol. 3, Wiley, New York, N. Y., 1961, p 1831.

(5) We are indebted to Mr. M. Sakoda, Department of Chemistry, Kyoto University, for his considerable assistance with the computer programs.

(6) The designations C₁ and C₂ refer to the position relative to the carbon atom which bears the unpaired electron.

Table I: Structures and Hyperfine Coupling Constants of the Intermediate Radicals^a

Substrate	Radical	Coupling constant, G			
		C ₁ -H	C ₂ -H	N	NH
Acetylglycine	CH ₃ CONHĊHCOOH	16.0		2.1	2.1
Glycylglycine	H ₃ ⁺ NCH ₂ CONHĊHCOOH	16.2	2.8 ^b		2.0
Acetylaniline	CH ₃ CONHĊ(CH ₃)COOH		18.1		1.4
Dimethylurea	CH ₃ NHCONHĊH ₂	17.9			
Ethylurea	NH ₂ CONHĊHCH ₃	16.9	21.9		
Urethan	CH ₃ ĊHOCONH ₂	17.3	23.2		

^a See ref 6 for the notations in column 3. ^b Coupling constant due to methylene protons. D. C. Borg and J. J. Elmore, Jr., assigned this splitting to the nitrogen hyperfine coupling in a private communication.

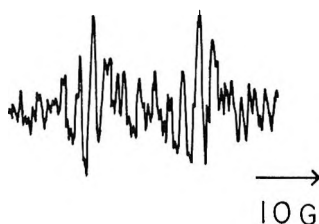


Figure 1. Electron spin resonance spectrum of the intermediate radical from 0.8 M acetylglycine.

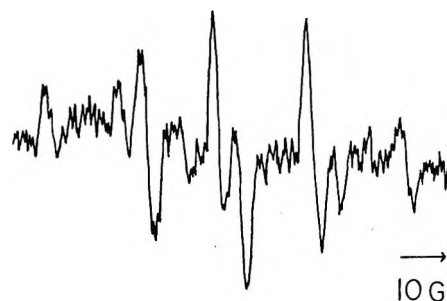


Figure 3. Electron spin resonance spectrum of the intermediate radical from 0.5 M ethylurea.

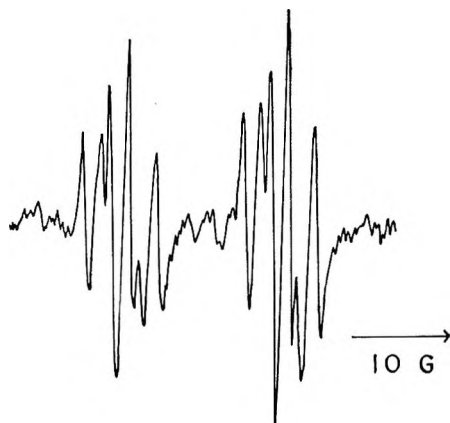


Figure 2. Electron spin resonance spectrum of the intermediate radical from 0.8 M glycylglycine.



Figure 4. Electron spin resonance spectrum of the intermediate radical from 1.0 M urethan.

small. The value obtained for the acetylglycine radical was 2.1 G. In the other radicals, the splitting was so small that we failed to observe the splitting as resolved peaks in the spectra. From the observed line widths and the modulation widths used for the recording, the nitrogen coupling constants could be less than about 1 G.

In the case of the glycylglycine radical, the methylenic protons located across the peptide group gave a splitting of 2.8 G, which is larger than the amide-proton coupling. Similar observation has been reported for the 1,4-diketopiperazine radical formed by X-irradiation at room temperature.⁷ It is noted that the observed coupling constants, a_{C_2-H} and a_N , are different between the structurally similar acetylglycine and glycylglycine radicals.

The long-range coupling across the alkoxy carbonyl group in the urethan radical was not resolved in the present study, while Smith, *et al.*,⁸ observed the coupling in aliphatic ester radicals of carboxylic acids.

It is interesting to note that the free radicals produced by X or γ irradiation of single crystals of acetylglycine,⁹ glycylglycine,⁹ acetyl-DL-alanine,¹⁰ and ethylurea¹¹ at room temperature were of the same species as the intermediate radicals in the present flow system.

(7) I. Miyagawa, *Tech. Rep. Inst. Solid State Phys. (Tokyo), Ser. A*, **27**, (1961); W. C. Lin and C. A. McDowell, *Can. J. Chem.*, **41**, 9 (1963).

(8) P. Smith, J. T. Pearson, P. B. Wood, and T. C. Smith, *J. Chem. Phys.*, **43**, 1535 (1965).

(9) R. S. Mangiaracina, *Radiat. Res.*, **32**, 27 (1967).

(10) M. Katayama, *J. Mol. Spectrosc.*, **9**, 429 (1962).

(11) T. S. Jaseja and R. S. Anderson, *J. Chem. Phys.*, **35**, 2192 (1961).

The hyperfine splitting due to the nitrogen nucleus was not observed in the solid radicals except in the methyl-deuterated acetylglycine radical (maximum value of nitrogen coupling, 2.0 G),⁹ and the broadening of the component lines of esr spectra has been believed to arise from the unresolved hyperfine interactions of the unpaired electron with the nitrogen nucleus and/or the proton in the NH group adjacent to C₁.

Calculation of π -Electron Spin Distribution. The π -electron spin densities were calculated by the simple LCAO-MO method and the LCAO-SCF method to examine the C₁-H coupling constants and to explain small nitrogen coupling constants. As for the parameters in the LCAO-MO calculations, we chose, after several trials, the values listed in Table II which were some modifications of Pullman's parameters.¹²

Table II: Parameters Used in Molecular Orbital Calculations

Group	Atom (X)	h_X^a	Bond (C-Y)	k_{CY}^b
C—O—	C	0.2	C—C	0.9
	O	2.0	C—O	0.9
C—C=O	C	0.2	C=O	2.0
	O	1.2		
N—C=O	C	0.27	C—N	0.8
	O	1.2		
C—CH ₃	C	-0.1	C—CH ₃	0.7
C—CH ₂	CH ₃	2.0	C—CH ₂	0.7
	CH ₂	2.0		
	N	1.6		
	N	2.0		

^a $h_X = (\alpha_X - \alpha_C)/\beta$ for Coulomb integral. The Coulomb integral, α_C , is taken to be that for carbon, and the resonance integral, β , is that for the C—C bond in benzene. ^b $k_{CY} = \beta_{CY}/\beta$ for resonance integral.

In the LCAO-SCF calculations, we adopted Yomosa's procedure¹³ in which the following formula was used

$$\alpha_r' = \alpha_r + \frac{2}{3}(X_{r+1} - X_r)Q_r\beta \quad (1)$$

for the Coulomb integral of heteroatom r. X_r is the electronegativity of the r atom with the net charge Q_r and X_{r+1} is that of the atom next to r in the periodic table. The spin density calculations were carried out until the differences between the successive eigenvalues became less than 0.0001 β . The results of the calculations are tabulated in Table III.

Putting the calculated spin densities and the observed hyperfine coupling constants into the equation, $a_{C_1-H} = Q\rho_{C_1}$, we obtained the proportional constants Q which were reasonable values as shown in Table III. The Q values for dimethylurea, ethylurea, and urethan

Table III: Calculated Spin Densities and Theoretical Nitrogen Hyperfine Coupling Constants^a

Radical	ρ_{C_1}	Q, G	ρ_N	$\sum_i \rho_{C_i}$	$\frac{N, a}{G}$
Acetylglycine	0.6727	23.8	0.1130	0.6794	1.16
Glycylglycine	0.6726	24.1	0.1133	0.6792	1.17
Acetyllalanine	0.6168	29.3 ^b	0.0812	0.6248	0.49
Dimethylurea	0.8564	20.9	0.1084	0.8672	0.57
Ethylurea	0.8226	20.5	0.0772	0.8388	0.14
Urethan	0.8111	21.3	0.0025	0.0162	0.02

^a See text and ref 6 for the notations. ^b Q value of C₁-CH₃ group.

radicals are slightly smaller, probably because of the inappropriate choice of parameters for methyl and methylene groups.

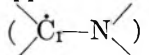
The spin density calculations by McLachlan's method¹⁴ were also carried out. The results, however, were not much improved because the small, rather localized π -electron system was treated.

Nitrogen Hyperfine Coupling Constant. The theoretical value of nitrogen hyperfine coupling depends not only on the π -electron spin density at the nitrogen atom, ρ_N , but also on the π -electron spin densities at the carbon atoms bonded to the nitrogen atom, $\sum_i \rho_{C_i}$, as shown in the following formula 2.¹⁵ The numerical values of Q_N^N and Q_{CN}^N were taken in this work to be

$$a_N = |Q_N^N \rho_N + Q_{CN}^N \sum_i \rho_{C_i}| \quad (2)$$

25.3 and -2.5 G, respectively, which are within an appropriate range of those proposed for the nitrogen splitting of substituted pyridine and pyrimidine anion radicals.¹⁶

The calculated values of a_N are less than about 1 G as shown in Table III, which are consistent with the experimental results except the acetylglycine radical.

The eq 2 originally presented for the delocalized π -electron system such as the nitrogen heterocyclic radical ions is applicable to the somewhat localized π -electron system () in this work.

Acknowledgment. The authors wish to express their gratitude to Professor Shun-ichi Ohnishi, Department of Biophysics, Kyoto University, for his helpful discussions and revisions of this manuscript.

(12) B. Pullman and A. Pullman, "Quantum Biochemistry," Interscience Publishers, Inc., New York, N. Y., 1963, p 104.

(13) S. Yomosa, *Biopolymers*, **1**, 1 (1964).

(14) A. D. McLachlan, *Mol. Phys.*, **3**, 233 (1960).

(15) J. C. M. Henning, *J. Chem. Phys.*, **44**, 2139 (1966), and references cited therein.

(16) P. T. Cottrell and P. H. Rieger, *Mol. Phys.*, **12**, 149 (1967).

Radiolysis Transients in Viscous Liquids. Biphenyl in Liquid Paraffin

by J. Fuller, N. Peteleski, D. Ruppel, and M. Tomlinson¹

Atomic Energy of Canada Limited, Whiteshell Nuclear Research Establishment, Pinawa, Manitoba, Canada
(Received February 18, 1970)

Formation and decay of transient species produced in pulse-irradiated solutions of biphenyl in liquid paraffin have been studied spectrophotometrically at temperatures from +20 to -20°. The rates of solute ion recombination and solute triplet quenching are correlated with the viscosity by $k_r \propto \eta^{-n}$ where $n = 0.5$. This departure from $n = 1$ for simple liquids is accounted for quantitatively by differences in solute-solvent and solvent-solvent interaction energies. Electron scavengers greatly reduce the yields of biphenyl ions and triplets. Since the same additives have little effect on photolytic triplets, this indicates that over 80% of radiolytic triplets are formed *via* routes not available in photolysis. A 60% increase of ion yields at -20° is attributed to paired ions whose recombination is retarded sufficiently to permit detection at a viscosity >100 P.

Introduction

The advantage of using viscous solvents to retard diffusion-controlled processes and facilitate their observation has been noted by Leone and Hamill.² These authors used liquid paraffin and squalane solutions to study recombination luminescence from radiolytic ions. Examination of viscosity effects has aided the study of triplet-state decay processes in flash photolysis work.^{3a,b} McCollum, Nevitt, and Wilson⁴ have combined flash photolysis and pulse radiolysis in a comparative study of the luminescence and triplet absorption of naphthalene, anthracene, and related solutes in liquid paraffin.

Observations of the formation and reaction of solute molecular ions in an appropriate viscous solvent can yield information about the motions of charged species and their contributions to the overall radiation chemical process. Similar information about electronically excited⁵ and free-radical species should also be forthcoming. Leone and Hamill² describe the time dependence of solute fluorescence in terms of recombination of solute anion + solute cation correlated pairs and electron + solute cation correlated pairs, *i.e.*, geminate recombination⁶ with ensuing formation of singlet excited state of the solute. There is an accumulation of evidence for formation of excited states, triplet as well as singlet, through ion recombination in other types of solvent.⁷⁻¹⁰

McCollum and Nevitt⁴ find that pulse radiolysis and flash photolysis give similar ratios of singlet and triplet yields for aromatic solutes in liquid paraffin and conclude that processes unique to radioexcitation—notably ion recombination—produce little or no triplet excitation. On the other hand, Theard, Peterson, and Holroyd¹¹ find that intersystem crossing is a minor mode of triplet excitation in pulse-irradiated liquid naphthalene and biphenyl. The experiments described here permitted observation of triplet excited solute molecules and solute molecular ions in the same solution. The effect

of additional solutes on these species revealed a clear distinction between pulse radiolysis and flash photolysis.

Empirical¹² and theoretical considerations¹³⁻¹⁵ show that diffusion processes in liquids normally proceed at a rate proportional to the fluidity, or more precisely the viscous friction factor T/η (T = absolute temperature, η = viscosity). Anomalous viscosity dependence has been observed for the disappearance of transient species in liquid paraffin solutions^{2,4} and other viscous solu-

- (1) To whom all correspondence should be addressed.
- (2) J. A. Leone and W. H. Hamill, *J. Chem. Phys.*, **49**, 5294 (1968).
- (3) (a) J. W. Hilpern, G. Porter, and L. J. Stief, *Proc. Roy. Soc., Ser. A*, **277**, 437 (1964); (b) M. Z. Hoffman and G. Porter, *ibid.*, **268**, 46 (1962).
- (4) J. D. McCollum and T. D. Nevitt, "Triplet Excitation Induced by Electron Irradiation," Aeronautical Systems Division report ASD-TDR-63-616, Clearinghouse for Federal Scientific and Technical Information, U. S. Department of Commerce, Springfield, Va., 1963; J. D. McCollum and W. A. Wilson, "Triplet Excitation Induced by Electron Irradiation II," Aeronautical Systems Division report ASD-TR-11, Clearinghouse for Federal Scientific and Technical Information, U. S. Department of Commerce, Springfield, Va., 1961; J. D. McCollum and W. A. Wilson, "Determination of Irradiation Produced Triplet Excitation by Flash Spectroscopy," Aeronautical Systems Division report ASD-TR-61-170, Clearinghouse for Federal Scientific and Technical Information, U. S. Department of Commerce, Springfield, Va., 1961.
- (5) B. Brocklehurst, *Nature (London)*, **221**, 921 (1969).
- (6) R. M. Noyes, *J. Amer. Chem. Soc.*, **77**, 2042 (1955).
- (7) J. K. Thomas, K. Johnson, T. Klippert, and R. Lowers, *J. Chem. Phys.*, **48**, 1608 (1968).
- (8) T. Saito, K. Takahashi, and S. Sato, *Bull. Chem. Soc. Jap.*, **41**, 2603 (1968).
- (9) G. R. A. Johnson and M. C. Sauer, *J. Chem. Phys.*, **51**, 496 (1969).
- (10) P. K. Ludwig, *Mol. Cryst.*, **4**, 147 (1968).
- (11) L. M. Theard, F. C. Peterson, R. A. Holroyd, *J. Chem. Phys.*, **51**, 4126 (1969).
- (12) P. Chang and C. R. Wilke, *J. Phys. Chem.*, **59**, 592 (1955).
- (13) S. Glasstone, K. J. Laidler, and H. Eyring, "Theory of Rate Processes," McGraw-Hill, New York, N. Y., 1941, p 516.
- (14) P. A. Egelstaff, "An Introduction to the Liquid State," Academic Press, New York, N. Y., 1967, p 151.
- (15) W. Jost, "Diffusion," Academic Press, New York, N. Y., 1967, p 462.

tions.^{3a} In the case of recombination of paired ions, the anomaly is attributed² to increased ion mobility at small ion separation distances. On the other hand, an explanation in terms of reactions of free radical quenchers is offered for the case of triplet quenching.⁴ Our experiments permitted a comparison of the effect of viscosity on triplet quenching and ion recombination processes. This suggested that "anomalous" viscosity dependence for diffusion-controlled reaction rates is a general characteristic of these solutions and the reasons for this will be discussed.

An increased ion yield at the highest viscosities is attributed to prolongation of the lifetime of some of the paired ions sufficient to permit detection in the early part of the pulse.

Experimental Section

Liquid paraffin (LP, Anachemia AC 7014) as received contained 39% carbon atoms in naphthenic rings, 61% carbon atoms in paraffinic chains, <0.05% wt hydrocarbons below C₂₄, no unsaturation detectable by ir examination, and 20 ppm of H₂O maximum. Repeated passes (typically 6) through an activated silica gel column removed a shoulder on the uv absorption edge to give over 95% transmission at 285 nm. Zone-refined biphenyl (James Hinton Co.) was used without further purification. Initial degassing of solvent (LP) was carried out with warming and shaking. Bubbling with dry nitrogen and reevacuation aided removal of residual oxygen. Final degassing of solutions was by several cycles of freeze, pump, thaw.

Irradiations were performed using conventional pulse radiolysis apparatus.¹⁶ The spectrophotometric detection equipment was mounted inside the accelerator room. The photomultiplier responses were calibrated periodically with a set of glass plates with known light transmission characteristics. A modified model GS Van de Graaff accelerator delivered 1.5-MeV electrons in pulses of 2 to 200 μ sec duration and up to 20 mA current into the target solution. The dose was monitored by measuring total charge input to the pulse radiolysis cell. Absolute dosimetry was performed by measuring absorption at 420 nm of ferricyanide ion produced by pulse irradiation of 5 mM K₄Fe(CN)₆ in neutral aerated water. $G(\text{ferricyanide}) = 3.2$ and decadic molar extinction coefficient ϵ_d 1000 were assumed.¹⁷ For a typical pulse the dose was 0.6 J in 40 μ sec at 10 mA giving 1.0×10^{18} eV/cm³ at 2.5×10^{22} eV/cm³ sec average in the region sampled by the light beam.

Supporting experiments were performed by the flash photolysis technique¹⁸ using the equipment of Singh, Scott, and Sopchysyn.¹⁹ This gave a 25 μ sec wide (at half-maximum amplitude) light flash from the 3 flash tubes containing air at ~ 0.02 Torr. The light was filtered by 2-mm Pyrex to prevent direct excitation of the solvent.

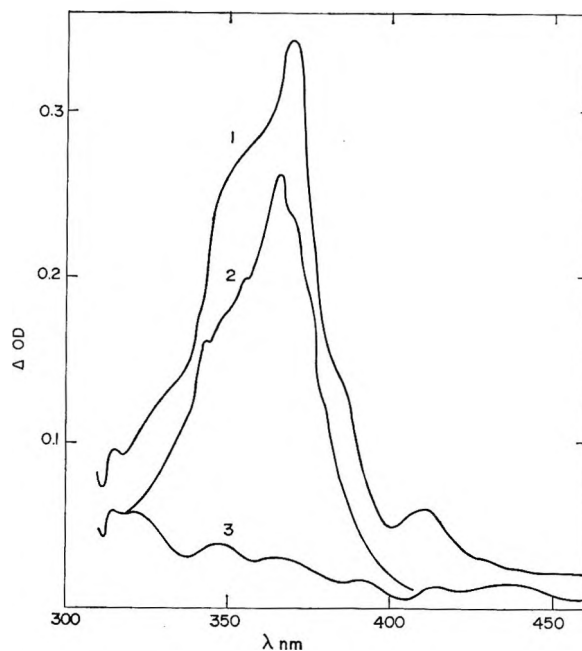


Figure 1. Absorption spectra of transients formed in biphenyl solutions in liquid paraffin. Curve 1: pulse radiolysis of 0.1 M (C₆H₅)₂ in LP, 20 μ sec after end of pulse; curve 2: flash photolysis of 10⁻⁴ M (C₆H₅)₂ in LP, at absorption maximum; curve 3: pulse radiolysis of 0.1 M (C₆H₅)₂ in LP, 900 μ sec after end of pulse (from photoelectrical measurements; points omitted for clarity).

Results

1. *Spectra.* Pulse irradiation of biphenyl in liquid paraffin was accompanied by light emission with a maximum at 310 nm attributable to biphenyl fluorescence. This died away with the pulse, *i.e.*, decay time <0.5 μ sec and was followed by light absorption over a broad band with a peak at 363 nm as shown in Figure 1. The transient absorption spectrum obtained by flash photolysis of biphenyl in liquid paraffin is shown for comparison. The latter was completely quenched by oxygen and corresponds to light absorption by the first triplet excited state of biphenyl.²⁰ Biphenyl triplet accounted for most of the pulse radiolysis spectrum shown but there were several additional components. The shoulder at 410 nm was due to biphenyl ions (see below). The triplet exponential decay time was 85 μ sec at 17°. The absorption spectrum after 900 μ sec when biphenyl triplets and ions had decayed is shown in Figure 1 and was due to at least two species. Subsequent decay of the light absorption in the region of 363 nm had a decay time of 3.5 msec.

(16) J. P. Keene, "Pulse Radiolysis," M. Ebert, J. P. Keene, and A. J. Swallow, Ed., Academic Press, New York, N. Y., 1965, p 1.

(17) G. E. Adams, J. W. Boag, and B. D. Michael, *Trans. Faraday Soc.*, **61**, 492 (1965).

(18) G. Porter, *Z. Elektrochem.*, **64**, 59 (1960).

(19) A. Singh, A. R. Scott, and F. Sopchysyn, *J. Phys. Chem.*, **73**, 2633 (1969).

(20) G. Porter and M. W. Windsor, *Proc. Roy. Soc., Ser. A*, **245**, 238 (1958).

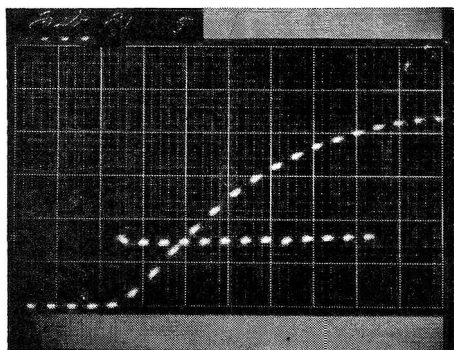


Figure 2. Formation of biphenyl triplet: upper trace, beam current to sample, 2 mA/div (downward deflection); lower trace, 363 nm absorption, 0.2/div. (upward deflection); sweep 2 μ sec/div.

The species responsible has not been identified. For convenience it will be referred to as Y. Decay of light absorption in the region of 310 nm continued with a decay time of 50 msec. This is tentatively attributed to phenylcyclohexadienyl radical.^{21,22}

In addition to the absorption shown in Figure 1, there was a weaker absorption band in the 600–700-nm region due to biphenyl ions.^{23–25} The main absorption band of the ions in the vicinity of 410 nm was obscured by the triplet band. No absorption was detected in the 600–700-nm region in flash photolysis. In liquid paraffin without biphenyl there was no absorption above 300 nm in pulse radiolysis. No change in characteristics with successive pulses was noted, except for a 10% decrease in the triplet decay constant after 100 light pulses.

2. Ion and Triplet Yields. Figure 2 shows the rise of the 363-nm absorption during a pulse and the associated current pulse. Triplet yields were estimated from the initial slope of traces of this type by fitting a second-degree polynomial to the first part of the curve up to $\Delta OD \sim 0.4$. The quadratic term allows for triplet decay in the pulse and the slow decrease of current during the pulse. A similar procedure for the 620-nm absorption gave the ion yield. For the 363-nm absorption, the rate of rise determined in this way was directly proportional to the electron beam current from 0.14 to 11 mA and independent of temperature from +20° to –20° corresponding to a product for triplet biphenyl $G \times \epsilon_D = 67000 \pm 3000$ (mean and standard deviation for 32 measurements) after correction for the absorption due to the long lived component Y. During the pulse this amounted to $(5.9 \pm 0.4)\%$ of the total change of optical density at 363 nm in 0.1 M $(C_6H_5)_2$, independent of dose, intensity, and temperature above –10°. The contribution decreased to 2.6% of ΔOD at –20° and increased to $(11.4 \pm 0.8)\%$ of ΔOD in 0.005 M $(C_5H_5)_2$.

The rate of rise of the absorption at 620 nm was also directly proportional to radiation intensity and independent of temperature from 0 to 20° corresponding

to a product $G\epsilon_D = 6000 \pm 500$ for biphenyl ions. The ion yield decreased for low biphenyl concentrations and increased at –20° as shown in Table I. Observations below –20° were hindered by opacity, believed due to formation of ordered regions.

Table I: Biphenyl Ion Formation

Biphenyl concn, mM	Temp, °C	d(OD)/dq, ^a 1/ μ C
113	20	0.45 \pm 0.04
	10	0.48
	0	0.48 \pm 0.08
	–7	0.52
	–20	0.65 \pm 0.05
5.7	–20	0.63 \pm 0.03
	20	0.34
1.1	20	0.35
0.3	18	0.20 \pm 0.02

^a d(OD)/dq = optical density increase per microcoulomb of injected charge (each value is the mean of 3 or more determinations).

The rate of biphenyl ion formation was reduced to less than $1/6$ the normal rate by addition of the electron scavengers SF₆ and N₂O, as indicated in Table II. The effect on the rate of triplet formation was very similar.

Table II: Effect of Additives on Biphenyl Ion and Triplet Yields

Additive	Additive concn, mM	Biphenyl concn, mM	Relative ion formation rate, Radiolysis	Relative triplet (formation rate) Radiolysis Photolysis	
SF ₆	sat ^a	5.7	0.11	0.20	1.02
		0.10			
N ₂ O	sat	5.7	0.14	0.16	0.91
		0.10			
CCl ₄	62	5.7	0.09	0.05	0.79
		28			
		0.10			
O ₂	sat	5.7	0.09	0.02	0.00
		0.10			
MTHF	100	28	0.55	0.42	1.00
		5.7			
		0.10			
<i>n</i> -BuOH	87	5.7	0.73	0.73	0.90
		0.10			
NH ₃	sat	100	0.55	0.79	0.88
		0.10			

^a Saturated solution at 1 atm pressure.

(21) L. M. Dorfman, I. A. Taub, and R. E. Buhler, *J. Chem. Phys.*, **36**, 3051 (1962).

(22) B. Cercek, *J. Phys. Chem.*, **72**, 3832 (1968).

(23) P. Balk, G. J. Hoijtink, and J. W. H. Schreurs, *Rec. Trav. Chim., Pay-Bas*, **76**, 813 (1957).

(24) J. Jagur-Grodzinski, M. Feld, S. L. Yang, and M. Szwarc, *J. Phys. Chem.*, **69**, 628 (1965).

(25) T. Shida and W. H. Hamill, *J. Chem. Phys.*, **44**, 4372 (1966).

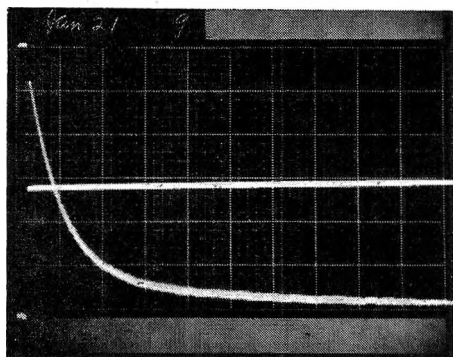


Figure 3. Triplet and long-lived decay: upper trace, charge input to sample, $0.05 \mu\text{C}/\text{div}$; lower trace, 363-nm absorption, $0.15/\text{div}$; sweep $200 \mu\text{sec}/\text{div}$.

Flash photolysis measurements showed that there was little direct effect of N_2O and SF_6 whereas O_2 caused complete triplet quenching. CCl_4 caused a small reduction in the photolytic yield of triplet which may have been due to radicals produced by photolysis of the CCl_4 . The pronounced reduction in radiolytic triplet yield by CCl_4 is consistent with its electron scavenging properties. The effects of the positive ion scavengers NH_3 , MTHF, and $n\text{-BuOH}$ were less pronounced and the distinction between photolysis and radiolysis was not as clear.

3. Ion and Triplet Decay Rates. The decay of the triplet absorption after pulse radiolysis is shown in Figure 3 and was essentially first order accompanied by a small contribution from the long-lived component Y. The decay of Y was determined from separate measurements over a longer time span and the Y contribution was subtracted to get the triplet contribution. A good fit was obtained assuming exponential decay of this part, *e.g.*, first-order decay better than second-order decay at the 99% confidence level (F test). Small second-order contributions to the decay were expected due to absorption at 363 nm by biphenyl ions and from triplet-triplet quenching. Assuming a diffusion limited rate, the latter was estimated to be less than 3% of the observed decay rate at the highest triplet concentration used. Absorption by the ions was estimated to be less than 7% of the initial 363 nm absorption and decayed at about the same rate in the region of measurements. No corrections have been applied for these contributions.

The observed triplet decay was independent of dose and biphenyl concentration as shown in Table III. The additives listed in Table II were also without detectable effect on the decay rate where measurable. The temperature variation is shown in Figure 4. The Arrhenius plot is curved like that for the viscosity in proximity to the glassy transition. The triplet decay rate in flash photolysis was considerably slower (exponential decay time = $3.0 \pm 0.3 \text{ msec}$ in $10^{-4} M (\text{C}_6\text{H}_5)_2$ at 20°) than in radiolysis ($t_0 = 0.10 \pm 0.01 \text{ msec}$ in $3 \times 10^{-4} M (\text{C}_6\text{H}_5)_2$ at 18°).

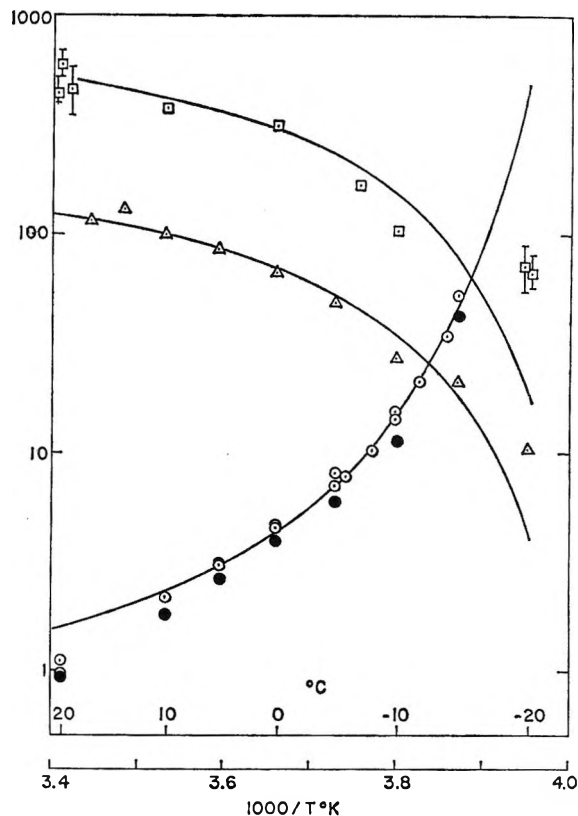


Figure 4. Temperature dependence of viscosity and radiolysis transient decay rate constants for liquid paraffin solution of biphenyl: \circ , viscosity (poises) of liquid paraffin; \bullet , viscosity (poises) of $0.1 M$ biphenyl-liquid paraffin solution; \square , ion recombination constant $k_2 = k_r/\epsilon D l$ ($10^3/\text{sec}$); \triangle , triplet-decay constant k_1 ($10^2/\text{sec}$); —, calculated.

Table III: Triplet Decay vs. Dose and Biphenyl Concentration

Biphenyl concn, mM	Temp, $^\circ\text{C}$	Pulse length, μsec	Dose, μC	Decay constant, $10^4/\text{sec}$
113	17	7.4	0.02-0.09	1.17 ± 0.11
		13	0.14	1.1
		40	0.03-0.3	1.5-2.3
28	20	65	0.64	0.99
			0.66	1.4
			0.60	1.15
			0.3	18

The decay of the ion absorption at 620 nm is illustrated in Figure 5. It was second order with k_2 independent of dose and biphenyl concentration. The temperature variation is shown in Figure 4. The variance of the replicate k values is due partly to the effects of low-frequency noise in the light source ($<0.5\%$ of the incident intensity).

Discussion

1. Ion and Triplet Formation. The biphenyl concentration ($0.1 M$) used in the majority of experiments is assumed adequate to capture most of the electrons

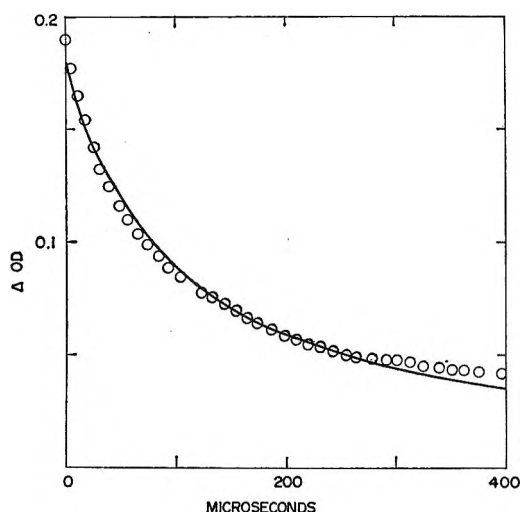
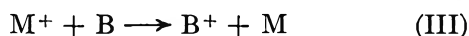
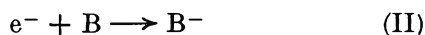
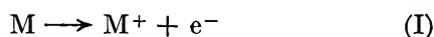


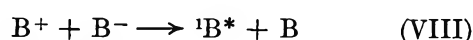
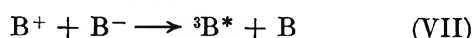
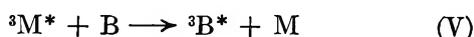
Figure 5. Ion decay; change in OD at 620 nm vs. time; observed points and fitted second-order line.

and positive holes generated by radiolysis of the solvent (reactions I-III). (The notation used is M = solvent,



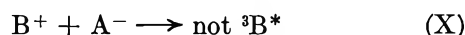
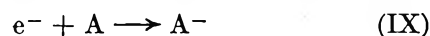
B = biphenyl, A = additive.) This view is supported by data from trapping experiments in hydrocarbon glasses.^{25,26} Two classes of ions are to be considered, those remaining paired and undergoing geminate recombination and free ions undergoing volume recombination.²⁷ The lifetimes of the paired ions are estimated below to be too short to permit their observation at 20° under the available pulse radiolysis conditions. Included in this class will be any charges which by virtue of short migration lengths are not captured by solute prior to recombination. The observed second-order recombination is characteristic of volume recombination of unpaired ions. If we assume for $B^+ + B^-$ an extinction coefficient $\epsilon_D \sim 25,000/\text{Mcm}$ at 620 nm²⁸ the observed product $G_{\epsilon_D} = 6000 \pm 500$ corresponds to a yield of ions $G(B^+) = G(B^-) \sim 0.24$ which is consistent with known free-ion yields for hydrocarbons.²⁹ A later section shows that detection of paired ions can account for the increased ion yield observed at -20°.

Possible routes for the formation of the solute triplet state in the radiolysis include³⁰ reactions IV-VIII.



For the photolysis only reaction VI is significant.

The reduction of triplet formation in radiolysis by electron scavengers which have little direct effect on triplets produced photolytically is a clear indication that at least 80% of the triplets which were formed in radiolysis did so by routes not available in photolysis. A contrary conclusion was reached by McCollum, Nevitt, and Wilson⁴ regarding naphthalene and anthracene in the same solvent, but without recourse to observations on ions or the effects of additives. The behavior with these solutes is not necessarily different from that of biphenyl. For example, no conflict is involved between our observations and those of McCollum, Nevitt, and Wilson if ion recombination leads first to singlet excited biphenyl and then by intersystem crossing to the triplet, *i.e.*, reactions VIII and VI. Removal of electrons by scavengers can interfere with these steps, *e.g.*, by competition from reactions IX and X. If the scavengers remove energetic (>2.8 eV)



electrons efficiently they can also interfere with reaction IV. Scavenging of positive charge may also interfere with triplet formation by reactions VI-VIII but not IV. However, the experimental evidence is not clear on this point.

The measured product $G_{\epsilon_D} = 67,000 \pm 3000$ for triplet biphenyl corresponds to $G(\text{triplet}) = 1.9 \pm 0.1$ on the basis of $\epsilon_D = 35,400$.³¹ This is equivalent to 60% conversion of all ion pairs to triplet if $G(\text{ion}) = 3$.

We found no indication of the growing-in of triplets as a result of the volume recombination of ions, but detection would be difficult because the mean lifetime of the observed ions was close to that of the triplet and the maximum amount which could be formed by this route was small (7% of total observed triplets on the basis of 60% conversion efficiency for free ions). Component Y cannot be identified with the triplets arising from volume recombination because this component persisted long after the ions had disappeared.

2. *Ion and Triplet Decay.* Various triplet decay processes have been described for solutions of this type.^{3b} The observed triplet decay is attributed to quenching by radicals generated by radiolysis or photolysis. The relatively long lifetime of the radicals results

(26) M. R. Ronayne, J. P. Guarino, and W. H. Hamill, *J. Amer. Chem. Soc.*, **84**, 4230 (1962).

(27) G. R. Freeman, *Advances in Chemistry Series*, No. 82, American Chemical Society, Washington, D. C., 1968, p 339.

(28) Based on the value $\epsilon_d = 12,500$ at 630 nm for B^- in methyl tetrahydrofuran²⁴ and the supposition that light absorption by B^+ is of the same magnitude as for B^- .

(29) W. F. Schmidt and A. O. Allen, *J. Phys. Chem.*, **72**, 3830 (1968).

(30) T. J. Kemp, J. P. Roberts, G. A. Salmon, and G. F. Thompson, "Proceedings of the Second Tihany Symposium on Radiation Chemistry," J. Dobo and P. Hedvig, Ed., Akademiai Kiado, Budapest, 1967, p 333.

(31) E. J. Land, *Proc. Roy. Soc., Ser. A*, **305**, 457 (1968).

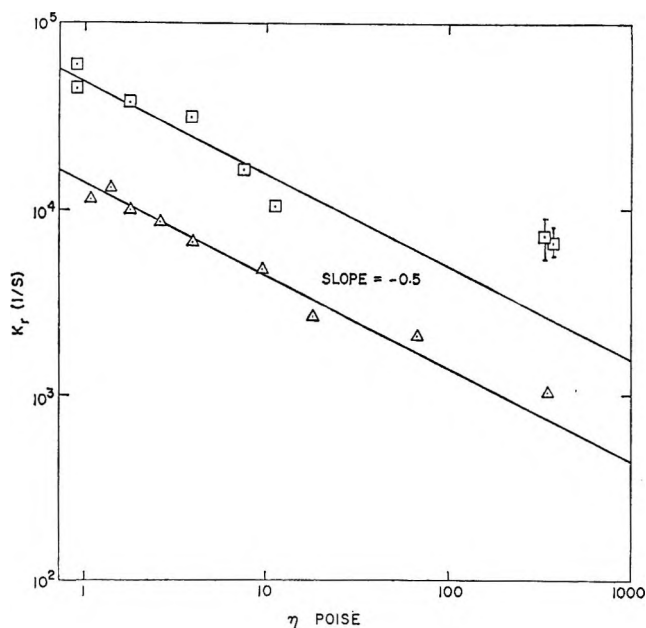


Figure 6. Ion recombination constant $k_2 = k_v/\epsilon D l$ (10/sec), \square , and triplet decay constant k_1 (1/sec), Δ vs. viscosity of 0.1 M $(C_6H_5)_2$ in LP (poises).

in pseudo-first-order kinetics of the decay. Triplet quenching in radiolysis is faster than in photolysis because of the greater number of reaction paths producing radicals and the consequent greater ratio of radicals to triplets.⁴ Thus the biphenyl triplet lifetime in radiolysis was 85 μ sec at 17° compared with 3 msec in photolysis.

Both the triplet quenching constant and the ion recombination rate constant exhibit curvature of the Arrhenius plot (Figure 4) which resembles the curvature of the corresponding viscosity plot as the glassy transition region is approached. In fact, the rate constants for both processes correlate with the -0.5 power of the viscosity into the region where the viscosity is rising very sharply with decreasing temperature as shown in Figure 6. A correlation with viscosity is to be expected if both reactions are diffusion limited processes but the -0.5 power is anomalous.

The rate constant for bimolecular diffusion-limited processes is obtained³² from eq 1, r_{ab} = separation

$$k_b = 4\pi r_{ab} D_{ab} C_s \quad (1)$$

distance of the molecular centers in the collision, $D_{ab} = D_a + D_b$ = the relative diffusion coefficient of the two centers (a, b), C_s = correction term to the Smoluchowski relation (where $C_s = 1$). The diffusion coefficient (D for individual center) is related to the friction coefficient f by Einstein's relation (eq 2).

$$D = kT/f \quad (2)$$

In the simple case where Stokes' law (eq 3) is applicable

to the molecular motion, eq 4 is obtained with $F =$

$$f = F/v = 6\pi\eta r \quad (3)$$

viscous drag force, v = velocity, r = radius of moving sphere, and η = viscosity (assuming equivalent centers with $r_{ab} = 2r$ and $D_{ab} = 2D$).

$$k_b = 8kT/3\eta \quad (4)$$

A correction factor for eq 3 to allow for discreteness of the molecular medium has been described by Gierer and Wirtz,³³ but the diffusion coefficient remains proportional to the viscous friction factor T/η . This inverse dependence on viscosity appears to be of general utility.¹²⁻¹⁵ In the case of ion recombination, the effective separation distance for reaction is given by the Onsager relation (5) (in dilute solutions), but the form of the viscosity dependence is unaffected.

$$r_v = e^2/\epsilon kT \quad (5)$$

r_v = critical ion separation for volume recombination, e = electronic charge, and ϵ = dielectric constant.

Anomalous viscosity dependence ($k \propto \eta^{-0.5}$) for triplet quenching in LP has been noted previously⁴ and attributed to a half-power dependence of the radical quencher concentration on viscosity. However, the details of this mechanism are not entirely self-consistent since a radical is required which has a lifetime that is short compared to the pulse duration and which also causes pseudo-unimolecular quenching. Similar viscosity dependence in ion recombination has been explained in terms of field dependent mobility of paired ions at small separation distances.² This mechanism does not apply to volume recombination of ions nor to triplet quenching. The anomalous behavior appears to be a general characteristic of diffusion-limited processes in viscous fluids. As suggested by Hilpern, Porter, and Stief,^{3a} it may be associated with the inapplicability of Stokes' law under these conditions. In essence the viscosity is related to solvent-solvent molecular interaction whereas the diffusion processes of interest are determined by solute-solvent interaction. In what follows we attempt to give quantitative expression to this concept.

3. Semiempirical Treatment of Viscosity-Diffusion-Temperature Correlations. From the many treatments of molecular transport in liquids¹³⁻¹⁵ we choose the semiempirical methods described by Bondi³⁴ as being the most appropriate for the transport properties for molecules which are too complex to be treated profitably by more rigorous methods. A principle of corresponding states is adopted, whereby the macroscopic properties of the liquid are expressed in dimensionless form in a

(32) A. M. North, "Collision Theory of Chemical Reactions in Liquids," Wiley, New York, N. Y., 1964, p 69.

(33) A. Gierer and K. Wirtz, *Z. Naturforsch., A*, **8**, 532 (1953).

(34) A. Bondi, "Physical Properties of Molecular Crystals, Liquids, and Glasses," Wiley, New York, N. Y., 1968.

manner which facilitates description by semiempirical relations common to large classes of liquids. The conversion factors for reduction to dimensionless form include measures of molecular size and molecular interaction energy which allow for the differences of these quantities for different liquids. A precise theoretical basis for these reducing factors exists for simple molecular fluids for which the form of the intermolecular potential function is invariant for the members of the class of fluids and for which the interaction is centrosymmetric.³⁵

In dimensionless form, the quantities of interest are the reduced viscosity η^* , reduced friction coefficient ζ^* and reduced temperature T^* given in Table IV. The values of the molecular parameters were calculated from the tables of group increments of molecular properties given by Bondi. A key parameter is E° , which is the measure of the molecular interaction energy and which is derived from latent heat of vaporization

ference between E° and E_s° which can account for the "anomalous" viscosity dependence of the diffusion limited processes.

The reduced viscosity follows the Vogel relation (eq 9) in the temperature region of interest, the constants B and A being approximately the same for all liquids.

$$\log \eta^* = \frac{B}{T^* - T_0^*} + \log A \quad (9)$$

The reduced friction coefficient follows a similar relation

$$\log \zeta^* = \frac{B'}{T^* - T_0^*} + \log A'$$

The ratio of these quantities may be expressed in the form of eq 10.

$$\frac{\log (\zeta^*/A')}{\log (\eta^*/A)} = \frac{B'/(T^* - T_0^*)'}{B/(T^* - T_0^*)} \quad (10)$$

Where ζ^* relates to diffusion of solvent molecules, the reduced temperatures in numerator and denominator of eq 10 are identical. Furthermore, as a matter of empirical observation, viscosity and solvent diffusion coefficient are proportional; therefore $B'/B = 1$. Where ζ^* relates to solute molecules the reduced temperatures in eq 10 are no longer the same in numerator and denominator because of the difference of energy parameter appearing in eq 8.

Converting back to ordinary quantities

$$\frac{\log T\delta/DA'}{\log \gamma\eta/A} = \frac{B'E_s^\circ zc}{BE^\circ z'c'}$$

i.e.

$$\log D = \log C - n \log \eta + \log T \quad (11)$$

or $D/T = C\eta^{-n}$, where $E_s^\circ = E^\circ$ value for solute

$$C = \frac{\delta}{A'} \left(\frac{A}{\gamma} \right)^n \quad (12)$$

$$n = B'E_s^\circ zc/BE^\circ z'c'$$

With appropriate changes of the constant C the same expression eq 11 applies for diffusion-limited rate constants with k_r ($k_r = k_b$ for neutral species, $k_r = k_v$ for ions) in place of D by substitution using relation 1. From the data in Table IV the value of the exponent n is 0.58 which is in satisfactory agreement with the data in Figure 6. (The change in the final $\log T$ term in (11) is negligible.)

The viscosity line in Figure 4 was obtained from a fit to the Vogel relation using $T_0 = -30^\circ$ based on the data in Table IV. Departures occur above 10° as the viscosity dependence passes over into the normal

Table IV: Transport Parameters

	Value for	
	LP	(C ₆ H ₆) ₂ in LP
$\zeta^* = N_0^{1/2}RTd_w/D(ME^\circ)^{1/2} = T\delta/D$		(6)
$\eta^* = N_0d_w^2/(ME^\circ)^{1/2} = \gamma\eta$		(7)
$T^* = zcRT/2E^\circ$		(8)
Quantity		
ζ^* = reduced friction coefficient		
d_w = average molecule thickness, Å	9.6	6.7
M = molar weight, g	390	154
E° = standard heat of vaporization, kcal/mol	32 ± 2	12 ± 1
= $\Delta H - RT$ at temperature where reduced density $\rho^* = 0.588$		
η^* = reduced viscosity		
z = number of nearest neighbors (molecules or "free" molecular segments) per molecule	10	10
c = $1/3$ number of external degrees of freedom per molecule (including rotation of chain links)	3.33	2.17
T^* = reduced temperature		
T_0^* = reduced effective glass transition temperature		
γ = constant defined by eq 7		
δ = constant defined by eq 6, poise ⁻¹		1.6×10^6

data. The value $E^\circ = 32 \pm 2$ kcal/mol for use in connection with properties of the solution was obtained by summation of group increments for various structures representative of the solvent. The solution was sufficiently dilute that correction for the solute was unnecessary in dealing with bulk properties. To extend the treatment to transport properties of solute species, the value $E_s^\circ = 12 \pm 1$ kcal/mol was used where applicable, based on biphenyl and corrected for low-energy CH₂ contacts in LP solution. It is the dif-

(35) R. M. Mazo, "Statistical Mechanical Theories of Transport Processes," Pergamon Press, Oxford, 1967, p 137.

Arrhenius form. The calculated curves for the ion ($k_r = k_v$) and triplet ($k_r = k_b$) decay constants in Figure 4 were obtained from relation 13 with T_0 as above; B_f the Vogel constant from the viscosity correlation; n calculated from (12) and the only disposable

$$\log(k_r/T) = \frac{nB_f}{T - T_0} + A_r \quad (13)$$

parameter A_r , a scaling factor chosen appropriately for the two decay curves.

Values of the viscosity exponent n in the range 0.6 to 1.0 have been reported² for quenching of various aromatic solute triplets in isopentane (IP) and propylene glycol (PG). The above treatment is consistent with these observations, the E° parameters being smaller for these solvents (7000 kcal/mol for IP) than for LP. The low values (0.6) for 1,5-dichloranthracene and 9-bromophenanthracene can only be accounted for if the quencher is a small weakly interacting atom or radical.

Exceptionally low values for n are anticipated where the solute-solvent interaction is very weak. Recent results for the electron-positive ion recombination in squalane³⁶ conform with this expectation. Detailed information on the viscosity dependence of electron reactions will permit an estimate of the short-range interaction energy of the electron with the solvent.

It is appropriate to note that the "free volume" theory of molecular transport of Cohen and Turnbull³⁷ is not applicable to the above problem as it stands because it contains explicitly the assumption that the diffusion coefficient is directly proportional to the fluidity ($1/\eta$). This assumption is not necessary for solute diffusion and with appropriate modifications a "free volume" treatment seems applicable. If one considers the energy parameter E° in the above analysis to be a measure of the energy required to form or redistribute the free volume, the two approaches are seen to be equivalent. Neither takes full account of molecular shape and the directionality of intermolecular forces.

4. *Paired Ion Lifetimes.* Combination of eq 1 and 5 gives Debye's relation (13a) for the ion recombination coefficient k_v for volume recombination of "free" ions.

$$k_v = \frac{4\pi e^2 D f_D}{ekT} \quad (13a)$$

The factor f_D allows for the effect of the counterion atmosphere on the potential due to an ion³⁸ and was in the range 0.5 to 1.0 under the conditions used. For ions, the friction factor f in (2) is obtained from the ion mobility u_\pm (u_+ or u_- according to ion) leading to the Nernst-Einstein and Langevin relations 14 and 15, respectively.

$$D_\pm/u_\pm = kT/e \quad (14)$$

$$k_v/u = 4\pi e/\epsilon \quad (u = u_+ + u_-) \quad (15)$$

The above relations 13-15 do not depend on the applicability of Stokes' law. From these and the measured ion recombination coefficients we obtain $D = 2 \times 10^{-6}$ cm²/sec and $u = 8 \times 10^{-5}$ cm²/V sec for biphenyl ions in LP at 20°. The value for D is an order of magnitude larger than that calculated from the Stokes-Einstein relation and three times larger than the value obtained after applying the Gierer and Wirtz correction. The discrepancies are even greater at lower temperatures and are accounted for in the preceding section.

As a first approximation the lifetime of paired ions is related to their separation distance³⁹ by the relation eq 16. From this we estimate that for a separation

$$t_r = \frac{\epsilon r^3}{uE} \quad (16)$$

distance of say, 40 Å, the recombination time for biphenyl ions in LP solution would be ~ 2 μsec at 20° and ~ 20 μsec at -20°. Thus paired ions of relatively small separation can account for the observed increase in initial ion yield at -20°. The effect of paired ions on the decay is to cause the observed recombination rate at -20° to exceed the volume recombination rate. Our failure to distinguish two contributions is associated with the low available pulse current and long pulse times.

Acknowledgments. We are grateful to C. F. Musick and R. B. Stewart for determination of viscosity and other data for liquid paraffin, and we thank Donna Wuschke for assistance with data processing. We are also indebted to A. Singh for valuable comments.

(36) H. A. Gillis and I. Taube, *J. Amer. Chem. Soc.*, **91**, 6507 (1969).

(37) M. H. Cohen and D. Turnbull, *J. Chem. Phys.*, **31**, 1164 (1959).

(38) P. Debye, *Trans. Electrochem. Soc.*, **82**, 265 (1942).

(39) F. Williams, *J. Chem. Phys.*, **48**, 4077 (1968).

A Far-Infrared Study of the Reaction of Phosphorus Oxychloride

Vapor with Ferric Chloride

by Eugene P. Scheide and George G. Guilbault

Department of Chemistry, Louisiana State University in New Orleans, Lakefront Campus, New Orleans, Louisiana 70122
(Received March 2, 1970)

A reaction cell specially designed for the study of chemisorption gas-solid reactions in the far-infrared is described. The far-infrared spectra of phosphorus oxychloride both before and after interaction with FeCl_3 are shown and assignments are made for all bands in the infrared spectra.

Introduction

Chemisorption reactions between gaseous ligands and metal or inorganic surfaces have received much attention in recent years¹⁻⁶ and infrared spectroscopy has been an invaluable tool in these investigations. Although the information obtained from the normal region of infrared is valuable in ascertaining what processes are occurring on the surface, other information is often needed to substantiate these results. Far-infrared spectroscopy can fulfill this need, especially when bonding occurs between a metal atom and some other atom. This is due to the fact that the infrared bands due to these types of vibrational modes appear in this region of the infrared spectrum, and not in the regular infrared region.

The present work describes an experimental technique for studying chemisorption reactions by use of far-infrared spectroscopy.

Experimental Section

A reaction cell which can be used to study chemisorption reactions by infrared spectroscopy has been previously described by the authors.⁷⁻⁹ The present study describes an extension of this experimental technique so that it can be applied to the far-infrared region.

The far-infrared cell (Figure 1) is of the same shape and construction as an ordinary gas cell, but with specially shaped windows made of high-density polyethylene. The windows were sealed onto the glass cell by machining them as close-fitting caps. Paraffin wax, when melted and applied around the outside of the window, provided the best seal. In this manner reaction pressures down to 10^{-4} Torr were obtained.

Reagent grade POCl_3 (Matheson Coleman and Bell) was further purified by degassing and redistilling several times on the vacuum line using the freeze-thaw method. Anhydrous reagent grade FeCl_3 was used without further purification.

The experimental procedure consisted of depositing a thin layer of FeCl_3 onto the inside surface of one of the cell windows, evacuating, and then exposing the

FeCl_3 surface to gaseous POCl_3 . The ir cell can be mounted in such a way as to extend the vacuum line into the ir sample compartment. In this way the reaction can be monitored by infrared continuously.

Results and Discussion

There has been much controversy and discussion concerning the bonding in complexes formed between POCl_3 and FeCl_3 . The two postulated reactions are shown below



With the use of infrared spectroscopy, it should be possible to differentiate between the two types of complexes formed.

When POCl_3 is allowed to react with FeCl_3 in solution,^{10,11} the infrared spectrum of the complex that is formed shows a large negative shift of the phosphoryl stretching frequency which indicates mechanism a and bonding between the metal and oxygen atoms.

There have also been reports^{12,13} of ion-pair formation, mechanism b, and it was to our interest to determine which mechanism occurred in the chemisorption

- (1) M. Courtois and S. J. Teichner, *J. Catal.*, **1**, 121 (1962).
- (2) R. M. Hammaker, S. A. Francis, and R. P. Eischens, *Spectrochim. Acta*, **21**, 1295 (1965).
- (3) E. P. Parry, *J. Catal.*, **2**, 371 (1963).
- (4) G. W. Poling and R. P. Eischens, *J. Electrochem. Soc.*, **113**, 218 (1966).
- (5) C. L. Angell and P. C. Schaffer, *J. Phys. Chem.*, **70**, 1413 (1966).
- (6) C. L. Angell and M. V. Howell, *ibid.*, **73**, 2551 (1969).
- (7) G. G. Guilbault, E. P. Scheide, and J. Das, *Spectrosc. Lett.*, **1**, 167 (1968).
- (8) S. J. DeLong and G. G. Guilbault, *ibid.*, **1**, 355 (1968).
- (9) G. G. Guilbault and J. Das, *J. Phys. Chem.*, **73**, 2243 (1969).
- (10) I. Lindquist, "Inorganic Adduct Molecules of Oxo-Compounds," Springer-Verlag, Berlin, 1963, and references therein.
- (11) J. C. Sheldon and S. Y. Tyree, *J. Amer. Chem. Soc.*, **80**, 4775 (1958).
- (12) V. Gutmann, *Rec. Trav. Chim. Pays-Bas*, **75**, 603 (1956).
- (13) H. Gerding and H. Houtgraaf, *ibid.*, **72**, 21 (1953).

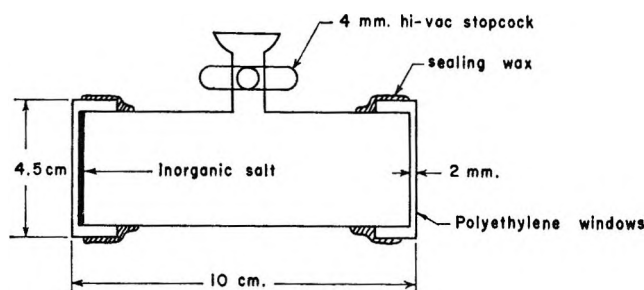


Figure 1.

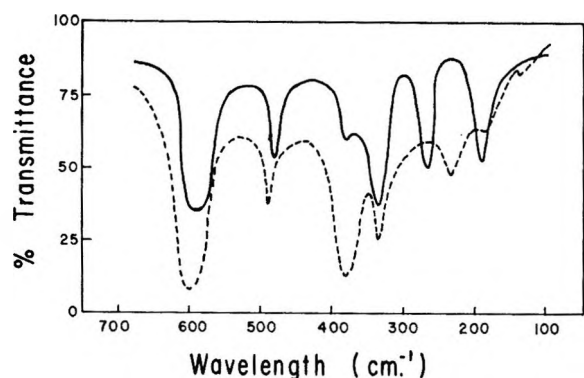


Figure 2.

reaction. Figure 2 shows the spectra of POCl_3 before and after interaction with FeCl_3 . The medium strength shoulder at 383 cm^{-1} in the spectrum of POCl_3 is attributed to be an overtone of the 191-cm^{-1} band, but upon complexation this band becomes very strong and has been assigned, first by Adams, *et al.*,¹⁴ and later by Driessen and Groeneveld,¹⁵ to the ν_3 mode of the tetrahedral ion FeCl_4^- . This accounts for the great increase in strength upon complexation and supports mechanism b. It is also evident that a shift of the P-Cl symmetrical deformation band from 268 cm^{-1} in the free POCl_3 to 236 cm^{-1} occurs after complexation. This negative shift would indicate a weakening of the P-Cl bond and the use of this Cl atom as a bridging atom as is implied by mechanism b. Finally, in the regular region of the infrared, instead of seeing a nega-

tive shift of the phosphoryl stretching frequency, a slight positive shift (from 1295 to 1300 cm^{-1}) and also an additional band at 1320 cm^{-1} are observed. A splitting on the high side of the P=O stretching band would indicate that the P=O bond is stronger in the complex than in the free state, instead of weaker as in a donor-acceptor complex of mechanism a.

From the evidence presented it can be concluded from far-infrared spectroscopy that the mechanism of formation of the $\text{FeCl}_3\text{-POCl}_3$ complex in solution is not the same one as in the chemisorption reaction and that a $\text{FeCl}_4^- \text{POCl}_2^+$ complex is formed in the chemisorption process (Table I^{16,17}).

Table I: Far-Infrared Bands and Assignments for POCl_3 before and after Interaction with FeCl_3

POCl_3 liquid	$\text{FeCl}_3\text{-}$ POCl_3	Assignment ¹⁶⁻¹⁷
587 (vs) ^a	600 (vs)	P-Cl asymmetrical stretch
481 (m)	490 (m)	P-Cl symmetrical stretch
383 (m, sh)	380 (vs)	In POCl_3 liquid, 191 cm^{-1} overtone, but in complex ν_3 of FeCl_4^-
334 (vs)	334 (s)	P-Cl asymmetrical deformation
268 (s)	236 (m)	P-Cl symmetrical deformation
191 (s)	195 (w)	P → O deformation
...	140 (vvw)	Tetrahedral $\text{FeCl}_4^- \nu_3$

^a vs = very strong, m = medium, vvw = very very weak, s = strong, w = weak, sh = shoulder.

Acknowledgment. The financial support of the Army Research Office (Grant No. Da-ARO-D-31-124-G906) is gratefully acknowledged.

(14) D. M. Adams, J. Chatt, J. M. Davidson, and J. Gerratt, *J. Chem. Soc.*, 2189 (1963).

(15) W. L. Driessen and W. L. Groeneveld, *Rec. Trav. Chim. Pays-Bas*, 87, 786 (1968).

(16) K. Nakamoto, "Infrared Spectra of Inorganic and Coordination Compounds," Wiley, New York, N. Y., 1963, p 112.

(17) M. L. Delwaille and F. Francois, *C. R. Acad. Sci.*, 220, 817 (1945).

Consecutive and Competing Metastable Ion Transitions in the Mass

Spectra of Monochlorophenols and Monobromophenols

by James C. Tou

Chemical Physics Research Laboratory, The Dow Chemical Company, Midland, Michigan 48640
(Received February 19, 1970)

The observed metastable ion corresponding to the transition $C_6H_5OX \cdot^+ \rightarrow C_5H_5^+$ in the case of monochlorophenols and monobromophenols was found to be a consecutive metastable ion for the transition $C_6H_5OX \cdot^+ \rightarrow C_6H_6O^+ + X \rightarrow C_5H_5^+ + X + CO$ (or $C_6H_5OX \cdot^+ \rightarrow C_5H_5X \cdot^+ + CO \rightarrow C_5H_5^+ + CO + X$). Hence, the mechanism involving ring-halogen rearrangement does not necessarily exist. The occurrence of the consecutive metastable ion is discussed in general in terms of the rates of decomposition.

Introduction

When an ion transition, $m_1^+ \rightarrow m_2^+ + (m_1 - m_2)$, occurs in the field-free region of a mass spectrometer, a diffuse metastable ion peak will appear in the mass spectrum.¹ The presence of a metastable ion peak has been used extensively by mass spectroscopists as direct evidence for one-step ion fragmentation.² However, Jennings³ reported that some of the metastable ions formed in the first free region between the ion source and the electrostatic analyzer (region 1) of a double focusing mass spectrometer decomposed further in the second field free region between the electrostatic analyzer and the magnet (region 2). These secondary metastable ions were termed as "consecutive metastable ions." Seibl⁴ also reported the necessity of the existence of such consecutive metastable ions for the explanation of the observation of some metastable ions which cannot be formed in a one-step process from the molecular ion without some unlikely skeletal rearrangements. Several studies⁵ of consecutive metastable ions have been carried out since then.

The consecutive metastable ion is very important in the interpretation of the ion fragmentation mechanism. It also provides an extra dimension for testing the validity of the quasiequilibrium theory of mass spectra.^{5b} In this study, we present another example of the observation of the so-called consecutive metastable ions. The importance of these ions in the elucidation of ion fragmentation mechanisms of monohalophenols is discussed.

Results and Discussion

The partial mass spectra of monochlorophenols and monobromophenols have recently been reported.⁶ The mass spectrum of *p*-chlorophenol is shown in Figure 1 as an example. In general, splitting off of small molecules such as CO and hydrogen halides, and/or radicals such as COH (or CO + H) and a halogen atom are involved in the fragmentation of the highly

excited molecular ion. The most intense fragment ion in the mass spectrum of a monohalophenol is the ion at m/e 65, which is confirmed to be $C_5H_5^+$ by high-resolution mass measurement. In the study of the generation of this ion by the defocusing metastable ion experiment,⁷ we have found three transitions. They are $93^+ \rightarrow 65^+ + 28$, $100^+ (102^+) \rightarrow 65^+ + 35 (37)$, and $128^+ (130^+) \rightarrow 65^+ + 63 (65)$ in the case of monochlorophenols, and $93^+ \rightarrow 65^+ + 28$, $144^+ (146^+) \rightarrow 65^+ + 79 (81)$, and $172^+ (174^+) \rightarrow 65^+ + 107 (109)$ in the case of monobromophenols. The ions at m/e 93 and 100 of monochlorophenols and those at m/e 93 and 144 of monobromophenols were found to be generated directly from their respective molecular ions. About one-fifth of the ion intensity of the peak at m/e 144 is due to the ¹³C contribution from the ion, $C_5H_4Br^+$, m/e 143⁺.

As a representative case, the defocusing metastable ion mass spectra of *p*-chlorophenol are shown in Figure 2 for those transitions discussed above. From the above information, the fragmentation path (eq 1 and 2) in the generation of the ion at m/e 65 can be derived where X stands for chlorine or bromine atom. Reaction 2 occurs if the observation of metastable ions represents a one-step process. If we assume that little or no back activation energy is involved in the ion decomposition, the difference in the heat of reaction near

(1) J. A. Hipple, R. A. Fox, and E. V. Condon, *Phys. Res.*, **69**, 347 (1946).

(2) H. Budzikiewicz, D. Djerassi, and D. H. Williams, "Mass Spectrometry of Organic Compounds," Holden-Day, San Francisco, Calif., 1967.

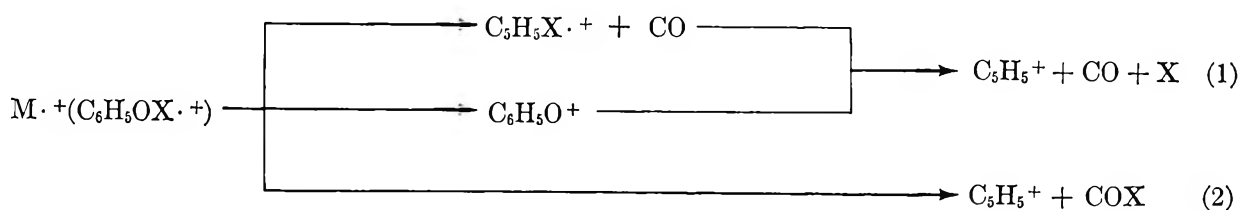
(3) K. R. Jennings, *Chem. Commun.*, 283 (1966).

(4) J. Seibl, *Helv. Chim. Acta*, **50**, 263 (1967).

(5) (a) U. Löhle and Ch. Ottinger, presented in 17th Annual Conference on Mass Spectrometry, Dallas, Texas, 1969, Paper No. 29; (b) L. P. Hills, J. H. Futrell, and A. L. Wahrhaftig, *J. Chem. Phys.*, **51**, 5255 (1969).

(6) T. L. Folk and L. G. Wideman, *Chem. Commun.*, 491 (1969).

(7) M. Barber and R. M. Elliott, Abstracts of papers of ASTM Committee E-14, 12th Annual Conference on Mass Spectrometry and Allied Topics, Montreal, 1964, p 150.



threshold, $\Delta H_1 - \Delta H_2$ for reactions 1 and 2 can be evaluated. In the case of monochlorophenols

$$\Delta H_1 - \Delta H_2 = \Delta H_{f\text{CO}} + \Delta H_{f\text{Cl}} - \Delta H_{f\text{COCl}}$$

where ΔH_f is the heat of formation. If the values of $\Delta H_{f\text{CO}} = 26.42 \pm 0.04 \text{ kcal mol}^{-1}$,⁸ $\Delta H_{f\text{Cl}} = 28.92 \pm 2 \text{ kcal mol}^{-1}$,⁸ and $\Delta H_{f\text{COCl}} = -4 \pm 3 \text{ kcal mol}^{-1}$,⁹ are used, then $\Delta H_1 - \Delta H_2 = 6.5 \pm 5 \text{ kcal mol}^{-1}$. From the thermodynamic point of view, reaction 2 requires even less heat than reaction 1 under our assumption and is therefore an energetically favored reaction.

If reaction 2 occurs in one step it must involve the rearrangement of the chlorine atom to the carbonyl group. This means that the chlorine atom on the aromatic ring of the molecular ion is labile and scrambles with the aromatic ring hydrogens. If reaction 2 is indeed a one-step process, this would be the first reported evidence for a halogen scrambling reaction. Scrambling of hydrogens on aromatic rings is well known in mass spectrometry.¹⁰

An alternative explanation for the existence of the metastable ion corresponding to the transition $\text{C}_6\text{H}_5\text{OX} \cdot^+ \rightarrow \text{C}_5\text{H}_5^+ + \text{COX}$, however, is that this metastable ion is due to a consecutive transition, which occurs in the field-free region, corresponding to reaction 1. This means reaction 2 is not a one-step process. If this explanation is correct, then the postulation of halogen atom scrambling on the aromatic ring is not necessarily true.

The technique of Jennings³ was used first and a CEC 21-110B mass spectrometer was employed. The metastable ion at m/e 42.25 was tuned in, using an accelerating voltage V_1 . This corresponds to the transition $100 \cdot^+ (\text{C}_6\text{H}_5\text{Cl} \cdot^+) \rightarrow 65^+ (\text{C}_5\text{H}_5^+) + 35 (\text{Cl} \cdot)$ in the mass spectrum of chlorophenol, which occurs in region

2. The accelerating voltage was then gradually increased to V_2 where a small peak appeared in the spectrum. This small peak corresponds to the above transition occurring in region 2 where m/e 100 is now

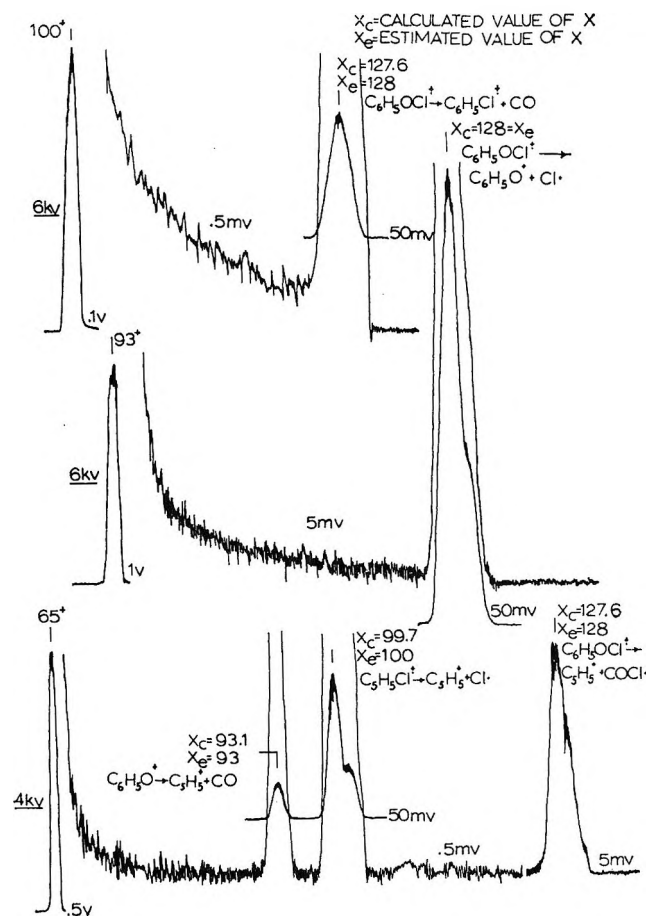


Figure 2. The defocusing metastable ion spectra for the transition of $\text{X}^+ \rightarrow \text{Y}^+ + \text{neutral}$ of *p*-chlorophenol, where $\text{Y}^+ = 100^+, 93^+, \text{ and } 65^+$.

a metastable ion formed in region 1. Experimentally, the mass of the precursor of the metastable ion from region 1, m/e 100, is calculated by $100 \times V_2/V_1$. In all of the cases concerning monochlorophenols the precursor of the region 1 metastable ion m/e 100 was found to be the molecular ion, m/e 128. Therefore, the small peak observed at the ion accelerating voltage V_2 is due

(8) "JANAF Thermochemical Tables," The Dow Chemical Co., Thermal Laboratory, Midland, Mich.

(9) L. C. Walker and H. Prophet, *Trans. Faraday Soc.*, **63**, 879 (1967).

(10) D. H. Williams, S. W. Tam, and R. G. Cooks, *J. Amer. Chem. Soc.*, **90**, 2150 (1968), and the references therein.

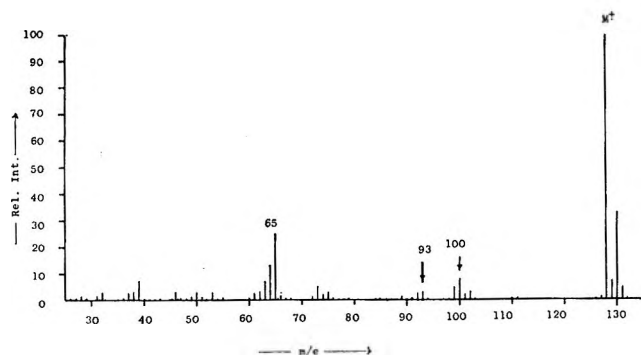


Figure 1. The mass spectrum of *p*-chlorophenol.

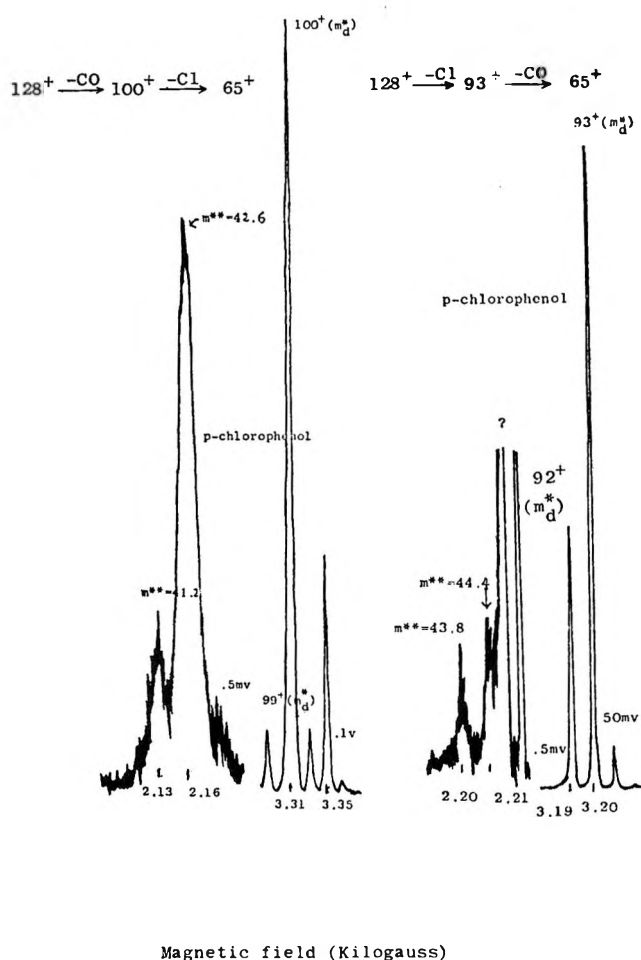


Figure 3. The observed consecutive metastable ions (m^{**}) for the listed transitions of *p*-chlorophenol; m_d^* = region 1 metastable ion.

to a metastable ion decomposing to yield another metastable ion. This is a direct observation of a "consecutive metastable ion" corresponding to reaction 1. This evidence unequivocally confirms that the metastable ion for the transition of $M^+ \rightarrow C_5H_5Cl^+ + CO$ can undergo further decomposition during analysis.

Because the intensities of some of the metastable ions in our study are very weak and are interfered with intense normal ion peaks, another technique was used in order to study all the consecutive metastable ions. The region 1 metastable ion for the transition of $C_6H_5OX^+ \rightarrow C_5H_5X^+ + CO$ (or $\rightarrow C_6H_5O^+ + X$) as shown in Figure 2 is tuned in by changing the accelerating voltage with fixed magnetic field, H_1 . When the magnetic field is scanned down to H_2 , a diffuse metastable ion peak appears at mass $m_{exptl}^* = m_{C_5H_5X^+}$ (or $m_{C_6H_5O^+}$) $\times H_2^2/H_1^2$, which corresponds to the transitions, $C_5H_5X^+ \rightarrow C_5H_5^+ + CO$ (or X) occurring in region 2. The detected consecutive metastable ions for the above transitions in the case of *p*-chlorophenol are shown in Figure 3. The theoretically calculated values and the experimentally determined values of the masses of the consecutive metastable ions

are listed in Table I. The discrepancies are mainly due to the inaccurate measurement of the magnetic field and the use of the approximation, $m/e = kH^2$.

Table I: The Observed Consecutive Metastable Ions (m^{**}) for the Reaction 1 in the Text

Reaction	Chlorophenol	
	$C_5H_5Cl^+ (100^+ \text{ and } 102) \rightarrow C_5H_5^+ (65^+) + Cl$	$C_6H_5O^+ (93^+) \rightarrow C_5H_5^+ (65^+) + CO$
m^{**}_{theor}	42.3 and 41.4	45.4
m^{**}_{exptl}		
ortho	43.9 and 42.3	44.1
meta	42.8 and 41.7	44.6
para	42.6 and 41.2	44.4
Reaction	Bromophenol	
	$C_5H_5Br^+ (144^+ \text{ and } 146^+) \rightarrow C_5H_5^+ (65^+) + Br$	$C_6H_5O^+ (93^+) \rightarrow C_5H_5^+ (65^+) + CO$
m^{**}_{theor}	29.3 and 28.9	45.4
m^{**}_{exptl}		
ortho	28.6 (not resolved)	44.9
meta	29.5 (not resolved)	45.2
para	29.0 (not resolved)	44.9

As noticed in Figure 3, some region 1 metastable ions with kinetic energy close to that of the tuned in region 1 metastable ion will also pass through the electrostatic analyzer but with less efficiency and are deflected by the magnetic field. Hence, these ions will be detected in the collector as the magnetic field is changed. This is why the isotopic ions of chlorine or bromine atom and the region 1 metastable ion of the transition $127^+ \rightarrow 92^+ + 35$ (or 36) and some other unidentified region 1 metastable ion (marked with question mark in Figure 3) were observed in the experiment. The isotopic pattern of the chlorine-containing consecutive region 2 metastable ion is well separated as shown in Figure 3 but that of the bromine-containing one is not. The region 1 metastable ions for the transition $(M-1)^+ \rightarrow (M-29)^+ + CO$ from the molecular ions, are also detected at m/e 99 in the case of monochlorophenols and at m/e 143 in the cases of monobromophenols. It was found that the relative intensities of the metastable ion peaks designated as m/e 99 ($127^+ \rightarrow 99^+$) and 100 ($128^+ \rightarrow 100^+$) for monochlorophenols are, as shown in Figure 3, approximately the same. The relative intensity of the similar peaks, m/e 143 ($171^+ \rightarrow 143^+$) and 144 ($172^+ \rightarrow 144^+$), in the case of *m*-bromophenol is much larger than that of *o*- or *p*-bromophenols. This reflects the differences in the relative intensities of the region 1 metastable ions corresponding to the above transitions. This is shown in Table II. Hence the bromine atom on the *meta* position of the phenolic ring affects the relative rates for the transition the most.

It was found⁶ that monobromophenols show intensive loss of bromine atom as contrasted to the competitive losses of chlorine atom and hydrogen chloride in the

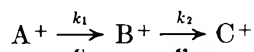
Table II: The Relative Intensities of the Region 1 Metastable Ions (m^*d) for the Transitions Shown

	$I_{m^*d,127^+ \rightarrow 92^+} / I_{m^*d,128^+ \rightarrow 100^+}$
Chlorophenol	
<i>ortho</i>	0.11
<i>meta</i>	0.10
<i>para</i>	0.09
	$I_{m^*d,171^+ \rightarrow 143^+} / I_{m^*d,172^+ \rightarrow 144^+}$
Bromophenol	
<i>ortho</i>	0.5
<i>meta</i>	2.1
<i>para</i>	0.6

case of monochlorophenols. This is also demonstrated in the present studies. In the case of monochlorophenols, both the intense region 1 metastable ion at m/e 92 ($128^+ \rightarrow 92^+ + 36$ or $127^+ \rightarrow 92^+ + 35$) and its consecutive metastable ion ($92^+ \rightarrow 64^+ + 28$) were observed. The calculated values of these consecutive metastable ions (43.5, 43.6, and 43.8) deviate from the expected value, 44.5, for the reasons stated previously. The relative intensities of these consecutive metastable ions among the three isomers differ according to those of their parent ions, which are the region 1 metastable ions. Because of the strong *ortho* effect,² the region 1 metastable ion of $128^+ \rightarrow 92^+$ (or $127^+ \rightarrow 92^+$) is much more intense than that of $128^+ \rightarrow 93^+$ in the case of *o*-chlorophenol. However, the region 1 metastable ions of $172^+ \rightarrow 92^+ + 80$ (or $171^+ \rightarrow 92^+ + 79$) are very weak in the case of monobromophenols and therefore their consecutive metastable ions are too weak to be detected. Only the region 1 metastable ion and its consecutive metastable ion, corresponding to the reaction sequence $C_6H_5OBr^+ \rightarrow C_6H_5O^+ + Br \rightarrow C_5H_5^+ + Br + CO$, were observed.

The above observations supports strongly that the observed region 1 metastable ion corresponding to the reaction $C_6H_5OX^+ \rightarrow C_5H_5^+ + ?$ is a consecutive metastable ion and is not necessarily generated from a one-step process. Hence reaction 2 is not likely to occur.

In terms of "Quasi-Equilibrium Theory,"¹¹ the reaction occurring in a mass spectrometer is a competing consecutive unimolecular rate process. For a hypothetical reaction series



the rates can be calculated as a function of internal energies, if the ion (ground state and activated state) structure parameters and activation energy, ϵ , are known. This is shown in Figure 4. The ions of A^+ with internal energy between ϵ' and ϵ'' will decompose with $\log k = 5-6.5$ (arbitrarily chosen) and yield the metastable ion corresponding to the transition $A^+ \rightarrow$

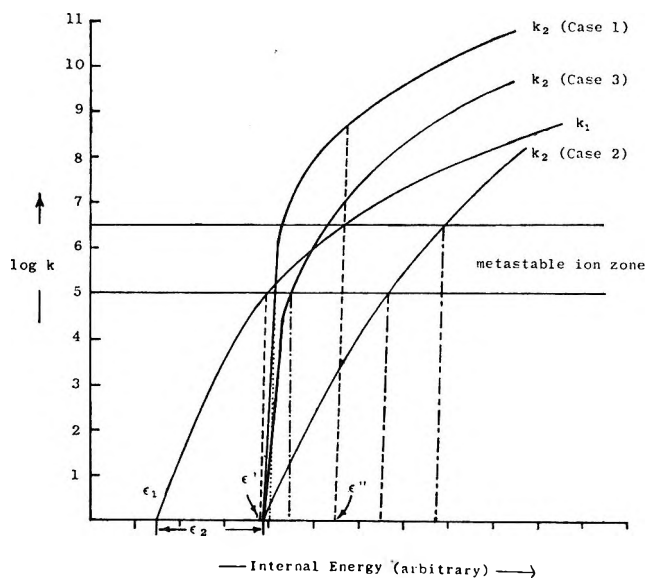


Figure 4. Internal energy-rate diagram for the generation of metastable ion and consecutive metastable ion.

B^+ . The internal energies of the metastable ion corresponding to $A^+ \rightarrow B^+$, thus range from $\epsilon' - \epsilon_1$ to $\epsilon'' - \epsilon_1$, if the neutral splitting off carries a very small amount of excess energy. This might be a good approximation for the case of the loss of small radicals, like $Cl\cdot$ or small molecules like CO . For the loss of a large neutral, statistical fluctuation of energy must be considered.^{12,13} Generally speaking, the upper limit of the energy that the metastable ion can have is $\epsilon'' - \epsilon_1$ when the molecular ion with internal energies between ϵ' and ϵ'' decomposes in the field-free region. Three cases of the rates for the reaction $B^+ \rightarrow C^+$ are considered here. The activation energy, ϵ_2 is arbitrarily chosen such that $\epsilon'' - \epsilon' \gg \epsilon_2 + \epsilon_1 - \epsilon'$. Case 1: the rates increase very rapidly with respect to internal energies near threshold, and the metastable ion energy window is very narrow. Hence, most of the metastable ions formed from the reaction $A^+ \rightarrow B^+$ will decompose rapidly to C^+ and thus an intense signal from the consecutive metastable ion should be observed. Case 2: the rates increase slowly with respect to energies and the metastable ion energy window does not overlap with that of reaction $A^+ \rightarrow B^+$. In this case, the metastable ion corresponding to $A^+ \rightarrow B^+$ with energies between $\epsilon' - \epsilon_1$ and $\epsilon'' - \epsilon_1$ will not have enough energy for further decomposition with rates $> \sim 10^5 \text{ sec}^{-1}$ and hence the consecutive metastable ion should not form. Case 3: this case is between the above two extremes. Only part of the metastable ions, corresponding to

(11) (a) H. M. Rosenstock, M. B. Wallenstein, A. L. Wahrhaftig, and H. Eyring, *Proc. Natl. Acad. Sci. U. S. A.*, **38**, 667 (1952); (b) J. C. Tou, L. P. Hills, and A. L. Wahrhaftig, *J. Chem. Phys.*, **45**, 2129 (1966).

(12) M. B. Wallenstein and M. Krauss, *ibid.*, **34**, 929 (1961).

(13) M. L. Vestal, *ibid.*, **43**, 1356 (1965).

$A^+ \rightarrow B^+$, will decompose to C^+ and hence the consecutive metastable ion as well as the metastable ion ($A^+ \rightarrow B^+$) should be observed.

Similar discussions can also be extended to the case of $\epsilon_2 < \epsilon' - \epsilon_1$. If $\epsilon_2 > \epsilon'' - \epsilon_1$, it is obvious that the metastable ion formed will not suffer further decomposition. Hence, the existence of the consecutive metastable ion is governed by the activation energy ϵ_2 and the shape of the energy-rate curve. The transitions studied here should belong to the third case, or possibly the first case if $1/2(\epsilon'' - \epsilon') \sim \epsilon_2 - (\epsilon' - \epsilon_1)$.

Most of the ion fragmentation reactions belong to case 2, or $\epsilon_2 > \epsilon'' - \epsilon_1$, where no consecutive metastable ion is observed, but the metastable ions for each step are detected. The strong metastable ion peak observed in the mass spectrum of ergosterol,⁴ corresponding to a loss of 33 mass units from the molecular ion, must fall into the case similar to case 1. Seibl⁴ reported that the generation of this metastable ion was a two-step process of consecutive splitting of water and methyl radical, based on the structure requirement.

Conclusion

The observed region 1 metastable ion corresponding to the transition $C_6H_5OX^+ \rightarrow C_5H_5^+$ in the case of monochlorophenols and monobromophenols was found to be a consecutive metastable ion for the transition $C_6H_5OX \cdot \rightarrow C_6H_5O^+ + X \rightarrow C_6H_5^+ + X + CO$ (or $C_6H_5OX \cdot + C_5H_5X \cdot \rightarrow C_5H_5^+ + CO + X$). Reaction 2 might not exist. Care should be taken in using metastable ions as a means of interpreting ion fragmentation mechanisms. The observation of a metastable ion does not necessarily denote a one-step process. The relative intensities of the region 1 metastable ion peaks corresponding to the transition of $127^+ \rightarrow 99^+$ and $128^+ \rightarrow 100^+ + 28$ in the case of monochlorophenols are approximately the same. The relative intensity of the similar region 1 metastable ion peaks ($171^+ \rightarrow 143^+ + 28$ and $172^+ \rightarrow 144^+ + 28$) in the case of *m*-bromophenols is much larger than that of *o*- or *p*-

bromophenol. In the case of monochlorophenols, both the intense region¹ metastable ion for the transition, $128^+ \rightarrow 92^+ + 36$ (or $127^+ \rightarrow 92^+ + 35$), and its consecutive metastable ion ($92^+ \rightarrow 64^+ + 28$) were observed. However, similar transition, $172^+ \rightarrow 92^+ + 80$ (or $171^+ \rightarrow 92^+ + 79$) in the case of monobromophenols was found to be very weak and its consecutive metastable ion ($92^+ \rightarrow 64^+ + 28$) was not detected. This is attributed to the fact that monobromophenols show intensive loss of bromine atom as contrasted to the competitive losses of chlorine atom and hydrogen chloride in the case of monochlorophenols.

Experiments

The defocusing metastable ion mass spectrum was obtained by using a CEC 21-110B double focusing mass spectrometer. A fraction of the accelerating voltage and the output from the electron multiplier were fed into a Model 2D-2A X-Y recorder of L. F. Moseley Co. The fraction of the accelerating voltage was measured using a Model 705B digital voltmeter of Computer Measurements Co. The mode of the operation can be found elsewhere.¹⁴

In the studies of the consecutive metastable ion, the voltage drop across a resistor in series with the magnet coil to ground and the output from the electron multiplier were fed into the X-Y recorder. The magnetic field was read out from the gaussmeter provided with the instrument.

The electron energy was maintained at 70 eV and the sample was introduced into the mass spectrometer through a molecular leak from a 5-l. reservoir.

Acknowledgment. The author would like to extend his appreciation to Professor F. W. McLafferty and Drs. L. A. Shadoff, R. T. Iwamasa, and H. T. Hu for many valuable discussions and to Mr. J. Storey for his careful experimental work.

(14) J. C. Tou, L. A. Shadoff, and R. H. Rigterink, *Org. Mass Spectrom.*, **2**, 355 (1969).

Derivation and Interpretation of the Spectrum of the Dimer of

Acridine Orange Hydrochloride, Dilute Aqueous

Solution, and Oriented Film Studies^{1a}

by T. Kurucsev^{1b}

Department of Physical and Inorganic Chemistry, The University of Adelaide, Adelaide, South Australia 5001

and Ulrich P. Strauss

School of Chemistry, Rutgers, The State University, New Brunswick, New Jersey 08903 (Received December 23, 1969)

The visible absorption spectra of acridine orange hydrochloride dissolved in water and potassium chloride solutions have been determined at low dye concentrations. These were analyzed in terms of an assumed equilibrium in solution between monomeric and dimeric species of the dye molecules. The results were consistent with a simple dimerization equilibrium model that does not involve chloride ions. Visible absorption spectra for the two species and equilibrium constants for the dimerization process have been derived. With the support of dichroic spectra obtained on stretched polyvinyl alcohol films dyed with acridine orange the spectrum of the dimeric species has been interpreted in terms of exciton interactions of the strong coupling type between the molecules.

Introduction

Lamm and Neville² derived two distinct sets of monomer-dimer spectra for acridine orange hydrochloride from dilute salt-free aqueous solution studies. One set, obtained by assuming that the anion participates in the dimerization equilibrium, is similar to the corresponding set described earlier by Zanker³ and the dimer spectrum of this set may be discussed in terms of exciton theory as representing relatively weak coupling⁴ of the transition dipoles of the dye molecules. The second set, based on the assumption that anions are not involved in the process of dimerization of the dyes, resembles spectra predicted by exciton theory for dimers with much stronger coupling between their transition moments. Although the nmr studies of Blears and Danyluk⁵ indicated subsequently preference for the strong coupling model, more direct methods are available for deciding on the correct choice between the two possibilities. We determined the spectra of aqueous acridine orange hydrochloride solutions in the presence of various concentrations of potassium chloride and found that a unique set of spectra is obtained only by assuming that the chloride ions do not participate in the dimerization equilibria. It will be shown in this publication that the dimer spectrum derived finds a satisfactory interpretation in terms of the perturbation approximation of the strong coupling vibronic case developed by McRae.^{6,7}

Experimental Section

Acridine orange hydrochloride (Merck, Germany) was purified by a method described elsewhere.⁸ The

purified sample contained no divalent metal ion impurities in detectable amounts.

Spectrophotometry. A Cary Model 11 spectrophotometer was calibrated by cobalt ammonium sulfate solutions.⁹

For the measurements of dichroic spectra, appropriately mounted polarizing prisms were placed in each of the reference and sample compartments. The instrumental response was found to depend on the polarization of the incident light. The prisms used were air-spaced Glan-Taylor types (Crystal Optics, Chicago, Ill.).

Solutions. Stock solutions of the dye were made up in Teflon bottles by weight. Solutions for spectrophotometry were prepared directly in the spectrophotometer cells by the addition of dye stock solution from an Agla micrometer syringe (Burroughs Welcome,

(1) (a) This work was supported in part by a grant (65/15799) from the Australian Research Grants Committee to T. Kurucsev and in part by a grant (GM 12307) from the U. S. Public Health Service to U. P. Strauss. (b) On Study Leave from the University of Adelaide.

(2) M. E. Lamm and D. M. Neville, *J. Phys. Chem.*, **69**, 3872 (1965).

(3) V. Zanker, *Z. Phys. Chem.*, **199**, 225 (1952).

(4) W. T. Simpson and D. L. Peterson, *J. Chem. Phys.*, **26**, 588 (1957).

(5) D. J. Blears and S. S. Danyluk, *J. Amer. Chem. Soc.*, **89**, 21 (1967).

(6) E. G. McRae, *Aust. J. Chem.*, **14**, 329 (1961).

(7) E. G. McRae, *ibid.*, **14**, 344 (1961).

(8) R. W. Armstrong, T. Kurucsev, and U. P. Strauss, *J. Amer. Chem. Soc.*, **92**, 3174 (1970).

(9) National Bureau of Standards (U. S.) Circular No. 484 (1949).

Tuckahoe, N. Y.) to known quantities of water or salt solutions. Matched pairs of cylindrical silica cells were used. Adsorption effects became noticeable, particularly with the 10-cm cells after about 20 to 30 min of preparing the solution. All measurements reported here refer to initial absorbance measured. Measurements were carried out at room temperature, near 22°.

Stretched Films. A 5% solution of polyvinyl alcohol (J. T. Baker, fully hydrolyzed, Lot 2-838) in 3:1 water-ethanol was poured into lucite trays with removable sides. These were floated on mercury pools placed in desiccators. After drying, the films were cut up, soaked in dye solutions of various compositions, and dried in air protected from light on sheet glass. The dyed polyvinyl alcohol films were stretched and mounted for spectrophotometry by a method to be described elsewhere.¹⁰

Curve Fitting. Standard least-squares fitting procedures were used. Calculations were carried out on a Wang 370 calculating system.

Results

In solutions containing a large excess of chloride ions the dimerization equilibrium constant, K , is independent of the anion concentration even if the anions were involved in the dimer formation. For these solutions the basic equations applicable to the spectra at any wavelength lead to the following two equations

$$C_T M_T = C_1 M_1 + K M_2 C_1^2 \quad (1)$$

$$4K C_1 = -1 + (1 + 8K C_T)^{1/2} \quad (2)$$

where the C_i and M_i refer to molarities and absorptivities. The subscript T stands for total and the subscripts 1 and 2 for monomer and dimer, respectively. The procedure used by Lamm and Neville² and adopted here consists of determining a best value of K from a regression analysis of the data according to eq 1. For this analysis data referring to the maximum at 496 nm were used since these values may be determined with high precision from the spectra recorded and since the largest changes with dye concentration also occur at this wavelength. Accordingly, for the purpose of the regression analysis the inclusion of data referring to other wavelengths was deemed to be of little advantage.

The use of eq 1 and eq 2 resulted in identical monomer-dimer spectral resolutions for all the solutions studied, including those containing no added salt.¹¹ The spectra resolved are shown in Figures 1 and 2. The data analyzed and the dimerization constants obtained showing the expected ionic strength dependence are summarized in Table I. At very low dye concentrations by expanding eq 2 one derives an equation that may be used directly for the determination of monomer absorptivities by computing the leading term

$$M_T C_T = M_1 C_T - (2M_1 - M_2) K C_T^2 + \dots \quad (3)$$

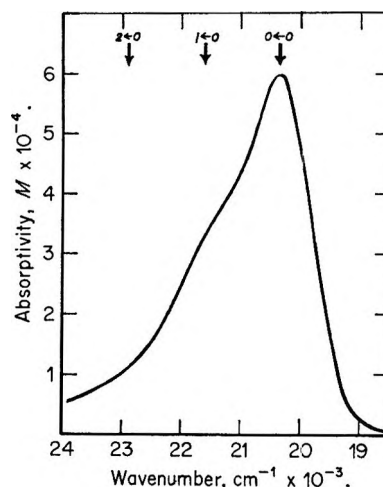


Figure 1. Spectrum of acridine orange monomer; arrows show positions of bands.

Some of the measurements (entry 2 of Table I, for example) were used for this purpose. In each case very good agreement was obtained with the monomeric spectral values derived from the analysis of the data by eq 1 and 2 of the more concentrated dye solutions. Standard errors given for the values of K in Table I were calculated from

$$\frac{[(M_1 \pm \Delta M_1) - M_T][2(M_1 \pm \Delta M_1) - (M_2 \pm \Delta M_2)]}{[2M_T - (M_2 \pm \Delta M_2)]} = KC_T \quad (4)$$

where ΔM_1 and ΔM_2 are the standard errors in the corresponding absorptivities obtained through the curve fitting of eq 1.

Table I: Experimental Conditions and Derived Dimerization Constants in Aqueous Acridine Orange Hydrochloride Solutions at 22°

Concn of KCl, M	Cell path length, cm	No. of soln used	Concn range of dye, $M \times 10^6$	$K \times 10^{-4}$
0	1 and 2	42	0.2-3.0	0.92 ± 0.04
0	10	30	0.03-0.16	
0.002	1	12	0.5-2.5	1.05 ± 0.06
0.02	1 and 2	39	0.2-2.4	1.25 ± 0.04
0.2	1 and 2	20	0.1-1.1	2.1 ± 0.2

Two representative results on the dyed polyvinyl alcohol films are shown in Figure 3. The absorbances, \bar{A} were calculated from the absorbances measured with the light polarized parallel, A_{\parallel} , and perpendicular, A_{\perp} , to

(10) T. Kurucsev and J. R. Zdysiewicz, manuscript in preparation.

(11) Conversely, the use of the anion participation model (appropriate equations given in ref 2) resulted in resolved spectra that changed significantly with the electrolyte content of the solutions and accordingly this incorrect model has not been considered further.

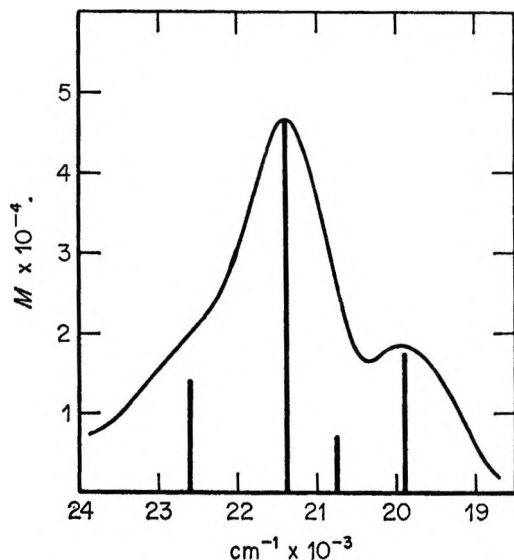


Figure 2. Spectrum of acridine orange dimer; thick vertical lines show the positions of, and are proportional to, the relative intensities of calculated transitions polarized along the long axis of the acridine ring.

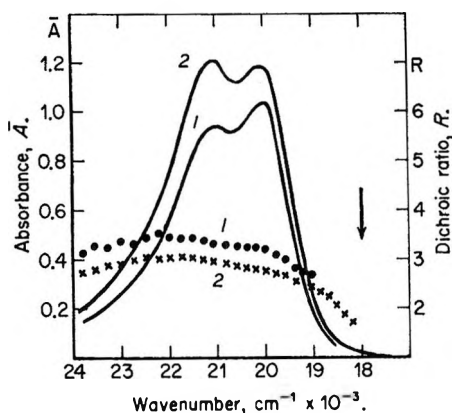


Figure 3. Spectra and corresponding dichroic ratios of dyed and stretched polyvinyl alcohol films: full lines; unpolarized spectra; dots and crosses, dispersion of dichroic ratios; for the meaning of the arrow see text.

the direction of the stretch according to the formula¹²

$$\bar{A} = (A_{\parallel} + 2A_{\perp})/3 \quad (5)$$

The differences in the absolute magnitudes of \bar{A} for the two spectra are due to the different thicknesses of the two films used. The shapes of the two spectra, when compared with spectra in solutions, suggest that in one of the samples (curve 1) about 30% of the total dye is in dimeric state, while for the other sample (curve 2) this figure is closer to about 45%.

The dichroic ratios, $R = A_{\parallel}/A_{\perp}$, for the two samples are also shown in Figure 3. As in the case of the absorbances, the differences between the absolute magnitudes of R of the two samples are of no significance from the point of view of this work. They are due to the different degrees of stretch to which the two samples were

subjected producing slight differences in the fractions of dye molecules oriented¹² in the polyvinyl alcohol matrix.

Discussion

The overall features of the spectra shown in Figures 1 and 2 are similar to the monomer and dimer spectra derived by Lamm and Neville² for acridine orange for the case of no anion participation. However, there are some significant differences. For example, isosbestic points were found at 474 nm and at or near 514 nm, compared with 470 nm and near 520 nm reported by Lamm and Neville; also the well-defined shoulder at around 22,500 cm^{-1} and the peak at 20,000 cm^{-1} shown in Figure 2 are absent in the dimer spectrum derived by the previous authors. The analysis of the spectra in this work has been confined to solutions where (M_T) the molar absorptivity at 496 nm was greater than about 48,000 since for more concentrated solutions the absorbance at 474 nm showed slight deviations from Beer's law. When solutions of these higher concentrations were included in the regression analysis of the data, the dimer spectrum derived agreed better with that shown by Lamm and Neville. Accordingly, it is probable that the differences in the dimer spectra referred to above may be attributed to the presence of some higher dye aggregates at the highest concentrations studied by Lamm and Neville.

It is now generally accepted^{13,14} that the transition moment associated with the absorption band studied is parallel to the long axis of the acridine ring system. The stretching of a polyvinyl alcohol matrix would be expected to produce partial alignment of the dyes embedded in this matrix with their long axes in the direction of stretch. Thus, as shown in Figure 3 such stretched films possess positive dichroism ($R > 1$). From the dichroic spectrum obtained the following important conclusion arises. In its simplest form exciton theory¹⁵ would assign an essentially "sandwich" type structure to the dimer on the basis alone that the most intense dimer transition is at higher energies than the monomer peak. However, on the basis of such a simple approach one might be led to assign a polarization perpendicular to the planes of the molecules to the dimer peaks that are red-shifted relative to the monomer maximum. As seen in Figure 3, except for the far red end of the spectrum, the dichroic ratios have essentially the same value right through the regions of appreciable absorption. Thus at least the more intense red-shifted dimer bands are polarized in the planes of the acridine system in the same way as the blue-shifted transitions.

(12) R. D. B. Fraser in "A Laboratory Manual of Analytical Methods of Protein Chemistry," Vol. 2, P. Alexander and R. J. Block, Ed., Pergamon Press, London, 1960, p 285.

(13) V. Zanker and J. Thies, *Z. Phys. Chem. (Frankfurt am Main)* **33**, 46 (1962).

(14) F. Dörr, *Angew. Chem.*, **78**, 457 (1966).

(15) For example, G. S. Levinson, W. T. Simpson, and W. Curtis, *J. Amer. Chem. Soc.*, **79**, 4314 (1957).

We found that the perturbation approximation described by McRae^{6,7} for the vibronic levels in the strong coupling limit leads to a satisfactory interpretation of the resolved dimer spectrum of acridine orange. A few details of the application of this theory to the system considered here are described in the Appendix. The calculated relative intensities of the dimer vibronic bands polarized in the plane of the molecules and their energy separations are illustrated in Figure 2 by the thick vertical lines. The energy calculated for each vibronic band has been reduced by the constant amount corresponding to 650 cm^{-1} . Since the theory does not take into account nonresonance interactions that would tend to lower the energy of the levels, this procedure may be considered to be justified as pointed out by McRae.⁷

From the application of this theory, one assigns to the resonance interactions an energy, ΔU , equivalent to about 3200 cm^{-1} . From Figure 1 the oscillator strength is estimated to be about 0.6 and using the dipole approximation¹⁶ the distance between the interacting dipoles is calculated to be about 4.2 \AA . In our opinion, the distance between molecular centers in the sandwich dimer is more likely to be the minimum van der Waals distance of 3.4 \AA . Accordingly the calculated figure of 4.2 \AA may indicate the breakdown of the dipole approximation in this case.

From the theory one can also calculate the position of the most intense transition that would be polarized perpendicular to the plane of the molecules in a sandwich dimer. This is indicated in Figure 3 by an arrow. Although the absorption in this region of the spectrum is very small, the observed drop in the values of the dichroic ratios at the far red end of the spectrum could be attributed to the presence of this transition.

Acknowledgment. We thank Dr. G. R. Bird of the School of Chemistry, Rutgers University, for reading and commenting on the manuscript.

Appendix

The knowledge of three molecular parameters is required for the application of the theory of McRae⁷ to the acridine orange dimer spectrum. One needs the energy separation between the vibrational levels of the monomeric upper electronic state, ν_1 , that of the ground state, ν_0 , and a constant M related to the harmonic oscillator properties of the molecule. The first of these parameters was obtained from the monomer spectrum shown in Figure 1 by assuming that each vibrational band has a Gaussian shape. This led to the approximate positions of the maxima in the monomer vibrational progression indicated in Figure 1. A similar analysis of the fluorescence spectrum¹⁷ of acridine orange resulted in an estimate for ν_0 . Finally, M was estimated from the intensities of the bands in the monomer progression, since $M^2 = I_{01}/I_{00} = 2I_{02}/I_{01}$ etc. where

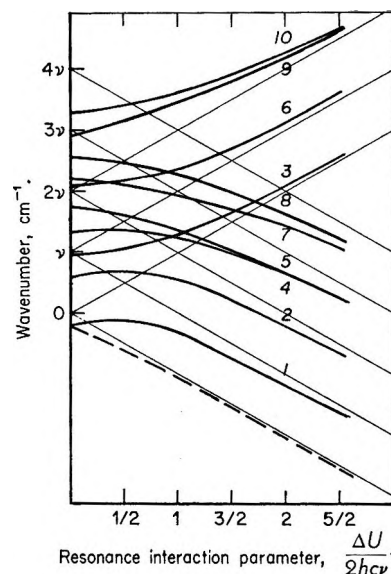


Figure 4. Energy level diagram for the A_u levels of acridine orange dimer: broken line corresponds to the lowest energy B_g level.

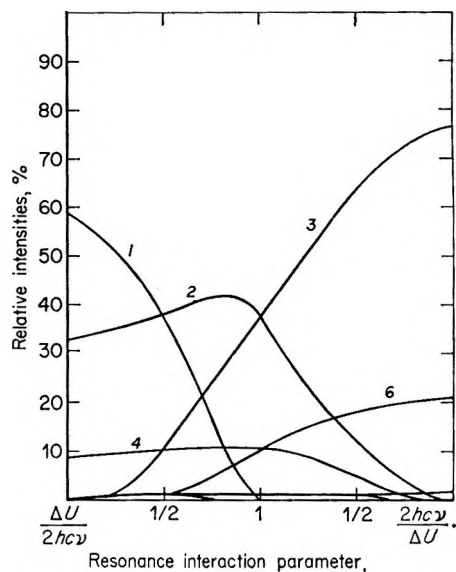


Figure 5. Relative intensities of transitions from ground state to the A_u levels of acridine orange dimer.

the I_{ij} are the intensities of the bands (i, j). The values used for the calculations were

$$\nu_1 = 1300\text{ cm}^{-1}$$

$$\nu_0 = 900\text{ cm}^{-1}$$

$$M^2 = 0.55$$

In the E-V coupling scheme the exciton wave functions are constructed from products of vibrational and electronic wave functions of the aggregates. Assuming

(16) For example, J. N. Murrell and J. Tanaka, *Mol. Phys.*, **7**, 363 (1963-1964).

(17) R. W. Armstrong, Ph.D. Thesis, Rutgers, 1970.

that the acridine orange dimer is a "sandwich" type of point symmetry C_{2h} , the allowed transitions polarized parallel to the long axis of the molecules involve EV functions that belong to the A_u representation. By solving the secular equations for first-order perturbation of degenerate levels we derived the zeroth-order wave functions for ten A_u levels of the ten lowest energy states for the hypothetical dimer with zero resonance energy, $\Delta U = 0$ and for the same levels at the points of resonance where the value of $\Delta U/2hc\nu$ equals $1/2$ or 1. Some of these functions have been listed by McRae.⁷ The parameter $\Delta U/hc\nu$ is used for convenience in presentation and ν is defined by $2\nu^2 = \nu_1^2 + \nu_0^2$.

The energies of the levels as a function of ΔU were calculated by second-order perturbation theory for $\Delta U = 0$ and for values of $\Delta U/2hc\nu$ greater than the region of resonance interactions, and the points were used to construct the smooth curves shown in Figure 4. This procedure leads to some ambiguity for the values of the energies at the lower regions of $\Delta U/2hc\nu$; however, the region of interest for the dimer spectrum considered in this case falls outside this range.

Absorption intensities as a function of ΔU were calculated, using the zeroth-order wave functions, from the overlap integral formula given by McRae⁷ at the points of resonance, at $\Delta U = 0$ and at $1/\Delta U = 0$ and drawing smooth curves through the points as shown in Figure 5. The numbering of the levels in Figures 4 and 5 is the same. It may be seen that the combined intensity contribution of the transitions to levels labeled 1, 2, 3, 4, and 6 constitutes 97% or more of the spectrum; accordingly the remaining five levels may be left out of consideration for this system.

For a sandwich dimer transitions to B_g energy levels are polarized perpendicular to the plane of the molecules. Since these are forbidden transitions we considered only one of the B_g levels. This is shown as a dotted line in Figure 4 and it would correspond to the highest intensity perpendicularly polarized transition.

Further information on the assumptions involved and on details of the calculations using this theory may be found in the papers of McRae^{6,7} or may be supplied upon request by one of the authors of this paper (T. K.).

On an Empirical Correlation between Nuclear Conformation and Certain Fluorescence and Absorption Characteristics of Aromatic Compounds¹

by Isadore B. Berlman

Argonne National Laboratory, Argonne, Illinois 60439 (Received February 12, 1970)

From an intercomparison of absorption and fluorescence spectra of a series of related compounds, it is deduced that certain spectroscopic parameters that depend on the conformation of a chromophore in its ground and first excited singlet state can be employed qualitatively as a spectroscopic "straightedge." As the nuclear conformation of a chromophore is made more planar and linear, the spectra become more structured, narrower, and positioned toward longer wavelengths, the Stokes loss becomes smaller, and the maximum value of the molar extinction coefficient, ϵ_{max} , becomes larger. Moreover, compounds planar in both the ground state and first excited states are generally more susceptible to excimer formation and/or concentration quenching than nonplanar compounds. The fluorescence and absorption characteristics of some of the analogs of biphenyl, certain indole derivatives, and several other compounds, are presented here as new data and are shown to be related to their nuclear topology. The configurations of many compounds in their ground state, as determined by other techniques, are used as standards of comparison for the spectroscopic data herein. Applying the above criteria to fluoranthene, it is predicted that this compound is nonplanar in its first excited singlet state.

Introduction

Fluorescence and absorption characteristics of an aromatic molecule can provide qualitative information concerning the conformation of the chromophore in the ground state, as well as the first excited state. The aim of this paper is to present an empirical correlation

between nuclear topology and spectroscopic data involving electronic transitions. To date, experimental information on the geometry of molecules in their ground state has been provided by diffraction (electron,

(1) Work performed under the auspices of the U. S. Atomic Energy Commission.

X-ray, and neutron), spectroscopic (microwave, infrared, and Raman), and dipole-moment techniques.² In a few cases,³⁻⁷ spectroscopic data of electronic transitions were used to determine the nuclear configuration, but generally only the absorption data, *i.e.*, the position, shape, and intensity of the absorption spectrum, were employed. Although theoretical work⁸ has provided some information on the equilibrium conformation of the excited state, there is no well-known experimental technique available to verify these results. Several articles have been published relating certain fluorescence parameters to conformation, but these publications have been concerned mostly with the explanation of anomalous results in terms of a change in conformation. Cherkasov and Voldaikina⁹ explain the diffuseness of the fluorescence spectrum of 9-vinylanthracene as being due to a change in configuration of a chromophore on excitation. In several cases^{10,11} an anomalously long lifetime has been explained by the following reasoning: a large intermolecular configurational change takes place during the lifetime of the excited state, resulting in a configuration that is unfavorable for the spontaneous fluorescence transition. In other words, the transition moment for absorption is different from the transition moment for emission. El-Bayoumi, *et al.*,¹² studied compounds that undergo a large increase in their static dipole moment on excitation and found that they have an anomalously short fluorescence lifetime. Evans and Leermakers¹³ used the characteristics of the fluorescence spectra to estimate the difference in conformation between ground and emitting excited states.

The fluorescence and absorption characteristics of a large number of aromatic compounds in solution have been measured and many have been published.¹⁴ An attempt is now made to correlate these data with the topology of a chromophore in the ground state, as well as in the excited state. Since π electrons are delocalized over the whole conjugated system, transitions involving π electrons, *i.e.*, π - π^* , are sensitive to changes in geometry of the system. Fluorescence is produced by π - π^* transitions from the lowest vibrational state of the first excited singlet state to any one of a manifold of vibrational states of the ground electronic state, and the long-wavelength absorption spectrum is produced by transitions from the zero-vibrational level of the ground state to various vibrational states of the first excited electronic state. Thus, specific characteristics of the fluorescence and the long-wavelength absorption processes are determined by the qualities of these two electronic states.

Materials and Procedures

The indole derivatives were made by Dr. H. O. Wirth and presented to Dr. D. Horrocks, who shared them with this author. A few grams of 3,4-benzo-

phenanthrene were given to me by Professor M. S. Newman and purified by Dr. J. Blum. The phenanthrene was purified by Pilot Chemical Co. and most of the other compounds were obtained from Aldrich Chemical Co. Our criteria for establishing the purity of our material are as follows: (1) the shape of the fluorescence spectrum is independent of the wavelength of the exciting radiation and (2) the fluorescence decay curve is composed of only one decay component.

Standard procedures¹⁴ are employed in making the measurements. Briefly, the fluorescence and absorption spectra of a compound in dilute, nitrogen-bubbled cyclohexane solution are recorded. The quantum yield Q is determined from the ratio of the areas of the fluorescence curve of the sample to that of 9,10-diphenylanthracene after proper adjustments are made as described in ref 14. The natural fluorescence lifetime τ_0 is computed from the data from both the fluorescence and absorption curves, according to the method of Strickler and Berg,¹⁵ rather than that of Förster described in ref 14. The fluorescence decay time τ is measured in a separate experiment. Stokes loss (in cm^{-1}) is determined from the energy difference between the 0-0 transition and the first moment of the fluorescence spectrum. Because the widths of the spectra of various compounds can vary by a factor of 2, a simple method is used to determine the relative breadth of each curve, namely measuring the full width (in cm^{-1}) at reciprocal "e" (FWRE) of the peak value. FWRE (F1) is a measure of the breadth of the fluorescence spectrum, and FWRE (Abs), that of the absorption spectrum. The measurement of a structured spectrum is inexact because it depends on an estimation of the wave number at which the curve has a value of 37% of the maximum. A better defined quantity, the statistical width W , is therefore also employed, and is defined by the equation

(2) P. J. Wheatley, "The Determination of Molecular Structures," Clarendon Press, Oxford, 1968, p 80.

(3) R. M. Hockstrasser, *Can. J. Phys.*, **39**, 459 (1961).

(4) H. Suzuki, *Bull. Chem. Soc. Jap.*, **33**, 381 (1960).

(5) H. H. Jaffe and M. Orchin, "Theory and Application of Ultraviolet Spectroscopy," Wiley, New York, N. Y., 1962, p 384.

(6) A. W. Jackson, *J. Org. Chem.*, **24**, 833 (1959).

(7) A. Heller, *J. Chem. Phys.*, **40**, 2839 (1964).

(8) H. Suzuki, "Electronic Absorption Spectra and Geometry of Organic Molecules; An Application of Molecular Orbital Theory," Academic Press, New York, N. Y., 1967, p 213.

(9) A. S. Cherkasov and K. G. Voldaikina, *Bull. Acad. Sci. USSR, Phys. Ser.*, **27**, 630 (1963).

(10) G. Briegleb, J. Trencseni, and W. Herre, *Chem. Phys. Lett.*, **3**, 146 (1969).

(11) J. B. Birks and D. J. Dyson, *Proc. Roy. Soc., Ser. A*, **275**, 135 (1963).

(12) M. A. El-Bayoumi, J. P. Dolle, and M. F. O'Dwyer, International Luminescence Conference, 1969, to be published.

(13) T. R. Evans and P. A. Leermakers, *J. Amer. Chem. Soc.*, **89**, 4380 (1967).

(14) I. B. Beriman, "Handbook of Fluorescence Spectra of Aromatic Molecules," Academic Press, New York, N. Y., 1965.

(15) S. J. Strickler and R. A. Berg, *J. Chem. Phys.*, **37**, 814 (1962).

Table I

	τ_0 , nsec	τ , nsec	Q	Stokes loss, cm ⁻¹	W_{SD} F1, cm ⁻¹	FWRE		ϵ_{max} l. M ⁻¹ cm ⁻¹	λ_{av} F1, Å
						F1, cm ⁻¹	Abs, cm ⁻¹		
Anthracene	12.5	4.9	0.36	1790	1346	3400	4000	9,800	4016
9,10-Diphenylanthracene	8.35	9.35	1.0	1820	1310	3750	4000	14,100	4282
3,4-Benzophenanthrene		76	0.12	2010	1317	3750			4010
Octamethylbiphenyl	(55)	23.6	0.18	1950	1326	3600	3900	930	2990
1,1-Diphenylethylene			0.003	3500	1666	4400			3154
1-Methyl-3,2-methylene- 2-phenyl indole	2.44	2.7	0.91	2450	1568	4100	5300	25,700	3740
1-Methyl-3,2-trimethylene- 2-phenyl indole	3.29	2.06	0.58	2860	1716	4900	5750	19,100	3738
Biphenyl	(2.3)	16	0.18	3310	1393	3750	6700	16,700	3160
Fluorene	13.5	10	0.80	1430	1147	2900		10,900	3135
Dibenzofuran	(3.48)	7.3	0.53	1900	1240	3050	4100	17,600	2990
Carbazole		16.1	0.38	1500	1173	3100		4,500	3490
Phenanthrene	373.5	57.5	0.13	1800	1342	3400		275	3670
9,10-Dihydrophenanthrene		6.6	0.55	2000	1441	3650		4,500	3225
1,3,6,8-Tetraphenylpyrene	2.28	2.67	0.90	1450	1304	3250	4150	39,700	4132
Fluoranthene	(15.2)	53	0.30	3900	1932	5500			4773
1,8-Diphenyloctatetraene	(3.7)	6.2	0.09	4300	1766	5150	4600	93,000	5277

$$W = [\bar{\nu}^{(2)} - \bar{\nu}^{(1)2}]^{1/2}$$

where $\bar{\nu}^{(1)}$ is the first moment of the spectrum $F(\bar{\nu})$ and $\bar{\nu}^{(2)}$ is the second moment, where

$$\bar{\nu}^{(n)} = \frac{\int \bar{\nu}^n F(\bar{\nu}) d\bar{\nu}}{\int F(\bar{\nu}) d\bar{\nu}}$$

W was not computed for the absorption spectra because of the frequent overlap of adjacent bands from other transitions.

The oscillator strength f of a transition is given by $f = A \int \epsilon d\bar{\nu}$ and an approximation is often made, that is $f \approx A \epsilon_{max} \Delta\bar{\nu}$, where A is a constant, $\bar{\nu}$ is the wave number, $\Delta\bar{\nu}$ is the width at half maximum of the long-wavelength absorption bands, and ϵ_{max} is the maximum value of the molar extinction coefficient ϵ . Values of ϵ_{max} , W , FWRE (F1) and FWRE (Abs), the latter a quantity proportional to $\Delta\bar{\nu}$, are assembled in Table I. Whereas ϵ_{max} is a function of the number of interacting π electrons, FWRE and $\Delta\bar{\nu}$ are not. In a comparison of bands of similar electronic origin in spectra of related compounds, it is frequently assumed that $\Delta\bar{\nu}$ is constant and f is proportional to ϵ_{max} alone. That such an assumption is inaccurate is seen in the large variation in FWRE (Abs) in Table I. For correct values of f , the integral should be employed.

If the strength of the fluorescence transition is equal to the absorption transition, $\tau/Q = \tau_0 \propto f^{-1} \bar{\nu}_0^{-2}$, where $\bar{\nu}_0$ is the wave number of the 0-0 transition. In all of the formulas in which τ_0 is computed by integrating over the long-wavelength absorption spectrum it is tacitly assumed that the strength of the fluorescence transition is equal to the absorption transition. If this assumption is true, the above relationship is expected to be correct, but if not, as for example when a

change in conformation takes place on excitation, then $\tau/Q \neq \tau_0$. In fact, τ and Q are the only measured parameters that are directly related to the fluorescence transition and are sensitive to changes in its strength.

A quantity λ_{av} is also presented for each fluorescence spectrum so that the relative positions of variously structured spectra can be compared. It is computed from the equation

$$\int_{\lambda_{min}}^{\lambda_{av}} F(\lambda) d\lambda = \frac{1}{2} \int_{\lambda_{min}}^{\lambda_{max}} F(\lambda) d\lambda$$

and represents the wavelength at which half of the total number of photons have smaller wavelengths and half, longer wavelengths. Although the definition of other parameters and symbols contained in the figures are not germane to the present discussion, they are retained for completeness and their definitions are given in ref 14.

Whereas the discussion above was concerned with the fluorescence and absorption characteristics of compounds in dilute cyclohexane solutions, mention is now made of the effect of the solute concentration on the intensity and shape of the fluorescence spectrum, the fluorescence decay time, etc. In the case of planar compounds, chromophores plus substituents, as the solute concentration is increased, the intensity and decay time of the monomer emission are both reduced by a process called self-quenching and/or a process called excimer formation (in which a new long-wavelength emission band is generated). The effects of both processes are proportional to the solute concentration. Since the radiative lifetime of excimer emission is generally longer than that of monomer emission, the emission decay curve from a solute containing excimers is usually composed of two components.

The magnitude of the error in each measurement is estimated to be as follows: the decay-time measurements <5%, quantum yield determinations about 10%, ϵ and ν_0 values, 5%.

Thesis and Examples

Certain correlations between conformation and spectroscopic data are well known:⁵ planar compounds that do not change their geometry on excitation generally have structured fluorescence and absorption spectra; nonplanar compounds generally have diffuse absorption spectra. Moreover, when the nuclear geometry of a chromophore in the ground state is made more planar, *e.g.*, by bridging, the absorption spectrum becomes more structured and red shifted, and the values of ϵ become larger. If the same chromophore is at the same time made more planar in the excited state, the fluorescence spectrum also becomes more structured and red shifted. On the other hand, when the nuclear topology is made more nonplanar, *e.g.*, by steric hindrance, the spectra becomes diffuse and blue shifted. As a rule of thumb, in a series of similar molecules, the larger the number of π electrons in a chromophore, the greater the shift to the red of the fluorescence and absorption spectra. Thus the characteristics of a planar chromophore can be interpreted as being due to the fact that in this configuration the number of functional π electrons is a maximum.

Somewhat less well known are the following: the width W of each spectrum and the Stokes loss become large when a change in conformation accompanies the electronic transition; the strength of the fluorescence transition as measured by Q/τ (where Q and ν are the fluorescence quantum yield and decay time, respectively) becomes larger with increased planarity; and the susceptibility to concentration quenching and excimer formation increases with the planarity of the whole molecule (chromophore and substituents). Thus the spectroscopic data can be related to the conformation of the main chromophore and the concentration studies to the conformation of the whole molecule.

It is our contention that the amount of structure in a spectrum depends on the planarity of the π system rather than its rigidity. Therefore, emphasis is placed on the correlation between spectroscopic data and planarity, not rigidity. Yet rigidity is important in maintaining a configuration on excitation or at least in restricting a change in configuration on excitation. In the present discussion a chromophore is considered rigid if there is no free or hindered rotation about a single bond by a component π system, such as a phenyl or vinyl group; and nonrigid, if there is rotation by such groups.

The emphasis of this study is on ring systems and not on the number and type of their substituents because the latter may introduce phenomena other than those of conformational changes. As an example, the subtle effects

of substituents are evident in the spectra of benzene derivatives. Whereas the fluorescence spectrum of benzene is structured, those of 1,3,5-trimethylbenzene and 1,2,4-trimethylbenzene are not.¹⁴ Whether this difference in the shape of the spectra is due solely to a modification in the amount and distribution of charge in the ring or is accompanied by changes in conformation on excitation (the substituted derivatives have a larger quantum yield for the formation of benzvalene and fulvene)¹⁶ is not known. Other substituents, *i.e.*, hydroxy and amine groups in phenol and aniline, respectively, modify the amount of charge in the ring and they also have structureless fluorescence spectra. Compounds with substituents will be used as examples but mainly to illustrate various phenomena related to conformation. A phenyl group is one of the most common types of substituent on scintillation materials. Because the ring system is generally prevented by steric hindrance from being coplanar with the main chromophore, a decision has to be made whether to include it as part of the functional chromophore in this discussion of the relationship between conformation and spectroscopic data. Our conclusion was that if the preferred angle between the plane of the ring and the plane of the chromophore is greater than about 60° so that the interaction between the two systems is small (the main effect being that the spectra are red shifted about 100 Å), the ring system (*s*) is not considered as part of the main chromophore; if the interplanar angle is less so that the interaction is greater, the ring system is considered as part of the active chromophore.

Spectroscopically, fluorescence compounds can be divided into five classes: those whose chromophores are (1) planar in the ground state and first excited state, (2) nonplanar in both states with the geometry preserved, in the main, on excitation, (3) nonplanar in the ground state and more planar in the excited state, (4) nonplanar in the ground state but more nonplanar in the excited state, and (5) planar in the ground state and nonplanar in the excited state. Whereas rigid and nonrigid chromophores can be in any of these classes, the majority of the rigid chromophores are found in the first two classes. The relative manner in which the absorption and fluorescence characteristics vary with respect to the conformation of a chromophore in its ground and first-excited, singlet state is tabulated in Table II.

Examples of the above classes are given below and some of their spectroscopic data are found in Table I. Anthracene¹⁴ is an example of a rigid compound that is planar in the ground state.¹⁷ Because the spectra are structured and narrow, and Stokes loss is small, it is inferred that this compound is also planar in the excited state (class 1). In solution, the fluorescence in-

(16) I. E. Denbesten, L. Kaplan, and K. E. Wilzbach, *J. Amer. Chem. Soc.*, **90**, 5868 (1968).

(17) V. C. Sinclair, J. M. Robertson, and M. A. Mathieson, *Acta Crystallogr.*, **3**, 351 (1950).

Table II

	Class 1 Planar both states	Class 2 Nonplanar both states	Class 3 Nonplanar-ground state planar- excited state	Class 4 Nonplanar-ground state more nonplanar- excited state	Class 5 Planar-ground state nonplanar- excited state
Absorption spectrum	Well structured Red shifted Narrow	Slightly structured Blue shifted Narrow	Diffuse Blue shifted Broad	Slightly structured Blue shifted Broad	Structured Red shifted Narrow
Fluorescence spectrum	Well structured Red shifted Narrow	Slightly structured Blue shifted Narrow	Structured Red shifted Narrow	Diffuse Red-shifted Broad	Diffuse Red shifted Broad
Mirror similarity	Yes	Sometimes	No	No	No
Stokes loss	Small	Small	Large	Large	Large
Concn sensitive	Yes	No	No	No	No
ϵ_{\max}	Large	Small	Small	Small	Large
Q/τ	Large	Small	Large	Small	Small
Example	Anthracene	3,4-Benzophen- anthrene	Biphenyl	1,1-Diphenyl- ethylene	Fluoranthene?

tensity is very sensitive to "self" quenching.¹⁸ When phenyl substituents are added to certain positions, *e.g.*, 9,10-diphenylanthracene,¹⁹ the concentration effects are completely eliminated. Jones²⁰ has estimated that in the ground state the plane of each phenyl group makes an angle of about 57° with the plane of the anthracene chromophore. Supporting evidence for this large angle is the small interaction between the two π systems and the resulting small red shift of the spectra,¹⁴ even though the substituents are positioned along the direction of the transition moment. The values of τ/Q for 9-phenylanthracene and 9,10-diphenylanthracene are about 30% larger than τ_0 obtained by integrating over the absorption curve, indicating that the strength of the fluorescence transition has become weaker than that of the absorption transition. For this to happen, either the phenyl rings assume a more perpendicular orientation with respect to the basic chromophore when the molecule becomes excited, or the anthracene chromophore becomes slightly warped. The former seems more likely.

Examples of nonrigid chromophores that remain planar in both states are rare. Most ring-chain systems such as *trans*-stilbene may be planar in the ground state, but apparently become nonplanar in the excited state^{21,22} (class 5).

The compound 3,4-benzophenanthrene (Figure 1) is an example of a rigid compound that is nonplanar in the ground state.²³ Because its spectra are slightly structured and narrow, Stokes loss is small, and it is relatively insensitive to concentration effects, it is presumed that this compound is also nonplanar in the excited state (class 2 or class 4). When this chromophore is made more planar by bridging, as in benzo[*ghi*]fluoranthene (Figure 2) (class 1), both spectra become more structured and are red shifted about 600 Å. Stokes loss and W remain small.

Octamethyl biphenyl²⁴ is a nonrigid compound that belongs to class 2 because it is nonplanar in both states.

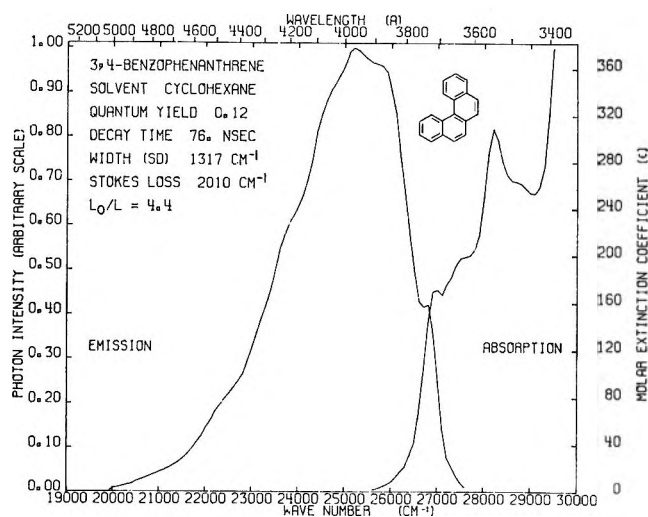


Figure 1. Spectra of 3,4-benzophenanthrene.

That the angle between the planes of the rings is so large that there is very little interaction between them is supported by the evidence that the fluorescence and absorption characteristics correspond to those of a single ring with alkyl substituents (*cf.* 1,3,5-trimethylbenzene in ref 14). Its absorption spectrum is slightly structured and narrow, and Stokes loss is small. Because each half of the molecule absorbs independently, the intensity of the absorption spectrum is about twice that of a single substituted ring. There is some interaction between the rings because the spectra are red

(18) H. Kallmann and M. Furst, *Phys. Rev.*, **79**, 857 (1950).(19) W. H. Melhuish, *J. Phys. Chem.*, **65**, 229 (1961).(20) R. N. Jones, *J. Amer. Chem. Soc.*, **67**, 2127 (1945).(21) P. Borrell and H. H. Greenwood, *Proc. Roy. Soc., Ser. A*, **298**, 453 (1967).(22) J. Saltiel, *J. Amer. Chem. Soc.*, **89**, 1036 (1967).(23) F. H. Herbstein and G. M. J. Schmidt, *J. Chem. Soc.*, 3302 (1954).(24) I. B. Berlman, *J. Chem. Phys.*, in press.

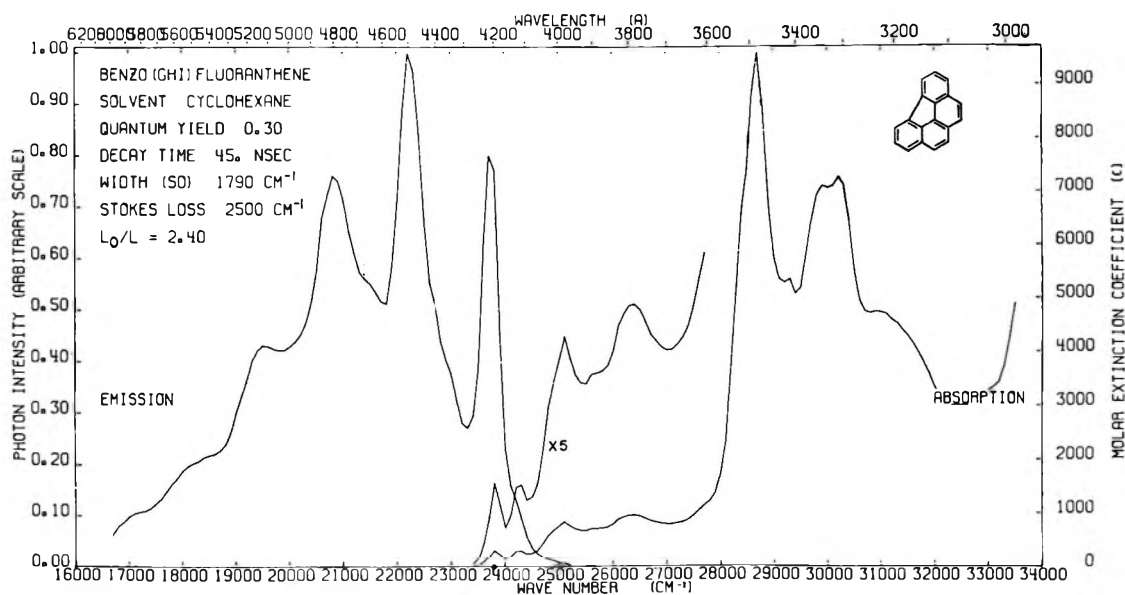


Figure 2. Spectra of benzo[ghi]fluoranthene.

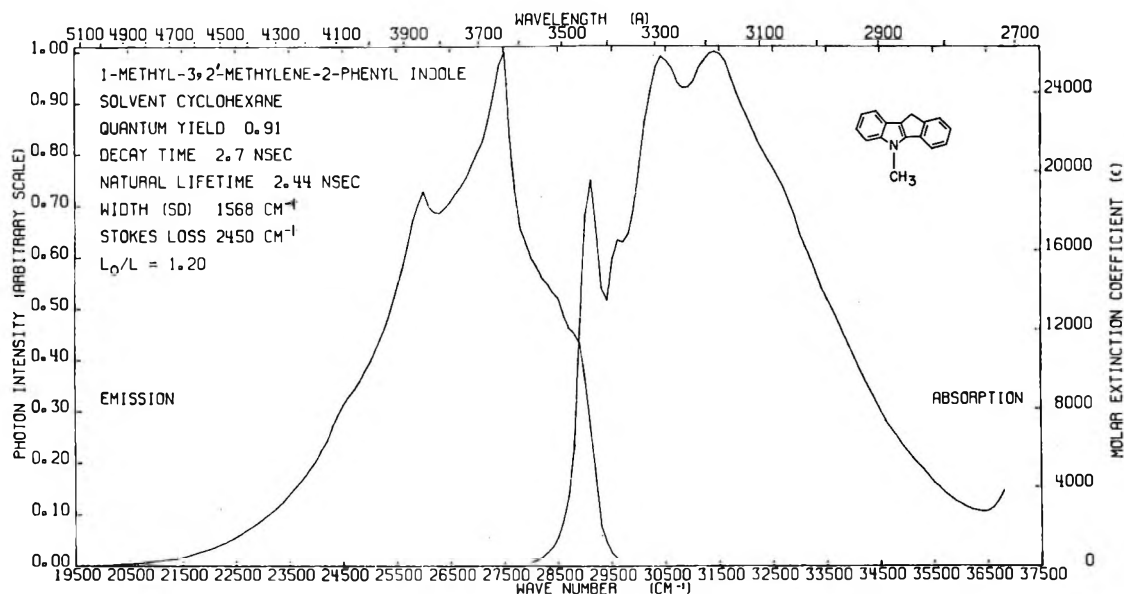


Figure 3. Spectra of 1-methyl-3,2'-methylene-2-phenylindole.

shifted with respect to alkyl-substituted benzene derivatives.

The compound 1,1-diphenylethylene is nonrigid and is made nonplanar in both states by steric hindrance. The angle between the plane of a phenyl ring and that of the ethylene bond is estimated²⁵ to be about 44° in the ground state. Because the spectra¹⁴ of this compound are diffuse, Stokes loss and FWRE (F1) are large, and the quantum yield is less than 0.01, it is conjectured that a large change in conformation takes place on excitation (class 4).

Compounds planar in the excited state generally have a larger quantum yield than related, nonplanar compounds. Thus, 1-methyl-3,2'-methylene-2-phenyl-

indole (class 1, Figure 3) which has the characteristics of being planar in both states has a quantum yield of 0.91, and 1-methyl-3,2'-trimethylene-2-phenyl indole (class 3, Figure 4) which has the characteristics of being nonplanar in the ground state and only slightly more planar in the excited state has a quantum yield of 0.58 (see Table I). (The latter of the above two compounds is also less sensitive to concentration quenching.²⁶) Moreover, *cis*-stilbene, whose rings in the ground state are about 30° out of plane, in a propeller configura-

(25) Reference 8, p 304.

(26) D. L. Horrocks and H. O. Wirth, *J. Chem. Phys.*, **49**, 2907 (1968).

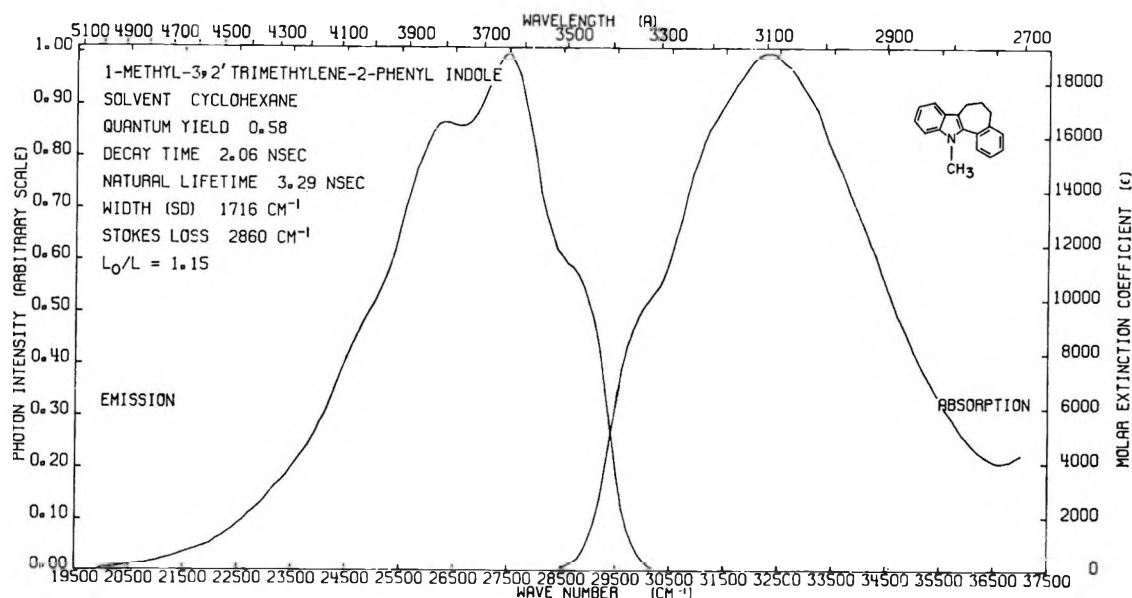


Figure 4. Spectra of 1-methyl-3,2'-trimethylene-2-phenylindole.

tion^{27,28} has almost zero fluorescence quantum yield at room temperature. Yet, phenanthrene (class 1), which can be considered a bridged and more planar analog of *cis*-stilbene, has structured spectra and a quantum yield of about 0.13. Triphenylene and *o*-terphenyl are similarly related compounds. The angle between the planes of adjacent rings of *o*-terphenyl in solution has been estimated²⁹ to be about 43°. Its absorption spectrum is diffuse and blue shifted,³⁰ and has a very small fluorescence quantum of less than 0.01.³¹ Triphenylene, which can be considered a bridged and relatively more planar analogue of *o*-terphenyl, has very structured spectra and a quantum yield of about 0.08.

Biphenyl is a nonrigid compound that belongs to class 3. Its absorption spectrum is diffuse and broad, the fluorescence is structured and narrow, and Stokes loss is large. All of the fluorescence characteristics of biphenyl, *i.e.*, the shape of its spectra, quantum yield, decay time, etc., are invariant over a concentration range from 0.1 to over 80 g/l. This immunity to concentration is characteristic of a molecule that is nonplanar in one or both of its states. Suzuki³² has estimated that in solution, the angle between the planes of the rings (in the ground state) is about 23°. Because the fluorescence spectrum is structured, it is inferred that this compound is relatively planar in the first excited state: The added resonance interaction between the rings in the excited state and the creation of some double-bond character in the coannular bond, are forces that coerce the rings into a more planar configuration.³³

When the rings of biphenyl are bridged as in fluorene,¹⁴ dibenzofuran (Figure 5), and carbazole,¹⁴ the spectra are structured and narrow, and Stokes loss is small—characteristic of compounds in class 1. Fluorene and dibenzofuran are sensitive to concentration,³⁴

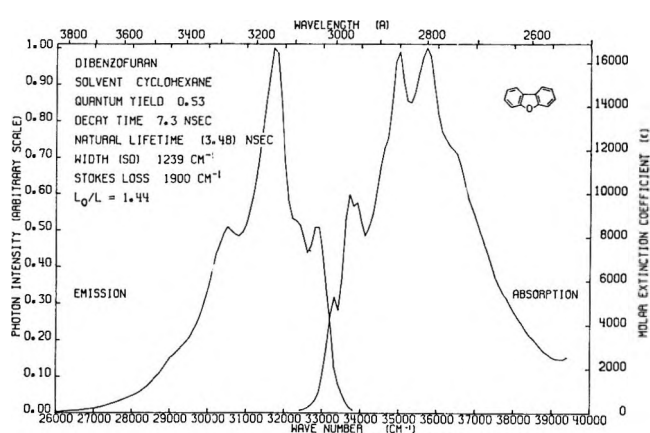


Figure 5. Spectra of dibenzofuran.

forming excimers, but the solubility of carbazole is too small to test for concentration effects. In 9,10-dihydrophenanthrene the rings are about 23° with respect to each other³⁵ (in the ground state) because the bridge joining them is larger than those of the above compounds. The absorption curve is structureless.²⁴ Because of the slight structure in the fluorescence spectrum it is assumed that the rings assume a more planar geometry in the excited state (class 3). Stokes loss

(27) D. L. Beveridge and H. H. Jaffe, *J. Amer. Chem. Soc.*, **87**, 5370 (1965).

(28) H. Suzuki, *Bull. Chem. Soc. Jap.*, **33**, 379 (1960).

(29) Reference 8, p 292.

(30) J. Dale, *Acta Chem. Scand.*, **11**, 650 (1957).

(31) Unpublished data.

(32) H. Suzuki, *Bull. Chem. Soc. Jap.*, **32**, 1340 (1959).

(33) Reference 5, p 339.

(34) D. L. Horrocks and W. Brown, *Chem. Phys. Lett.*, **5**, 117 (1970).

(35) G. H. Beaven, D. M. Hall, M. S. Leslie, and E. E. Turner, *J. Chem. Soc.*, 854 (1952).

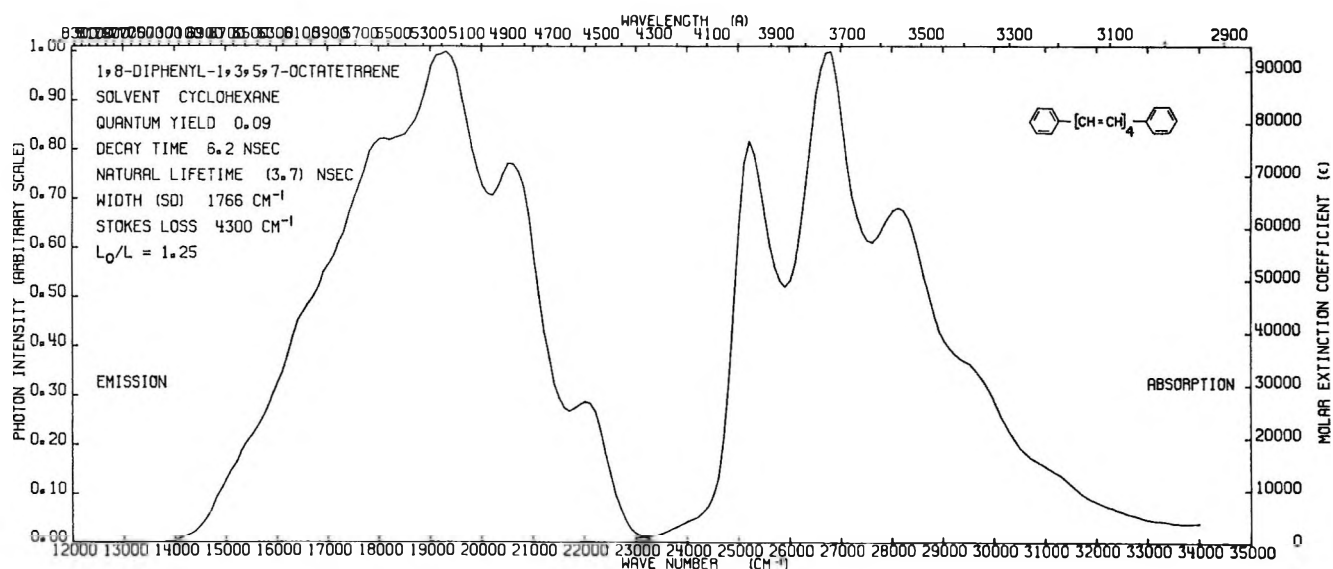


Figure 6. Spectra of 1,8-diphenyloctatetraene.

and W , although small, are nevertheless larger than those of the above-bridged biphenyl compounds (Table I). There is no evidence of concentration effects over a range from 0.1 to 20 g/l.

Ring-chain systems, such as *trans*-stilbene, 1,6-diphenylhexatriene,¹⁴ and 1,8-diphenyloctatetraene (Figure 6) have characteristics of members of class 5. Their absorption spectra are well structured and the absorption transitions are very strong (ϵ_{max} is large), indicating that at least in the ground state they are planar (all *trans* form). Yet, each of these has peculiar fluorescence characteristics. That *trans*-stilbene on excitation rotates with a finite probability into the *cis* form is well known.²⁷ The fluorescence decay time of the other two compounds is more than 10 times larger and the quantum yield is smaller than would be expected if the fluorescence transition were equal to that of the absorption. Independent studies of polarization by Anderson³¹ have shown that the fluorescence characteristics of the latter two compounds are not produced by a "hidden" transition. Therefore, it is assumed herein and in ref 9 that these large decay times are produced by molecules assuming various isomeric forms on excitation. In these forms, the fluorescence transition is much weaker than the absorption transition of the all *trans* form. The very broad spectra and large Stokes loss support this contention of a change in configuration on excitation. Förster³⁶ has also suggested that the large value of Stokes loss for 1,8-diphenyloctatetraene could be explained by a large change of the nuclear configuration on excitation.

Pyrene has been found to be slightly nonplanar in the crystalline state³⁷ but it was suggested by the authors of the above reference that this nonplanarity may be due to crystalline packing forces. The spectroscopic evidence appears to be that in solution it is relatively planar, the spectra are sharply structured and narrow,

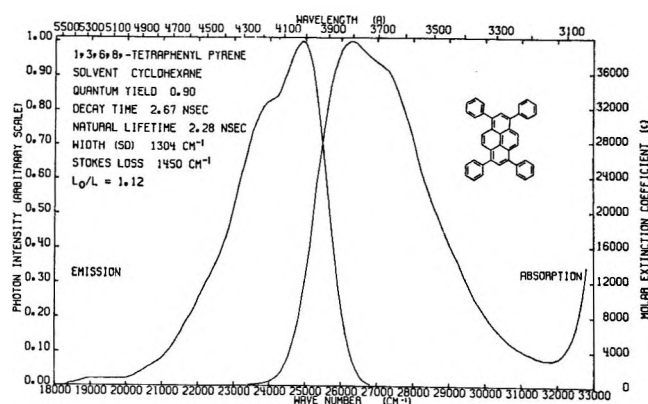


Figure 7. Spectra of 1,3,6,8-tetraphenylpyrene.

and Stokes loss is small. Pyrene is also very susceptible to excimer formation.³⁸ When phenyl substituents are added to certain positions, e.g., 1,3,6,8-tetraphenylpyrene (Figure 7), the concentration effects are either completely eliminated or drastically reduced. Whereas about 50% of the emission from a 0.1 g/l. solution of pyrene in cyclohexane is from excimers, there is no evidence of excimer emission from a 0.1 g/l. solution of 1,3,6,8-tetraphenylpyrene in benzene (approximately a saturated solution). The planes of the phenyl rings probably have a preferred angle of about 50° with respect to the plane of the main chromophore, when the latter is in the ground state, very much like that in 1-phenylnaphthalene.³⁹ In the excited state the phenyl groups probably make a larger angle with the pyrene chromophore because the ratio of $\tau/Q > \tau_0$.

(36) Th. Förster, "Floreszenz Organischer Verbindungen," Vandenhoeck und Ruprecht, Göttingen, 1951, p 136.

(37) A. Camerman and J. Trotter, *Acta Crystallogr.*, **18**, 636 (1965).

(38) Th. Förster and K. Kasper, *Z. Phys. Chem. (Frankfurt am Main)*, **1**, 19 (1954).

(39) B. Tinland, *Theor. Chim. Acta*, **11**, 385 (1968).

Fluoranthene was shown⁴⁰ to possess some anomalous spectroscopic characteristics. When the aforementioned diagnostic techniques are applied to this compound to provide some information concerning the conformation of this compound, it is observed that the absorption spectrum is structured, whereas the fluorescence spectrum is not, the Stokes loss and FWRE (F1) are abnormally large, and this compound is immune to concentration quenching and/or excimer formation from a concentration of 0.1 to over 100 g/l. Thus, it may be concluded that at least one of the states is nonplanar. Because the spectroscopic and X-ray⁴¹ data indicate that this compound is flat in the ground state, it follows that it must be warped in the first excited singlet state, *i.e.*, class 5. When sophisticated pulsed nmr measurements can be made on compounds that are simultaneously excited by a pulsed laser radiation, this contention and others made in this paper can be tested.

Discussion

Structureless spectra are also produced by inter- and intramolecular interactions such as hydrogen bonding, but these effects are strongly influenced by the solvent and are easily recognized. These studies are not included in the present discussion.

The effect of large solute concentrations on the fluorescence characteristics, whether in the formation of excimers or in self-quenching, depends on the diffusional close approach of two molecules so they can interact during the excitation lifetime, times of the order of 1 to 100 nsec. Temperature and solvent influence this diffusional process. Many theoretical studies⁴² on the mechanism(s) involved in excimer formation have been published but these will not be discussed. The inhibition of excimer formation and of self-quenching produced by large substituents or by a nonplanar chromophore is a purely steric one; they act as "bumpers" and prevent an interaction by inhibiting a close mutual approach.

Our results can be summarized as follows: a system planar in the ground state has a more structured ab-

sorption spectrum and larger values of ϵ than a similar nonplanar one. A chromophore planar in the excited state has a more structured fluorescence spectrum and larger fluorescence quantum yield than a similar nonplanar system. When there is no change in configuration on excitation, Stokes loss is small, the spectra are narrow, and $\nu/Q = \tau_0$. When a change in configuration does take place on excitation, Stokes loss is large, the spectra are relatively broad, and $\tau/Q \neq \tau_0$. If the change in topology on excitation is from a nonplanar to a more planar configuration, then the absorption spectrum is more diffuse and broader than the fluorescence spectrum. On the other hand, when the conformational change on excitation is from a planar or nonplanar to a less planar configuration, the absorption spectrum is more structured and narrower than the fluorescence spectrum. Theoretical justification for some of these statements may be found in ref 5 and 8.

Our limited results appear to indicate that when a phenyl substituent makes an angle of about 50° or larger with the main chromophore in the ground state, the angle becomes larger in the excited state. When the angle in the ground state is less than 25°, it becomes smaller in the excited state.

In conclusion, it may be stated that spectroscopic data can be used as a "straightedge" to provide qualitative evidence concerning the planarity of an aromatic chromophore in its ground and first excited singlet state.

Acknowledgment. The author would like to thank Dr. F. F. Rieke for his many valuable suggestions on the presentation of this paper and Dr. W. G. Brown for bringing ref 22 to his attention.

(40) I. B. Berlman, O. J. Steingraber, and H. O. Wirth, *J. Amer. Chem. Soc.*, **90**, 566 (1968).

(41) M. A. Lasher, *Acta Crystallogr.*, **17**, 1588 (1964).

(42) S. P. McGlynn, A. T. Armstrong, and T. Azumi, "Modern Quantum Chemistry," Part III, O. Sinanoglu, Ed., Academic Press, New York, N. Y., 1965, p 203.

Geminate Retention from Nuclear Isomeric Transition and Radiative Neutron Capture in Carbon Tetrabromide-Ethanol Solutions

by Gerald P. Gennaro and Kenneth E. Collins

Department of Chemistry, State University of New York at Buffalo and Research Department, Western New York Nuclear Research Center, Buffalo, New York 14214 (Received December 3, 1969)

Geminate retentions of radiobromine atoms activated by nuclear transformations have been measured in $\text{CBr}_4\text{-C}_2\text{H}_5\text{OH}$ solutions at low CBr_4 concentrations in the presence of iodine. At 21° the geminate retentions from the $^{79}\text{Br}(n,\gamma)^{80\text{m}}\text{Br}$ and the $^{80\text{m}}\text{Br}(\text{I.T.})^{80\text{g}}\text{Br}$ transformations and from the $^{81}\text{Br}(n,\gamma)(\text{I.T.})^{82\text{g}}\text{Br}$ transformation sequence are 0.19%, 5.0%, and 0.07%, respectively. The geminate retention from a singly converted isomeric transition is deduced to be 10%. The bases for these values are discussed in terms of the distances of fragment separation and the charging which accompanies a portion of the nuclear transformation events. Geminate retention for CBr_4 in CH_3OH solution is lower than in $\text{C}_2\text{H}_5\text{OH}$ solution while the geminate retention of CBr_4 in $n\text{-C}_3\text{H}_7\text{OH}$ solution is higher than either.

Introduction

In their study of the fate of recoil ^{80}Br atoms produced by radiative neutron capture in gas phase alkyl bromides, Gordus and Hsiung¹ found that less than 1% of the ^{80}Br atoms from the $^{79}\text{Br}(n,\gamma)^{80}\text{Br}$ process did not undergo C-Br bond rupture. In CBr_4 vapor scavenged by nitric oxide only $0.031 \pm 0.006\%$ of the ^{80}Br atoms failed to break their C-Br bonds. This small yield of ^{80}Br atoms in the parent bromide form was discussed in terms of the small but plausible likelihood that some fraction of these nuclei undergo deexcitation by γ ray cascades in which the angular distributions of the γ rays give a net recoil momentum less than that required for bond rupture.

The probability that a recoil ^{80}Br atom fails to rupture its C-Br bond following (n,γ) activation in a target CBr_4 molecule present in a condensed phase might be expected to be similar to the gas phase probability or perhaps even greater. For example, when the recoil energy of a bromine atom is not much greater than that required to break its C-Br bond, the wall of solvent molecules surrounding the affected CBr_4 molecule might absorb or dissipate some fraction of this kinetic energy, giving a contribution to the "probability of bond survival" which would not be present in the gas phase case. The solvent wall might also collisionally deexcite certain excited states of the parent bromide which would otherwise decompose or the solvent wall might tend to stabilize the parent molecular ion resulting from the nuclear transformation by giving favorable charge redistribution paths. Any loss in the recoil momentum attained by the recoiling atom or any deexcitation of the excited parent molecular ion would presumably tend to decrease the likelihood of bond rupture. In addition, secondary "caging" reactions, whereby parent-type molecules can be reconstructed from separated fragments after a bond rupture, might occur and thus obscure the measurement

of probability of bond survival in the condensed phase by giving higher values.

However, in contrast to the finite *gas phase* value of the bond survival probability¹ it has been reported that there is *no* retention of $^{80\text{m}}\text{Br}$ as parent $\text{CBr}_4(^{80\text{m}}\text{Br})$ in a 6.5×10^{-4} mole fraction (mf) liquid phase solution of CBr_4 in $\text{C}_2\text{H}_5\text{OH}$.^{2,3} In these experiments, CBr_4 was separated following neutron activation by precipitation with water.

These observations of *zero* retention in dilute $\text{CBr}_4\text{-C}_2\text{H}_5\text{OH}$ solution introduce the possibilities that some factors previously not considered, such as solvent molecules *assisting* in the rupture of the $\text{Br}_3\text{C-Br}$ bond (for instance, by reacting with an excited but intrinsically stable state of the CBr_4), may play a role in the hot atom chemistry of bromine atoms or that previous investigators were not concerned with yields as low as 1% or lower.

The work reported in the present paper was intended to examine whether the CBr_4 retention is indeed *zero* or whether it is a small but finite amount. Analytical methods capable of accurately determining yields of less than 0.1% were used. After establishing a nonzero value we then investigated the influence of various controllable parameters on the CBr_4 retention.

Experimental Section

Solutions. Solutions of CBr_4 in ethanol were prepared from redistilled absolute ethano (Pharmco) and resublimed CBr_4 (Eastman No. 1314). Resublimed iodine (Fisher No. I-37) was also added to most of the solutions. Solutions were freshly prepared in dim light for each experiment. Quantities (10 ml) were sealed in cleaned polyethylene vials, usually in the presence of air

(1) A. A. Gordus and C.-H. Hsiung, *J. Chem. Phys.*, **36**, 954 (1962)

(2) W. F. Libby, *J. Amer. Chem. Soc.*, **62**, 1930 (1940).

(3) R. M. Iyer and J. E. Willard, *Radiochim. Acta*, **7**, 175 (1967).

These samples were then shielded from light until they were analyzed following irradiation.

Neutron Irradiations. Neutron irradiations were conducted in the pneumatic conveyer of the Western New York Nuclear Research Center. The thermal neutron flux was $6 \times 10^{12} \text{ cm}^{-2} \text{ sec}^{-1}$ at a γ exposure dose rate of $1.0 \times 10^7 \text{ R hr}^{-1}$.

Temperature control during irradiation was obtained by preequilibrating samples at a desired temperature prior to irradiation, then rapidly placing the (insulated) samples into the irradiation position. The change during a 15-sec irradiation was less than 2° in all cases. When desired, samples were cooled to -78° after the irradiation and stored until analyzed. No effect of such storage was detectable for storage times of up to 3 days.

Analysis for $^{80\text{m}}\text{Br}$. When analyzing for $\text{CBr}_4(^{80\text{m}}\text{Br})$ resulting from the $^{79}\text{Br}(n,\gamma)^{80\text{m}}\text{Br}$ transformation, 300 mg of inactive CBr_4 was dissolved in 10 ml of the irradiated solution; then 2 ml of 1 *M* Na_2SO_3 was added to reduce the iodine to iodide. Ten ml of water was then added to precipitate most of the CBr_4 . After centrifugation the CBr_4 precipitate was transferred to a vacuum sublimation apparatus for purification. After weighing, the sublimed CBr_4 was dissolved in 95% carbon tetrachloride–5% acetone nonscintillating solution in a conventional polyethylene “liquid scintillation” counting vial for measurement of Cerenkov radiation from the daughter $^{80\text{g}}\text{Br}$ after $^{80\text{m}}\text{Br}$ – $^{80\text{g}}\text{Br}$ secular equilibrium had been established.⁴ For a reference value, the total $^{80\text{m}}\text{Br}$ activity was measured by taking an aliquot of a second $\text{CBr}_4\text{-C}_2\text{H}_5\text{OH}$ solution of the same CBr_4 concentration, but with no iodine added, which had been irradiated at the same time and at the same flux as the first solution. A liquid scintillation spectrometer (Packard Model 3375) was used to measure the Cerenkov radiation of the counting samples.⁴

Analysis for ^{82}Br . In the case where the $^{81}\text{Br}(n,\gamma)\text{-}(I.T.)^{82}\text{Br}$ transformation sequence was studied samples were stored, after a 15-sec irradiation, at the temperature of the irradiation until the $^{82\text{m}}\text{Br}$ (6.1 min) had decayed by isomeric transition. The $\text{CBr}_4\text{-C}_2\text{H}_5\text{OH}$ solutions were then stored at -78° until analyzed, during which time the ^{128}I (25 min) activity and $^{80\text{m}}\text{Br}$ (4.4 hr) activity had decayed. The analysis consisted of taking two 2-ml aliquots of the irradiated solution, one of which was used as a reference (100%) sample. CBr_4 was precipitated and purified from the other aliquot as in the $^{80\text{m}}\text{Br}$ analysis (above). The purified CBr_4 was then weighed and dissolved in $\text{C}_2\text{H}_5\text{OH}$ for counting. Both counting samples were counted integrally in a well-type $\text{NaI}(\text{Tl})$ scintillation counting system. Low activity samples were counted repetitively for 60-min periods to optimize counting statistics.

Analysis of $^{80\text{g}}\text{Br}$. To study the chemistry of the $^{80\text{g}}\text{Br}$ atoms resulting from the $^{80\text{m}}\text{Br}(I.T.)^{80\text{g}}\text{Br}$ trans-

formation, $^{80\text{m}}\text{Br}$ -labeled CBr_4 , prepared by sublimation purification of neutron irradiated solid CBr_4 , was dissolved in $\text{C}_2\text{H}_5\text{OH}$ (+ I_2) to give a solution of the desired composition. The solution was maintained at the desired temperature for about 4 hr while secular equilibrium between $^{80\text{m}}\text{Br}$ and $^{80\text{g}}\text{Br}$ was attained. Then two rapid purifications of the CBr_4 were made: either one precipitation followed by sublimation, as described above for the $^{79}\text{Br}(n,\gamma)^{80\text{m}}\text{Br}$ case, or two precipitations by addition of water to an ethanol solution of the CBr_4 . The purified samples were then rapidly dissolved in 95% carbon tetrachloride–5% acetone in a counting vial and transferred to the liquid scintillation spectrometer for measurement of the $^{80\text{g}}\text{Br}$ via its Cerenkov radiation. A record of the timing history of each sample was kept for calculation of a correction factor for the final measurement. Repetitive 1-min counts of the $^{80\text{g}}\text{Br}$ activity were made for a period of more than 4 hr to characterize the growing in of the $^{80\text{g}}\text{Br}$ daughter from the decay of the $^{80\text{m}}\text{Br}$ parent. The data were analyzed by means of a digital computer program which determined the relative amounts of $^{80\text{m}}\text{Br}$ and $^{80\text{g}}\text{Br}$ (as well as the relevant statistical errors in these quantities) at the time the counting was begun. A correction was then made, based on the timing history of the individual sample, to take into account the periods of time the $^{80\text{m}}\text{Br}(I.T.)\text{-}^{80\text{g}}\text{Br}$ transformation was taking place in the solid (precipitated) state and in the solution phase during the steps of purification. The parent retention for the isomeric transition occurring in the solid state at room temperature (21°) is 88%,⁵ while the corresponding parent retention in the ethanol solution is about 5% (this value is discussed later). Thus to determine the $\text{CBr}_4(^{80\text{g}}\text{Br})$ content of the CBr_4 at the moment of the initial separation it was necessary to correct for the loss of 12% of the new $^{80\text{g}}\text{Br}$ growing in from $^{80\text{m}}\text{Br}$ decay during the time the CBr_4 was present as reprecipitated solid and for the 95% loss of the new $^{80\text{g}}\text{Br}$ produced during the time the CBr_4 was in the solution step of the purification procedure. These losses occur when the non- CBr_4 activity is separated from the CBr_4 activity in the processes of purification. A small positive correction is thus made in the value of the $^{80\text{g}}\text{Br}$ computed to the starting time of the counting to give the value of the $^{80\text{g}}\text{Br}$ present at the moment of the initial precipitation.

Results and Discussion

Many types of reactions can accompany nuclear transformation events in liquid phase systems.⁶ These include several possible paths by which the activated atom may be incorporated into the parent-type mole-

(4) G. P. Gennaro and K. E. Collins, *J. Radioanal. Chem.*, in press.

(5) G. P. Gennaro, unpublished data.

(6) S. Goldhaber and J. E. Willard, *J. Amer. Chem. Soc.*, **74**, 318 (1952).

cule (in the present case, CBr_4). One such path is collisional deexcitation of intrinsically unstable excited states of the affected parent molecule, resulting in a failure to rupture the molecular bonds. Other possibilities involve breakage of bonds and the subsequent reassembly of the activated atom into a parent-type molecule. Bond breakage in the case of the CBr_4 parent molecules might give different sets of fragments, e.g., $\text{CBr}_3 + \text{Br}$, $\text{CBr}_2 + \text{Br}_2$, $\text{CBr}_2 + 2\text{Br}$, $\text{C} + 4\text{Br}$, etc. For reconstruction, such fragments would have to recombine. Other fragments containing atoms from the affected parent molecule might result from reactions of any of the above fragments with neighboring molecules yielding, for example, BrX or CBr_3Y , where X and Y are atoms or groups of atoms not present in the initially affected parent molecule. These new fragments might then undergo reaction with other species to yield CBr_4 as a product. Ionic fragments, such as CBr_3^+ or Br^- , might also play some role.

Thus, the incorporation of the activated atom into parent-type molecular form can be classified into three cases. Case I. All bonds of the initially affected parent molecule survive the nuclear transformation event; this is *probability of bond survival*. Case II. All atoms from the initially affected parent molecule are reassembled after bond rupture to give a parent-type molecule which necessarily contains the radio-activated atom. Case III. One or more atoms not part of the initially affected parent molecule enter into the assembly of a parent-type product molecule which contains the radio-activated atom. This classification relates to the measured quantity, the *parent retention*,⁷ as follows: in most instances, the measured retention in the parent molecular form is expected to include contributions of all three types. When the conditions of the experiment exclude contribution from Case III events (discussed below) the parent retention measurement represents the sum of Case I and Case II events. Case I events might similarly be obtained, in principle, under conditions which would also exclude contributions from Case II events.

The gross *parent retention*, consisting of radio- CBr_4 molecules from Case I + II + III events, is measured directly as the parent retention in $\text{C}_2\text{H}_5\text{OH}$ solutions having no scavengers added deliberately to interfere with Case III processes. In the present work the solvent $\text{C}_2\text{H}_5\text{OH}$ molecules themselves as well as the small concentrations of O_2 molecules and other impurity species in the air-saturated solutions can, presumably, interfere with some of the Case III processes; however, quantitative measurements of the radio- CBr_4 from the Case III processes are not of special interest in the present work; hence the gross parent retention, as measured, serves only as a qualitative indication of such processes.

The *geminate retention* is the parent retention obtained only from Case I + II events. We thus shall

use this expression for situations in which we believe Case III contributions are negligible.

In the $\text{CBr}_4\text{-C}_2\text{H}_5\text{OH}$ system the fragment species containing (or consisting of) the radio-Br atom from a nuclear transformation event can, in general, obtain other atoms to complete a CBr_4 molecule only from other fragments of the same parent molecule (Case II) or from other CBr_4 molecules it might encounter after thermal diffusion in the medium (Case III). Other bromine-containing species, initially present as impurities or introduced as radiolysis products from ambient radiations present at the time of the nuclear transformation events, might be present in low concentrations. The concentrations of such species must, however, be so small compared to the concentrations of CBr_4 and I_2 (when present) that their potential contribution to the production of radiobromine-labeled CBr_4 , even if they are very reactive, is expected to be negligibly small.⁸

Thus, to determine a value for the *geminate retention*, it is necessary to measure the parent (CBr_4) retention under conditions which minimize or eliminate the secondary (Case III) reactions with CBr_4 molecules from the bulk solution. These reactions might be due to CBr_4 molecules in the immediate vicinity of the nuclear event or far from that event. "Local" reactions of this type can be minimized by working at very low concentrations in an "inert solvent."^{2,9} In this context an "inert solvent" is one which cannot contribute atoms or groups of atoms to the assembly of parent-type molecules: $\text{C}_2\text{H}_5\text{OH}$ is considered to be "inert" since it contains no Br atoms to contribute to the formation of CBr_4 . Reactions of radio-Br species with CBr_4 molecules initially many molecular diameters away from the site of the transformation can be eliminated by the use of a suitable scavenger additive which will react with diffusing radio-Br species and thereby prevent diffusive radio- CBr_4 formation. Thus, if sufficiently dilute solutions are used and if iodine is, indeed, a suitable scavenger, Case III reactions will be essentially eliminated.

Figure 1 gives $\text{CBr}_4(^{82}\text{Br})$ -retention values obtained from air-saturated solutions of 6.5×10^{-4} mf CBr_4 (the same concentration used by Libby² and by Iyer and Willard³) containing various concentrations of scavenger iodine. The iodine decreases the parent retention, hence interferes with one or more Case III reac-

(7) *Parent retention* is that fraction (or percentage) of a nuclide product of a nuclear transformation which is in precisely the same chemical form as was the precursor nuclide prior to the transformation. In the present study the parent retention is the fraction of radiobromine atoms, resulting from nuclear transformation events occurring in bromine atoms of CBr_4 , that are subsequently found in radio- CBr_4 molecules.

(8) The ionizing radiation dose of 4×10^4 rads ($\sim 2.4 \times 10^{18}$ eV/g) accompanying nearly all neutron irradiations corresponds to less than one part in 10^4 of bromine atoms as radiolytic Br-products, assuming a $G(\text{Br-products})$ of 3.

(9) I. G. Campbell, *Adv. Inorg. Chem. Radiochem.*, 5, 135 (1963).

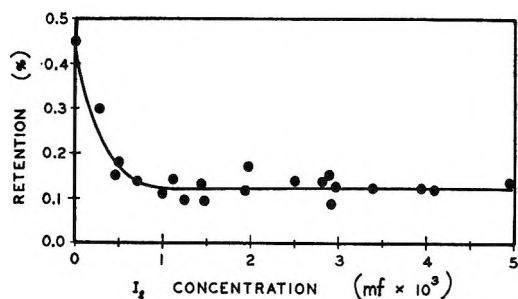


Figure 1. $\text{CBr}_4(^{82}\text{Br})$ retention as a function of iodine concentration. Concentration of CBr_4 , 6.5×10^{-4} mf.

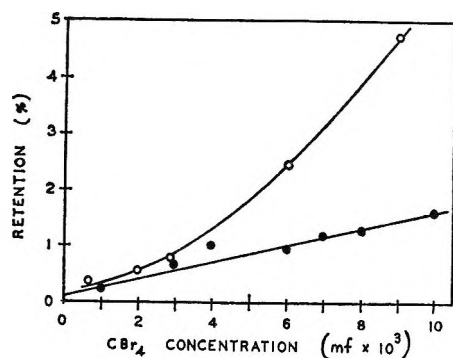


Figure 2. $\text{CBr}_4(^{82}\text{Br})$ retention as a function of CBr_4 concentration in the presence and absence of iodine scavenger: upper curve (O), no iodine present; lower curve (●), 0.002 mf iodine present.

tions (involving CBr_4 molecules) which otherwise would give radio- CBr_4 product molecules. The leveling off at concentrations greater than 10^{-3} mf indicates that these radio- CBr_4 -producing reactions are eliminated in these solutions by such concentrations of iodine.¹⁰ At a concentration of about 10^{-3} mf the iodine probably does not appreciably affect the *local* (Case II) reactions of the geminate fragments from the CBr_4 molecule directly involved in the nuclear transformation event occurring in one of its Br atoms. This is so because there is but a very short time (10^{-10} sec) available to the neighboring fragments in which recombination can occur before these fragments diffuse apart.¹¹ After diffusing apart, the radiobromine tagged species can react with iodine, oxygen, or perhaps a solvent molecule before it can encounter a CBr_4 with which it could react.

Since the radio- CBr_4 yield remains constant when the iodine concentration is increased by a factor of 6 (Figure 1) it is tempting to assume that all of the radio-Br species which escape geminate recombination have been prevented by the iodine from reacting with non-labeled CBr_4 to yield radio- CBr_4 . However, when the concentration of CBr_4 is changed it is seen (Figure 2) that iodine does not scavenge *all* of the diffusing radiobromine-containing fragments. The lower curve of Figure 2 shows that, at a constant iodine concentration of 0.002 mf, the radio- CBr_4 yield increases with CBr_4

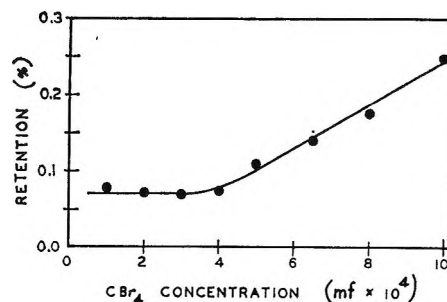


Figure 3. $\text{CBr}_4(^{82}\text{Br})$ retention from solutions of low CBr_4 concentration containing 0.002 mf of iodine.

concentration. Some of the diffusing radiobromine-containing species (fragments) appear to escape from their neighborhood of origin and from the scavenger iodine to form radio- CBr_4 by reaction with molecules of CBr_4 . A comparison of the upper (no I_2 present) and lower (I_2 present) curves of Figure 2 suggests that there are (at least) two routes whereby such radiobromine species can interact with CBr_4 molecules to form radio- CBr_4 . One of these routes is scavenged by iodine while the other is not. These different routes might be due to different radiobromine species (molecules, radicals, or ions) reacting with CBr_4 or I_2 . Alternatively, competing reactions of the same species with CBr_4 and I_2 might lead to the differences between the curves of Figure 2.

In her comprehensive study of solutions of cyclopentadienylmanganesetricarbonyl and dimanganesedecacarbonyl in organic solvents, Zahn¹² was able to measure geminate retention by extending the concentration range to such low values that the radiomanganese fragment species formed had no significant probability of reacting with another parent molecule. Similarly, Figure 3 shows that a limiting CBr_4 -retention value of 0.07% is obtained for CBr_4 concentrations below 4×10^{-4} mf. This limiting value is interpreted as the *geminate retention* for the $^{81}\text{Br}(n,\gamma)(\text{I.T.})^{82}\text{Br}$ transformation sequence in ethanol solutions at 21° .

Investigation of the temperature dependence of the $\text{CBr}_4(^{82}\text{Br})$ retention (in a 6.5×10^{-4} mf $\text{CBr}_4\text{-C}_2\text{H}_5\text{OH}$ solution containing 2×10^{-3} mf iodine) shows that the same retention, within experimental error, is obtained over the temperature range -78 to 21° . This lack of a significant temperature dependence over such a wide range implies either that there is a very small activation energy for the local reactions which contribute to the geminate retention or that the relevant *local* temperature is governed by the transient thermal "spike" from energy deposited by the nuclear transformation. The 10^{-10} sec lifetime of the high-temperature "spike"¹³

(10) In subsequent experiments 2×10^{-3} mf iodine was included as scavenger in all solutions.

(11) R. M. Noyes, *J. Chem. Phys.*, **22**, 1349 (1954).

(12) U. Zahn, *Radiochim. Acta*, **7**, 170 (1967).

(13) G. Harbottle and N. Sutin, *J. Phys. Chem.*, **62**, 1344 (1958).

Table I: Geminate Retentions as $\text{CBr}_4(^{82}\text{Br})$ from Solutions of CBr_4 in CH_3OH , $\text{C}_2\text{H}_5\text{OH}$, and $n\text{-C}_3\text{H}_7\text{OH}$ and Selected Physical Constants of the Solvents

Solvent	Geminate retention ^a (%)	Physical constants of solvent			
		Density ^b (g/mol at 20°)	Viscosity ^b (cP at 20°)	Mol wt ^b	IP, V
CH_3OH	0.05 ± 0.01	0.7914	0.579	32.04	10.85, ^c 10.97 ^d
$\text{C}_2\text{H}_5\text{OH}$	0.07 ± 0.01	0.7893	1.200	46.07	10.48, ^c 10.65 ^d
$n\text{-C}_3\text{H}_7\text{OH}$	0.19 ± 0.02	0.7796	2.256	60.09	9.98, ^c 10.42 ^d

^a Geminate retentions were obtained from the low ($<5 \times 10^{-4}$ mf) concentration portions of curves of $\text{CBr}_4(^{82}\text{Br})$ retention *vs.* CBr_4 concentration for solutions containing 2×10^{-3} mf iodine. Data based on triplicate determinations. ^b "Handbook of Chemistry and Physics," 44th ed, Chemical Rubber Publishing Co., Cleveland, 1963. ^c R. W. Kiser, "Introduction to Mass Spectrometry and Its Applications," Prentice Hall, Englewood Cliffs, N. J., 1965. ^d I. Omura, K. Higasi, and H. Baba, *Bull. Chem. Soc. Jap.*, **29**, 504 (1956).

may be sufficiently long to control most of the (thermal) reactions between the localized fragments before they diffuse apart.

Geminate retentions in CH_3OH , $\text{C}_2\text{H}_5\text{OH}$, and $n\text{-C}_3\text{H}_7\text{OH}$ are given in Table I. Each of these values was obtained from the limiting plateau of a parent retention *vs.* mf CBr_4 curve (*viz.* Figure 3) in CBr_4 -solvent systems containing 2×10^{-3} mf of iodine. Several relevant physical properties of these solvents are also listed. The density property appears to trend in the wrong direction to relate to an increasing effectiveness of the solvent in confining ("caging") the fragments. However, it might be argued that each of the remaining listed properties for the three solvents could account, at least qualitatively, for the observed differences.

If "caging" is important, the increase in viscosity would be expected to give an increase in geminate recombination, hence a higher geminate retention. However, the temperature coefficient of viscosity must also be considered; a change of greater than 10 in viscosity accompanies the change of temperature from 21 to -78° .¹⁴ Since no significant change in geminate retention occurred over this temperature range, this might be evidence that the viscosity is not an important controlling factor. A similar conclusion has been obtained from certain studies of recombination of fragments after photolysis in a wide variety of solvents.¹⁵ In the present case, however, the local "spike" temperature might well control the local "viscosity" to such a degree that the bulk viscosity of the solution at the ambient temperature is not directly relevant to the reactions which occur in the "spike" region.

The molecular weight of solvent might directly affect the resistance to separation of high-energy fragments, with the heavier molecules giving a sturdier "cage." This possibility has been discussed by Milman.¹⁶ Although the mass of solvent molecules is related to the bulk viscosity of the solution, the above-mentioned possibility that viscosity is not an important parameter, *per se*, may imply that the efficiency of a given solvent in "caging" high-energy fragments depends upon the

inertia of individual molecules but not on the collective (bulk) motions of these molecules.

Alternatively, the ionization potential of the solvent molecules, relative to that of CBr_4 , might be important in the determination of geminate retention; this point is discussed in detail later in conjunction with the possible reactions occurring as a result of the $^{80\text{m}}\text{Br}$ (I.T.)^{80g}Br transformation.

The value of $0.07 \pm 0.01\%$ for $\text{CBr}_4(^{82}\text{Br})$ retention in iodine-scavenged solution (Figure 3) is interpreted as *geminate* retention, with no significant contribution from secondary (Case III) processes. Geminate retention values, similarly obtained, for other nuclear transformations in ethanol solutions are given in Table II. Interpretation of the differences between the values obtained from the different nuclear transformations requires consideration of several factors. The following

Table II: Geminate Retentions of CBr_4 from Different Nuclear Processes in $\text{CBr}_4\text{-C}_2\text{H}_5\text{OH}$ Solutions. Concentration of CBr_4 ; 6.5×10^{-4} mf. Concentration of Iodine Scavenger; 2×10^{-3} mf

Nuclear process	CBr_4 retention, %
$^{79}\text{Br}(n,\gamma)^{80\text{m}}\text{Br}$	0.19 ± 0.01
$^{80\text{m}}\text{Br}(\text{I.T.})^{80\text{g}}\text{Br}$	5.0 ± 1.0 ^a
$^{81}\text{Br}(n,\gamma)(\text{I.T.})^{82\text{g}}\text{Br}$	0.07 ± 0.01

^a This value results from the *two* transitions which occur in this case. A value of 10% for the geminate retention from a *single* transition is discussed in the text.

(14) E. A. Moelwyn-Hughes, "Physical Chemistry," 2nd ed, Pergamon Press, New York, N. Y., 1961.

(15) K. Chakravorty, J. M. Pearson, and M. Szwarc, *J. Amer. Chem. Soc.*, **90**, 283 (1968).

(16) (a) M. Milman, *Radiochim. Acta*, **2**, 180 (1964). (b) We are grateful to a referee for observing that while the collision diameters for CH_3OH , $\text{C}_2\text{H}_5\text{OH}$, and $n\text{-C}_3\text{H}_7\text{OH}$ are less dissimilar than their corresponding viscosities (3.69, 4.31, and 4.71 Å, respectively), consideration of the energy degradation of the bromine atom by the solvent molecules (which is controlled by a factor $[(M - m)/(M + m)]^2$ and is computed to be 0.192, 0.079, and 0.024 for the three solvents, respectively) would indicate clearly that propanol is the more effective moderator.

discussion will consider, in turn, factors relating to the geminate retention resulting from the recoil suffered by $^{80\text{m}}\text{Br}$ in the (n,γ) transformation, from the charging accompanying the (I.T.) transformation in $^{80\text{m}}\text{Br}$ decay and from the (n,γ) (I.T.) transformation sequence in the ^{82}Br case.

Geminate Retention from the $^{79}\text{Br}(n,\gamma)^{80\text{m}}\text{Br}$ Transformation. Nearly all of the 7.8 MeV of excitation energy of the ^{80}Br nucleus formed upon neutron capture by a ^{79}Br nucleus is very rapidly emitted as a set of γ ray quanta. Such γ ray cascades generally include one or more γ rays of sufficiently high energy to make it probable that the recoil experienced by the nucleus will result in breakage of the chemical bonds of the directly affected atom. Internal conversion of certain excited states of the nucleus, whereby an orbital electron rather than a photon carries off energy from the nucleus, may occur as well.¹⁷ When this does occur a positive charge of 1 or more than 1 is very rapidly ($<10^{-15}$ sec) placed on the atom.¹⁷ This "charging" can initiate bond breakage and possibly other chemical reactions of the affected molecule. If we assume that the likelihood of survival or reconstitution of all of the chemical bonds of a CBr_4 molecule is negligible for those events which involve both recoil and charging (as compared to those events with only recoil or charging) we can evaluate factors which might contribute to the geminate retention after some fraction of the recoil events. According to Wexler and Davies,¹⁸ in the $^{79}\text{Br}(n,\gamma)^{80\text{m}}\text{Br}$ reaction the recoil-only events are more probable by a factor of about 8 than events which occur with both recoil and charging.

The actual recoil energy attained by a given $^{80\text{m}}\text{Br}$ atom as a result of its particular γ cascade depends upon the vector sum of the contributions from the γ rays involved provided these γ rays are emitted rapidly ($<10^{-14}$ sec), as is usually the case with the energetic γ rays which contribute most significantly to the recoil.^{9,17,19} The recoil energy distribution associated with the $^{79}\text{Br}(n,\gamma)^{80\text{m}}\text{Br}$ transformation has not yet been determined. However, if the probability distribution for the recoil energies from the $^{35}\text{Cl}(n,\gamma)^{36}\text{Cl}$ transformation is used to approximate that of the $^{79}\text{Br}(n,\gamma)^{80\text{m}}\text{Br}$ transformation, as appears to be valid in the $^{79}\text{Br}(n,\gamma)^{80\text{g}}\text{Br}$ case,¹ then the likelihood of a given $^{80\text{m}}\text{Br}$ nucleus receiving a recoil energy of less than 1 eV is negligibly small ($<0.01\%$). It is estimated, from this assumed distribution, that about 1% of the bromine atoms have recoil energies less than 20 eV. The gas-phase bond survival value of 0.031% for the $^{79}\text{Br}(n,\gamma)^{80\text{g}}\text{Br}$ transformation in CBr_4 was shown by Gordus and Hsiung¹ to correspond on this distribution curve to a recoil energy in good agreement with the calculated minimum recoil energy required for bond rupture in CBr_4 (2.98 eV).²⁰

The ethanol solution value of 0.19% (Table II) might similarly correspond to those $^{80\text{m}}\text{Br}$ atoms having

recoil energies of 10 eV or less. This is plausible in a rough qualitative sense since, after expending perhaps 3 eV in bond breaking, the fragments resulting from low-energy recoils are expected to remain within a few molecular diameters of one another where their encounter and recombination probabilities are expected to be significant. On the other hand, some recoils of somewhat higher energy, for example 10–30 eV, probably do not separate fragments more than 1–2 molecular diameters and may contribute to the geminate recombination.⁹ The geminate retention value of 0.19% may thus correspond to a kind of averaging of recoil events over a rather wide range of recoil energies, with the decrease in the probability of geminate recombination with recoil energy *per event* (due to the usually larger separation distances at higher recoil energies) being partially compensated by the *increase* in the number of recoil events of higher energy.

Geminate Retention Resulting from the $^{80\text{m}}\text{Br}$ (I.T.)- $^{80\text{g}}\text{Br}$ Transformations. Interpretation of the geminate retention value for this case (Table II) is complicated by the fact that all of the atoms undergoing this isomeric transition pass through two transformations. The first of these is a 49-keV transformation which is 99.7% converted²¹ to give a short-lived (7.4×10^{-9} sec)²² intermediate 37-keV state which decays to ground state $^{80\text{g}}\text{Br}$. The transition from the intermediate state to the ground state is about 57% converted.²¹ Thus 57% of the radiobromine nuclei undergo *two* internal conversions while 43% undergo only one. In the events where the second transition is not converted, only low-energy photons (37 KeV) are emitted, giving very little recoil (<0.01 eV) to the resulting atom and no (additional) charge. Thus, in 43% of the events the second transition does not (further) affect the chemistry of the $^{80\text{g}}\text{Br}$ atom.

Since fragments from the CBr_4 bond ruptures resulting from the first *converted* transition will have either undergone geminate recombination or will have escaped from each other in less than 10^{-9} sec,¹¹ it appears likely that the chemical form of the intermediate (7.4×10^{-9} sec) nuclear state prior to its decay to the ground state has been stabilized either as molecular CBr_4 or in inorganic form and that these species are located in neighborhoods made up of nonfragmented $\text{C}_2\text{H}_5\text{OH}$ molecules. It thus seems reasonable to assume that approximately the same probability of survival should apply to a CBr_4 molecule from either of the *converted*

(17) S. Wexler in "Actions Chimiques et Biologiques des Radiations; Huitieme Serie," M. Haissinsky, Ed., Masson et Cie, Paris, 1965.

(18) S. Wexler and T. H. Davies, *J. Chem. Phys.*, **18**, 376 (1950).

(19) C.-H. Hsiung, H.-C. Hsiung, and A. A. Gordus, *ibid.*, **34**, 535 (1961).

(20) C.-H. Hsiung and A. A. Gordus, *ibid.*, **36**, 947 (1962).

(21) W.-D. Schmidt-Ott, K.-W. Hoffman, I. Y. Krause, and A. Flammersfeld, *Z. Physik*, **158**, 242 (1960).

(22) W. Flauger and H. Schneider, *Nucl. Phys.*, **55**, 207 (1964).

transitions. If this is so, then the geminate retention expected for a *single* converted transition is 10%, with the 5% value reported in Table II representing the survival percentage after 57% of the ^{80m}Br atoms have decayed by two internal conversion transitions while 43% have decayed by one.²³

It is now necessary to consider why the geminate retention for a single-transformation isomeric transition is so much higher than that from an (n,γ) reaction. Perhaps the simplest answer is that in 10% or more of the events the formation and subsequent events accompanying an inner shell vacancy in a bromine atom of a CBr_4 molecule in $\text{C}_2\text{H}_5\text{OH}$ solution do not cause the bromine atoms to move from their initial positions so that they have a good chance of giving product radio- CBr_4 .

When Auger electrons are ejected from atoms having inner shell vacancies this ejection takes place very rapidly ($<10^{-15}$ sec), at least an order of magnitude more rapidly than the atoms (*i.e.*, nuclear positions) can respond to the electronic changes. In bromine from one to more than a dozen electrons may be ejected, with energies ranging from about 10 to greater than 10^3 eV.⁹ When this ejection occurs in the gas phase the electrons rapidly leave the vicinity of the charged atom. If the charged atom is initially part of a molecule the atomic charge is redistributed rapidly over the molecule and this multiply charged "ion assembly" then undergoes a "coulombic explosion,"²⁴ effectively separating the two or more charged fragments.

Similar explosions have been suggested for the condensed phase.²⁵ However, they may not occur with high efficiency as solution phase electronic redistribution may discharge most or all of the multiply charged assemblies before the atomic (ionic) motion of an "explosion" can occur. The high potential gradient in the neighborhood of the multiply charged species would undoubtedly attract and transfer electrons not only from the other atoms of the target molecule (as occurs in the gas phase),²⁴ but also from other neighboring molecules.

In considering the rapid electronic redistributions taking place within the neighborhood of a CBr_4 molecule in $\text{C}_2\text{H}_5\text{OH}$ solution as a result of having an inner shell vacancy generated within one of the bromine atoms of the CBr_4 molecule it is convenient to picture this as occurring in two stages, first the Auger charging of the CBr_4 molecule to give the CBr_4^{n+} "ion assembly," and then the discharging of the ions of the assembly. If "coulomb explosion" were to occur,²⁵ the second stage would begin with this explosion, with discharging of the resulting ionic fragments occurring afterwards. If, as appears likely, ion motion does not have time to occur before electrons are transferred to the assembly, the "explosion" would not occur. However, even if complete discharging were to occur before significant atomic (nuclear) motion takes place, the survival of the assem-

bly as a CBr_4 molecule would by no means be assured. Since discharging reactions brought about by free electrons or negative ions resulting from the local Auger radiolysis²⁶ are generally exothermic by 8–11 eV or more per event (tens or even hundreds of eV for multiply charged ions), fragmentation of the neutralized but activated CBr_4 assembly is expected and local reactions with the adjacent solvent molecules, for example hydrogen abstraction by atomic bromine, may drastically affect the likelihood of deexcitation-recombination reactions which could possibly give molecular CBr_4 .

A much more plausible route is available, however, whereby a fraction of the CBr_4^{n+} assemblies can survive as CBr_4 molecules after discharging. This route is electron transfer from neighboring $\text{C}_2\text{H}_5\text{OH}$ molecules. A Br^+ ion of the CBr_4^{n+} assembly might be discharged by electron transfer from a neighboring molecule, this



transfer having an exothermicity of about 1.3 eV based on gas phase ionization potentials of 10.48 eV for $\text{C}_2\text{H}_5\text{OH}$ ²⁷ and 11.8 eV for Br .²⁷ If all of the individual ions of the CBr_4^{n+} assembly were so discharged before significant atom motion occurred, then the individual atoms of the initial CBr_4 molecule would be in precisely the configuration for CBr_4 molecular bond reconstruction. This route is the more plausible the smaller the charge on the CBr_4^{n+} assembly, due to the accumulated energy deposition from several electron transfers occurring by reaction 1. The special case in which *only* the conversion electron is emitted from the initial inner shell vacancy (*i.e.*, the case of no Auger cascade) is particularly favorable since *no* opportunity for coulombic explosion exists and only about 1 eV of excitation energy need be dissipated. Even more favorable energetically would be electron transfer from a $\text{C}_2\text{H}_5\text{OH}$ molecule to *molecular* CBr_4^+ , since the exothermicity of this transfer is probably less than 0.5 eV, based on ionization potentials of 10.48 eV for $\text{C}_2\text{H}_5\text{OH}$ ²⁷ and 10.5–11.0 for CBr_4 .²⁸ However, the likelihood of this electron transfer in the liquid phase is unknown and could be very small if, for instance, the ionization potentials were both about 10.5 eV.

(23) If 10% of the CBr_4 molecules in which the $^{80m}\text{Br}(\text{I.T.})^{80g}\text{Br}$ decay is occurring survive the internal conversion processes accompanying the *first* transition, then $(10 \times 0.43)\% = 4.3\%$ of these CBr_4 molecules will survive the second transition since in 43% of the events the second transition occurs without internal conversion. The other $(10 - 4.3)\% = 5.7\%$ of the CBr_4 molecules which survive the first transition suffer internal conversion from the second transition. If the CBr_4 molecule survives about 10% of these events, these would contribute an additional $(0.1 \times 5.7)\% = 0.57\%$ to the geminate retention.

(24) S. Wexler, *J. Chem. Phys.*, **36**, 1922 (1962).

(25) A. R. Kazanjian and W. F. Libby, *ibid.*, **42**, 2778 (1965).

(26) P. R. Geissler and J. E. Willard, *J. Phys. Chem.*, **67**, 1675 (1963).

(27) R. W. Kiser, "Introduction to Mass Spectrometry and Its Applications," Prentice Hall, Englewood Cliffs, N. J., 1965.

(28) R. Thorburn, *Brit. J. Appl. Phys.*, **16**, 1397 (1965).

Although the fraction of $^{80\text{m}}\text{Br}(\text{I.T.})^{80\text{g}}\text{Br}$ decay events which occur without emission of Auger electrons from the resulting CBr_4^+ (with its inner shell vacancy) is not known, a rough estimate may be made based on the data of Wexler and Anderson²⁹ for the amount of $\text{CH}_3\text{Br}^{(80\text{g}}\text{Br})^+$ surviving isomeric transition in $\text{CH}_3\text{-Br}^{(80\text{m}}\text{Br)}$. The observed value of 10% may represent an upper estimate^{17, 29} for the CH_3Br^+ surviving the two-step isomeric transition. Hence a value of perhaps 10–20% might be a reasonable estimate for the probability of survival of a singly converted transition. A similar value for the probability of formation of CBr_4^+ from a singly converted transition could account for all of the observed $\text{CBr}_4^{(80\text{g}}\text{Br)}$ in the present case.

It is thus possible that most, if not all, of the 10% geminate retention from a singly converted isomeric transition is due to electron transfer from neighboring $\text{C}_2\text{H}_5\text{OH}$ molecules to those CBr_4^+ ions which suffer no Auger charging although some contribution could occur from geminate recombination reactions of, for example, $\text{CBr}_3 + \text{Br}$, where the Br results from decharging of a nonbonded Br^+ (or Br^{2+}).

Geminate Retention Resulting from the $^{81}\text{Br}(\text{n},\gamma)\text{-}(\text{I.T.})^{82\text{g}}\text{Br}$ Transformation Sequence. In the activation of ^{81}Br by thermal neutrons about 10% of the events go by the $^{81}\text{Br}(\text{n},\gamma)^{82\text{g}}\text{Br}$ reaction and 90% by the $^{81}\text{Br}(\text{n},\gamma)^{82\text{m}}\text{Br}$ reaction, followed by the $^{82\text{m}}\text{Br}(\text{I.T.})^{82\text{g}}\text{Br}$ transformation.³⁰ Assuming that the geminate retentions from each of the (n,γ) reactions is the same as from the $^{79}\text{Br}(\text{n},\gamma)^{80\text{m}}\text{Br}$ reaction, *i.e.*, 0.19%, and that the geminate retention contribution from the $^{82\text{m}}\text{Br}(\text{I.T.})^{82\text{g}}\text{Br}$ transformation is 10%, as indicated by the $^{80\text{m}}\text{Br}(\text{I.T.})^{80\text{g}}\text{Br}$ data, the geminate retention for the overall sequence is predicted to be about 0.035%. The difference between this value and the observed value of $0.07 \pm 0.01\%$ (Table II) may result from an inapplicability of the ^{79}Br data to the ^{81}Br activation cases or it may be caused, as discussed below, by the chemical forms of the *intermediate* bromine species present during the sequence of transformations (*i.e.*, at the time of the second transformation).

In a *sequence* of nuclear transformations, such as the $^{81}\text{Br}(\text{n},\gamma)(\text{I.T.})^{82\text{g}}\text{Br}$ sequence, generally only the first transformation occurs exclusively in the selected target species; the second and subsequent transformations occur in the spectrum of chemical product species which result from the preceding transformation, thus complicating or even destroying the known specification of the system.

After the (n,γ) activation of ^{81}Br in CBr_4 only a small fraction, presumably about 0.2%, of the $^{82\text{m}}\text{Br}$ is present in radio- CBr_4 form; the remaining 99.8% is present in other forms. These other forms include CH_3Br , $\text{C}_2\text{H}_5\text{Br}$, and $\text{C}_2\text{H}_4\text{BrOH}$,³ and very likely also BrI , HBr , CHBr_3 , and CH_2Br_2 . When the converted

isomeric transition occurs in one of these compounds it might generate an intermediate species capable of efficient reaction with low-concentration (inactive) CBr_4 molecules. Alternatively, one or more of the products from the (n,γ) reaction could complex with a CBr_4 molecule *before* the (I.T.) transformation occurred. Such a complex would presumably permit radio- CBr_4 formation from the localized fragments after the (I.T.) event. A charge transfer species such as CBr_5 , analogous to the CCl_5 postulated by Louwrier and Hamill,³¹ is one conceivable species of this type. Either of these chemical routes, or other factors, could undoubtedly account for the twofold difference between the calculated and the experimental geminate retention for the $^{81}\text{Br}(\text{n},\gamma)(\text{I.T.})^{82\text{g}}\text{Br}$ sequence.

Conclusions. The small (0.19%) geminate retention from the $^{79}\text{Br}(\text{n},\gamma)^{80\text{m}}\text{Br}$ reaction can be attributed to a small but finite probability that the mechanical recoil which the nucleus experiences from its deexcitation γ rays has a very low (<30 eV) value as a result of the near cancellation of momenta from the emitted γ rays. The larger recoil energies in most of the (n,γ) events would break bonds and carry the recoil atom too far from its geminate partners to permit geminate recombination. Using the gas phase bond survival value of 0.03%¹ as an estimate of that (Case I) component of this geminate retention leads to the conclusion that most of the observed geminate retention from the (n,γ) reaction is due to geminate recombination (Case II) reactions.

The relatively large (5%) geminate retention from the two transitions of the $^{80\text{m}}\text{Br}(\text{I.T.})^{80\text{g}}\text{Br}$ process can be attributed to those internal conversion events in which only the conversion electron is emitted from the atom or perhaps to those events in which one or two Auger electrons are also emitted. The decharging of the CBr_4^+ (and perhaps CBr_4^{2+} and CBr_4^{3+}) species may occur as simple electron transfers from adjacent solvent molecules. Thus, the geminate retention from (I.T.) might result largely from bond survival (Case I) in contrast to the recombination (Case II) route proposed for most of the (n,γ) events.

Acknowledgments. The authors are grateful to Mr. Adrian Adelman and Dr. C. H. Collins for valuable contributions during the course of this work and to the U. S. Atomic Energy Commission for the partial support of this work through Contract AT(30-1)3941. This paper constitutes Document NYO-3941-3.

(29) S. Wexler and G. R. Anderson, *J. Chem. Phys.*, **33**, 850 (1960).

(30) (a) O. U. Anders, *Phys. Rev.*, **138**, B1 (1965); (b) J. F. Emery, *J. Inorg. Nucl. Chem.*, **27**, 903 (1965).

(31) P. W. F. Louwrier and W. H. Hamill, *J. Phys. Chem.*, **73**, 1702 (1969).

The Molecular Composition of Liquid Sulfur

by Robert E. Harris

Department of Chemistry, University of Missouri, Columbia, Missouri 65201 (Received June 20, 1969)

A model of the molecular composition of equilibrium liquid sulfur is constructed to agree with the composition of sulfur vapor, the maximum in the heat capacity, and the CS₂-insoluble sulfur content of liquid quenched from 160 to 184°. Aten's S_r is interpreted as partially fractionated ring material other than S₈. For comparison with experiment it is assumed S₂₉ and larger rings are retained in the insoluble sulfur. The predictions of the model are compared with the experimental molecular formula of S_r, the content of S_r and insoluble sulfur in quenched sulfur, and the self-depression of the freezing point of sulfur. The agreement between experimental results and predictions of the model is satisfactory.

Introduction

Anyone who has handled liquid sulfur is familiar to some extent with its peculiar properties. The changes of color and viscosity with temperature are prominent. A vast body of experimental work on such a common element of such uncommon properties is to be expected.¹⁻⁴

The experimental evidence suggests that at least three classes of molecular species must be considered in order to account for the observed properties. One class of species is produced when crystalline (orthorhombic or monoclinic) sulfur melts to the molecular species of the crystal, S₈. The second class of species is important only above 159° and is a mixture of linear polymers. The third class of species, often referred to as S_r, manifests itself mainly in the properties of the liquid below 159°. The rest of the Introduction is devoted to summarizing some of the experimental results and theories attempting to explain them and outlining the model of this paper. The next two sections are devoted to defining the model in quantitative terms and examining the probable accuracy of the theory used in the model. The Discussion contains comparisons between experimental and calculated properties of sulfur.

Liquid sulfur at any temperature which is quenched at low temperatures and allowed to age near room temperature yields a CS₂-insoluble fraction. Smith and Holmes⁵ took the position that if the quenched material were not aged the insoluble sulfur would be emulsified and pass through the filter with the soluble sulfur, so they aged the quenched material to allow it to harden before extraction. Smith and his coworkers found that the amount of insoluble sulfur increases with the temperature of equilibration of the liquid, with the rate of increase much larger above 160° than below. They studied the rate of formation of the precursor of insoluble sulfur at 130 and 140° and the effect of acidic and basic substances on the amount of insoluble sulfur.^{6,7}

Aten⁸ showed that prompt extraction of sulfur quenched from any temperature gives less insoluble sulfur than is found in sulfur aged before extraction. He showed that the CS₂ extract contains, on cooling to -80°, dissolved sulfur in excess of the solubility of ordinary sulfur at that temperature. He called the excess dissolved sulfur S_r. He also showed that solutions, containing variable amounts of S₆ and saturated with S₈, which were then saturated with sulfur which had been heated to 170°, gained sulfur beyond the sulfur content of solutions simultaneously saturated with S₆ and S₈, which shows the presence of some extractable species other than S₆ and S₈ in the 170° sulfur.⁹

Wahl¹⁰ showed that sulfur quenched from 130° and aged near room temperature yields insoluble sulfur in amounts increasing from none initially to a maximum with increasing time of aging. The amount decreases very slowly beyond the maximum. The rate of formation of insoluble sulfur and the maximum amount increase with increasing aging temperature. Aten presented data which shows the rise in insoluble sulfur content is accompanied by a decay of most of the S_r, while the slow decay of the insoluble sulfur is accompanied by a slow decay of the S_r.⁸

(1) J. W. Mellor, "A Comprehensive Treatise on Inorganic and Theoretical Chemistry," Vol. 10, Longmans, Green and Co., London, 1930, pp 23-87.

(2) W. N. Tuller, Ed., "Sulfur Data Book," compiled by the technical staff, Freeport Sulphur Co., McGraw-Hill Publications, New York, N. Y., 1954.

(3) B. Meyer, *Chem. Rev.*, **64**, 429 (1964).

(4) B. Meyer, Ed., "Elemental Sulfur," Interscience Publishers, New York, N. Y., 1965.

(5) A. Smith and W. B. Holmes, *J. Amer. Chem. Soc.*, **27**, 979 (1905).

(6) A. Smith, W. B. Holmes, and E. S. Hall, *ibid.*, **27**, 797 (1905).

(7) C. M. Carson, *ibid.*, **29**, 499 (1907).

(8) A. H. W. Aten, *Z. Phys. Chem.*, **86**, 1 (1914).

(9) A. H. W. Aten, *ibid.*, **88**, 321 (1914).

(10) W. H. Wahl, M.S. Thesis, Purdue University, 1956.

Schenk and Thümmeler¹¹ carried out a cryoscopic investigation of the molecular weight of S_x in CS_2 and concluded that the average formula was 8.3 atoms per molecule, assuming the S_x is quantitatively converted to insoluble sulfur on evaporation of the CS_2 . They later found that about 55% of the S_x was converted.¹²

The presence of species other than S_8 in the liquid results in a self-depression of the freezing point. Smith and Holmes¹³ studied the relation between freezing point and insoluble sulfur content and found a linear relation. Schaum¹⁴ and Wiewiorowski, *et al.*,¹⁵ have studied the development of the self-depression of the freezing point as a means of following the temperature-dependent rate of formation of the non- S_8 part of the liquid. These data, together with Carson's data on the rate of increase of insoluble sulfur content,⁷ agree with an activation energy of about 30 kcal for the process involved in producing the initial part of the insoluble sulfur; the data show some inconsistencies and probably are not very reliable.

Additional evidence bearing on the nature of liquid sulfur comes from studies of the temperature dependencies of heat capacity, viscosity, electron spin resonance, and magnetic susceptibility. West¹⁶ found that the heat capacity rises to a maximum at 159° and then decreases. Bacon and Fanelli¹⁷ found that the viscosity decreases to a minimum at 155°, rises slightly to 159°, then increases rapidly above 159° to a maximum at about 185°. The electron paramagnetic resonance data reported by Gardner and Fraenkel¹⁸ and the magnetic susceptibility data reported by Poullis, Massen, and van der Leeden¹⁹ indicate that the concentration of unpaired electrons is large at high temperature.

The first attempt to give a quantitative explanation of the viscosity in terms of high polymers was made by Powell and Eyring.²⁰ Both Tobolsky²¹ and Flory²² pointed out that the failure of the Powell and Eyring treatment lay in approximation of the activity of linear polymer species by mole fraction rather than by concentration. Gee²³ offered the first successful description of the properties of liquid sulfur, assuming an equilibrium between S_8 and linear polymer and treating the insoluble sulfur content as a measure of the polymer content of the liquid and the viscosity as a measure of the average molecular weight of the polymer. Fairbrother, Gee, and Merrall²⁴ used the rise in heat capacity at 159° as a measure of the heat of polymerization. They rejected the possibility of large ring species, since the heat capacity curve they used did not show a large rise below 159°.

Gardner and Fraenkel interpreted their spin resonance data in terms of Gee's model, and Poullis and Derbyshire²⁵ did the same for the spin resonance and magnetic susceptibility data taken together.

Tobolsky and Eisenberg²⁶ reformulated Gee's theory in rather clearer terms, with the polymer species restricted to integer multiples of eight atoms per chain. This restriction was removed in a later paper.²⁷ Tobolsky and Eisenberg's theory is based on substantially the same results of the theory of polymer solutions as is Gee's and the characterization of the Tobolsky and Eisenberg theory as unified or unitary is to be understood only in the sense that Gee made approximations in the calculations which, although accurate, are not particularly convenient in the original form of the Tobolsky and Eisenberg treatment. Touro and Wiewiorowski²⁸ have interpreted the viscosity in terms of the Tobolsky and Eisenberg model.

The S_8 -linear polymer models account for the magnetic and viscous properties. They predict negligible polymer content with low average molecular weight below 159°. The insoluble sulfur content rises with increasing temperature in a way which suggests the polymer must be responsible for part of the insoluble sulfur, but the quantity of insoluble sulfur does not agree with the polymer content.

The interpretations of liquid sulfur below 159° have often been in terms of S_8 and one other species. Schenk and Thümmeler summarized much of the previous speculation. They suggested on the basis of their molecular weight work that S_x is either S_8 chain or a ring mixture. They rejected the ring mixture on grounds that the experimental properties of sulfur do not agree with what might be expected from a ring mixture.¹¹ Wiewiorowski and Touro suggested the S_8 chain is complexed by S_8 , since the polymer theories predict a negligible content of free S_8 chain.

(11) P. W. Schenk and U. Thümmeler, *Z. Elektrochem.*, **63**, 1002 (1959).

(12) P. W. Schenk and U. Thümmeler, *Z. Anorg. Allg. Chem.*, **315**, 271 (1962).

(13) A. Smith and W. B. Holmes, *Z. Phys. Chem.*, **42**, 469 (1903).

(14) K. Schaum, *Justus Liebig's Ann. Chem.*, **308**, 18 (1899).

(15) T. K. Wiewiorowski, A. Parthasarathy, and B. L. Slaten, *J. Phys. Chem.*, **72**, 1890 (1968).

(16) E. D. West, *J. Amer. Chem. Soc.*, **81**, 29 (1959).

(17) R. F. Bacon and R. Fanelli, *ibid.*, **65**, 639 (1943).

(18) D. M. Gardner and G. K. Fraenkel, *ibid.*, **78**, 3279 (1956).

(19) J. A. Poullis, C. H. Massen, and P. v. d. Leeden, *Trans. Faraday Soc.*, **58**, 474 (1962).

(20) R. E. Powell and H. Eyring, *J. Amer. Chem. Soc.*, **65**, 648 (1943).

(21) A. V. Tobolsky, *J. Chem. Phys.*, **12**, 402 (1944).

(22) P. J. Flory, *ibid.*, **12**, 425 (1944).

(23) G. Gee, *Trans. Faraday Soc.*, **48**, 515 (1952).

(24) F. Fairbrother, G. Gee, and G. T. Merrall, *J. Polymer Sci.*, **16**, 459 (1955).

(25) J. A. Poullis and W. Derbyshire, *Trans. Faraday Soc.*, **59**, 559 (1963).

(26) A. V. Tobolsky and A. Eisenberg, *J. Amer. Chem. Soc.*, **81**, 780 (1959).

(27) J. A. Poullis, C. H. Massen, A. Eisenberg, and A. V. Tobolsky, *ibid.*, **87**, 413 (1965).

(28) F. J. Touro and T. K. Wiewiorowski, *J. Phys. Chem.*, **70**, 239 (1966).

They invoked an acidic character for the rings and a basic character for the chains, citing solubility evidence for the acidic character of the rings and the enhancement of insoluble sulfur content by acidic substances for the basic character of the chains.²⁹

Semlyen has suggested a mixture of rings larger than S_8 as the explanation of S_x . Semlyen's arguments are mainly based on theoretical studies of the configurations of sulfur chains, although he cites the production of insoluble sulfur from S_x and other known ring species as an argument in favor of a ring mixture. Semlyen rejects rings smaller than S_8 on the basis of energy considerations.³⁰

None of the models of S_x mentioned above agrees with experimental results on all points. Semlyen's model cannot give an average formula of S_x which agrees with S_8 . Wiewiorowski and Touro's model has the same difficulty, unless the complexed S_8 rings come off the chains in some unexplained way during the separation of S_x . The solubility arguments for the acidic character of rings depend on data which Scott has interpreted (without acid-base assumptions) in terms of solubility parameter theory,³¹ and the enhancement of insoluble sulfur content by acidic substances has been recognized for many years as the result of base catalysis of interconversion of sulfur species and acid inhibition of the catalysis.^{32,33} The simple S_8 -chain model suggests that the equilibrium constant for the reaction of S_8 to form the chain should be proportional to the ratio of the S_x fraction to the S_8 fraction, so that a plot of the logarithm of the ratio vs. reciprocal absolute temperature should be nearly linear below 159°. The available data give distinctly curved plots.¹¹

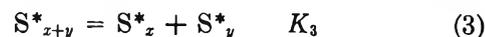
The present paper consists of a model of the composition of liquid sulfur based on equilibrium among ring species S_8 and larger and linear polymer species, an explanation of S_x and insoluble sulfur, and comparisons between predicted and experimental freezing points, S_x and insoluble sulfur contents, and the formula of S_x . It is interesting to note that no model of liquid sulfur predicts accurately the amount of insoluble sulfur found after quenching, so that one of the oldest and best-known phenomena connected with liquid sulfur remains something of a puzzle.

Model of Liquid Sulfur

The composition of liquid sulfur assumed in this paper is a mixture of ring species, predominantly S_8 , and linear high polymers. The treatment of the equilibrium between S_8 and linear polymer is substantially the same as that first suggested by Flory²² and later carried out by Gee²³ and by Tobolsky and Eisenberg.^{25,26} This paper assumes that all activities may be approximated by concentrations. It also assumes that the temperature dependence of equilibrium constants may be represented by the form

$$K = A \exp\{-[\Delta H/R][(1/T) - (1/T_0)]\} \quad (1)$$

where T_0 is an arbitrarily chosen temperature; $1/T_0$ is $2.275 \times 10^{-3} \text{ } ^\circ K^{-1}$ throughout this paper. The evaluation of an equilibrium constant means the determination of both A and ΔH , unless a particular temperature is specified. Linear species are written with asterisk superscripts: S_n^* . The assumed reactions and equilibrium constants are



(Ring species S_4 and smaller are ignored, so that K_3 and K_4 always refer to reactions 2 and 3.)

The linear species may be dealt with by assuming sulfur atoms form either two bonds or one bond to other sulfur atoms. An atom with only one bond is the terminal atom of a chain and has one unpaired electron in lieu of a second bond. Calling the unpaired electron a bond not terminated, let the probability that a given bond of a particular chain sulfur atom is terminated by another sulfur atom be p and the probability that it is not terminated be r . Then the application of simple statistical argument,³⁴ or of a more complex polymer solution theory treatment,²² leads to the concentration of chains containing x S atoms in terms of the total concentration of chain sulfur atoms, C_c

$$[S_x^*] = r^2 p^{x-1} C_c \quad (5)$$

Note that

$$p + r = 1 \quad (6)$$

The concentration of unpaired electrons, C_e , is given by

$$C_e = 2rC_c \quad (7)$$

Substitution of (5) into the equilibrium constant expressions for reactions 2 and 3 leads to

$$K_4 = C_8/p^8 \quad (8)$$

$$K_3 = r^2 C_c/p \quad (9)$$

where C_8 is the concentration of S_8 .

Following Jacobson and Stockmayer,³⁵ one may write for reaction 4

(29) T. K. Wiewiorowski and F. J. Touro, *J. Phys. Chem.*, **70**, 3528 (1966).

(30) J. A. Semlyen, *Trans. Faraday Soc.*, **64**, 1396 (1968).

(31) R. L. Scott, ref 4, Chapter 17.

(32) E. Beckmann and C. Platzmann, *Z. Anorg. Allg. Chem.*, **102**, 201 (1918).

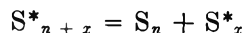
(33) P. D. Bartlett, G. Lohaus, and C. D. Weis, *J. Amer. Chem. Soc.*, **80**, 5064 (1958).

(34) P. J. Flory, "Principles of Polymer Chemistry," Cornell University Press, Ithaca, N. Y., 1953, p 319.

(35) H. Jacobson and W. H. Stockmayer, *J. Chem. Phys.*, **18**, 1600 (1950).

$$C_n = Bp^n/n^{2.5} \quad (10)$$

where B is independent of n so long as n is large enough that the heat of reaction for



is zero. It is assumed that B is independent of temperature. For n small enough that (10) does not apply with a constant B

$$C_n = K_n C_8^{n/8} \quad (11)$$

where each K_n must be evaluated individually. The conservation of total sulfur makes possible the solution of the equilibrium problem if the various equilibrium constants are known. In this paper the various concentrations are referred to the volume containing 55.22048 g-atoms of S. The concentration units are abbreviated by the symbol M , which is to be understood as molar when corrected to the density of sulfur at 160°. Then

$$55.22048 = 5C_5 + 6C_6 + \dots + C_8 \quad (12)$$

represents the conservation of sulfur.

The various concentrations in (12) may be replaced by expressions involving C_8 and the equilibrium constants, which reduces the problem to finding the root of a nonlinear equation in a single variable, C_8 . Writing p for $(C_8/K_4)^{1/8}$ and x for C_8 otherwise, the equation becomes

$$55.22048 = 5K_5x^{5/8} + 6K_6x^{3/4} + 7K_7x^{7/8} + 8x + 9K_9x^{9/8} + 10K_{10}x^{5/4} + Bf(p) + pK_3/(1-p)^2 \quad (12a)$$

where $f(p)$ is the sum from $n = 11$ to infinity of terms $p^n/n^{2.5}$. (Calculations for this paper were carried out with a digital computer. The equation was solved by Newton's method. The values of $f(p)$ and its derivative with respect to p were stored as tables.)

The equilibrium constants to be evaluated are divided below into categories according to the mode of evaluation. Where necessary, it is assumed that other equilibrium constants are reasonably well known. The results are not self-consistent, since calculations based on estimates of other equilibrium constants were not always revised when the estimated equilibrium constants had been evaluated. The new estimates were made, and the effects of changes on the final results were found to be small enough to justify the further neglect of the corrections in view of the semi-quantitative nature of both the initial assumptions and the interpretation of available experimental results.

The evaluations of K_5 – K_{14} were based on the available data on sulfur vapor together with assumptions about the liquid–vapor equilibrium. The calculations were based on the following assumptions.

1. The heat of vaporization of pure liquid S_n is given, independent of temperature, by

$$\Delta H_v = 4.404n^{2/3} \text{ kcal/mol} \quad (13)$$

Gee's estimate of the heat of vaporization of S_8 at 150°²³ leads to the factor 4.404, and the heats of vaporization of the cycloparaffins C_3H_8 through C_8H_{18} , calculated from the variation of boiling point with pressure,³⁶ are given to within 2% by $2.3037n^{2/3}$ kcal/mol.

2. The heat of vaporization and the boiling point of pure liquid S_n follow the empirical correlation, approximately valid for many substances³⁷

$$\Delta H_v = 17T_b + 0.009T_b^2 \text{ cal/mol} \quad (14)$$

3. The species present in liquid sulfur at 150° obey Raoult's law so that the partial pressure of any one species in the vapor over the liquid is given by

$$P_n = X_n P_n^\circ \quad (15)$$

The first two assumptions allow the calculation of the normal boiling point of pure S_n on the assumption that the heat of vaporization is independent of temperature. Once the boiling point is known, the vapor pressure of pure S_n at 150°, P_n° , can be calculated from the integrated form of the Clausius–Clapeyron equation. The ratio P_n°/P_8° is what is needed; this ratio is relatively insensitive to small temperature dependencies and other errors in the heats of vaporization.

Berkowitz and Marquart³⁸ report equilibrium constants K_n for n equal to 5, 6, and 7 in the gas phase. Mass spectral ion intensities relative to S_8^+ from the saturated vapor at 356°K are also reported for S_9^+ and S_{10}^+ . In order to fix values for K_9 and K_{10} in the gas phase, this paper assumes that the partial pressures of S_8 , S_9 , and S_{10} are proportional to the intensities of the corresponding ions and that the gas-phase enthalpies of formation of S_9 and S_{10} are 5.2 and 2 kcal/mol of S_8 consumed, respectively. The enthalpies are based on examination of molecular models with the idea that the main contribution to the enthalpy of formation of S_n from S_8 comes from displacement of the dihedral angle about S–S bonds away from the value of the dihedral angle found in S_8 .³⁹ Models suggest that the dihedral angles in S_7 and S_9 are displaced mainly around one bond, so the enthalpy of adding $1/4S_8$ to S_7 to make S_9 should be small. The model of S_{10} suggests that the dihedral angle of S_8 is nearly available in S_{10} so the enthalpy of formation of S_{10} ought to be less than the enthalpies of formation

(36) "Selected Values of Properties of Hydrocarbons and Related Compounds," API Project 44, Carnegie Institute of Technology, Pittsburgh, Pa., April 30, 1954, Table 23-2-(3.100)-a. Table originally carried No. 34a.

(37) J. H. Hildebrand and R. L. Scott, "Solubility of Nonelectrolytes," 3rd ed, Dover Publications, Inc., New York, N. Y., 1964, p 427.

(38) J. Berkowitz and J. R. Marquart, *J. Chem. Phys.*, **39**, 275 (1963).

(39) L. Pauling, *Proc. Natl. Acad. Sci. U. S.*, **35**, 495 (1949).

of the other small ring sulfur species. The vapor pressure of sulfur⁴⁰ at 356°K allows the calculation of the gas-phase K_9 and K_{10} . The gas-phase K 's at 150° together with the vapor pressure allow the calculation of the partial pressures of S_5 – S_{10} in the vapor.

Write $C_n = X_n C_8 / X_8$, substitute the mole fractions using (15); then substitute the resulting expression for C_n in (11). The result is

$$K_n = (P_8^\circ P_n / P_8 P_n^\circ) C_8^{1-(n/8)}$$

which is used to evaluate liquid phase K_n at 150° from the vapor pressures calculated as indicated above together with the assumption that liquid S at 150° is 92% S_8 . The gas-phase enthalpies of the reaction are converted to liquid phase values by adding the differences between the enthalpies of vaporization of $(n/8)S_8$ and S_n to the gas-phase enthalpies of the reaction. A summary of the estimated equilibrium constant parameters is given in Table I.

Table I: Parameters for Equilibrium Constants^a

n	A_n^b	ΔH_n , kcal/mol
3	1.487×10^{-12}	33.28
4	5.546	-4.00
5	1.975×10^{-4}	11.18
6	3.062×10^{-2}	4.25
7	5.787×10^{-2}	4.50
9	1.893×10^{-2}	6.47
10	1.190×10^{-2}	4.09

^a To be used in eq 1. ^b Units are mol/55.22048 g-atoms raised to the first power for $n = 3, 4$; the $1 - (n/8)$ power otherwise.

The values of K_4 and B are adjusted to fit the heat capacity and extraction data. The average heat capacity of a system over a temperature interval, ΔT , may be expressed by $C_p(\text{av}) = \Delta H / \Delta T$, where ΔH is the enthalpy change accompanying the temperature change. For a mixture of sulfur species, ΔH may be represented as the sum of the enthalpy changes for three steps: converting the initial mixture to pure S_8 at the initial temperature, changing the temperature of the S_8 to the final temperature, and converting the S_8 to the final mixture of species at the final temperature. The enthalpy changes associated with the first and third steps may be lumped together to give a contribution of reactions to the heat capacity, while the second step gives the average heat capacity of S_8 over the temperature interval. The model being developed here has no heat of mixing terms and no temperature dependencies in the heats of reaction, so the reaction contribution to the heat capacity may be found once the composition has been found at

each end of a temperature interval. The experimental heat capacity less the calculated contribution of reactions to heat capacity should represent the heat capacity of S_8 if the basic assumptions and numerical values of the model are correct.

The experimental heat capacity work by West seems to be superior to other investigations.¹⁶ The heat capacities reported are taken from smooth curves drawn to agree with the experimental average heat capacity, but the data needed to recover the average heat capacities are given. The average heat capacities were recalculated from the data given and were used in the present work.

First efforts were devoted to adjusting K_4 and B to obtain a smooth difference curve when the experimental heat capacity less the calculated reaction contribution was plotted against temperature. It became clear that ΔH_4 must lie somewhere in the range -3.5 to -4.5 kcal. These calculations showed that the value of A_4 fixed the location of the peak of the reaction contribution to the heat capacity and had slight effect on the shape of the reaction contribution *vs.* temperature. Most satisfactory results were obtained when A_4 was chosen to make the maximum in the reaction contribution fall at 158.65°. The values of B and ΔH_4 affect the height and width of the peak in the reaction contribution *vs.* temperature, but have slight effect on the shape close to the maximum: the reaction heat capacity rises rapidly with increasing temperature to a break over into a slow rise which turns over into a fall in a range of about 0.5°. The form is agreeable with an abrupt change of slope at about 2° resolution. It became apparent that no definite choice of values of both B and ΔH_4 could be made from fitting the heat capacity, so ΔH_4 was fixed at -4.0 kcal to make the insoluble sulfur content and the linear polymer content increase in parallel over the range 160–184°, following Gee's original method.²³ The heat capacity differences were then used to choose a value for B . The calculated differences are plotted in Figure 1. The irregularities near 160° cannot be eliminated by modest changes in B , A_4 , and ΔH_4 .

Fairbrother, Gee, and Merrall²⁴ have derived an equation for determining ΔH_4 from the jump in heat capacity at the onset of polymerization. Aside from the difficulties in deciding what part of the rise in the experimental heat capacity should be included in the jump, their method cannot be employed if a significant portion of the heat capacity below the temperature of the onset of polymerization is the result of equilibrium between S_8 and other low molecular weight species, since such equilibrium results in an apparent negative jump in the heat capacity at the

(40) W. A. West and A. W. C. Menzies, *J. Phys. Chem.*, **33**, 1880 (1929).

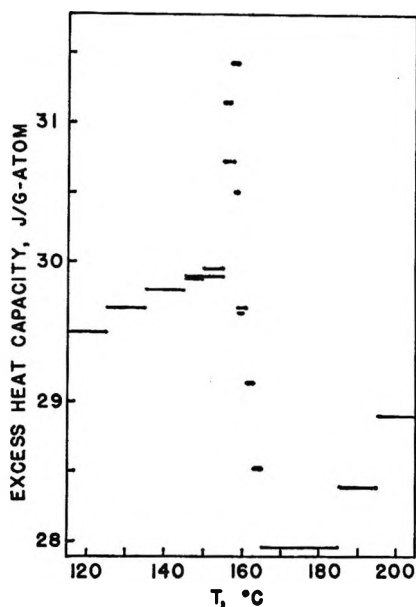


Figure 1. Excess of experimental heat capacity over contributions of reactions to heat capacity *vs.* temperature. The horizontal lines extend over the temperature intervals of the experimental determinations, taken from ref 16. The reaction contributions were calculated as indicated in the text.

temperature of onset of polymerization. This is so without regard to the particular reactions involved. Figure 2 shows that the slopes of the concentration *vs.* temperature curves for ring species become more negative above 159°, the temperature of onset of polymerization. The slopes of these curves depend on ΔH_4 above 159°, so simply subtracting the contributions of these species from the heat capacity below that temperature does not result in a heat capacity jump amenable to the jump treatment as it has been employed. The value of ΔH_4 , -3.2 kcal, found by the jump method seems unlikely to be accurate.

The evaluation of K_3 was carried out by eliminating p and r among (9), (6), and (7). The result gives K_3 in terms of C_e and C_c . The concentrations of unpaired electrons, C_e , were calculated from esr data reported by Gardner and Fraenkel,¹⁸ and C_c was calculated at the same temperatures using a preliminary estimate of K_3 . The derived K_3 values were used in a least-squares straight-line fit of $\ln K_3$ *vs.* $1/T$. The values of ΔH_3 and A_3 were used to provide the K_3 estimate required to repeat the procedure until the derived values agreed with the values employed in making the estimate. The results presented in this paper are not sensitive to substantial variations in ΔH_3 and A_3 .

Approximations in the Model

The treatment of the S_3 -linear polymer equilibrium is equivalent to assuming that the thermodynamics of mixing polymer and S_8 (ignoring other ring species for the moment) can be described by the concentrated

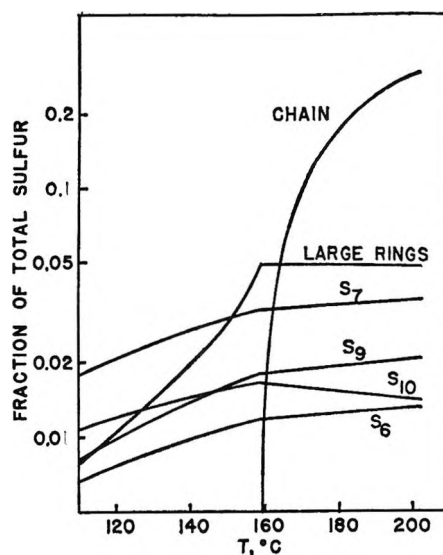


Figure 2. Calculated composition of liquid sulfur *vs.* temperature. The curve labeled "chain" represents the total of all linear species, and the curve labeled "large rings" represents the total of all ring species S_{11} and larger.

polymer solution formalism with a free energy interaction parameter equal to zero at all temperatures. The mixing would be athermal, since the temperature derivative of the free energy parameter is proportional to the enthalpy interaction parameter. This may be a reasonable estimate of the true state of affairs, but it is probable that the mixing is not athermal. A small enthalpy of mixing would not introduce enough temperature dependence in the free energy parameter to seriously affect the concentrations calculated by the methods of this paper. For example, an enthalpy parameter of 0.1 would produce a temperature derivative of the free energy parameter of about -0.0003 deg⁻¹ and temperature derivatives of a similar magnitude in the activity coefficients. The same enthalpy parameter, 0.1, would introduce a heat of mixing term in the calculated heat capacity of about 0.4 J/g-atom deg at 160°. (Presumably, very large rings would show the same heat of mixing effects. If all species S_{11} and larger acted as very large rings, a heat of mixing contribution of about 2.0 J/g-atom deg would appear at 157°.)

The treatment of large rings by eq 9 is subject to some uncertainty. Brown and Slusarczuk⁴¹ reported for polydimethylsiloxane (PDMS) in toluene the equivalent of K_n of this paper as a function of n . They found a limiting exponent of -2.86 for n , while the Jacobson and Stockmayer treatment gives -2.5 ; the difference is ascribed to the fact that toluene is not a θ solvent for PDMS under the condition of the experiments. They also found a range of ring sizes, roughly 12–26 bonds, for which the experimental K_n values fall below

(41) J. F. Brown, Jr., and G. M. J. Slusarczuk, *J. Amer. Chem. Soc.*, **87**, 931 (1965).

the values extrapolated back from large n , being about one-fourth the extrapolated values. According to Brown and Slusarczuk, the exponent of n can be shown to be $-(2 + a)$, where a is the exponent of the molecular weight in the intrinsic viscosity-molecular weight relation. The author of the present paper has carried out some preliminary calculations on the viscosity of sulfur which suggest an exponent of 0.7-0.8 for the intrinsic viscosity-molecular weight relation. Assuming sulfur and PDMS are comparable, the large and small rings are overestimated relative to the intermediate sizes by the Jacobson and Stockmayer treatment.

Flory and Semlyen⁴² gave a modification of the Jacobson and Stockmayer treatment and made calculations which are applicable to PDMS in a θ solvent. For large n the theory approaches the Jacobson and Stockmayer treatment. Using 2.06 Å for the S-S bond length and the S atom as the monomer unit, Flory and Semlyen's treatment would give $B = 1.92$ for sulfur for large n , assuming the difference between PDMS and sulfur lies only in the bond length and number of links per monomer unit.

Jacobson, Beckmann, and Stockmayer⁴³ treated their experimental results for the formation of cyclic decamethylene adipates by the equivalent of eq 10. Assuming the differences between sulfur and the decamethylene adipates lie in the bond length and number of links per monomer unit, the value of B would be 1.26 M . However, the major portion of the cyclic decamethylene adipates probably was material with 18 and 36 atoms per ring, which would be expected to appear in lower concentration than the Jacobson and Stockmayer theory would predict if the PDMS results have general validity.

Semlyen's treatment of the large ring equilibrium in sulfur amounts to using the Jacobson-Stockmayer treatment for rings larger than S_8 in the equivalent of eq 10 and the equivalent of eq 10 multiplied on the right by $\exp(-\Delta H_4/RT)$ for S_8 .³⁰ From the latter relation it is easy to calculate the value of B which would be appropriate for his treatment. The result is 10 M , when $C_8 = 6 M$. (Semlyen took ΔH_4 as -3.2 kcal. The value estimated here is based on $\Delta H_4 = -4.0$ kcal.)

On the basis of the above discussion it appears that the Jacobson and Stockmayer treatment yields a fair approximation for the large ring content if a suitable value is assigned to B . The value assigned here, 4.4 M , is somewhat larger than would be expected by comparison with the PDMS data, but it is smaller than the value obtained from Semlyen's analysis of configurations of sulfur chains. Since the viscosity suggests the low molecular weight material is not a θ solvent for the linear polymer, one expects the correct exponent of n in eq 9 to be more negative than -2.5 , and taking the exponent as -2.5 results

in a B smaller than would result from nearly free rotation about bonds and the correct exponent of n .

Discussion

Nearly the only data resulting from experiments not involving extraction of quenched sulfur are the freezing points of equilibrium liquid sulfur as a function of temperature of equilibration. The assumptions involved in interpreting the experimental results are that the melting of monoclinic sulfur produces S_8 and equilibration slowly develops other species which depress the freezing point of S_8 . The calculated freezing points are obtained from the Raoult's law equation

$$-\ln X_8 = \frac{\Delta H}{R} \left(\frac{1}{T} - \frac{1}{T_0} \right) \quad (16)$$

where X_8 is the mole fraction of S_8 and ΔH and T_0 are the enthalpy and temperature of fusion of monoclinic sulfur to pure S_8 . West's value of the enthalpy of fusion to equilibrium liquid is 1717.6 J/g-atom at 115.21°,¹⁶ which yields, on correction for the calculated enthalpy of forming equilibrium sulfur from S_8 , a value of 1584.2 J/g-atom for the fusion of monoclinic sulfur to pure S_8 . The melting point to pure S_8 , as calculated from (15) with X_8 and ΔH derived from this model, is 120.683°. The calculated freezing points of equilibrium sulfur are presented in Table II together with experimental results.

Table II: Freezing Point as a Function of Equilibration Temperature

Equil temp. °C	Fp	
	Calcd	Exptl
114.5	115.26°C	114.5°C ^a
121.4	114.66°C	113.55°C ^b
131.1	113.73°C	112.5°C ^b
140.6	112.74°C	111.6°C ^b
130.0	386.98°K	387.0°K ^c
140.0	385.96°K	386.0°K ^c
150.0	384.80°K	384.3°K ^c

^a Reference 7. ^b Reference 14. ^c Reference 15.

The calculated freezing points would be in excellent agreement with Schaum's results if 1.16° were added to all of Schaum's freezing points. Carson's value of 114.5° for the equilibrium freezing point is the result of combining his data on the insoluble sulfur content as a function of temperature with Smith and Holmes's data on the dependence of freezing point on insoluble sulfur content. The calculated freezing point of liquid equilibrated at 114.5° lies 0.76° higher. It is thought that early methods of purifying sulfur

(42) P. J. Flory and J. A. Semlyen, *J. Amer. Chem. Soc.*, **88**, 189 (1966).

(43) H. Jacobson, C. O. Beckmann, and W. H. Stockmayer, *J. Chem. Phys.*, **18**, 1607 (1950).

were ineffective,⁴⁴ and the lower freezing points found by the early workers can be reasonably understood as the result of impurities present at concentrations of about 1 mol %. The calculated results are in excellent agreement with the recent work of Wiewiorowski, *et al.*, at 130 and 140°. The disagreement at 150° indicates the calculated composition is 0.5 mol % too high in S_8 at this temperature. It seems unlikely that a gross error in the amounts of species smaller than S_{11} is responsible, since the error becomes appreciable between 140 and 150° and these species are all present in large concentration at 140°, except S_5 which is estimated to be 5×10^{-3} mol % at 150°. The total amount of the larger ring species changes rapidly with temperature in this range. The likely errors in the treatment of the larger species have been discussed, and it is possible that this is a result.

Comparison of the calculated melting temperature of monoclinic sulfur to pure S_8 with the prompt melting points found by experiment is not satisfactory. The calculated temperature, 120.68°, is much above all experimental values. Wiewiorowski, *et al.*, obtain 118.85°, Smith and Holmes obtain 119.25° by extrapolation to zero insoluble sulfur content, and Schaum gives 118.75°. If we take 0.76° impurity lowering for Smith and Holmes and 1.16° for Schaum, the three values become 118.85°, 120.01°, and 119.91°. The discrepancies are still large and the worst agreement is for data taken with well-purified sulfur. The lifetime of the non- S_8 material is very long at low concentration in the solid near room temperature. Aten gives one case of sulfur quenched from 170° which gave 1.1% S_π after 150 days.⁸ If the decay process had an activation energy of 9 kcal/mol, the decay would be 30 times faster at 95° than at 25°. It might be necessary to age the solid for many days at elevated temperature to obtain reasonably pure S_8 if the sulfur initially contained much non- S_8 material.

Aten's S_π

Aten's S_π is the product of extraction of quenched liquid sulfur with CS_2 and cooling of the extract to a low temperature which is accompanied by precipitation of crystalline sulfur. These steps result in separation of sulfur species. Aten's S_π is the sulfur other than S_8 remaining in the extract. The interpretation of Aten's S_π in terms of the present model is based on the interpretation of these separations. There is no evidence whether or not species other than S_8 are precipitated from the extract at -80°. The extraction step involves the transfer of sulfur species from an amorphous sulfur-rich phase to a CS_2 -rich phase, and one may assume that the concentration of any particular sulfur species in the CS_2 phase would, at equilibrium, be controlled by the distribution coefficient of that species between the two phases. The average chain length of the linear polymer species is given

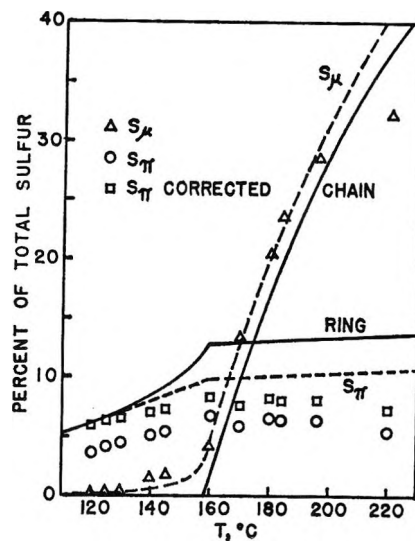


Figure 3. S_π and insoluble sulfur contents vs. temperature. The dashed curves represent calculated approximations to the S_π and S_μ contents, and the squares represent recalculation of Aten's S_π results, as indicated in the text. See Table III for another representation of these data.

by r^{-1} , and the average chain length is large when the linear polymer content is an appreciable fraction of the total sulfur. It is assumed that the linear polymer species make a negligible contribution to the sulfur content of the CS_2 extract. It is also assumed that ring species of high molecular weight give a negligible contribution to the sulfur content of the CS_2 extract. The distribution coefficients of linear polymer species between polymer-rich and solvent-rich phases vary with chain length approximately as $\exp(\alpha x)$, where x is the chain length and α depends on the compositions of the two phases and other factors.²² Assuming a similar behavior for the distribution coefficients of ring species leads to the conclusion that the lower molecular weight ring species are extracted in preference to the higher molecular weight species. The extraction of quenched sulfur is not an equilibrium process, but one expects the higher molecular weight species to diffuse out into the solvent more slowly than the lower molecular weight species, leading to qualitatively similar results. As an approximation to this, it is assumed that species S_{29} and higher are left in the sulfur-rich phase and species of lower molecular weight are quantitatively extracted into the CS_2 rich phase. The division at S_{28} is chosen to make Aten's insoluble sulfur content agree with the calculated insoluble sulfur content over the range 160–184°. The dashed lines in Figures 3 and 4 represent, on this basis, the content and average formula of S_π .

The retention of ring sulfur in the polymer-rich phase is partially confirmed by Aten's finding that the S_π content is larger if the quenched sulfur is

(44) B. Meyer, ref 4, pp 73–76.

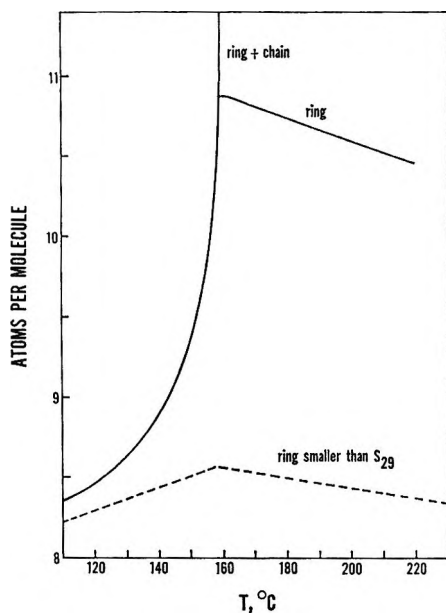


Figure 4. Calculated average formulas of sulfur fractions vs. temperature. S_8 is excluded from the rings represented here. The dashed curve represents an approximation to S_x .

repeatedly extracted with CS_2 .⁸ Smith and Holmes¹³ corrected their data on insoluble sulfur content for the solubility of insoluble sulfur in CS_2 . Precipitation of ring species in the polymer-rich phase has been experimentally demonstrated in PDMS.⁴¹

The calculated S_x content, represented by the curve labeled "ring S_{28} and smaller" in Figure 3, lies well above Aten's values. A reduction of 40% by weight in the calculated S_x would be required to bring agreement. At 120° the major part of the calculated S_x is rings close to S_8 , so even a large change in B would not produce much change in agreement between calculation and experiment. Part of the discrepancy may be removed by recalculating Aten's results. Aten arbitrarily assumed 50% of the sulfur in a particular CS_2 solution saturated with S_8 at -80° was S_x . He constructed a ternary phase diagram by diluting repeatedly with CS_2 while maintaining S_8 saturation at -80° and analyzing for total sulfur after each dilution. In order to correct for the arbitrary initial assumption, he assumed that all the S_x lost from quenched sulfur on aging is converted to insoluble sulfur and got from this a factor, 0.78, by which the S_x content from the phase diagram was multiplied to get the final S_x content.⁸ Schenk and Thümmeler assumed that the solubility of S_8 in CS_2 at Dry Ice temperature is independent of the S_x content and showed on that basis that 64% of the S_x is converted to insoluble sulfur after the CS_2 is evaporated.¹¹ Later they showed by direct analysis that 55% of the S_x is converted to insoluble sulfur under these circumstances,¹² so it appears the S_8 solubility in CS_2 is, if anything, slightly suppressed by S_x . Aten's phase diagram indicates enhancement of the S_8 solubility

by the presence of S_x . Aten gave enough information to allow his S_x results to be calculated back to the total sulfur concentration in the CS_2 extract at -80° , and he indicated that 10 g of S and 20 ml of CS_2 were used in each experiments, so that the total sulfur content in the extract can be calculated and the fraction of S_x in the quenched sulfur can be found on the assumption of constant S_8 solubility in the CS_2 extract at -80° . The S_x content has been recalculated on the assumption that the S_8 is 2.53% of the solutions at -80° . The resulting S_x contents are plotted as squares in Figure 3. The total of Aten's S_x , recalculated as indicated, and his insoluble sulfur may be compared with the total non- S_8 sulfur calculated from the model. Table III gives the comparison. The comparison eliminates the assumption of a sharp division at S_{28} between S_x and insoluble sulfur. The agreement between calculation and experiment is excellent below 160°. Over the range 160–184° the discrepancies are consistent with Aten's thermometer readings being about 2.5° below the temperature scale of this paper, which can easily happen if a thermometer calibrated for total immersion is used in partial immersion without correction. At 184° and above the rate of quenching obtained by Aten probably is comparable with the rates of the reactions involved in equilibrating the sulfur.

Figure 4 shows the average formula of the non- S_8 sulfur and the average formula of S_x based on the assumption that S_x is all the non- S_8 ring material smaller than S_{29} . Schenk and Thümmeler's results,¹¹ recalculated on the basis that 55% of the S_x is converted to insoluble sulfur on evaporation of the CS_2 extract, give an average formula of 8.14 atoms per molecule with a standard deviation of 0.29 for sulfur quenched from temperatures in the range 130–165° and 8.16 atoms per molecule with a standard deviation of 0.36 for sulfur quenched from 350°. Schenk and Thümmeler reported few details of their extraction, but it is clear that they obtained concentrated solutions, since assuming 55% conversion leads to negative calculated S_8

Table III: Calculated and Experimental Non- S_8 Content as a Function of Temperature

Temp. °C	Wt %	
	Exptl ^a	Calcd
120	5.9	6.0
125	6.5	6.5
130	6.8	7.1
140	8.3	8.3
145	9.0	9.1
160	12.0	14.0
170	20.9	22.6
180	26.6	29.9
184	31.5	32.6
196	36.6	40.4
220	39.4	51.2

^a Sum of Aten's S_x and S_x corrected as indicated in the text.

content in a few cases. (These negative S_8 contents were treated as acceptable in the recalculation since otherwise one would either treat some of the results in a different way from others or else assume some larger conversion for all samples, which disagrees with the later experiments.) The dashed curve is calculated to agree with Aten's work with much less concentrated solutions of S_x . One might expect that Schenk and Thümmeler's extraction conditions would be more effective in excluding large rings from the CS_2 extract than Aten's conditions. If it is assumed that the dashed line of Figure 4 represents what would be found with experiments free of any random error, the result of a series of experiments carried out at the same temperatures as Schenk and Thümmeler used in the range 130–165° would be 8.50 with a standard deviation of 0.09. The agreement between experiment and the present calculation is fairly satisfactory without attempting to adjust the calculation to unknown extraction conditions.

The development of insoluble sulfur on aging the quenched liquid can be explained in terms of the model presented here. It seems unlikely that the aging process involves free radical reactions. Rates of equilibration of liquid sulfur extrapolated back to room temperature suggest times of the order of years for processes involving the formation of radicals, and the effect of iodine on the amount of S_x found immediately after quenching and the amount of insoluble sulfur after aging suggests that the presence of free radicals before quenching is unimportant. Reactions of the type $S_n + S_m \rightleftharpoons S_{n+m}$ might be expected to have much lower activation energies and more negative activation entropies than reactions in which ring opening to form diradical chains occurs. The main equilibration reactions at high temperature would then be expected to involve radical formation and destruction, while the main reactions at low temperatures would be expected to be of the direct-ring fusion-fission type. So long as n and m are large (larger than 10 for the present model), these reactions are in equilibrium at the same composition at all temperatures. The change of equilibrium composition with temperature comes from the reactions in which n and m are not both large. It is easy to show that the initial changes in composition after the temperature of a system initially in equilibrium is changed involve only the reactions in which n and m are not both large, and that these changes are in the direction of establishing the equilibrium at the new temperature. The aging of quenched sulfur is complicated by the crystallization of S_8 during the aging process. Partial crystallization of S_8 increases the concentrations of the other species in the amorphous phase, and the result of the increased concentrations is to put all of the reactions out of equilibrium. The new position of equilibrium lies at higher large ring concentrations

and lower small ring concentrations for each reaction except those reactions in which S_8 appears. The effect is a very substantial shift toward high molecular weight because the large rings appearing on the right in one set of reactions appear on the left in another set of reactions leading to still larger rings. Although a quantitative realization of this explanation of the formation of insoluble sulfur on aging is beyond the scope of this paper, the qualitative results are in agreement with the available experimental results: the fraction of S_8 increases continuously, and the fraction of insoluble sulfur increases to a maximum followed by a slow decrease.^{8,10}

Conclusions

The model of the molecular composition of liquid sulfur offered in this paper together with the interpretation of S_x as a partially fractionated mixture of ring species gives a good account of experimental non- S_8 content, freezing point, and molecular weight of S_x as functions of temperature. The model and interpretation of S_x are constructed to agree with the experimental equilibrium vapor composition, insoluble sulfur content over 160–184°, and heat capacity and do not conflict with any evidence known to the author. The viscosity of liquid sulfur in the range 150–160° should be amenable to treatment in terms of the model. The development of insoluble sulfur after quenching from temperatures below 150° may be less easy to treat in quantitative terms. The author hopes to offer accounts of both these matters in the future. A number of points could be cleared up by experimentation. The total non- S_8 content probably could be determined by reaction of quenched samples with triphenyl phosphine. The melting point of monoclinic sulfur in contact with freshly melted sulfur could be determined in a way which would remove doubts about the purity of the S_8 in the solid before melting. The various ring species might be separated by gel permeation chromatography. The author hopes that if anyone does these things, the work will be carried out and reported in such a way as to relieve future speculators of the burden of guessing what the results mean.

Acknowledgments. I am indebted to many for help. Dr. C. Basch insisted I read Aten's paper. Professor H. E. Bent raised questions about phase equilibrium. Dr. D. Bayfuss and Professor R. W. Kiser suggested references, and Dr. I. Taha brought one into my office. Professor H. Kim read the manuscript and made some useful suggestions. The computations were mainly carried out at the Computer Center and financed by the Research Activities Office of the University of Missouri. A significant part of the literature work was carried out in the Pomona College Chemistry Department Library. The work was partially supported by DOD Contract No. DAAA13-68-C-0033.

Relative Cation Mobilities in Silver Bromide-Potassium Bromide Melts¹

by Richard W. Laity and Albert S. Tenney

School of Chemistry, Rutgers University, New Brunswick, New Jersey 08903 (Received October 24, 1969)

Direct current transference experiments have been used to compare the rates of cation migration relative to bromide at a number of temperatures and concentrations of the system AgBr-KBr. Individual cation conductance isotherms have been calculated from a combination of these data with Λ values for the same mixtures. Both mobilities decrease with decreasing concentration of AgBr, that of the initially more mobile silver ion falling considerably more rapidly. The resulting "crossover point" shifts toward higher concentrations of AgBr as temperature increases. Although no frits or other porous materials were employed in this work, the observed behavior is remarkably similar to that found in previous transference experiments on other binary mixtures. It is contrary, however, to the equality of cation mobilities at all concentrations implied by some emf values reported in the literature for AgBr-KBr concentration cells with transference. By dividing the potentials predicted for such cells into four "components" in such a way that contributions due to thermodynamic nonideality and to inequality of cation mobilities ("liquid junction potentials") are evaluated separately, it is shown that the results of some new emf measurements are consistent with the transference behavior observed directly and do not support conclusions based on the earlier reports of concentration-cell emf's.

Previous transference experiments on molten LiCl-KCl mixtures revealed a strong and unexpected dependence of relative cation mobilities on concentration.² Subsequently, similar behavior was observed in such other systems as NaNO₃-KNO₃^{3a,b} and LiNO₃-KNO₃.⁴

As was pointed out previously,⁵ however, emf measurements reported by Murgulescu and Marchidan⁶ indicate significantly different behavior: equal cation mobilities over the entire concentration range studied in a number of systems.

Although most of the latter systems have not been the subject of direct transference experiments, the system PbCl₂-KCl had been found by Duke and Fleming⁷ to have unequal cation mobilities that should have given rise to substantially larger liquid junction potentials⁸ than the "less than 1 mV" reported by Murgulescu and Marchidan.⁶

In an attempt to identify the source of this discrepancy, Behl and Egan⁸ carried out additional emf measurements on PbCl₂-KCl. They found results consistent with the transference measurements of Duke and Fleming.⁷

Since capillary tubing had been used to isolate the electrode compartments described by Murgulescu and Marchidan, while porous materials of relatively high internal surface area were used both in the emf measurements of Behl and Egan and in the transference work of Duke and Fleming (as well as in most other transference determinations), the possibility that such materials introduced a "wall effect" on the relative cation mobilities could not be ruled out.

The present studies are part of a thorough investigation of transport properties of the systems silver bromide-alkali bromide, for which equal cation mobilities were also indicated by Murgulescu's emf measurements.

The concentration dependence of the equivalent conductance in AgBr-KBr has been found^{9,10} to be remarkably similar to that of LiCl-KCl. In both systems Λ shows such strongly negative deviations from additivity of the pure salt values that conductance *vs.* composition isotherms pass through a minimum. It would therefore be surprising if cation mobilities in AgBr-KBr were equal at all concentrations.

The aim of this work has been to determine the relative mobilities of the cations in this system with good precision over substantial ranges of composition and temperature, employing a Hittorf-type transference method in which no frits or other porous materials separate the compartments. In addition, some relatively crude emf measurements on concentration cells with transference have been included to check for consistency with values calculated using the experimental transference numbers obtained in this work.

- (1) This work is part of a program sponsored by the U. S. Atomic Energy Commission.
- (2) C. T. Moynihan and R. W. Laity, *J. Phys. Chem.*, **68**, 3312 (1964).
- (3) (a) F. Lantelme and M. Chemla, *Bull. Soc. Chim. Fr.*, 2200 (1963); (b) E. P. Honig and J. A. A. Ketelaar, *Trans. Faraday Soc.*, **62**, 190 (1966).
- (4) F. Lantelme and M. Chemla, *Electrochim. Acta*, **10**, 663 (1965).
- (5) R. W. Laity and C. T. Moynihan, *J. Phys. Chem.*, **67**, 723 (1963).
- (6) I. G. Murgulescu and D. I. Marchidan, *Russ. J. Phys. Chem.*, **34**, 2534 (1960); *Stud. Cercet. Chim.*, **8**, 383 (1960).
- (7) F. R. Duke and R. A. Fleming, *J. Electrochem. Soc.*, **106**, 130 (1959).
- (8) W. K. Behl and J. J. Egan, *J. Phys. Chem.*, **71**, 1764 (1967).
- (9) B. S. Harrap and E. Heymann, *Trans. Faraday Soc.*, **51**, 259 (1955).
- (10) S. Petrucci and R. W. Laity, to be published.

Experimental Section¹¹

Materials. Matheson Coleman and Bell purified AgBr was used without further purification. The KBr was Baker reagent grade. Salt mixtures were prepared by heating the solids together in the transference vessel slowly (2 days) to 300° under vacuum, then melting under dry nitrogen. The composition could then be varied by adding one of the pure salts which had also been dried at 300°. KCN was reagent grade from either Matheson Coleman and Bell or Baker.

Apparatus. The transference vessel, furnace, and devices for regulating and measuring temperature were those employed by Moynihan and Laity.¹

As anodes, both bromine and silver electrodes were used. To avoid difficulties resulting from dendritic growth of silver, only bromine electrodes were used as cathodes. Bromine vapor was introduced into a porous carbon cathode by first passing a stream of dry nitrogen through a liquid bromine trap. A bromine anode was simply a short graphite rod. A silver anode consisted of 99.99% silver wire about $\frac{1}{8}$ in. in diameter.

A sheath enclosing the contents of each electrode compartment was made from a Pyrex tube, tapered at the bottom so that contact to the bulk was made through a capillary 3 to 4 cm long and about 1 mm in diameter. This capillary was bent upward so that the salt could not run out of the compartment as the cell was raised at the end of a run.

Run procedure was similar to that of Moynihan and Laity¹ except that cathode, as well as anode, compartments were analyzed.

Analysis. Several analytical techniques were investigated. By far the greatest accuracy and precision were obtained using a completely gravimetric method in which KBr was first leached with hot water from a previously weighed sample consisting of both salt and electrode material fragments. After reweighing, the AgBr was dissolved in excess KCN solution and the remaining material weighed a third time.

Some mixtures were analyzed as many as 15 times. In such cases the standard deviation in mole fraction of silver bromine was found to be less than one part per thousand.

Emf Measurements. Except for the use of silver metal electrodes in both compartments, essentially the same apparatus and materials as had been used in the transport number experiments were employed in the emf experiments.

The procedure consisted of putting different concentrations of salt on each side of a cell, immersing the cell in a molten salt bath, monitoring the emf of the cell until it became stable, and removing and analyzing the salt in the compartments as in the transport number experiments.

Although this was a rather crude method, it was possible to investigate the approximate effect of cation mobility differences on the emf of concentration cells

with transference over a wide range of compositions quickly and easily.

Calculation of Results

Mobility Ratios. Since the assignment of transport numbers depends on the choice of reference frame, which is arbitrary in molten salts,¹² it is convenient for the purpose of comparing cation mobilities to choose the transport number of the bromide ion, t_{Br} , equal to 0 and hence assign cation transference numbers such that $t_{Ag} + t_K = 1$. The actual transport numbers of each cation relative to bromide must vary from 1 to 0 as the concentration changes from pure salt to infinite dilution. Thus it is more instructive to describe results of transference experiments in a way that reflects any variations of *mobility* with concentration. However, it is desirable to make use of a quantity whose value is not dependent on the reliability of conductance measurements. Thus, Moynihan and Laity¹ employed the "per cent mobility difference," Q . Present results will be expressed in terms of the mobility ratio R , defined as $R = \lambda_{Ag}/\lambda_K$, where λ_i is the equivalent conductance of cation i relative to Br. R is related to Q by $Q = 100(R - 1)$. It is calculated from experimental data by the relation

$$R = \frac{\phi_{Ag} N_K}{N_{Ag} \phi_K}$$

where ϕ is the "transport fraction" whose calculation from experimental data is described by Moynihan and Laity¹ for the case where halogen electrodes are used. An analogous expression can be employed to obtain the same quantity when the anode is silver metal.

Calculation of Emf from Thermodynamic and Transport Data. The basic equation for the emf of the concentration cell $Ag|(AgBr + KBr)_A|| (AgBr + KBr)_B|Ag$ is

$$\epsilon_{cell} = \frac{RT}{F} \int_A^B \frac{\phi_2}{N_2} d \ln a_1$$

where 1 refers to Ag, 2 to K, and A and B to two different concentrations,¹³ B richer in AgBr.

To distinguish the explicit dependence of the emf on activity coefficients and on transport number values it is instructive to divide the total emf into a sum of four "contributions": ϵ_N , ϵ_γ , ϵ_ϕ , and $\epsilon_{\gamma\phi}$.

I. For an *ideal solution* with equal cation mobilities, $\epsilon_I = \epsilon_N$, where

$$\epsilon_M = \frac{RT}{F} \int_A^B d \ln N_1 = \frac{RT}{F} \ln \frac{N_{1B}}{N_{1A}} \quad (1)$$

(11) For a more complete description of apparatus and procedure see A. S. Tenney III, Ph.D. Thesis, Rutgers University, 1970.

(12) R. W. Laity, "Fused Salt Transport Numbers" in "The Encyclopedia of Electrochemistry," C. A. Hampel, Ed., H. Reinhold Publishing Corp., New York, N. Y., 1964.

(13) R. W. Laity, *J. Amer. Chem. Soc.*, **79**, 1849 (1957).

II. For a *nonideal solution with equal cation mobilities*, $\varepsilon_{II} = \varepsilon_N + \varepsilon_\gamma$, where

$$\varepsilon_\gamma = \frac{RT}{F} \int_A^B d \ln \gamma_1 \quad (2)$$

Integration in this case (as in many molten salt mixtures) is facilitated by the fact that the system is thermodynamically "regular." Thus Hildebrand and Salstrom have shown that $RT \ln \gamma_1 = AN_2^2$ in a mixture of AgBr with alkali bromides, A being a constant whose value is $-1480 \text{ cal mol}^{-1}$ in AgBr-KBr.¹⁴ ε_{II} is the emf predicted for a cell in which cation mobilities are equal over the concentration range from A to B .

III. For an *ideal solution with unequal cation mobilities*, $\varepsilon_{III} = \varepsilon_N + \varepsilon_\phi$, where

$$\varepsilon_\phi = \frac{RT}{F} \int_A^B \left(\frac{\phi_2}{N_2} - 1 \right) d \ln N_1 \quad (3)$$

The value of ϕ_2/N_2 is obtained from the results of the transport number experiments. From the values of R measured for AgBr-KBr, it was found that ϕ_2/N_2 could be represented within experimental precision as a linear function of N_1 over the concentration range studied in the emf experiments.

IV. Finally, for *nonideal solutions with unequal cation mobilities*, $\varepsilon_{IV} = \varepsilon_N + \varepsilon_\gamma + \varepsilon_\phi + \varepsilon_{\gamma\phi}$, where

$$\varepsilon_{\gamma\phi} = \frac{RT}{F} \int_A^B \left(\frac{\phi_2}{N_2} - 1 \right) d \ln \gamma_1 \quad (4)$$

may be considered an additional "correction" that is required wherever cation mobilities are unequal in a nonideal system. By comparison of ε_{IV} with ε_{II} it is seen that the quantity $\varepsilon_\phi + \varepsilon_{\gamma\phi}$ may be taken as the "liquid junction potential."

Since ε_{IV} includes all four contributions to the emf, it is equivalent to the quantity designated $\varepsilon_{\text{cell}}$ at the beginning of this section.

Results and Discussion

The results for the cation mobility ratios at four temperatures are plotted in Figure 1 as functions of equivalent fraction AgBr. They may be summarized as follows: at 350° and $N_{\text{Ag}} = 0.72$ (only the eutectic region was accessible), $R = 1.69 \pm 0.04$; at 450° and $0.55 \leq N_{\text{Ag}} \leq 0.9$, $R = 0.67 + 0.89N_{\text{Ag}} \pm 0.04$; at 500° and $0.55 \leq N_{\text{Ag}} \leq 0.75$, $R = 0.58 + 0.85N_{\text{Ag}} \pm 0.03$; at 550° and $0.55 \leq N_{\text{Ag}} \leq 0.9$, $R = 0.58 + 0.53 \cdot N_{\text{Ag}} \pm 0.04$; at 550° and $N_{\text{Ag}} = 0.48$, $R = 0.90 \pm 0.04$.

Each point in Figure 1 is the average of the results of a number of determinations. The error bar indicates the average deviation, except that when five or more determinations were made, the standard deviation is used. The errors indicated in the summary equations are the averages of the errors in each contributing point.

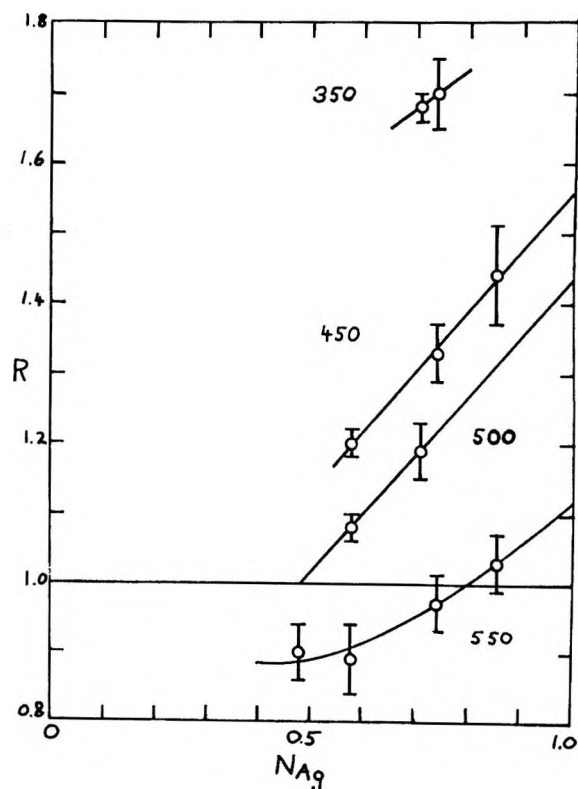


Figure 1. Isotherms of the $\text{Ag}^+:\text{K}^+$ ion mobility ratio R in molten AgBr-KBr mixtures at temperatures from 350 to 550° . (Br^- ion is reference.)

Although remarkably good precision was achieved in comparison with previous measurements of this type, the error in our chemical analysis is not large enough to account for the random errors in R . Such variations could be caused by a slight mixing between salt in the electrode compartments and that in the bulk. It should be noted that significant mixing of this type would yield an apparently smaller cation mobility difference, *i.e.*, R closer to unity, for compartments with bromine electrodes. In such cases the true cation mobility differences would be at least as large as those indicated by the R values reported here. In the case of silver anodes, on the other hand, mixing would yield high values of R . No systematic difference could be found among the results obtained with bromine cathodes, bromine anodes, or silver anodes. The agreement among all three was within the random error indicated by the precision of repeated runs with electrodes of each type.

Pure AgBr melts at 432° , KBr at 730° ; the two salts form a eutectic mixture at $69 \text{ mol } \%$ AgBr which melts at about 280° .¹⁵ Although the range of concentrations available at the experimental temperatures was thus

(14) J. H. Hildebrand and E. J. Salstrom, *J. Amer. Chem. Soc.*, **54**, 4257 (1932).

(15) S. F. Zhemchuzhni, *Z. Anorg. Allgem. Chem.*, **153**, 56 (1926); summarized in "Physico-Chemical Constants of Binary Systems, Vol. 3, J. Timmermans, Ed., Interscience Publishers, New York, N. Y., 1960, p 86.

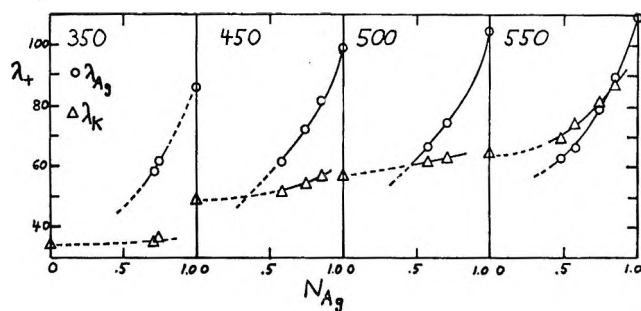


Figure 2. Isotherms of individual ionic conductances of Ag^+ and K^+ in molten mixtures of $\text{AgBr} + \text{KBr}$ based on R values in Figure 1 and Δ for the same mixtures.

limited, enough values have been obtained to indicate the dependence of R on both concentration and temperature over a wide range of values. Thus, it is clear that at temperatures below 500° , Ag^+ is the more mobile cation ($R > 1$) for $N_1 > 0.5$, while at 550° , K^+ is more mobile for $N_1 < 0.8$.

To assign numerical values to cationic mobilities or conductances (relative to Br) it is necessary to know the equivalent conductance of each mixture as well as the transport numbers. Using the results of Laity and Petrucci,¹⁰ we find the concentration dependence of the individual ionic conductances shown in Figure 2.

Both the temperature and composition dependence of the relative cation mobilities in AgBr-KBr are remarkably similar to those in KCl-LiCl^1 and in alkali nitrates.²⁻⁴ In all of these systems both mobilities increase monotonously with increasing concentration of the better-conducting (when pure) salt. The mobility of the cation of this salt has significantly greater concentration dependence than that of the other cation, resulting in the "crossover" of mobilities indicated for our system by each pair of isotherms in Figure 2. As the temperature is increased, the crossover point moves toward higher concentrations of the better-conducting salt. This means that the mobility of the cation of this salt is less temperature dependent than that of the other cation. Thus, the apparent "activation energy" for conductance of Ag^+ (based on the temperature dependence of λ_{Ag}) is less than that of K^+ at all concentrations studied, as shown by the isotherms of E^\ddagger plotted in Figure 3. Perhaps more noteworthy in this system, however, is the fact that while both $E^\ddagger_{\lambda_{\text{K}}}$ and $E^\ddagger_{\lambda_{\text{Ag}}}$ apparently decrease with increasing KBr concentration, the E^\ddagger_{Δ} (the quantity obtained from conductance measurements alone) increases. This apparent anomaly is due to the trivial fact that as one ionic species increases in concentration, it contributes more to the conductivity of the mixture.

Results of emf measurements on concentration cells with transference are presented in Table I along with values calculated for each of the "components" indicated. In view of the relatively poor precision of the observed emf's, their accuracy is not expected to be

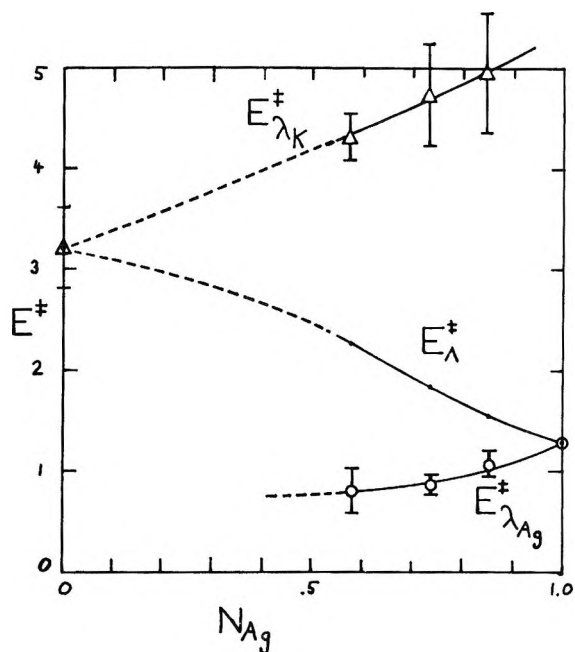


Figure 3. Activation energies for Δ_{mixt} and for individual cationic conductances in molten $\text{AgBr} + \text{KBr}$ mixtures at 500° .

much better than ± 2 mV. For example, although the second and sixth runs were performed on identical concentrations at nearly identical temperatures, the emf's measured differed by more than 1 mV. The uncertainties in the concentrations determined by direct analysis of overall electrode compartment contents, as well as in the emf measurement itself, were not nearly large enough to account for such discrepancies. The main source of error was probably attributable to the difficulty of maintaining uniform concentrations within the electrode compartments. The mixing that resulted from both interdiffusion and the mass flow between compartments that took place as each was stirred between emf readings may not have been negligible in some of these experiments; in such cases the concentrations analyzed were not necessarily identical with those that determined the emf at the electrodes. In an effort to reduce this error several experiments were performed in which excess solid KBr in one compartment (whose temperature was accurately known) fixed the liquid concentration at a value which could be taken from the phase diagram. Unfortunately, the uncertainty in the available N_{Ag} value at a particular temperature amounted to about ± 0.01 .¹⁵

To test whether the emf results were consistent with the transport number results, it was necessary to study a concentration range over which ε_ϕ and $\varepsilon_{\gamma\phi}$ were large compared to the uncertainties in the method. This accounts for the choices of composition and temperature at which our emf experiments were conducted. Note that a crossover in cation mobilities within the interval spanned by the electrode compartment compositions

Table I: Observed and Calculated Emf's for the Concentration Cell with Transference Ag|AgBr + KBr (A)||AgBr + KBr (B)|Ag

Run	Temp, °C	Concn's		Components of predicted emfs, mV				Predicted emf's, mV		Obsd emf's, mV ϵ_{exp}
		N_{Ag} A	N_{Ag} B	ϵ_N	ϵ_γ	ϵ_ϕ	$\epsilon_{\gamma\phi}$	ϵ_{II}	ϵ_{IV}	
1	455	0.500	1.000	44	16	-8	-3	60	49	50.9
2	453	0.52 ^a	1.000	41	15	-8	-3	56	45	43.2
3	452	0.796	1.000	14	3	-4	-1	17	12	12.0
4	451	0.636	0.918	23	8	-5	-2	31	24	26.6
5	482	0.628	0.907	24	9	-4	-2	33	27	29.0 ^b
6	451	0.52 ^a	1.000	41	15	-8	-3	56	45	42.1
7	431	0.541	0.665	13	6	-2	-1	19	16	13.2
8	443	0.726	1.000	20	5	-5	-1	25	19	16.5
9	447	0.53 ^a	1.000	39	14	-8	-2	53	43	41.5
10	446	0.53 ^a	1.000	39	14	-8	-2	53	43	44.5

^a Determined from phase diagram:¹⁵ pure solid KBr was in contact with these solutions. ^b Compartments were separated by a coarse fritted Pyrex disk.

would result in a decrease of the liquid junction potential $\epsilon_\phi + \epsilon_{\gamma\phi}$.

Several sources of error contribute to the uncertainty in values tabulated for the components of ϵ_{IV} . The random error in the activity coefficients reported by Hildebrand and Salstrom¹⁴ is about 4%, which gives rise to $\pm 4\%$ uncertainty in the values calculated for ϵ_γ and $\epsilon_{\gamma\phi}$. More seriously, the uncertainty in our own values of R results in uncertainties of about $\pm 15\%$ in ϵ_ϕ and $\epsilon_{\gamma\phi}$. From these figures the total uncertainty in predicted emf values is about $\pm 1\%$ (< 1 mV) for ϵ_{II} and 3 to 5% (1 to 2 mV) for ϵ_{IV} , considering only those cells in which compartment A was analyzed directly. The additional uncertainty for both ϵ_{II} and ϵ_{IV} in experiments with excess solid KBr is about ± 2 mV (resulting from inaccuracy of the phase diagram).

Examination of the four contributions to the emf reveals the following generalizations. (a) The signs of ϵ_N and ϵ_γ are positive (free energy and excess free energy of mixing are both negative), while the signs of ϵ_ϕ and $\epsilon_{\gamma\phi}$ are negative (Ag^+ is more mobile than K^+ in the concentrations studied). (b) All emf components increase in magnitude as N_{Ag} (A) decreases in the concentration range studied (due mainly to the fact that the sign of each integral in eq 1-4 remains unchanged while the range of integration increases). (c) ϵ_N is the largest and $\epsilon_{\phi\gamma}$ the smallest of the contributions at all concentrations studied. At high silver bromide concentrations, where R is large and γ_{AgBr} nearly unity, $|\epsilon_\phi| > |\epsilon_\gamma|$, but as N_{Ag} (A) decreases, R decreases and γ_{AgBr} decreases, so that

ϵ_γ eventually becomes greater than $-\epsilon_\phi$. Thus, for the large concentration differences needed to obtain experimental emf's of sufficient magnitude for valid comparisons of ϵ_{exp} with predicted values, contributions due to the nonideality of the solution comprise as much as one third of the total, while the (negative) contributions to ϵ_{IV} due to unequal cation mobilities, $\epsilon_\phi + \epsilon_{\gamma\phi}$, are generally less than one-fourth the magnitudes of ϵ_{II} and ϵ_{IV} .

$\epsilon_\phi + \epsilon_{\gamma\phi}$ has been called the "liquid junction potential." It reaches a maximum of only about -11 mV, even at the "optimum" ranges of composition and temperature chosen. For most of the cells listed, however, comparison of both ϵ_{IV} and ϵ_{II} with the observed emf provides a crude but justifiable basis for ascertaining the presence (or absence) of a liquid junction potential. From the data in Table I it is apparent that within experimental error, emf results for the concentration cells studied are consistent with the transport number results reported here. Our emf measurements do not support the conclusion that cation mobilities are equal in this system. It should be clear, furthermore, that since the magnitude of $\epsilon_\phi + \epsilon_{\gamma\phi}$ is likely to be relatively small in many systems, it is difficult to draw reliable conclusions about relative mobilities of like-charged ions from the emf's of concentration cells. The values of R reported here for the system AgBr-KBr show that even in the absence of porous separators such information can be obtained directly with considerably greater precision by a dc transference method.

New Compounds Consisting of Sodium *p*-Toluenesulfonate, Water, and a Polar Benzenoid Nonelectrolyte

by Joseph Steigman,¹ Richard DeIasi,² and Judah Lando

Department of Chemistry, Polytechnic Institute of Brooklyn, Brooklyn, New York 11201 (Received March 2, 1970)

Sixteen new crystalline compounds consisting of sodium *p*-toluenesulfonate, water, and an aromatic nonelectrolyte have been prepared. Analysis of these compounds indicates a molar ratio (solute:salt:water) ranging from 1:2:2 to 1:5:5. Half of these new compounds have a molar ratio of 1:4:4. These ratios suggest an expanded structure, possibly one in which the aromatic solute acts as a guest molecule in a two-dimensional cage of sodium tosylate and water. This hypothesis is supported by the large cell dimensions obtained from the X-ray diffraction measurements of single crystals of three of these new compounds. The compounds with *o*-toluic acid and *o*-nitroaniline (both with molar ratios 1:4:4) are orthorhombic, space group Pncb, with $a = 37.06 \text{ \AA}$, $b = 23.72 \text{ \AA}$, $c = 10.21 \text{ \AA}$, and $a = 36.97 \text{ \AA}$, $b = 24.02 \text{ \AA}$, $c = 10.20 \text{ \AA}$, respectively, while that with *p*-nitrophenol (molar ratio 1:3:3) is orthorhombic, space group Pccn, with $a = 38.16 \text{ \AA}$, $b = 18.20 \text{ \AA}$, $c = 10.19 \text{ \AA}$. The rotation photographs of these compounds mounted along the *c* axis show sharp spots for *l* even but diffuse spots for *l* odd. Similarly, the Weissenberg photographs of the *l* odd layers show diffuse, almost continuous festoons. This suggests that these compounds are layer crystals which are made up of symmetrical molecules but are not completely ordered. Sodium *p*-toluenesulfonate exists as a stable hemihydrate at room temperature, crystallizing in a monoclinic unit cell: space group P2₁/c, with $a = 17.93 \text{ \AA}$, $b = 14.83 \text{ \AA}$, $c = 6.73 \text{ \AA}$, and $\beta = 90^\circ$. Room-temperature infrared spectra of these new compounds were investigated, with particular emphasis placed upon the O-H (st), O-H (b), and S-O (st) modes. Very small differences were observed in these modes for all of the new compounds investigated, but these modes were different from the corresponding modes in the starting materials. It was concluded that the water in all of these new compounds was hydrogen bonded primarily to the common structural unit, *i.e.*, sodium tosylate. Differential scanning calorimetry combined with high-temperature infrared spectroscopy of several of these compounds indicates that the decomposition of these compounds probably takes place in two steps. The first step involves the breakdown of the cage system into free solute, water, and sodium tosylate hemihydrate, followed by the release of water from the tosylate hemihydrate during the second step.

Introduction

The effects of neutral salts on the solubility in water of a nonelectrolyte are often described by the empirical Setschenow equation

$$\log f = \log (S_0/S) = K_s C_s \quad (1)$$

in which f is the activity coefficient of the solute, S_0 is its solubility in water, S is its solubility in the electrolyte solution of concentration C_s , and K_s is the Setschenow constant. Inorganic salts usually cause salting out of organic solutes. Equation 1 holds fairly well for relatively insoluble nonelectrolytes in inorganic salt solutions whose concentrations may range from dilute to 2 *M*.³ Organic electrolytes like the alkali metal *p*-toluenesulfonates and various quaternary ammonium compounds almost always salt in organic nonelectrolytes. The equation is usually satisfactory to 0.5 *M* salt³ and has been shown to hold for some salts in solutions as concentrated as 2 *M*.⁴

A previous paper from this laboratory briefly reported that Setschenow plots for *p*-nitroaniline in concentrated aqueous solutions of sodium and potassium *p*-toluenesulfonates showed maxima at approximately 1.7 and 1.0 *M*, respectively and that the decrease in the

solubility of nitroaniline appeared to be associated with the formation of a solid phase consisting of alkali metal tosylate, *p*-nitroaniline, and water.⁵

Similar compounds were reportedly formed from aqueous sodium *p*-toluenesulfonate solutions of concentrations greater than 1.0 *M* during an investigation of the solubility of *o*- and *m*-dinitrobenzene in certain organic and inorganic salts.⁶ We have found 13 additional compounds formed from substituted benzoic acids, anilines, and phenols with sodium tosylate. Four compounds of this type are formed from an aqueous potassium tosylate solution and one is formed from an aqueous lithium tosylate solution. Some of these nonelectrolytes also show solubility maxima in aqueous solutions of tetra-*n*-butylammonium bromide;

(1) To whom inquiries should be addressed.

(2) Submitted in partial fulfillment of the requirements for the degree of Doctor of Philosophy to the Graduate School of the Polytechnic Institute of Brooklyn, June 1968.

(3) F. A. Long and W. F. McDevit, *Chem. Rev.*, **51**, 119 (1952).

(4) R. L. Bergen, Jr., and F. A. Long, *J. Phys. Chem.*, **60**, 1131 (1956).

(5) J. Steigman and J. L. Lando, *ibid.*, **69**, 2895 (1965).

(6) A. G. Leiga and J. N. Sarmousakis, *ibid.*, **70**, 3544 (1966).

however, the new phases which appear are oils which melt below room temperature.⁷

Experimental Section

A. Materials. The purification of *p*-nitroaniline, the substituted benzoic acids, the substituted phenols, and the alkali metal salts of *p*-toluenesulfonic acid have already been described.^{5,8} *o*-Nitroaniline (Matheson Coleman and Bell, highest quality) and 2,4-dinitroaniline (Eastman, highest purity) were recrystallized several times from aqueous ethanol and ethanol, respectively.

B. Apparatus and Procedure. 1. *Sample Preparation.* (a) *Room-Temperature Phase.* Approximately 50–100 mg of solute was added to 10 ml of 3.0 *m* NaPTS solution. The mixture was heated to ensure dissolution of the solute and then was permitted to cool slowly. Upon cooling, a solid phase usually appeared. If no solid phase appeared when the temperature of the mixture returned to 25° or if the solid:solution ratio was greater than 0.35, an additional amount of solute or salt solution was added and the procedure was continued until the desired solute:solvent ratio was achieved. The solid phase was subsequently filtered and air dried for 1 hr.

A similar procedure was followed for the compounds formed from 2.0 *m* LiPTS.

(b) *Low-Temperature Phase.* Approximately 20 mg of solute was added to 10 ml of 2.0 *m* NaPTS solution. The solute was dissolved by heating the solution slightly. This solution was then placed in an ice-water bath and after several minutes a solid phase appeared. The solid phase was separated from the solution by means of an International portable refrigerated centrifuge, Model PR-1, which was maintained at approximately 0° throughout the separation. The filtration element was a fritted extraction thimble placed inside a polyethylene centrifuge tube.

2. *Sample Analysis.* The water content in a known weight of each compound was obtained by desiccating to constant weight over barium oxide. The per cent solute in the compounds containing substituted phenols and anilines was analyzed spectrophotometrically using a Cary Model 14 spectrophotometer. These compounds which contained substituted carboxylic acids were analyzed for solute by potentiometric titration with standard base. Titrations were performed with a Beckman Model G pH meter using a glass electrode and a saturated calomel electrode. The compounds which contained *o*- and *m*-dinitrobenzene as the solutes were analyzed by placing the anhydrous compound in a heated oven and subliming off the solute. In all cases the weight of the salt of *p*-toluenesulfonic acid was obtained by difference.

3. *Infrared Spectroscopy. Solid Phase.* *i. Room Temperature.* Nujol mulls were prepared and run between NaCl or KBr plates. The infrared measure-

ments were made on a Perkin-Elmer Model 521 recording infrared spectrophotometer which was calibrated with water vapor. The resolution desired for all band location spectra was approximately 0.8 cm⁻¹. In order to achieve this resolution, the wave number scale was increased by a factor of 12.5 and the scanning rate was decreased to 3 cm⁻¹/min.

ii. Low Temperature. The sample which had been prepared and collected at 0° was suspended in Nujol by means of a tissue homogenizer which was maintained at 0°. The entire procedure was performed in a nitrogen atmosphere. The temperature required for the low-temperature spectra (~0°) was achieved by mounting the stainless steel cell on a stainless steel block which was almost entirely immersed in an ice-water bath. The bath was covered with Styrofoam in order to prevent an excess of water vapor from condensing on the cell. A stream of nitrogen was passed through the cell compartment and a second stream of nitrogen was directed at the cell windows to prevent condensation.

4. *Differential Scanning Calorimetry (DSC).* The Perkin-Elmer differential scanning calorimeter (DSC-1) was used for the calorimetry. The sample, weighing approximately 25 mg, was placed in a pan and the lid was crimped on. Holes were made in the lid in order that the volatile components could evolve. The scan rate was set at 10°/min and a sensitivity of 10 mcal/sec was employed. The carrier gas was nitrogen (20.5 cm³/min) which carried the volatile components to the detector at which the effluent gas was compared with that which originally entered the cell.

5. *X-Ray Diffraction.* Single crystals were prepared by slowly cooling saturated solutions. Space groups, cell dimensions, and densities were determined from oscillation, Weissenberg, and precession photographs. Rotation photographs were recorded on a Phillips X-ray diffraction unit using polychromatic Cu radiation. Weissenberg and precession photographs were recorded on a Picker X-ray diffraction unit using Ni-filtered Cu K α radiation. The new compounds crystallized in a needle shape, whereas the hemihydrate crystallized in platelets. All specimens were mounted along the *c* axis.

6. *Density.* The density of the compounds was determined by the flotation method⁹ using ethyl ether and carbon tetrachloride as the immersion liquids.

Results and Discussion

Since new solid compounds had been reported consisting of NaPTS, water, and three aromatic compounds,^{5,6} it was decided to examine the behavior of a

(7) D. Sussman, Ph.D. Dissertation, Polytechnic Institute of Brooklyn, 1966.

(8) J. Steigman and D. Sussman, *J. Amer. Chem. Soc.*, **89**, 6400 (1967).

(9) "International Tables of X-Ray Crystallography," Vol. III, Kynoch Press, Birmingham, England, 1962, p 18.

large number of different aliphatic and aromatic solutes in concentrated solutions of NaPTS. A concentration of 3.0 *m* (2.2 *M*) NaPTS was chosen because it was considerably higher than the concentrations used by the previous investigators.^{5,6} A study of the effect of salt concentration on the formation of these new compounds showed that most of them formed in the concentration range 0.7–1.3 *M* indicating that 2.2 *M* is a suitable working concentration. None of the aliphatic solutes investigated yielded compounds of the new type. Table I lists the aromatic solutes which react

Table I

Solutes forming new compounds	Solutes not forming compounds
<i>o</i> -Dinitrobenzene	<i>p</i> -Dinitrobenzene
<i>m</i> -Dinitrobenzene	<i>m</i> -Hydroxybenzoic acid
<i>p</i> -Hydroxybenzoic acid	<i>m</i> -Toluic acid
<i>o</i> -Toluic acid	<i>p</i> -Nitrobenzoic acid
<i>o</i> -Nitrobenzoic acid	<i>p</i> -Fluorobenzoic acid
<i>m</i> -Nitrobenzoic acid	<i>p</i> -Chlorobenzoic acid
Benzoic acid	2-Methyl-5-nitroaniline
<i>o</i> -Fluorobenzoic acid	<i>p</i> -Bromobenzoic acid
<i>o</i> -Bromobenzoic acid	<i>p</i> -Iodobenzoic acid
<i>o</i> -Chlorobenzoic acid	Terephthalic acid
<i>p</i> -Aminobenzoic acid	<i>m</i> -Aminobenzoic acid
<i>o</i> -Aminobenzoic acid	2,3,6-Trichlorobenzoic acid
<i>o</i> -Nitroaniline	<i>o</i> -Iodobenzoic acid
<i>p</i> -Nitroaniline	<i>o</i> -Methoxybenzoic acid
2,4-Dinitroaniline	<i>p</i> -Methoxybenzoic acid
4-Chloro-2-nitroaniline	<i>m</i> -Nitroaniline
<i>o</i> -Nitrophenol	2,4,6-Trinitroaniline
<i>p</i> -Nitrophenol	3-Nitro-4-chloroaniline
2,4-Dinitrophenol	2,5-Dinitrophenol
	Lauric acid
	Valine
	Urea
	Diethylamine
	α -Naphthol
	β -Naphthol

with the electrolyte solution to produce a new solid phase, as well as some which do not.

NaPTS appears to be unique among simple aromatic sulfonate salts in its ability to form these new compounds readily. Most of the solutes which react with it were obtained unchanged from a 3 *m* LiPTS solution; only *p*-aminobenzoic acid formed a new phase. Four unstable new phases were obtained from concentrated KPTS solution: *o*-aminobenzoic acid, *o*-dinitrobenzene, *o*-nitroaniline, and 4-chloro-2-nitroaniline. Their instability is not unexpected, since the hydrate of KPTS is itself unstable at room temperature and decomposes to the anhydrous salt within several minutes after exposure to air. A more limited investigation showed that *p*-nitroaniline did not form a new solid phase in saturated CsPTS solution, that 2,4-dinitrophenol did not do so in a concentrated sodium xylenesulfonate solution, and that neither *p*-nitroaniline nor 2,4-dinitro-

phenol reacted with sodium benzenesulfonate. It is quite possible, of course, that under different conditions and with other neutral solutes these arylsulfonate salts will also form compounds.

Table II shows the compositions of the various com-

Table II: Analyses of the Compounds Formed from a 3.0 *m* NaPTS Solution

Solute	Stoichiometric ratios	Integral molar ratio (solute:salt:water)
<i>o</i> -Dinitrobenzene	1:2.9:2.7	1:3:3
<i>m</i> -Dinitrobenzene	1:3.7:3.6	2:7:7
<i>p</i> -Hydroxybenzoic acid	1:4.2:4.0	1:4:4
<i>o</i> -Toluic acid	1:4.2:4.1	1:4:4
<i>o</i> -Nitrobenzoic acid	1:5.2:5.3	1:5:5
Benzoic acid	1:2.9:3.1	1:3:3
<i>o</i> -Bromobenzoic acid	1:2.2:2.1	1:2:2
<i>p</i> -Aminobenzoic acid	1:4.3:4.1	1:4:4
<i>o</i> -Aminobenzoic acid	1:4.6:4.6	2:9:9
<i>p</i> -Nitroaniline	1:3.2:3.2	1:3:3
4-Chloro-2-nitroaniline	1:4.4:4.2	1:4:4
<i>o</i> -Nitroaniline	1:4.2:4.0	1:4:4
2,4-Dinitroaniline	1:4.4:4.4	2:9:9
<i>o</i> -Nitrophenol	1:5.0:5.3	1:5:5
<i>p</i> -Nitrophenol	1:3.3:3.2	1:3:3
2,4-Dinitrophenol	1:4.6:4.5	2:9:9
Sodium <i>p</i> -toluenesulfonate hemihydrate	0:1.9:1.0	0:2:1

pounds form in 3.0 *m* NaPTS solution. The exact ratios are listed, together with suggested (idealized) molar ratios. The nonintegral ratio values obtained from the analyses themselves are at least in part due to the method of handling the samples. Since each of these compounds forms only in concentrated aqueous NaPTS solution and since washing would alter their compositions, it is inevitable that a varying proportion of the mother liquor would adhere to the crystals, leaving some hemihydrate of NaPTS. In addition, the new phases themselves are less stable than the hemihydrate and might lose some water.

The integral molar ratios (solute:salt:water) range from 1:2:2 for *o*-bromobenzoic acid to 1:5:5 for *o*-nitrophenol and *o*-nitrobenzoic acid. Half of the compounds show the ratio 1:4:4. All of these are consistent with an expanded structure, perhaps of a cage type, in which the nonelectrolyte molecules are surrounded by water and salt.

Table III contains the crystallographic data obtained from single crystals of three of the compounds formed from a 3.0 *m* NaPTS solution. These compounds were selected because they formed single crystals quite readily in contrast to many of the others. A single crystal of sodium *p*-toluenesulfonate hemihydrate was also examined. All three of the compounds studied crystallize in orthorhombic unit cells, whereas the

Table III: Crystallographic Data of Sodium *p*-Toluenesulfonate Hemihydrate and Three Compounds Formed from a 3.0 *m* NaPTS Solution

Compound	<i>o</i> -Toluic acid	<i>o</i> -Nitroaniline	<i>p</i> -Nitrophenol	Sodium <i>p</i> -toluenesulfonate hemihydrate
Space group	Pncb	Pncb	Pccn	P2 ₁ /c
<i>a</i> , Å	37.06	36.97	38.16	17.93
<i>b</i> , Å	23.72	24.02	18.20	14.83
<i>c</i> , Å	10.21	10.20	10.19	6.73
β , deg	90
<i>Z</i>	8	8	8	4
Formula wt	984.99	986.98	775.74	406.40
<i>V</i> , Å ³	8975.2	9057.8	7077.1	1789.5
<i>D</i> _{calcd} , g/cm ³	1.458	1.448	1.457	1.509
<i>D</i> _{exptl} , g/cm ³	1.41	1.43	1.42	1.50

hemihydrate crystallizes in a monoclinic unit cell. It can be seen that the crystallographic data for the compounds formed from *o*-toluic acid and *o*-nitroaniline are almost identical. This is not unexpected since the analysis of both of these compounds indicates a molar ratio (solute:salt:water) of 1:4:4. Thus it appears that the common structural units, namely, NaPTS and water, are primarily responsible for determining the unit cell dimensions. The slight differences in cell dimensions can be attributed to the somewhat different sizes of the functional groups attached to the aromatic ring.

Two of the unit cell dimensions obtained for the compound formed from *p*-nitrophenol are in agreement with the corresponding cell dimension for the other two compounds listed, but the third dimension is approximately 25% smaller than that of the other compounds. Thus the volume of the *p*-nitrophenol compound is approximately 75% of that of the other two compounds. This occurs because *Z* (the number of molecules per unit cell) is the same in all three cases but the analysis of the compound formed from *p*-nitrophenol indicates a molar ratio of 1:3:3 whereas that of the other two compounds is 1:4:4. These results suggest that two of the cell dimensions are fixed by a fixed number of salt and water molecules, whereas the third dimension may depend in addition on the ability of the particular organic solute to hydrogen bond to water.

The results listed in Table III may also explain why an aromatic nucleus is necessary for the formation of these new compounds. The common structural matrix (NaPTS and H₂O) probably forms a stable cage into which only solutes of a particular size and shape can fit without disruption. It is quite possible that naphthalene derivatives and small aliphatic solutes could also fit into such cages if they exist in solution, but these particular solutes probably cannot stabilize these cage systems sufficiently.

The photographs of single crystals of these compounds possess several anomalies which cannot be explained on

the basis of ordered structures. The oscillation photographs contain sharp reflections only for alternate layers, *i.e.*, $l = 0, 2, 4, 6, \dots$, whereas the reflections for l odd are diffuse streaks. The corresponding Weissenberg photographs of these layers possess sharp reflections for the l even layers but diffuse, almost continuous festoons extending in both the a^* and b^* directions for l odd. In more detail, the space groups Pncb and Pccn correspond to systematic absences of spots on the zero-level Weissenberg photographs for $k = 2n + 1$ for the 1:4:4 compounds and for $h + k = 2n + 1$ for the 1:3:3 compound. For other even l levels, the systematic absence of spots with $h = 0$ and $k = 2n + 1$ was observed for the 1:4:4 compounds but none were observed in the 1:3:3 compound. On the odd l levels, the streaks for $k = 0$ are absent for all three compounds, whereas the streaks for $h = 0$ are absent for the 1:3:3 material, but the 1:4:4 compounds have absences corresponding to $h = 0$ and $k = 2n$. The space group P2₁/c observed for the hemihydrate corresponds to systematic absences of spots with $h = 0, l = 0$, and $k = 2n + 1$, as well as when $k = 0$ and $l = 2n + 1$.

It has been suggested^{10,11} that phenomena of this type arise from the existence of layer crystals which are made up of symmetrical molecules but are not completely ordered. These crystals may be thought of as consisting of ordered layers, having the same internal structure, perpendicular to [001] stacked in random fashion such that successive layers fail to be in register as far as the x and y coordinates of the molecule are concerned. Therefore the lack of order is due to translations of the layers parallel to their own planes. Dornberger-Schiff¹² has classified structures of this type as "OD structures" (order-disorder structures). This term includes structures with stacking disorders if the lack of order in the stacking results from the fact that there are two geometrically and hence energetically equivalent ways in which neighboring layers may be placed relative to one another. Since the solute itself is not symmetrical, any rotation about an axis perpendicular to the plane of the molecule in this configuration for the 1:4:4 compounds would produce two slightly different structures with identical molecular dimensions. This may be the cause of the disorder in these compounds. A similar effect could produce disorder in the *p*-nitrophenol compound.

The 1:4:4 compounds listed in Table III may well have layer structures. Each contains five aromatic rings per complex molecule, which could lie in the same plane, with the water and tosylate units located symmetrically around the benzenoid nonelectrolyte. The large " a " and " b " cell dimensions and the relatively

(10) S. Hendricks and E. Teller, *J. Chem. Phys.*, **10**, 147 (1942).

(11) S. Glauser and M. G. Rossmann, *Acta Crystallogr.*, **21**, 175 (1966).

(12) K. Dornberger-Schiff, *ibid.*, **9**, 593 (1956).

Table IV: O-H (str), O-H (bend), and SO- (str) Frequencies of Compounds Formed in 3.0 *m* NaPTS Aqueous Solution

Solute	$\bar{\nu}_{\text{O-H(asy)}},$ cm ⁻¹	$\bar{\nu}_{\text{O-H(sym)}},$ cm ⁻¹	$\bar{\nu}_{\text{O-H(bend)}},$ cm ⁻¹	$\bar{\nu}_{\text{S-O(asy)}}, \text{cm}^{-1}$	
<i>o</i> -Dinitrobenzene	3613 sh	3541	1619	1205	1167
	3595	3522			
<i>m</i> -Dinitrobenzene	...	3542	1617	1204	1165
	3598	3522			
<i>m</i> -Nitrobenzoic acid	3615 sh	3543	1616	1204	1168
	3602	3527			
<i>p</i> -Hydroxybenzoic acid	3613 sh	3538 sh	1618	1204	1164
	3602	3529			
<i>o</i> -Toluic acid	3605	3534	1618	1205	1167
	3593 sh	3522 sh			
<i>o</i> -Nitrobenzoic acid	3610 sh	3537	1616	1204	1166
	3596	3523			
Benzoic acid	3605	3535	1618	1206	1167
	3590 sh	3521 sh			
<i>o</i> -Bromobenzoic acid	3612	3548	1616	1205	1169
	3597	3529			
<i>p</i> -Aminobenzoic acid	3612	3540	1618	1205	1168
	3596	3524			
<i>p</i> -Aminobenzoic acid	3612	3542	1618	1205	1165
	3595	3525			
<i>p</i> -Nitroaniline	3612	3542	1617	1204	1163
	3583	3507			
4-Chloro-2-nitroaniline	3613	3540	1619	1203	1164
	3580	3521			
<i>o</i> -Nitroaniline	3612	3540	1618	1203	1161
	3595	3520 sh			
2,4-Dinitroaniline	3616	3543	1619	1203	1163
	3596	...			
<i>o</i> -Nitrophenol	1615	1204	1166
	3601	3529			
<i>p</i> -Nitrophenol	3612	3538	1617	1202	1162
	3598	3527			
2,4-Dinitrophenol	3618	3544	1613	1202	1160
	3600	3526			
NaPTS·0.5H ₂ O	3475	3368	1658	1215	1193
NaPTS (anhydrous)	1234	1202

smaller "c" dimension are also consistent with a layer structure in which the solute molecule is surrounded in the same plane by salt and water units.

The 10.20-Å spacing suggests layers that are 2.5 Å apart which is impossibly close, or 5 Å apart, which would require considerable tilting of the aromatic rings. Thus it would be extremely difficult, if not impossible, to reconstruct the structure of a unit cell containing such a large number of atoms solely from molecular packing.

The infrared spectrum of the stable hemihydrate of NaPTS is different from those of the new compounds; in turn, the latter all show certain common features in the O-H (str), the O-H (bend), and the S-O (str) regions. Table IV shows the O-H stretching, the O-H bending, and asymmetric S-O stretching modes of the NaPTS hemihydrate and of all of the new compounds listed in Table I, with the exception of *o*-fluorobenzoic and *o*-chlorobenzoic acids.

In the spectrum of NaPTS·0.5H₂O, the symmetric and antisymmetric O-H stretching modes of the water

appear at 3475 and 3368 cm⁻¹, whereas the corresponding modes are found in all the new compounds at considerably higher frequencies—approximately 130 and 165 cm⁻¹ higher, respectively. In the same vein, the O-H bending mode of the water appears at 1658 cm⁻¹ in the hemihydrate but is shifted to lower frequencies by approximately 40 cm⁻¹ in all of the new compounds listed in Table IV. The shift to higher frequencies in the O-H stretching mode and that to lower frequencies in the bending mode both are consistent with a decrease in the strength of hydrogen bonding of the water in the new compounds relative to that in the hemihydrate of sodium *p*-toluenesulfonate.

In the tosylate hemihydrate there is one O-H anti-symmetric stretching mode and one symmetric stretching mode. In almost all of the new hydrates, each of the two modes is split into two double potential bands, whose maxima are shown in Table IV. Since this splitting is only approximately 15 cm⁻¹ in magnitude, it is improbable that it is due to two drastically different structures like X-H...Y and X...H-Y. It could be

due to a small difference in the environment of one or two of the water molecules compared to that of the remaining waters. Thus, while all of the water molecules may be hydrogen bonded to the sulfonate group, one or two would tend to be closer than the others to the hydrogen-bonding groups of the benzenoid nonelectrolyte. This proximity might cause a small change in the vibrational modes of adjacent water molecules and produce a small splitting.

Anhydrous sodium *p*-toluenesulfonate has two asymmetric S-O (str) modes at 1234 and 1202 cm^{-1} . The two bands are hydrogen bonded in the hemihydrate and appear at 1215 and 1193 cm^{-1} , respectively. These two stretching frequencies are shifted to still lower frequencies in the various compounds listed in Table IV. They appear at about 1204 and 1165 cm^{-1} in almost all cases. This would indicate that the sulfonate group is more strongly hydrogen bonded in these compounds than in the hemihydrate. This appears to contradict the conclusion that the water in these compounds is less strongly hydrogen bonded (presumably to the S-O bonds) than in the hemihydrate. There is no real contradiction in the sense that there is a greater proportion of water to sulfonate in the new compounds than in the hemihydrate, and hence the sulfonate group could be more strongly hydrogen bonded, and the water less so.

The O-H (str) frequencies of water in the compounds are considerably higher than in the tosylate hemihydrate, pointing to a lower stability. This decreased stability also showed itself in differential scanning calorimetric studies of a number of these compounds. The hemihydrate itself showed a transition which began at 119°, rose to a sharp maximum at 123°, and decreased gradually to 147°. Seven compounds—those containing *o*-nitroaniline, *p*-nitroaniline, 4-chloro-2-nitroaniline, *o*-toluic acid, *o*-nitrobenzoic acid, *p*-aminobenzoic acid, and *o*-nitrophenol—all showed broad transitions starting near 49° and finishing near 121°, with a maximum between 83 and 104°. If there are differences among them, they are small and will require more precise measurements for differentiation. The common maximum is ascribed to the loss of water from the crystals. The hemihydrate was left after the decomposition of each compound. This was confirmed by the study at different temperatures of the infrared spectra of the tosylate compound containing *o*-toluic

acid (one of the 1:4:4 compounds listed in Table II). The spectrum of 25° showed two sharp, well-defined O-H bands at 3605 and 3535 cm^{-1} . At 49° the bands are more diffuse, but they are still quite definite. At 86° the bands are still more diffuse and broadened. At 102° the spectrum became markedly different. The bands at 3605 and 3535 cm^{-1} virtually disappeared, and strong bands were seen at 3480 and 3370 cm^{-1} which are assigned to the hemihydrate of sodium *p*-toluenesulfonate. At still higher temperature—127°—the two bands of the hemihydrate disappeared, and the spectrum showed one broad band from 3700 to 3200 cm^{-1} , which is probably that of water alone.

A study was also made of the effect of temperature on the infrared spectrum of the 1:4:4 compound formed from 4-chloro-2-nitroaniline and NaPTS. The compound was formed, collected, and measured at 25°; another sample was formed at 0° but was collected and measured at 25°. A third sample was formed, collected, and measured at 0°. The three mulls showed virtually identical spectra, with the exception of a broadened peak at 1200 cm^{-1} in the third sample. It can be concluded that low-temperature hydrates different from those found at room temperature probably do not form.

It was found possible to prepare at least one of the new compounds from a solution in which the largest part of the water had been replaced by either methanol or ethanol. 4-Chloro-2-nitroaniline formed the compound with NaPTS from 3.0 *m* NaPTS in water, aqueous methanol (50% v/v) saturated with NaPTS, and aqueous methanol (75% CH_3OH , 25% H_2O v/v) saturated with NaPTS. The only solid substance obtained from pure methanol saturated with NaPTS and the solute was the unchanged solute. Similarly, the compound with NaPTS was obtained from 95% ethanol (v/v) saturated with NaPTS. Identification was made from the infrared spectra of mulls of the solid phases. Evidently the reaction with water is quite specific, and as little as 5% water in 95% ethanol suffices for the new hydrate to form.

Acknowledgment. This research was supported in part by an R. E. Kirk fellowship from the Science Development Program of the National Science Foundation and in part by AEC Grant AT(30-1)-2544.

On the Mechanism of Charging and Discharging Ionic

Double Layers at Electrodes

by Chaim Yarnitzky and Fred C. Anson

Gates and Crellin Laboratories of Chemistry, California Institute of Technology, Pasadena, California 91109
(Received March 9, 1970)

The ionic double layers created at electrode surfaces when sudden changes are made in the charge density on the electrode have transient compositions which differ from those prevailing after equilibrium is attained. By creating such nonequilibrium double layers in electrolytes containing ions which undergo faradaic reactions at the electrode it becomes possible to assay the initial compositions of these nonequilibrium double layers and to draw conclusions about the mechanisms by which they are formed. Comparison of such experimental assays with those calculated on the basis of a simple model involving only relative ionic mobilities and concentrations leads to good agreement. Some possible ramifications of the transient existence of double layers with nonequilibrium compositions are considered.

A number of recent papers have examined the processes by which very rapidly created diffuse double layers at electrodes relax to their equilibrium dimensions and ionic compositions.¹⁻⁴ These previous studies have been confined to cases where no faradaic reactions proceeded; they concentrated on relaxation transients and frequency-dependent capacitances arising from the finite velocities with which ions move into and out of diffuse double layers. One of the conclusions reached¹ was that the instantaneously created diffuse layer would have a transient composition reflecting the relative concentrations and mobilities of the ions in the bulk of the solution rather than the equilibrium composition based on the Gouy-Chapman-Stern model of the diffuse layer. Consequently, when positively charged diffuse layers are created rapidly in electrolyte solutions containing equal concentrations of two cations bearing the same charge, the instantaneously formed diffuse layer will be richer in the more mobile cation. The presence of this effect is not readily detectable in the absence of faradaic discharge of either cation because the capacitance of the diffuse layer is affected very little by substitution of one kind of ion for another so long as their charges are the same.⁵ However, when one of the ions contained in the diffuse layer can undergo faradaic reduction (or oxidation) it becomes possible to assay the composition of the diffuse layer and thus to test the prediction that the more mobile ion will be disproportionately present. In this paper we report the results of experiments designed to determine the instantaneous composition of diffuse double layers at mercury electrodes. The experimental technique, charge-step chronocoulometry,⁶ previously employed to assay equilibrium diffuse layer compositions,⁷ has been modified to permit measurements at much shorter times so that the assay is obtained before the instantaneous diffuse layer achieves its equilibrium composition.

Experimental Section

Apparatus. The cell and specially drawn thin and tapered capillary electrodes described previously¹ were employed. A block diagram of the overall apparatus is shown in Figure 1. A new charge injection circuit was desired in order to decrease significantly the time during which ohmic potential drops perturbed the measurements. A high voltage, constant current pulse circuit was therefore substituted for the previously employed capacitance charge injection circuit. The circuit employed in this galvanostat is shown in Figure 2.

The potential-time transients were photographed from the screen of an oscilloscope (Tektronix Type 536, Type T time base, Type W vertical amplifier) and the data read directly from the photographs.

Reagents. Triply distilled water and recrystallized reagent grade salts were employed. Solutions were deoxygenated with prepurified nitrogen which was further treated by passage over copper turnings at 400°. Measurements were conducted at $25 \pm 1^\circ$.

Results and Discussion

All of the experiments employed the technique of charge-step chronocoulometry.⁶ This involves the measurement of the change of electrode potential with time at open circuit following the very rapid injection of charge into the electrode in electrolytes made up of both reducible and nonreducible ions.

(1) F. C. Anson, R. F. Martin, and C. Yarnitzky, *J. Phys. Chem.*, **73**, 1835 (1969).

(2) J. Newman, *ibid.*, **73**, 1843 (1969).

(3) R. P. Buck, *J. Electroanal. Chem.*, **23**, 219 (1969).

(4) S. W. Feldberg, *J. Phys. Chem.*, **74**, 87 (1970).

(5) D. C. Grahame, *J. Electrochem. Soc.*, **98**, 343 (1951).

(6) F. C. Anson, *Anal. Chem.*, **38**, 1924 (1966).

(7) F. C. Anson, *J. Phys. Chem.*, **72**, 727 (1968).

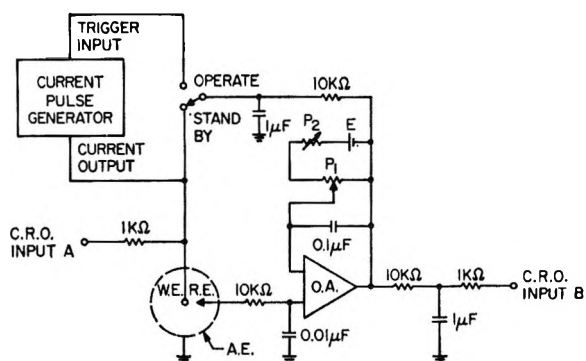


Figure 1. Schematic diagram of apparatus for charge-step chronocoulometry with dilute solutions: O.A., operational amplifier—Philbrick Model P-75; P₁, 10-kilohm ten-turn precision potentiometer; P₂, 3-kilohm + 1-kilohm trimpot; E, 2.7-V battery; CRO inputs A & B are the two inputs of a Tektronix W plug-in amplifier operated in the differential mode; W.E., hanging mercury drop working electrode; R.E., reference electrode; A.E., platinum gauze auxiliary electrode.

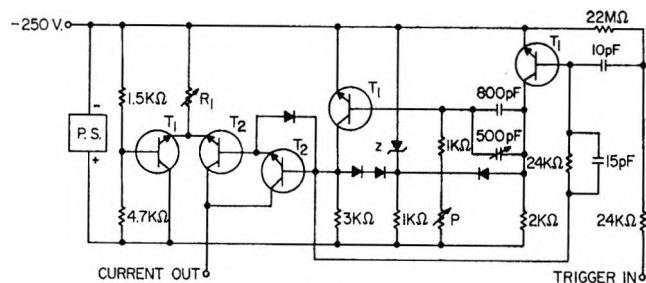


Figure 2. Circuit of the current pulse generator for injection of negative charge: all diodes are 1N 645; T₁, 2N 3607 transistor; T₂, RCA 40327 transistor; R₁, current determining resistor, 100 ohms–10 kilohms; P, ten-turn precision potentiometer, 100 kilohms; P.S., 9-V power supply; Z, 5.2-V zener diode.

Following the small and rapid initial potential decay, arising from the spatial relaxation of the overextended double layers that are created in the dilute solutions employed,¹ a more gradual decay of the potential is observed as the reducible ion diffuses to the electrode surface and consumes the charge on the electrode. Independent measurements on solutions of the same ionic strength but containing no reducible ions established the relationship between the electrode potential and the charge on the electrode from which the observed potential–time transients were converted to the corresponding charge–time transients. Conditions were chosen so that semiinfinite linear diffusion of the reacting ions to the electrode surface determined the rate of consumption of charge.⁷ The resulting charge–time data might be expected to obey the simple relation given by eq 1

$$Q = q_0^m + Q_{inj} + 2FC_r \left(\frac{D_r t}{\pi} \right)^{1/2} + F\Gamma_r \quad (1)$$

where Q is the charge density on the electrode at time t , q_0^m is the initial charge density on the electrode, Q_{inj}

is the (negative) charge injected per cm², and C_r and D_r are the bulk concentration and diffusion coefficient of the singly charged reactant ion. Γ_r is the total amount of reactant ion present in the compact and diffuse layers in mol/cm². Plots of Q vs. $t^{1/2}$ are expected to be linear with intercepts given by $q_0^m + Q_{inj} + F\Gamma_r$. Thus, the intercept of a Q vs. $t^{1/2}$ plot should differ from the known values of $q_0^m + Q_{inj}$ by an amount corresponding to whatever reactant is incorporated into the diffuse layer because of the charge injection.

This analysis is oversimplified because it has so far ignored the fact that a layer of essentially salt-free water is generated when the exposed cations move rapidly to the electrode surface following the charge injection.^{1,2} The diffusion of reactant to the electrode is delayed initially by the intervention of this water layer and the expected charge–time behavior will not be accurately described by eq 1, especially at times very soon after the injection. A modified equation was therefore derived by taking the existence of the water layer into account at the outset of the solution of the mass transfer problem. This derivation, which is given in the Appendix, leads to eq 2.

$$Q = q_0^m + Q_{inj} + 2FC_r \left(\frac{D_r}{\pi} \right)^{1/2} \times \left[t^{1/2} \exp\left(-\frac{\tau}{t}\right) - (\pi\tau)^{1/2} \operatorname{erfc}\left(\frac{\tau}{t}\right)^{1/2} \right] + F\Gamma_r \quad (2)$$

where

$$\tau = \frac{d^2}{4D_r} \quad (3)$$

and d is the thickness of the salt-free layer created by the charge injection. For injection of negative charge, d is determined by the transference number, T_- , and concentration, C_- , of the anion present.¹ If the electrode is initially uncharged

$$d = \frac{|Q_{inj}|T_-}{FC_-} \quad (4)$$

while if the electrode has an initial positive charge density, q_0^m

$$d = \frac{[|Q_{inj}|T_- - q_0^m]}{FC_-} \quad (5)$$

Plots of Q vs. the function inside the brackets in eq 2 were prepared. For all but the shortest values of time, eq 2 was accurately approximated by substituting the first terms of the small argument series expansions for the exponential and complementary error functions. The simpler equation resulting from this approximation is

$$Q = q_0^m + Q_{inj} + \frac{2FC_r D_r^{1/2}}{\pi^{1/2}} \left(\left[t^{1/2} \left(1 + \frac{\tau}{t} \right) - (\pi\tau)^{1/2} \right] \right)$$

Table I: Calculated and Observed Compositions of Nonequilibrium Diffuse Layers in Mixtures of Tl^+ with Various Electrolytes

Salt concn, mM	T_{Tl^+}	T_-	$-Q_{inj}$, $\mu C/cm^2$	q_0^m	τ , ^a μsec	$F\Gamma_{Tl^+}$, $\mu C/cm^2$, calcd ^b	$F\Gamma_{Tl^+}$, $\mu C/cm^2$, obsd ^c
0.1 $TlClO_4$ -0.9 $HClO_4$	0.020	0.18	15	2.0	0.7	0.38	1.0 ± 0.2
0.1 $TlClO_4$ -0.9 $KClO_4$	0.053	0.48	15	2.0	36	1.33	1.4 ± 0.2
0.1 $TlClO_4$ -0.9 $LiClO_4$	0.067	0.61	15	1.8	72	1.73	1.8 ± 0.3
0.2 $TlClO_4$ -0.8 $HClO_4$	0.041	0.19	15	2.0	1	0.79	0.9 ± 0.2
0.2 $TlClO_4$ -0.8 $KClO_4$	0.11	0.48	15	2.0	36	2.69	2.9 ± 0.3
0.2 $TlClO_4$ -0.8 $LiClO_4$	0.13	0.59	15	1.8	67	3.39	3.3 ± 0.4
0.5 $TlClO_4$ -0.5 $HClO_4$	0.13	0.24	15	2.0	3	2.75	2.2 ± 0.4
0.5 $TlClO_4$ -0.5 $KClO_4$	0.26	0.47	15	2.0	34	6.47	5.5 ± 0.7
0.5 $TlClO_4$ -0.5 $LiClO_4$	0.30	0.54	15	1.9	52	7.61	6.7 ± 0.9
0.5 $TlOH$ -0.5 KOH	0.14	0.71	15	2.0	101	6.27	6.0 ± 0.9

^a Calculated from eq 3 and 5. ^b Calculated from eq 8. ^c Obtained from the intercepts of plots like those in Figure 4 with the listed values of τ used in calculating the abscissa values.

These plots were linear and the differences between their intercepts on the charge axis and the value of $q_0^m + Q_{inj}$ gave the observed values of $F\Gamma_r$ listed in Table I.

In the absence of specific adsorption of reactant, Γ_r represents the amount of reactant that would be present in the nonequilibrium diffuse layer at the end of the rapid charge injection if no discharge of the reactant had occurred. For injection of negative charge with cationic reactants, Γ_r includes two components, Γ_m and Γ_e . The first, Γ_m , counts the amount of reactant that migrates all the way up to the electrode surface during the charge injection. When the initial electrode potential is positive of the potential of zero charge (pzc), anions are ejected from the disappearing diffuse layer until the negative charge injected equals the initial positive charge on the electrode. During the same time cations from the bulk of the solution migrate to the electrode surface to pair up with the ejected anions.⁸ As a result, the concentrations of both reactant and supporting electrolytes (e.g., $KClO_4$ and $TlClO_4$) are increased at the electrode surface. If sufficient negative charge is injected to make the net charge on the electrode become negative, then some or all of the cations which have migrated to the surface will be incorporated into the resulting diffuse layer. If the negative charge injected is insufficient to bring the electrode to the pzc, these cations will remain as components of the local excess of neutral electrolyte just outside the diffuse layer. In all of the experiments to be discussed below in which thallos ion is the reactant, the total negative charge injected was sufficiently large to cause all of the cations in the excess electrolyte produced at the electrode surface up to the pzc to be incorporated into the diffuse layer. The necessary condition for this to be true is: $q_0^m(T_{Tl^+} + T_+) < |Q_{inj}|$, where T_{Tl^+} and T_+ are the transference numbers of thallos ion and the nonreactant cation, respectively. For any value of $|Q_{inj}|$, however, Γ_m will be given by

$$\Gamma_m = \frac{|Q_{inj}|}{F} T_r \quad (6)$$

where T_r is the transference number of the reactant in the bulk of the solution.

The second component of Γ_r , Γ_e , is made up of the cations that are left exposed (i.e., unneutralized by anions) by the anions that migrate away from the electrode during the charge injection. These cations are driven very rapidly to the electrode surface by the high electric field generated by the negative charge on the electrode,² so that the reactant portion of these cations can be regarded as being at the electrode surface at times very soon after injection. Exposure of cations does not commence until the injected charge reaches q_0^m/T_- because a local excess of electrolyte containing this quantity of cations (and anions) is created at the electrode surface by the migration of cations to the electrode surface as its positive charge is reduced to zero. These cations are used to populate the diffuse layer that is formed when the electrode's charge starts to become negative. The anions present in the excess of electrolyte that was created at the electrode surface during the first part of the injection migrate away from the electrode where the creation of cations unmatched by anions is delayed until the supply of anions in the excess is exhausted. That part of the injected charge which leads to exposed cations is thus $(|Q_{inj}| - q_0^m/T_-) T_-$, and the reactant portion of these exposed cations is given by

$$\Gamma_e = \left(|Q_{inj}| - \frac{q_0^m}{T_-} \right) \frac{T_- C_r}{FC_-} \quad (7)$$

where C_- and T_- are, respectively, the concentration and transference number of anions in the bulk of the solution, and C_r is the bulk concentration of reactant. With combinations of Q_{inj} , q_0^m , and T_- for which

(8) F. C. Anson, *J. Phys. Chem.*, **71**, 3605 (1967).

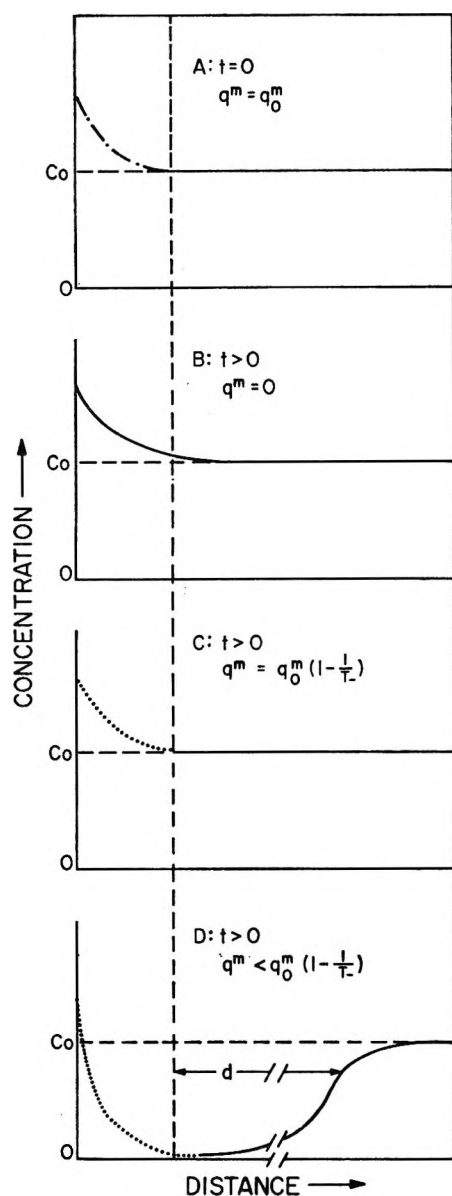


Figure 3. Approximate concentration profiles developed at electrode surfaces by rapid charge injection with dilute electrolytes. Solid lines represent the concentration of the single neutral electrolyte present. The dotted and dashed line represents the concentration of anions. The dotted lines represent cation concentrations. The vertical dashed line marks the outer edge of the original, equilibrium diffuse double layer. A, before injection; the electrode bears an initial positive charge density, q_0^m ; B, after injection of an amount of negative charge just equal to the initial positive charge on the electrode; C, the amount of negative charge injected is just great enough to consume all of the cations in the excess electrolyte at the electrode as shown in B; D, enough negative charge has been injected to expose cations at large distances from the electrode which leads to a salt-free layer of width d (see eq 5).

$|Q_{inj}| - q_0^m/T_- < 0$, $\Gamma_e = 0$. The total reactant in the nonequilibrium diffuse layer is thus

$$\Gamma_r = \Gamma_m + \Gamma_e = \frac{|Q_{inj}|}{F} T_r + \left(|Q_{inj}| - \frac{q_0^m}{T_-} \right) \frac{T_- C_r}{FC_-} \quad (8)$$

with the proviso that the second term can never be negative.

Although the ionic migration processes we have discussed are all relatively simple, describing them with words alone is, as the persevering reader will have already concluded, cumbersome. For this reason, it may be helpful to depict graphically some of concentration profiles that develop near the electrode surface during charge injection. Solutions to the necessary mass transfer equations are available^{2,9} so that exact concentration profiles could be calculated. For the present illustrative purposes, however, we have prepared in Figure 3 a set of approximate profiles which indicate the chief concentration changes that result with dilute solutions of a single electrolyte when no faradaic reaction occurs at the electrode. In Figure 3A, the uniform concentration profile existing before any charge is injected is depicted for an electrode bearing an initial positive charge density q_0^m . The equilibrium diffuse layer is populated entirely by anions.

In Figure 3B, just enough negative charge has been injected to reduce the charge density on the electrode to zero. No diffuse layer is present, but a higher concentration of neutral electrolyte, produced by the pairing-up of ejected anions with migrating cations, is present in the region formerly occupied by the diffuse layer.

In Figure 3C, the negative charge injected exceeds the initial positive charge on the electrode by an amount just sufficient for all of the cations in the excess electrolyte generated up to the pzc to have been incorporated into the new diffuse layer. The necessary condition for this to be true is $|Q_{inj}| = q_0^m/T_-$.

Figure 3D displays the profile which results when $|Q_{inj}| > q_0^m/T_-$ so that cations are exposed during the charge injection and are driven very rapidly to the electrode surface by the resulting nonequilibrium electric field generated.² The layer of essentially salt-free water that results extends over a distance, d , given by eq 5. The concentration profile depicted corresponds to the conditions that would prevail just before any faradaic process commenced in the charge-step chronocoulometric experiments with electrolytes containing both a reacting and nonreacting salt; e.g., $TiClO_4$ and $KClO_4$.

Figure 4 shows a set of chronocoulometric plots for electrolytes containing mixtures of $TiClO_4$ and $KClO_4$ with the total ionic strength maintained at 1.00 mM. The initial charge on the electrode was $+2.0 \mu C/cm^2$ ($E = -300$ mV vs. SCE) and $-15 \mu C/cm^2$ of charge was injected, which took the electrode to -1240 mV vs. SCE in 1 mM $KClO_4$. As expected from eq 2, the plots are linear with slopes proportional to the concentration of thallium. As the ratio Tl^+ to K^+ increases, the intercepts of the lines on the charge axis decrease, corresponding to the incorporation of more and more Tl^+ into the diffuse layer during its creation.

(9) K. B. Oldham, *Anal. Chem.*, **40**, 1799 (1968).

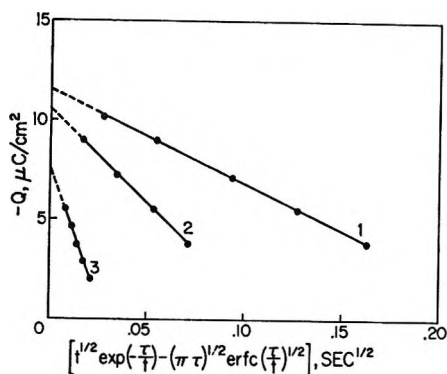


Figure 4. Charge-step chronocoulometric plots for KClO_4 - TlClO_4 mixtures: 1, 0.1 mM TlClO_4 -0.9 mM KClO_4 ; 2, 0.2 mM TlClO_4 -0.8 mM KClO_4 ; 3, 0.5 mM TlClO_4 -0.5 mM KClO_4 ; $q_0^m = +2 \mu\text{C}/\text{cm}^2$; $Q_{\text{inj}} = -15 \mu\text{C}/\text{cm}^2$.

Since the instantaneous electrode potential that results from the charge injection corresponds to a very rapid rate of reduction of Tl^+ , all of the thallos ions within the diffuse layer react with electrons in the electrode at a rate too fast to measure and what is observed is the slower, diffusion limited consumption of the remaining negative charge on the electrode by thallos ions which diffuse to the electrode.

For comparison with the experimental results, the amount of Tl^+ that is present within the diffuse layer just after its creation was calculated from eq 8. (To avoid possible confusion it may be well to point out that the "amounts of reactant in the diffuse layer," referred to throughout this paper, are not identical with the thermodynamic surface excesses reckoned with respect to water.¹⁰ Our nonequilibrium measurements give the total amount of a given kind of ion contained within the instantaneous diffuse layer without regard to the concentration of the same ion in the bulk of the solution. On this basis, the total amount of cationic charge contained in the diffuse layer is always equal to the negative charge on the electrode surface. None of the charge within the nonequilibrium diffuse layer arises from "missing anions.") The resulting values of $F\Gamma_{\text{Tl}^+}$ calculated for the concentrations and transference numbers corresponding to the three plots in Figure 4 are 1.3, 2.6, and $6.5 \mu\text{C}/\text{cm}^2$; the corresponding experimental values obtained from Figure 4 are 1.4 ± 0.2 , 2.9 ± 0.3 , and $5.5 \pm 0.7 \mu\text{C}/\text{cm}^2$. This reasonable agreement supports the main features of the analysis which lead to the calculated intercepts.

A further test of eq 8 was provided by experiments in which the mobility of the supporting electrolyte cation was varied by substituting lithium or hydrogen for potassium. As Figure 5 shows, the intercepts of the chronocoulometric plots for these mixtures increase as the transference number of thallos ion increases even though the equilibrium diffuse double layers (if no faradaic reaction occurred) would contain the same amount of thallos ion in all three cases. A comparison

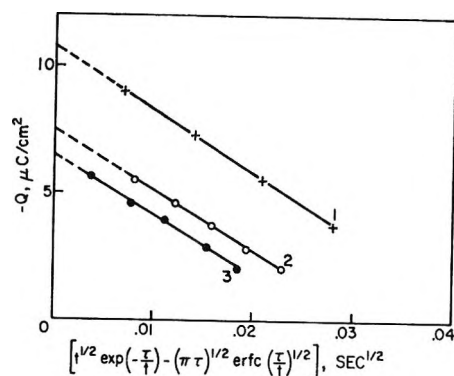


Figure 5. Charge-step chronocoulometric plots for 0.5 mM TlClO_4 in electrolytes with varying cationic mobilities: second electrolyte present: 1, 0.5 mM HClO_4 ; 2, 0.5 mM KClO_4 ; 3, 0.5 mM LiClO_4 ; other conditions as in Figure 4.

of calculated and observed values of $F\Gamma_{\text{Tl}^+}$ for a number of mixed electrolytes is shown in Table I. The reasonable agreement obtained between the calculated and observed diffuse layer compositions in all of these cases adds support to our portrayal of the mechanism by which diffuse layers are formed during charge injection. An especially convincing piece of evidence is the good agreement between the calculated and observed values of $F\Gamma_{\text{Tl}^+}$ for both the TlClO_4 - HClO_4 and TlOH - KOH mixtures: The experimental charge-time transients obtained with these two electrolytes are almost identical, even though the values of $F\Gamma_{\text{Tl}^+}$ calculated from eq 8 are quite different. However, when the chronocoulometric plots are made with the appropriately different values of τ indicated in Table I very good agreement with the calculated values results.

It should be noted that throughout this analysis it has been assumed that the only cause of the decay of potential following the charge injection is the faradaic discharge of reactant. In fact, there is a second component of the observed decay which reflects the relaxation of the instantaneous diffuse layer created by the charge injection. The thickness of the initial diffuse layer is greater than its equilibrium thickness;¹ this nonequilibrium diffuse layer has a smaller capacitance which makes the overall double-layer capacitance lower so the observed potential relaxes to smaller values as the diffuse layer attains equilibrium and the double-layer capacitance rises. Fortunately, in the experiments reported here, the magnitude and duration of this second component of potential decay were so small that they produced only minor perturbations on the potential decay arising from the diffusion limited faradaic reactions.

Absence of Supporting Electrolyte. If, instead of a mixed electrolyte, a pure solution of a reducible cation is employed, the diffuse layers created by injection of negative charge consist entirely of the reducible cation.

(10) D. M. Mohilner in "Electroanalytical Chemistry," Vol. 1, A. J. Bard, Ed., Marcel Dekker, New York, N. Y., 1966.

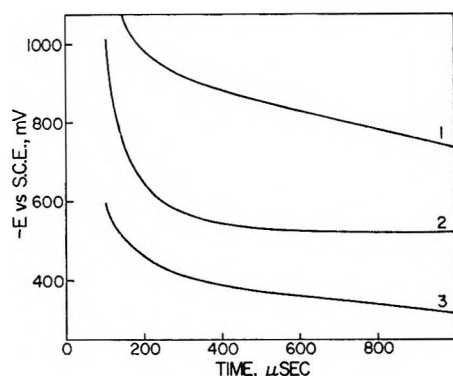


Figure 6. Potential decay curves for TiClO_4 and $\text{Cu}(\text{ClO}_4)_2$ electrolytes: 1, 0.5 mM TiClO_4 -0.5 mM KClO_4 ; $q_0^m = +2 \mu\text{C}/\text{cm}^2$; $Q_{\text{inj}} = -15 \mu\text{C}/\text{cm}^2$; 2, 1.0 mM TiClO_4 ; $q_0^m = +2 \mu\text{C}/\text{cm}^2$; $Q_{\text{inj}} = -15 \mu\text{C}/\text{cm}^2$; 3, 0.5 mM $\text{Cu}(\text{ClO}_4)_2$; $q_0^m = +12 \mu\text{C}/\text{cm}^2$; $Q_{\text{inj}} = -20 \mu\text{C}/\text{cm}^2$.

For cations like Tl^+ , which are very rapidly reduced, the instantaneously created diffuse layer annihilates itself at a rate too high to measure as the electrons on the negatively charged electrode combine with the thallos ions in the diffuse layer. The net result is a reduction of thallos ions at a rate much higher than the diffusion limited rate measured by the slopes of chronocoulometric plots such as those in Figures 4 and 5. Figure 6 compares the potential-time transient for 0.5 mM TiClO_4 -0.5 mM KClO_4 with that for 1.0 mM TiClO_4 . When the potassium ions are removed, the potential decays very rapidly to the vicinity of the half-wave potential for the $\text{Tl}/\text{Tl}(\text{Hg})$ couple where the back oxidation of the amalgam becomes significant. With pure TiClO_4 solutions potential decay curves resembling curve 2 in Figure 6 are obtained no matter how much negative charge is injected, because injection of additional charge moves additional thallos ions into the diffuse layer where they rapidly consume the additional charge on the electrode.

The behavior of thallos ions after the initial potential decay depends upon the fact that the half-wave potential for the $\text{Tl}^+/\text{Tl}(\text{Hg})$ couple is close to the pzc. When the experiment is repeated with cupric ions, which have a half-wave potential quite positive of the pzc, a somewhat different behavior is expected and observed. Curve 3 in Figure 6 shows a potential decay curve for a solution of Cu^{2+} . Note that the very rapid decay (due to reaction between cupric ions in the diffuse layer and electrons in the electrode) mimics the rapid decay obtained with thallos ions down to the pzc at which point all of the cupric ions within the diffuse layer have been consumed and no diffuse layer remains. The much slower continued potential decay occurs as cupric ions diffuse to the electrode surface and are reduced, producing a positively charged electrode. Chronocoulometric plots of charge vs. $(\text{time})^{1/2}$ prepared from potential transients such as curve 3 have slopes proportional to the bulk concentration of Cu^{2+} and intercepts very close to the pzc.

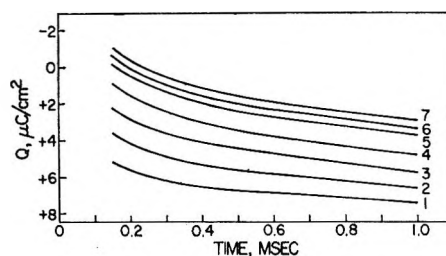


Figure 7. Charge decay curves for a 0.5 mM $\text{Cu}(\text{ClO}_4)_2$ solution; $q_0^m = +12 \mu\text{C}/\text{cm}^2$, $-Q_{\text{inj}}$, $\mu\text{C}/\text{cm}^2$: 1.12; 2.16; 3.20; 4.24; 5.28; 6.32; 7.36.

Cupric ions are reduced at potentials quite positive of the pzc so that it is possible to commence at potentials where the electrode bears a high positive charge and inject negative charge to take the electrode potential towards the pzc. Figure 7 displays the potential decay curves resulting from a series of such experiments in which increasing quantities of negative charge were injected. The noteworthy feature in this figure is the larger separation of the relaxation transients when the charge injected is less than enough to bring the electrode to the pzc. Under these conditions, the diffuse layers contain only perchlorate anions so the rate of potential change is determined by the diffusion of cupric ions to the electrode. When the charge injected exceeds the amount needed to reach the pzc, the excess charge is matched by an equivalent quantity of cupric ions in the diffuse layer and a much more rapid relaxation ensues until all the Cu^{2+} is consumed. This is the reason that the curves in Figure 7 are bunched together near the pzc. Except for the differences in the copper amalgam concentrations and the changing values of the pzc with each amalgam, the observed transients obtained would be expected to be essentially identical for all values of injected charge great enough to bring the electrode beyond the pzc.

Chronocoulometric plots prepared from the transients in Figure 7 in which the injected charge was insufficient for the electrode to attain the pzc have intercepts below the values calculated from the injected charge in spite of the fact that no cupric ions populate the diffuse layer during the experiment. The explanation for this behavior has been mentioned earlier: cupric cations migrate to the exterior of the anionic diffuse layer to pair up with the anions ejected by the injection of the negative charge. A concentration "spike" of $\text{Cu}(\text{ClO}_4)_2$ results and the cupric ions in this "spike" are reduced much more rapidly than those ions which must diffuse to the electrode. This gives the appearance of "adsorbed" Cu^{2+} and leads to the lowered intercepts in the chronocoulometric plots. The amount of Cu^{2+} in the spike is given by $|Q_{\text{inj}}| T_{\text{Cu}^{2+}}$, where Q_{inj} is the amount of negative charge injected (less than the initial charge on the electrode in this case) and $T_{\text{Cu}^{2+}}$ is the transference number of Cu^{2+} . Table II compares the calculated values with those obtained from chronocoulometric

Table II: Calculated and Observed Excesses of $\text{Cu}(\text{ClO}_4)_2$ Generated at Electrode Surfaces by Injecting Negative Charge into Positively Charged Electrodes

Soln compn	Initial charge on electrode, $\mu\text{C}/\text{cm}^2$	Charge injected, $\mu\text{C}/\text{cm}^2$	FF Cu^{2+} in the $\text{Cu}(\text{ClO}_4)_2$ "spike"	
			Calcd from $Q_{\text{inj}}/T_{\text{Cu}^{2+}}$, $\mu\text{C}/\text{cm}^2$	From chronocoul plots, $\mu\text{C}/\text{cm}^2$
0.5 mM $\text{Cu}(\text{ClO}_4)_2$	+10.4	-15	6.5	8.0 ± 1
	+13.0	-22	9.7	11 ± 1
	+15.6	-25	11.3	12 ± 1
0.25 mM $\text{Cu}(\text{ClO}_4)_2$ +0.5 mM KClO_4	+10.4	-20	4.4	4.5 ± 1
	+13.0	-20	4.4	6.0 ± 1

plots prepared from Figure 7. The agreement is reasonably good considering the approximations involved in the simple analysis employed; the existence of the concentration "spike" of cupric ions is clearly demonstrated by these data.

Anionic Reactant in the Diffuse Layer. Anionic reactants, being repelled from negatively charged electrodes, would be expected to give rise to potential decay curves that differ from those with cationic reactants. A comparison of the decay curves for Cu^{2+} and FeY^- (Y^{4-} = ethylenediaminetetraacetate anion) is provided in Figure 8. (This particular pair of ions was chosen because the cation and anion have nearly identical half-wave potentials.) Note that the initial potential decay is much faster for the Cu^{2+} than for the FeY^- solution because FeY^- is ejected from the diffuse layer by the charge injection while Cu^{2+} is drawn into the diffuse layer. The decay rate for Cu^{2+} falls to a value comparable to the FeY^- rate only after all the cupric ions in the positive diffuse layer have been consumed and the potential, therefore, has become more positive than the pzc.

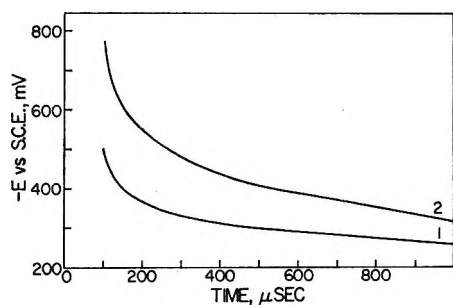


Figure 8. Potential decay curves for $\text{Cu}(\text{ClO}_4)_2$ and NaFeY solutions (Y = ethylenediaminetetraacetate); in each case $q_0^m = +10 \mu\text{C}/\text{cm}^2$ and $Q_{\text{inj}} = -20 \mu\text{C}/\text{cm}^2$; 1, 0.5 mM $\text{Cu}(\text{ClO}_4)_2$; 2, 1.0 mM NaFeY .

Conclusions

The experiments described here establish the conditions under which diffuse layers containing nonequilibrium quantities of reactants can be created and examined. The generally good agreement between

measured transient compositions of the diffuse layers and those calculated on the basis of relative ionic mobilities and bulk concentrations appears to justify the very simple description proposed for the mechanism by which diffuse layers are created.

A number of potential applications of the results of this study can be suggested. For example, it would appear to be feasible, by selection of supporting electrolytes, to generate transient diffuse layers containing much greater or much smaller quantities of various charged reactants than the corresponding equilibrium values. In this way, overall current efficiencies for desired reactions might be enhanced while those of undesired side reactions are reduced by performing electrolyses in a series of brief charge injections, followed by open-circuit reaction of the components in the resulting nonequilibrium diffuse layers.

The fact that very different potential decay curves result from cationic, neutral, or anionic reactants suggests possible application to the determination of the net charge on reactants, *i.e.*, ion-pairing or complex formation between reactants and components of the supporting electrolytes might be observable.

Finally, it is clear that in electrode kinetic measurements with dilute electrolytes and charged reactants, attention must be paid to the possibility that the nonequilibrium diffuse layers created by the electrical perturbations applied to the electrode may not achieve their equilibrium compositions by the time kinetic data are taken. The data and analysis presented here could be utilized to make appropriate corrections when data must be obtained under nonequilibrium conditions, *e.g.*, when a very rapid electrode reaction is studied in the presence of little or no supporting electrolyte.

Acknowledgment. We are grateful to Professor George Gavalas for helpful discussions and to Dr. Keith Oldham for pointing out errors in a previous version of the Appendix. This work was supported by the U. S. Army Research Office (Durham).

Appendix

The salt-free layer created at electrode surfaces by rapid charge injection changes the boundary conditions of the mass-transfer problem that must be solved to calculate the rate at which reactants diffuse to the electrode to consume charge. The problem is to solve eq A1

$$\frac{\partial C(x,t)}{\partial t} = D \frac{\partial^2 C(x,t)}{\partial x^2} \quad (\text{A1})$$

for the boundary condition

$$C(0,t) = 0 \quad t \geq 0 \quad (\text{A2})$$

and the initial conditions

$$C(x,0) = 0 \quad 0 \leq x < d \quad (\text{A3})$$

$$C(x,0) = C^0 \quad d < x < \infty \quad (\text{A4})$$

where d is the thickness of the salt-free layer of water created at the electrode surface at time $t = 0^+$, and C^0 is the concentration of reactant in the bulk of the solution.

A full solution of eq A1 is not required for the present purpose. It suffices to obtain $[\partial C(x,t)/\partial x]_{x=0}$, because the charge consumed per unit area by the diffusing reactant is given by

$$Q = \int_0^t FD \left[\frac{\partial C(x,t)}{\partial x} \right]_{x=0} dt' \quad (\text{A5})$$

The LaPlace transform of the derivative needed can be obtained by standard methods.^{9,11} In the region $0 \leq x < d$ the result is

$$D \frac{\partial \bar{C}(x,s)}{\partial x} = \frac{C^0}{2} \sqrt{\frac{D}{s}} \left\{ \exp \left[\sqrt{\frac{s}{D}} (x-d) \right] + \exp \left[-\sqrt{\frac{s}{D}} (x+d) \right] \right\} \quad (\text{A6})$$

where s is the LaPlace transform variable.

Since the LaPlace transform of $\int_0^t [\partial C(x,t')/\partial x]_{x=0} dt'$ is $1/s [\partial \bar{C}(x,s)/\partial x]_{x=0}$ we set $x = 0$ in eq A6 and multiply the result by $1/s$ to obtain

$$\frac{D}{s} \left[\frac{\partial \bar{C}(x,s)}{\partial x} \right]_{x=0} = \frac{C^0 \sqrt{D}}{s^{3/2}} \exp \left(-\sqrt{\frac{s}{D}} d \right) \quad (\text{A7})$$

The inversion of the right-hand side of eq A7 yields eq 2 in the main text.

(11) H. S. Carslaw and J. C. Jaeger in "Conduction of Heat in Solids," 2nd ed, Oxford University Press, 1959, Chapter XII.

The Vaporization Thermodynamics of Samarium Oxide Fluoride

by Dale E. Work and Harry A. Eick

Department of Chemistry, Michigan State University, East Lansing, Michigan 48823 (Received March 12, 1970)

Samarium oxide fluoride has been studied at high temperatures by X-ray diffraction and target collection Knudsen effusion techniques and found to vaporize over the temperature range 1614–2017°K to the sesquioxide and gaseous trifluoride. At 1815°K, $\Delta H^\circ_{\tau} = 101.5 \pm 1.1$ kcal/gfw and $\Delta S^\circ_{\tau} = 34.73 \pm 0.63$ eu. Combination of these values with estimated and measured heat capacity data yields for $\text{SmOF}(s) \Delta H^\circ_{f,298} = -274.6 \pm 2.5$ kcal/gfw, and $\Delta S^\circ_{f,298} = -42.6 \pm 4.0$ eu. Second- and third-law vaporization enthalpies are presented and discussed.

Introduction

Samarium oxide fluoride has been known for many years and several of its physical properties have been investigated,¹ but its high-temperature decomposition mode has never been characterized. Indeed, aside from the vaporization mode of NdOF^2 (for which no thermodynamic data were given), the high-temperature decomposition modes of MOF and the corresponding thermodynamic studies constitute a virtually unexplored area. Thermodynamic data have not been reported for either the lanthanide oxide fluorides or, aside from a few recent studies,^{3,4} for the other lanthanide oxide halide systems. This dearth of thermodynamic experimental data probably stems from a scarcity of thermodynamic and spectroscopic data for the corresponding trihalides. The purposes of this investigation were: (1) to characterize the vaporization mode of $\text{SmOF}(s)$ and thus to define more clearly the phase diagram of $\text{SmO}_n\text{F}_{3-2n}$ at $n = 1$; and (2) to

determine the thermodynamics of vaporization, thus providing a predictive tool for decomposition reactions of related species.

Experimental Section

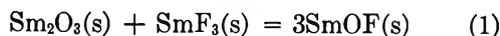
Preparative. Samarium oxide fluoride was prepared as described by Shinn and Eick.² The trifluoride, prepared from a mixture of Sm_2O_3 (>99.9% pure, Michigan Chemical Corp., St. Louis, Mich.) and excess ammonium fluoride (reagent grade, J. T. Baker Chemical Co.), and sesquioxide were mixed in a mortar with a pestle and were placed in a Pt boat inside a Vycor tube. They reacted according to eq 1. Heating the mixture

(1) L. Mazza and A. Iandelli, *Atti. Acad. Ligure Sci. Lett., Genoa*, **7**, 44 (1951).

(2) D. B. Shinn and H. A. Eick, *Inorg. Chem.*, **8**, 232 (1969).

(3) J. M. Haschke and H. A. Eick, *J. Amer. Chem. Soc.*, **92**, 4550 (1970).

(4) A. K. Baev and G. I. Novikov, *Zh. Neorgan. Khim.*, **10**, 2457 (1965).



gradually to 1050° in an inert atmosphere and maintaining it at that temperature for 5 hr yielded the white crystalline oxide fluoride. The products from two such preparations and a samarium oxide fluoride sample prepared 42 months earlier by Shinn and Eick⁵ were studied.

Analytical. The various crystalline species involved in this study were identified by X-ray powder diffraction (Haegg-type Guinier camera Cu K α_1 radiation, $\lambda_{\alpha_1} = 1.54051 \text{ \AA}$, $T = 24 \pm 1^\circ$, internal standard KCl, $a = 6.2930_0 \pm 0.0000_9 \text{ \AA}$).

Vaporization. The thermal decomposition of SmOF(s) under vacuum was traced by a series of X-ray diffraction patterns obtained as the decomposition progressed. The net weight loss of each of the three oxide fluoride preparations used was also determined. In each case, a weighed specimen was heated by induction under vacuum (10^{-6} Torr) in an outgassed molybdenum effusion cell to a temperature above 1500° for several hours until the weight of the solid residue was invariant.

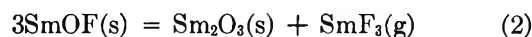
The vapor pressure was measured over the temperature range 1614–2017°K, using the Knudsen effusion target collection apparatus and technique as described elsewhere.⁶ In experimental run 11, in which exceptionally long exposure times were required, a Latronics Coloratio pyrometer–analog controller system was used to improve temperature stability and these data points were assigned double weight in the corresponding thermodynamic calculations. The one other data point which involved a similarly long exposure time was also assigned double weight. Calculated fractions of the effusate⁷ were collected on liquid nitrogen-chilled aluminum targets which were then analyzed for samarium by an X-ray fluorescence procedure using a previously determined calibration graph. Power settings and electronic circuitry were adjusted to provide maximum sensitivity to Sm L- β_1 radiation according to the method suggested by Neff,⁸ and the analysis was standardized as described elsewhere.⁹ Symmetrical molybdenum effusion cells previously outgassed at 1900° under vacuum (10^{-6} Torr) were used for the vaporization measurements and no crucible–sample interaction was observed either visually or by X-ray diffraction. Circular knife-edged orifices with areas ranging from 9×10^{-4} to $120 \times 10^{-4} \text{ cm}^2$ were used without apparent effect on the equilibrium pressure measurements.

The sticking coefficient of the oxide fluoride on the aluminum collection targets was determined by a bouncing experiment in which a thin aluminum disk was exposed to the effusate over the temperature range 1600–1700° via a 6.0 mm diameter hole in the disk. The disk was mounted 5.0 mm from the face of a chilled aluminum collection target.

Results

The diffraction pattern of the air-insensitive product of reaction 1 matched that of the SmOF sample⁵ prepared by Shinn and Eick and stored in a desiccator 42 months earlier, and is in good agreement with that calculated from published lattice parameters for SmOF.¹⁰ Metal analysis for the phase is consistent with the formula SmO₁F₁.⁶

X-Ray diffraction results showed clearly the solid product of the oxide fluoride decomposition was monoclinic B-Sm₂O₃. The diffraction pattern of the reaction product matched that of reagent grade Sm₂O₃ heated to >1200°. The successive X-ray diffraction patterns obtained as the decomposition progressed revealed no intermediate crystalline phase between the oxide fluoride and the sesquioxide for the temperature and pressure ranges studied. This observation suggested that SmOF decomposes incongruently according to reaction 2. Further evidence that this is the decomposition



mode was obtained by net weight loss experiments in which the observed weight losses of the three oxide fluoride preparations used were 99.7 ± 1.0 , 96.5 ± 1.0 , and $100.5 \pm 1.0\%$ of the theoretical loss expected according to reaction 2. The rapidity with which the initial equilibration was attained for the second sample was taken as additional evidence that the sample yielding 96.5% of the theoretical weight loss contained excess Sm₂O₃.

The sticking coefficient determination revealed that no detectable trifluoride had been reflected by the chilled aluminum target to the back of the disk, even though approximately 18 μg was collected on the chilled target. Accordingly, the sticking coefficient was taken to be ≥ 0.95 .

Six independent vaporization experiments were performed, the last two on the oxide fluoride sample prepared by Shinn and Eick. The linear least-squares fit of the $34 \log P_{\text{SmF}_3} \text{ vs. } 1/T$ data points ($R = 1.987 \text{ eu}$) presented in Figure 1, is described with standard deviation as

$$R \ln P_{\text{SmF}_3(\text{atm})} = -[(101.5 \pm 1.1) \times 10^3]/T + (34.73 \pm 0.63)$$

From this equation the thermodynamic data for reaction 2 at the median temperature, together with their

(5) D. B. Shinn, Ph.D. Thesis, Michigan State University, East Lansing, Mich., 1968.

(6) J. M. Haschke and H. A. Eick, *J. Phys. Chem.*, **72**, 4235 (1968).

(7) J. L. Margrave in Bockris, White, and Mackenzie, "Physicochemical Measurements at High Temperatures," Butterworths Scientific Publications, London, 1959, p 225 ff.

(8) H. Neff, *Arch. Eisenhüttenw.*, **34**, 903 (1963).

(9) J. M. Haschke, R. L. Seiver, and H. A. Eick, U. S. Atomic Energy Commission Report, COO-716-033, 1968.

(10) N. C. Baenziger, J. R. Holden, G. E. Knudsen, and A. I. Popov, *J. Amer. Chem. Soc.*, **76**, 4734 (1954).

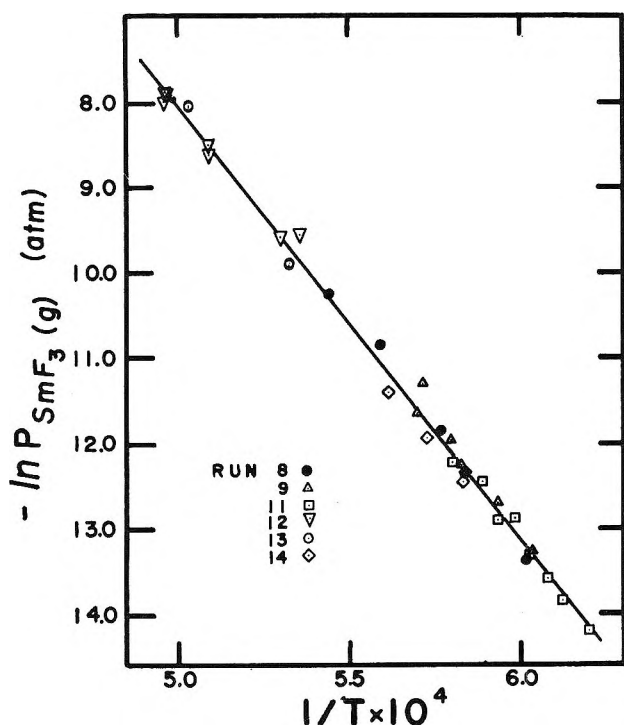


Figure 1. Graph of the logarithm of the partial pressure of $\text{SmF}_3(\text{g})$ in equilibrium with condensed Sm_2O_3 and SmOF as a function of reciprocal temperature.

standard deviations, are: $\Delta H^\circ_{1815} = 101.5 \pm 1.1$ kcal/gfw of $\text{SmF}_3(\text{g})$ and $\Delta S^\circ_{1815} = 34.73 \pm 0.63$ eu. To reduce these second-law data to 298°K, published heat capacities were used for B- Sm_2O_3 ^{11,12} and a Kopp's rule approximation¹³ was employed for the heat capacity of SmOF : $C_p[\text{SmOF}(\text{s})] = 18.355 + 2.32 \times 10^{-3}T - 2.15 \times 10^5 T^{-2}$ ($298 \leq T \leq 1195^\circ\text{K}$), and $C_p[\text{SmOF}(\text{s})] = 21.43$ ($1195 < T \leq 2000^\circ\text{K}$). The enthalpy of transition of SmOF at 524° was estimated as 1.25 kcal/gfw ($\Delta S_{\text{tr}} = 1.57$ eu), and the enthalpy of transition of B- Sm_2O_3 at 922° was taken to be 0.25 kcal/gfw ($\Delta S_{\text{tr}} = 0.21$ eu).¹¹

The heat capacity of $\text{SmF}_3(\text{g})$ also had to be approximated. Heat capacity data for 16 gaseous MX_3 species¹⁴ ($X = \text{halogen}$) with masses ranging from 71 to 456 amu, ten of which are pyramidal, four of which are trigonal planar, and two of which are T-shaped, were examined. Above 1000° , these data showed the heat capacity of $\text{MX}_3(\text{g})$ to be surprisingly invariant and virtually mass independent, but at lower temperatures the magnitude of the heat capacity became decisively mass dependent. The four $\text{BX}_3(\text{g})$ species exhibited exceptionally low heat capacities at lower temperatures with respect to the other twelve compounds, and were disregarded. For the remaining compounds the heat capacities, when given, were averaged at 1000, 1500, and 2000° and were found with their standard deviations to be 19.46 ± 0.42 , 19.79 ± 0.07 , and 19.91 ± 0.08 , respectively. Because of the close agreement of the heat capacity of $\text{AsF}_3(\text{g})$ with

these average values, and because the heat capacity of $\text{AsF}_3(\text{g})$ agrees well with an independent estimate for $\text{SmF}_3(\text{g})$ at lower temperatures,¹⁵ the heat capacity of $\text{SmF}_3(\text{g})$ was taken to be that of $\text{AsF}_3(\text{g})$: $C_p[\text{AsF}_3(\text{g})] = 19.04 + 0.52 \times 10^{-3}T - 3.12 \times 10^5 T^{-2}$ ($298^\circ \leq T \leq 2000^\circ\text{K}$). Combining these data according to reaction 2 yields

$$\Delta H^\circ_T - \Delta H^\circ_{1195} = -8.35T + 0.26 \times 10^{-3}T^2 - 3.12 \times 10^5 T^{-1} + 9346 \quad (1195^\circ < T \leq 2000^\circ\text{K})$$

$$\Delta H^\circ_T - \Delta H^\circ_{298} = -5.275T - 0.9 \times 10^{-3}T^2 + 0.97 \times 10^5 T^{-1} - 2424 \quad (298^\circ \leq T \leq 1195^\circ\text{K})$$

$$\Delta S^\circ_T - \Delta S^\circ_{1195} = -8.35 \ln T + 0.52 \times 10^{-3}T + 1.56 \times 10^5 T^{-2} + 58.44 \quad (1195^\circ < T \leq 2000^\circ\text{K})$$

$$\Delta S^\circ_T - \Delta S^\circ_{298} = -5.275 \ln T - 1.80 \times 10^{-3}T + 0.485 \times 10^5 T^{-2} + 25.33 \quad (298^\circ \leq T \leq 1195^\circ\text{K})$$

The corrected values obtained, with the listed error indicating a composite of the standard deviation and an estimated error of 1.4 kcal/gfw in the reduction (and including a 2 eu uncertainty in $\Delta S_{\text{sub}}[\text{SmF}_3]$), are: $\Delta H^\circ_{298} = 115.9 \pm 2.5$ kcal/gfw of $\text{SmF}_3(\text{g})$ and $\Delta S^\circ_{298} = 51.9 \pm 4.0$ eu.

The second-law enthalpy (of reaction 2) has been combined with the enthalpy of formation of B- Sm_2O_3 ,¹² the enthalpies of formation¹⁶ and sublimation of $\text{SmF}_3(\text{s})$,¹⁵ and the estimated heat capacity of $\text{SmF}_3(\text{g})$, to yield for $\text{SmOF}(\text{s})$: $\Delta H^\circ_{298} = -274.6 \pm 2.5$ kcal/gfw. The error limit in this value reflects a composite of the standard deviation and estimated error in reduction. Similarly, the entropy change for reaction 2 has been combined with published data for B- Sm_2O_3 ,¹⁷ F_2 ,¹⁸ O_2 ,¹⁸ and $\text{SmF}_3(\text{s})$ ^{15,16} and the estimated heat capacity for $\text{SmF}_3(\text{g})$ to yield $\Delta S^\circ_{298}[\text{SmOF}(\text{s})] = -42.6 \pm 4.0$ eu. The absolute entropy of $\text{SmOF}(\text{s})$ is calculated to be

(11) L. B. Pankratz, E. G. King, and K. K. Kelley, U. S. Bureau of Mines Report of Investigations, No. 6033, U. S. Department of the Interior, Mines Bureau, Pittsburgh, Pa., 1962.

(12) C. E. Holley, Jr., E. J. Huber, Jr., and F. B. Baker, "Progress in the Science and Technology of the Rare Earths," Vol. 3, L. Eyring, Ed., Pergamon Press, New York, N. Y., 1968, pp 379-384.

(13) J. M. Haschke and H. A. Eick, *Inorg. Chem.*, 9, 851 (1970).

(14) K. K. Kelley, U. S. Bureau of Mines Bulletin No. 584, U. S. Department of the Interior, Mines Bureau, U. S. Government Printing Office, Washington, D. C., 1960.

(15) K. F. Zmbov and J. L. Margrave, *Advances in Chemistry Series*, No. 72, American Chemical Society, Washington, D. C., 1968.

(16) C. E. Wicks and F. E. Block, U. S. Bureau of Mines Bulletin No. 605, U. S. Department of the Interior, Mines Bureau, U. S. Government Printing Office, Washington, D. C., 1960.

(17) E. F. Westrum, Jr., *Advances in Chemistry Series*, No. 71, American Chemical Society, Washington, D. C., 1967.

(18) G. N. Lewis and M. Randall, revised by K. S. Pitzer and L. Brewer, "Thermodynamics," 2nd ed, McGraw-Hill, New York, N. Y., 1961.

$S^\circ_{298} = 22.5 \pm 4.0$ eu. The reported error represents the composite of the experimental errors and the estimated errors.

A third-law enthalpy change has been calculated using thermodynamic data published for B-Sm₂O₃^{11,12} and the sublimation enthalpy of SmF₃(s),¹⁵ together with the appropriate heat capacity approximations cited previously. Since no independent experimental value for $S^\circ_{298}[\text{SmOF}]$ is available, a value of $S^\circ_{298} = 22.16$ eu was employed in accord with Latimer's¹⁹ technique for estimating standard entropies and Westrum's procedure for including the magnetic contribution.¹⁷ This calculation yielded a value of $\Delta H^\circ_{298} = 117.59 \pm 0.50$ kcal/gfw with a 0.2 kcal temperature trend evident over the temperature range 1614–2017°K. However, when free-energy functions based on $S^\circ_{298} \text{SmOF} = 22.46$ eu were used (an increase of 0.3 eu), a value of $\Delta H^\circ_{298} = 116.01 \pm 0.49$ kcal/gfw was obtained with no temperature trend observed. The very close agreement between the $S^\circ_{298} \text{SmOF}$ value used here and that calculated above was not by design, and although the agreement is certainly significant, the precision of the agreement must be considered with respect to the approximations employed.

Discussion

The phase diagram of the SmO_nF_{3-2n} has been established for $0.7 \leq n \leq 1.0$,²⁰ and the present study indicates that phases corresponding to higher values of n do not exist at the temperature and pressure regions investigated. The incongruent decomposition mode is analogous to that of LnOCl species,⁴ but different from that of EuOBr(s).³ The observed mode is not surprising in view of earlier work on NdOF² and the predominantly trivalent character of samarium.

The enthalpy and entropy values given above are reasonable in view of the earlier work¹⁵ by Zmbov and Margrave on the sublimation of condensed SmF₃ over the temperature range 1362 to 1506°K: $\Delta H^\circ_T = 96.8$ kcal/gfw; $\Delta S^\circ_T = 45 \pm 2$ eu; and $\Delta H^\circ_{298} = 107 \pm 5$ kcal/gfw. Since gaseous SmF₃ is the only vapor species in equilibrium with the oxide fluoride, its vapor pressure must be less than the corresponding pressure over condensed SmF₃. As expected, the slope of the $-\ln P$ vs. $1/T$ plot for the SmOF decomposition is more negative than that for the SmF₃ sublimation.

The enthalpy of sublimation for the trifluoride was also useful for checking the suitability of the SmF₃(g) heat capacity approximation. From Zmbov and Margrave's data at 298°K, and from published enthalpy data for SmF₃(s),¹⁶ ΔH°_{298} for SmF₃(g) is found to be about -273.0 ± 5.0 kcal/gfw. Use of $C_p(\text{AsF}_3) \sim C_p(\text{SmF}_3)$ in conjunction with Zmbov and Margrave's $\Delta H^\circ_{\text{sub}}{}_{1434}$ data yields $\Delta H^\circ_{298}[\text{SmF}_3(\text{g})] = -274.5$ kcal/mol, well within the error limit of the earlier study. Correcting C_p at lower temperatures for the SmF₃-AsF₃ mass difference yields a net change of less

than 1 kcal/mol. It is also significant that use of the anomalous $C_p(\text{BF}_3)$ rather than $C_p(\text{AsF}_3)$ in the above calculation yields for SmF₃(g) $\Delta H^\circ_{298} = -271.8$ kcal/gfw, further evidence of the very similar C_p values for MX₃(g) species. The consistency of these approximations is evidenced by the value of ΔS°_{1434} calculated for the reaction: SmF₃(s) = SmF₃(g) using the second-law value for ΔS°_{1815} and the various C_p and transition approximations cited previously. The calculated value of 44.05 eu is in good agreement with Margrave and Zmbov's value of 45 ± 2 eu.

The entropy of samarium oxide fluoride and the third-law calculation have presented some interesting features. Incorporating Westrum's¹⁷ approximation for the magnetic contribution to the entropy of SmOF with Latimer's¹³ estimation of the atomic contribution yields a value of 22.16 eu, while the second-law result obtained in the present investigation is 22.5 ± 4.0 eu. Although the discrepancy may seem small with respect to the error limit, the uncertainty in the third-law calculation stems largely from an error limit of ± 2 eu in Zmbov and Margrave's study¹⁵ on the sublimation enthalpy of SmF₃, and may not represent a true uncertainty. Further, according to the stoichiometry of reaction 2, a 1.0 eu difference in S°_{298} of SmOF results in a change of about 5 kcal in the third-law value of ΔH°_{298} . The fact that the third-law value (117.59 kcal/gfw) obtained by using $S^\circ_{298} \text{SmOF} = 22.16$ is about 1.7 kcal higher than the second-law value (115.9 kcal/gfw) and exhibits a slight temperature trend may suggest an error in the third-law computation which did not enter into the second-law calculation. Since estimated heat capacities were used in both calculations, but the estimated standard entropy of SmOF was employed only in the third-law calculation, the value of $S^\circ_{298}[\text{SmOF}]$ is suspect. Latimer mentions that the value for the fluorine contribution to the entropy is an estimated rather than an empirical entity, but this does not account for a difference of 0.3 eu, though it may account for part of it. Rather, it seems that the discrepancy arises from the very basis of the approximation. Latimer's approximation is based on atomic contributions to the entropy in binary compounds, and although this approximation would hold for many ternary species, difficulty might well be expected in a compound such as SmOF(s), in which are present two comparably sized anions which can assume ordered or disordered positions in the lattice. Thus, it seems probable that the entropy of the oxide fluoride should be somewhat higher than that predicted by Latimer or more near the 22.5 eu value. The third-law value of ΔH°_{298} is seen to

(19) W. M. Latimer, "The Oxidation States of the Elements and Their Potentials in Aqueous Solutions," 2nd ed, Prentice-Hall, Inc., Englewood Cliffs, N. J., 1952.

(20) U. Roether, Ph.D. Thesis, University of Freiburg i. B., Germany, 1967.

be quite sensitive to the approximations used, and the good agreement between the second- and third-law values gives further credence to the validity of the approximations employed in this investigation.

Acknowledgment. The partial support of the U. S. Atomic Energy Commission (AT(11-1)-716) and a National Science Foundation Fellowship to D. E. W. are gratefully acknowledged.

Polymorphism of the Crystalline Methylchloromethane Compounds.

III. A Differential Scanning Calorimetric Study

by Lawrence Silver and Reuben Rudman

Department of Chemistry, Adelphi University, Garden City, New York 11530 (Received March 30, 1970)

The methylchloromethane compounds and carbon tetrabromide have been studied from above their melting points to 115°K using differential scanning calorimetry. Carbon tetrachloride, methyl chloroform (1,1,1-trichloroethane), and 2,2-dichloropropane each form two successive high-temperature, disordered crystalline phases (Ia and Ib) when cooled from the melt, but when warmed from the low-temperature, ordered modification (phase II), phase Ib forms and persists until the melt. *t*-Butyl chloride (2-chloro-2-methylpropane), neopentane (2,2-dimethylpropane), and carbon tetrabromide form only one crystallographic modification in the high-temperature region. Enthalpies of transition and fusion have been obtained for all but the two weakest phase transitions involved. These include $\Delta H_{Ia \rightarrow L, CCl_4} = 419$ cal/mol, $\Delta H_{Ia \rightarrow L, CH_3CCl_3} = 217$ cal/mol, $\Delta H_{Ib \rightarrow L, (CH_3)_2CCl_2} = 537$ cal/mol, and $\Delta H_{II \rightarrow Ib, (CH_3)_3CCl} = 1415$ cal/mol. The other data, with one exception, are in agreement with previously published values. It was not possible to obtain accurate data for $\Delta H_{II \rightarrow Ib, CH_3CCl_3}$ inasmuch as the heat capacity is rapidly changing in the high-temperature phase. Similar difficulties were encountered by previous investigators; the two sets of results are compared.

Introduction

The methylchloromethane (MCM) compounds, $(CH_3)_nCCl_{4-n}$, where n varies from 0 to 4, consist of nearly spherical molecules and exhibit a number of solid-solid phase transitions. The high-temperature phases of such materials are generally termed "plastic crystals," inasmuch as they are soft, waxy, and easily extruded. An initial low-temperature survey^{1,2} of these compounds revealed that carbon tetrachloride ($n = 0$) exhibits unusual crystallographic behavior. It was found that, on cooling from the melt, a face-centered cubic (fcc) phase is formed which transforms to a rhombohedral phase, followed by a transformation to a monoclinic phase. On warming the monoclinic phase, the rhombohedral phase is formed; this phase persists until the melting point. Subsequent study by differential thermal analysis³ and differential scanning calorimetry (DSC)⁴ verified the results of the X-ray investigation.

The X-ray investigation² of methyl chloroform ($n = 1$) and 2,2-dichloropropane ($n = 2$) revealed the existence of high-temperature structures similar to that of the rhombohedral phase of carbon tetrachloride. However, no evidence for the existence of any fcc phase was

discovered for these compounds, even though *t*-butyl chloride ($n = 3$) and neopentane ($n = 4$), as well as carbon tetrachloride, form fcc phases with similar unit cells and X-ray intensity distributions.

The present study was undertaken in an attempt to investigate systematically the solid-solid phase transitions of all five MCM compounds, from their melting points to -160° . In addition, the possibility of similar phase transitions in carbon tetrabromide, which is isomorphous with carbon tetrachloride in the fcc and monoclinic phases, was investigated. The existence of fcc phases in methyl chloroform and 2,2-dichloropropane was uncovered during the course of the DSC investigation and verified by low-temperature single-crystal X-ray diffraction techniques. The results of the X-ray diffraction studies have been described elsewhere.⁵ The present paper is limited to a description

(1) R. Rudman and B. Post, *Science*, **154**, 1009 (1966).

(2) R. Rudman and B. Post, *Mol. Cryst.*, **5**, 95 (1968).

(3) K. Kotake, N. Nakamura, and H. Chihara, *Bull. Chem. Soc. Jap.*, **40**, 1018 (1967).

(4) A. P. Gray, personal communication; *Instr. News*, **17**, 3 (1967); and Perkin-Elmer DSC literature.

(5) R. Rudman, *Mol. Cryst. Liquid Cryst.*, **6**, 427 (1970).

of the various phase transitions and the thermodynamic data derived from the DSC thermograms of the MCM compounds and of carbon tetrabromide. These data are compared, where possible, with previously reported data.

Experimental Section

Materials. The MCM samples used were the highest quality commercially available and were treated as follows. Carbon tetrachloride, methyl chloroform, 2,2-dichloropropane, and *t*-butyl chloride were redistilled and examined by vapor-phase chromatography using both polar and nonpolar columns. Analysis of the chromatograms showed that methyl chloroform was 99.9% pure and *t*-butyl chloride was 99.7% pure, while both carbon tetrachloride and 2,2-dichloropropane showed no indication of any impurities even at the highest resolution of the instrument and were assumed to be >99.95% pure. J. T. Baker CP grade neopentane, rated at 99.0% pure, was obtained in a pressurized cylinder and was used without further purification or analysis. The carbon tetrabromide was recrystallized by sublimation.

Equipment. A Perkin-Elmer DSC-1B differential scanning calorimeter equipped with a low-temperature adapter was used.⁶ The DSC was calibrated with 99.9999% pure indium, using ranges of 8 and 16 with a chart speed of 1.5 in./min. An instrument constant of 10.92 ± 0.06 mcal/cm² was obtained, using ΔH_f of indium equal to 0.775 kcal/mol.⁷ With this constant, ΔH_f for a 99.99+ % pure sample of lead was found to be 1.113 kcal/mol, compared to the reported value of 1.141 kcal/mol.⁷ Appropriate corrections were made for other ranges and chart speeds.

A further indication of the accurate calibration of the energy input and temperature readings of the DSC was provided by the good agreement between the present and previously reported values for a number of the MCM transitions. Possible explanations for the discrepancies which were observed in a few cases are found in the Discussion.

Each of the transitions was investigated at two or more scan rates, ranging from 0.625 to 10°/min. All readings for a given transition were in agreement, within the limits of error. The thermogram peaks were each measured several times with a compensating polar planimeter accurate to 0.1 cm². Areas ranging from 0.4 to 21 cm² were measured.

The manufacturer's specifications state that the temperature of the DSC-1B is accurate to better than 2°. The observed phase changes were reproducible to within 1° for sharp changes and agreed as well with previously reported values. For example, the monoclinic to rhombohedral phase transition in carbon tetrachloride was observed at 226.6°K, which compared quite favorably with the value of 225.6°K reported by Dunlop.⁸ Temperatures were read at the intersection of the base

line and the peak slope (on the ascending side of the peak).

A difficult problem arose in determining the accurate melting point of the MCM compounds with $n = 0, 1,$ and 2 . These compounds melted over considerable ranges of temperatures. It is known that the considerable premelting phenomena which have been observed for these compounds⁹ prevent the determination of a sharp melting point. In fact, it might not even be proper to speak of a sharp melting point when discussing these compounds. The soft, plastic nature of these phases and the large degree of self-diffusion that is known to occur¹⁰ suggest that it might be most practical to speak of a melting point range. In the present investigation it was found that the end of the peak always occurred at the same temperature. It was decided to report the (reproducible) temperature at which melting is completed rather than the (variable) temperature at which premelting phenomena begin to occur. It was later found that similar difficulties had induced Rubin, *et al.*,¹¹ to report the melting point of methyl chloroform for the *completely* melted system.

Sample Preparation. The mass was determined to ± 0.01 mg for samples ranging in size from 2 to 10 mg. All samples used were quite volatile and the sample holders had to be sealed before weighing. A few sets of sample holders were weighed, sealed without *any* sample, and reweighed. No change in mass was determined. Aluminum sample holders were initially used. However, for MCM compounds where $n = 1, 2,$ and 3 they exploded while they were being sealed or corroded very soon after sealing. A search of the literature revealed that a strongly exothermic reaction occurs between heated aluminum metal and alkyl halides resulting in the formation of air-sensitive liquid alkyl-aluminum sesquihalides.^{12,13} Evidently the crimping process generates sufficient heat to initiate the reaction.

(6) The temperature calibration of the instrument only reached -100° , so it was necessary to offset the controls in the rear of the instrument and to recalibrate the dial settings with a series of known materials. Instructions for this are included with the instrument, but the suggested standards, as well as a number of other materials we tested, did not melt sharply. A straight-line calibration curve of dial reading *vs.* temperature was obtained by using the following sharp, reproducible transitions of the $(\text{CH}_3)_n\text{CCl}_{4-n}$ compounds (n , transition, transition temperature in degrees Kelvin): 3, I \rightarrow L, 248.2; 2, Ib \rightarrow L, 239.4; 0, II \rightarrow Ib, 225.5; 3, II \rightarrow I, 219.7; 2, II \rightarrow Ib, 188.2; 3, III \rightarrow II, 183.2; 4, II \rightarrow I, 140.0. In this notation, II \rightarrow I indicates a transition from phase II to phase I; L represents the liquid state.

(7) "Handbook of Chemistry and Physics," 49th ed, The Chemical Rubber Publishing Co., Cleveland, Ohio, 1968-1969, p D-33.

(8) A. Dunlop, *J. Amer. Chem. Soc.*, **77**, 2016 (1955).

(9) A. R. Ubbelohde, "Melting and Crystal Structure," Oxford University Press, London, 1965, p 230.

(10) E. O. Stejskal, D. E. Woessner, T. C. Farrar, and H. S. Gutowsky, *J. Chem. Phys.*, **31**, 55 (1959).

(11) T. R. Rubin, B. H. Levedahl, and D. M. Yost, *J. Amer. Chem. Soc.*, **66**, 279 (1944).

(12) A. V. Grosse and J. M. Mavity, *J. Org. Chem.*, **5**, 106 (1940).

(13) G. E. Coates, M. L. H. Green, and K. Wade, "Organometallic Compounds," Vol. I, 3rd ed, Methuen and Co., London, 1967, p 297.

Table I: Carbon Tetrachloride

	Phase transition					
	L → Ia	Ia → Ib	Ib → II	II → Ib	Ib → L	Ia → L
Temp, °K						
This work	245.2	234.0	217.3	226.6	247.8	244.8
Dunlop ^a					250.41	
Hicks, <i>et al.</i> ^a			225.28	225.48		
Kotake, <i>et al.</i> ³		Obsd ^b			x^b	$x - 3.86$
Gray ⁴	244.8	234.3	220.9	225.1	250.3	245.9
ΔH , cal/mol						
This work	-407	-164	-1063	1070	596	419
Hicks, <i>et al.</i> ^a				1095	601	
Gray ⁴	-421	-163	-1050	1087	601	421
ΔS , eu						
This work	-1.66	-0.70	-4.89	4.72	2.41	1.71
Hicks, <i>et al.</i> ^a				4.859	2.401	
Gray ⁴	-1.72	-0.70	-4.75	4.83	2.40	1.71

^a J. Hicks, J. Hooley, and C. Stephens, *J. Amer. Chem. Soc.*, **66**, 1064 (1944). ^b Observed but not reported.

Gold pans were used for these compounds and for carbon tetrabromide. All samples were sealed with the Perkin-Elmer volatile-sample sealer in special volatile-sample pans and covers. As suggested by the manufacturer, small disks were placed inside the pans to prevent the vapors from depositing on the covers. The samples were weighed after investigation and remained constant within 0.01 mg, indicating no sample loss during the course of the DSC study.

Errors. Enthalpy. Calculations of ΔH are based on the measured peak areas, the experimentally obtained instrumental constant, weight of the sample, and the C-12 system for molecular weights. The errors involved in each of these measurements, combined with the agreement between the experimental and literature values of ΔH_f for Pb, indicate that ΔH is accurate to within 4%, with a precision of 2%, except for the weak, broad melting point transitions where an error of 8% is estimated.

Temperature. The error in temperature accuracy is between 1 and 2°. For temperatures in the range of 140–250°K the error is no larger than 1%.

Entropy. The error in the calculated entropy is the square root of the sum of the squares of the errors in enthalpy and temperature. This is approximately 4% for the sharp transitions and 8% for the broad melting points.

Results and Discussion

The five methylchloromethane compounds are now known to form a total of fifteen distinct crystallographic phases between their melting points and 113°K, at atmospheric pressure.¹⁴ Enthalpies of fusion and transition have been obtained from the DSC study for all but two of these. The results of this investigation are presented in Tables I–VI and, where possible, are compared with similar data obtained by other investigators.

Table II: Carbon Tetrabromide

	Phase transition			
	L → I	I → II	II → I	I → L
Temp, °K				
This work	367.8	310.4	320.0	367.4
Marshall, <i>et al.</i> ^a			320.0	
Aston ^b			319.4	366.7
ΔH , cal/mol				
This work	-846	-1563	1581	854
Marshall, <i>et al.</i> ^a			1594.5	
Aston ^b				880
ΔS , eu				
This work	-2.33	-5.03	4.94	2.33
Marshall, <i>et al.</i> ^a			4.98	
Aston ^b				2.4

^a J. G. Marshall, L. A. K. Staveley, and K. R. Hart, *Trans. Faraday Soc.*, **52**, 19 (1956). ^b J. G. Aston, "Physics and Chemistry of the Organic Solid State," Vol. I, D. Fox, M. Labes, and A. Weissberger, Ed., Interscience, New York, N. Y., 1963, p 545.

In an attempt to prevent confusion between this and other papers,^{2,5,14} the phases have been labeled as in the previous studies. In order to accommodate the newly discovered phases, the high-temperature phases for $n = 0, 1,$ and 2 have been labeled Ia and Ib, where the Ia phase forms directly from the melt and, upon cooling, transforms to Ib. When the low-temperature modification (II) is warmed, it always forms Ib which persists until the melting point; phase Ia is never formed by warming phase Ib. When the sample is cooled, the formation of phase Ib is extremely rapid. This is shown by the nearly perpendicular rise of the chart pen as the transition to phase Ib occurs. This sharp rise is characteristic of the formation of phase Ib and was

(14) C. E. Weir, G. J. Piermarini, and S. Block, *J. Chem. Phys.*, **50**, 2089 (1969), have detected the presence of yet another phase for carbon tetrachloride using high-pressure X-ray techniques.

Table III: Methyl Chloroform

	Phase transition							
	L → Ia	Ia → Ib	Ib → II	II → III	III → II	II → Ib	Ib → L	Ia → L
Temp, °K								
This work	227	214.3	178	220.5	239.2	231.9
Rubin, <i>et al.</i> ¹¹					206	224.20	240.2	
Crowe and Smyth ^b					205	223.6	240.1	
ΔH , cal/mol								
This work	-226	-162	-1433	<i>a</i>	<i>a</i>	1227	451	217
Rubin, <i>et al.</i> ¹¹					...	1786	450	
Crowe and Smyth ^b					50	1780	450	
ΔS , eu								
This work	-0.99	-0.76	-8.09	5.56	1.87	0.93
Rubin, <i>et al.</i> ¹¹						7.967	...	
Crowe and Smyth ^b					0.24	7.92	1.85	

^a Too small to be measured accurately. ^b R. W. Crowe and C. P. Smyth, *J. Amer. Chem. Soc.*, **72**, 4009 (1950).

Table IV: 2,2-Dichloropropane

	Phase transition				
	L → Ia	L → Ib	Ib → II	II → Ib	Ib → L
Temp, °K					
This work	<i>a</i>	226.7	184.8	187.0	240.2
Turkevich and Smyth ^b		232.9	187.2	188.2	239.4
ΔH , cal/mol					
This work		-544	-1373	1415	537
van de Vloed ^c				>750	790
ΔS , eu					
This work		-2.40	-7.43	7.57	2.24
van de Vloed ^c				>4	3.3

^a Observed during X-ray diffraction investigation; see text.
^b A. Turkevich and C. P. Smyth, *J. Amer. Chem. Soc.*, **62**, 2468 (1940). ^c A. van de Vloed, *Bull. Soc. Chim. Belg.*, **48**, 229 (1939).

noted on all the thermograms that were obtained in the present investigation and by Gray,⁴ even when the rate of cooling was as low as 0.625°/min.

A comparison of the present data with previously reported values shows that in nearly all cases the DSC-based enthalpies are lower. This is due to the (partly) subjective choice of base line and is pronounced in those cases where the thermograms show broad, relatively small peaks. The difficulty in choosing a proper base line has been recognized as a potential source of error.⁴ In spite of this, the only major discrepancy appears in the transition between phases Ib and II of methyl chloroform. However, in this particular instance both sets of previous investigators^{11,15} reported difficulties in the determination of the heat capacities.

Carbon Tetrachloride. The data for carbon tetrachloride are found in Table I. The agreement between the present data and those of previous investigators is well within the experimental error. It should be noted that Gray⁴ used $\Delta H_{II \rightarrow Ib}$ and $T_{Ib \rightarrow L}$ as internal heat capacity and temperature standards, respectively.

The peaks corresponding to the melting of phases Ia and Ib were always broad and poorly defined. This was true regardless of the scan rate and sample size. Surprisingly, the thermograms obtained by Gray showed clearly defined, nearly identical peaks for the formation and melting of these phases. We could not duplicate this. However, it is noted that the areas under the two sets of peaks were equivalent and corresponded to equal enthalpy changes, within the experimental limits of error. Similar broad curves were obtained by us for the corresponding transitions of methylchloroform and 2,2-dichloropropane.

In the original X-ray study,² it was thought that the metastable phase Ia transformed spontaneously to the stable phase Ib, after standing for several hours. However, the present study shows that this transition becomes kinetically favorable at a definite temperature, resulting in a sharp peak appearing on the thermogram. This was reproducible over several runs and at different cooling rates and agrees with the observations of Gray.⁴ Holding the sample temperature above 234°K for a long period of time did not result in the formation of phase Ib; the moment the temperature was lowered, phase Ib was formed. (A similar effect was noted for methyl chloroform.) It is most likely that during the X-ray investigation, momentary cooling of the sample resulted in the formation of phase Ib. The X-ray cooling apparatus was accurate to $\pm 3^\circ$, the nominal temperature was 238°K, and occasional fluctuations in the air pressure over a period of several hours could very easily have lowered the temperature.

An interesting phenomenon is that the melting point of phase Ia is approximately 4° lower than that of phase Ib. This fact has already been reported by several investigators.^{3,4}

Carbon Tetrabromide. Carbon tetrabromide is known to crystallize in a manner similar to that of car-

(15) R. W. Crowe and C. P. Smyth, *J. Amer. Chem. Soc.*, **72**, 4009 (1950).

Table V: *t*-Butyl Chloride

	Phase transition					
	L → I	I → II	II → III	III → II	II → I	I → L
Temp, °K						
This work	245.2	209.8	178.5	181.0	220.3	250.3
Kushner, <i>et al.</i> ^a				183.2	219.7	248.2
Dworkin and Guillamin ^b				182.9	219.2	247.5
ΔH , cal/mol						
This work	-414	-1298	-401	394	1281	410
Kushner, <i>et al.</i> ^a				410	1390	480
Dworkin and Guillamin ^b				446.3	1405.1	495.0
ΔS , eu						
This work	-1.69	-6.19	-2.25	2.18	5.81	1.64
Kushner, <i>et al.</i> ^a				2.3	6.4	1.9
Dworkin and Guillamin ^b				2.44	6.41	2.00

^a L. M. Kushner, R. W. Crowe, and C. P. Smyth, *J. Amer. Chem. Soc.*, **72**, 1091 (1950). ^b A. Dworkin and M. Guillamin, *J. Chim. Phys.*, **63**, 53 (1966).

Table VI: Neopentane

	Phase transition			
	L → I	I → II	II → I	I → L
Temp, °K				
This work ^a	255	134.4	139.0	253.8
Aston and Messerly ^b			140.02	256.5
ΔH , cal/mol				
This work	-724	-623	612	774
Aston and Messerly ^b			615.9	778.2
ΔS , eu				
This work	-2.84	-4.64	4.40	3.05
Aston and Messerly ^b			4.39	3.03

^a Based on calibration curve described in ref 6. ^b J. G. Aston and G. H. Messerly, *J. Amer. Chem. Soc.*, **58**, 2354 (1936).

bon tetrachloride. The possibility that CBr₄ also forms a phase analogous to phase Ib was investigated. The data in Table II show that this is not the case; only two crystalline phases are formed between 115 and 370°K.

Methyl Chloroform. The present investigation revealed the existence of a previously unknown crystalline phase. In the initial X-ray diffraction survey,² phase Ia was not discovered. The DSC thermogram clearly showed that it formed as the sample cooled and that its behavior is similar to that of carbon tetrachloride. Subsequent X-ray diffraction studies⁶ showed that this phase is face-centered cubic with $a = 8.39 \text{ \AA}$ with 4 molecules/unit cell. This phase was not found originally due to the extensive supercooling that methyl chloroform exhibits.

It will be seen from the data in Table III that the L → Ia transition does not form until 227°K (the temperature, though not reproducible, did fall within a 3° range). This is nearly the same temperature as the II → Ib transition observed by us on warming and reported by others.^{11,15} During the first X-ray study,

when it was discovered that the temperature was approaching that of the major solid-solid transition and the liquid had not yet solidified, the tube containing the sample was touched with the tip of a cotton swab dipped in a Dry Ice-acetone slurry. This immediately initiated crystallization, but, as is now known, of phase Ib. However, on the basis of the DSC data, the X-ray sample was allowed to cool without disturbance until the material crystallized and phase Ia was then identified.

Although the temperature of the Ia → Ib transition is sharply reproducible, the supercooled Ib → II transition occurs within a 2° range. Phase III has been identified by heat capacity,¹⁵ dielectric constant,¹⁵ and nmr measurements¹⁰ as well as by X-ray diffraction.² In the present case, no indication of the formation of this phase was found during the cooling cycle. A small peak, of approximately the correct area, was found at 205°K on warming. However, this peak was not significantly above the base line variation and was too small to be measured accurately.

The melting point of phase Ia is more than 7° below that of phase Ib. It is clear from the data in Table III that previous investigators studied phase Ib. This is consistent with the fact that they were heating the sample from below 125°K.

The enthalpy of transition between phases Ib and II determined in the present investigation does not agree with that determined on the basis of heat capacity measurements.^{11,15} In the latter case, the enthalpies of transition and fusion were estimated on the basis of the running time in excess of that required by the normal heat capacity of the material in the transition or melting range.¹⁶ This in turn requires a reasonably accurate

(16) L. M. Kushner, R. W. Crowe, and C. P. Smyth, *J. Amer. Chem. Soc.*, **72**, 1091 (1950).

determination of the heat capacity on either side of the transition. Both sets of investigators^{11,15} obtained similar heat capacity *vs.* temperature curves. However, in both cases the heat capacity between the temperature of transition and the melting point is seen to be sharply rising and not well defined. As these authors indicate, it was extremely difficult to determine C_p in this region. As a result their values for ΔH_t and ΔH_m are only approximations. In fact, ΔH_m is reported as 450 ± 300 cal/mol.¹¹ Methyl chloroform is quite different from the other compounds in this series. A comparison of available data¹⁷ shows that in all cases except methyl chloroform the heat capacities are well defined on either side of the transition and the use of the approximation formula (eq 2, ref 16) is valid. However, in the case of methyl chloroform it does not appear to be valid. Crowe and Smyth¹⁵ emphasized this point by stating that the heat capacity values between the transition point and melting point are extremely uncertain and that it is difficult to estimate the energies involved in the two processes with accuracy. Rubin, *et al.*,¹¹ made similar statements; *e.g.*, "premelting effects occur to obscure the course of the true heat capacity curve."

On the other hand, a difficulty in the interpretation of the thermogram lowers the accuracy of the data obtained by the DSC method. In order to measure accurately the area under the peak a suitable base line must be drawn. It is generally very easy to choose this parameter, since the base line on either side of the peak is clearly defined and lies along a straight line of nearly constant slope. In the case of methyl chloroform, because of the rapidly changing heat capacity, the base line above the $\text{II} \rightarrow \text{Ib}$ transition is quite different in slope from that below the transition. A large error enters because of the ambiguity in choice of base line. However, it is important to point out that, regardless of the choice of base line, it was not possible to obtain as large a value for ΔH_t as was previously reported.^{11,15} The present value was determined on the basis of a straight line drawn from the beginning to the end of the peak. By judicious choosing of a base line we were able to obtain nearly equivalent enthalpies of transition for $\text{Ib} \rightarrow \text{II}$ and $\text{II} \rightarrow \text{Ib}$, which fell between the two values reported in Table III. However, there was no justification for this choice and so these data are not reported. In addition, there is the strong possibility that not all of the liquid froze during the cooling process until the $\text{Ib} \rightarrow \text{II}$ transition occurred. This would account for a larger enthalpy of transition for $\text{Ib} \rightarrow \text{II}$ than for $\text{II} \rightarrow \text{Ib}$. Similar effects have been reported elsewhere for cases of severe supercooling.¹⁸

It is of interest to note that during one cooling run a small shoulder was noted on the low-temperature side of the $\text{L} \rightarrow \text{Ia}$ peak. In this run the three enthalpies of transition were 245, 164, and 1369 cal/mol, respectively. It would seem that, in this case, supercooling effects were negligible. However, it was not repeated during any other scan.

The conclusion drawn by the present authors is that neither the DSC nor the heat capacity value is accurate. The former method underestimates the enthalpy, while the latter overestimates it.

2,2-Dichloropropane (Table IV). Von de Vloed¹⁹ determined the enthalpy values on the basis of freezing curves of binary mixtures. This method gives only approximate values and is not reliable. (For example, a value of ΔS_m of 4.5 eu was determined for methyl chloroform.) No other reports of heat capacity or enthalpy data were found for 2,2-dichloropropane.

The thermogram showing the $\text{L}(?) \rightarrow \text{Ib}$ transition was identical in appearance with the formation of phases Ib of carbon tetrachloride and methyl chloroform. However, a slight increase in the base line just prior to the onset of this transition was noted. A sample was set up on an X-ray diffraction camera and allowed to cool until crystallization was initiated, at which time it was quickly warmed. X-Ray diffraction photographs showed the presence of a face-centered cubic unit cell with $a = 8.45 \text{ \AA}$ and 4 molecules/unit cell.⁵ Evidently the formation of phase Ia occurs nearly simultaneously with that of Ib and involves a very small enthalpy change.

t-Butyl Chloride and Neopentane. Each of these compounds exhibits only one phase (fcc) prior to the major crystallographic transition. The observed transitions are in agreement with those reported by previous investigators, as shown in Tables V and VI.

Acknowledgments. Acknowledgment is made to the donors of the Petroleum Research Fund, administered by the American Chemical Society, and to the Research Corp. for partial support of this research. The authors thank R. Fyans for helpful discussions concerning the operation of the DSC-1B.

(17) Figure 1, J. Hicks, J. Hooley, and C. Stephens, *J. Amer. Chem. Soc.*, **66**, 1064 (1944) ($n = 0$); Figure 1, ref 11, and Figure 1, ref 15 ($n = 1$); Figure 3, ref 16 ($n = 3$); Figure 1, J. G. Aston and G. H. Messerly, *ibid.*, (58, 2354 (1936) ($n = 4$); 2,2-dichloropropane $n = 2$) was determined by another method.

(18) E. M. Barrall, II, R. S. Porter, and J. F. Johnson, *J. Phys. Chem.*, **71**, 1224 (1967).

(19) A. van de Vloed, *Bull. Soc. Chim. Belg.*, **48**, 229 (1939).

NOTES

Catalytic Polarographic Current of a Metal Complex. IX.^{1,2} The Effect of Lithium Hexafluorophosphate Supporting Electrolyte on the Nickel(II)-*o*-Phenylenediamine System

by Hubert C. MacDonald, Jr., and Harry B. Mark, Jr.

Department of Chemistry, the University of Michigan, Ann Arbor, Michigan 48104 (Received August 18, 1969)

Recent studies of the polarographic prewave which is observed to arise at potentials anodic to the main hexaaquonickel(II) wave in the presence of *o*-phenylenediamine(OPDA) have shown that this prewave is the result of the reduction of a 1:1 nickel(II)-OPDA complex.^{1b,d,e} Further study of the effect of the concentration and nature of supporting electrolyte upon the prewave, Ψ effects, showed that the complex is formed at the electrode surface and not in the "bulk" of the solution.^{1b,d,e,f,g,3,4} The analysis of the data for all systems investigated, however, showed that the quantitative correlation of theory^{1a,g,4} and experimental data indicated that the charge of the cation involved in the chemical reaction preceding electron transfer was +1.^{1d,f} This result was surprising as the theory of the effect of the potential within the Helmholtz double layer on the rate of chemical reaction at the electrode surface should be related to the bulk charge of the ion(s) involved in the chemical reaction.^{1f,g,4,5} A value of $z = +2$ was expected for the reaction of the hexaaquonickel(II) ion and neutral OPDA at a pH of 7.⁶ On extensive study of the adsorption of OPDA by differential capacitance measurements as a function of the nature and concentration of the supporting electrolyte indicated that anion coadsorption was a possible explanation.^{1g,7} It was felt that a study of the nickel(II)-OPDA prewave in the presence of an anion of the supporting electrolyte which was known to exhibit a minimum tendency toward specific adsorption might provide more direct evidence for an anion coadsorption mechanism. Although alkali metal fluoride salts have been shown to exhibit a negligible tendency toward specific adsorption at a mercury electrode,⁸ they cannot be employed in this study as the fluoride ion exhibits a strong complexing effect toward the nickel(II) ion.⁹ However, the hexafluorophosphate salts, LiPF₆ and KPF₆, exhibit a similar lack of specific adsorption of the anion on mercury^{10,11} and do not form complexes with nickel(II). Thus a study of the nickel(II)-OPDA prewave current as a function of the lithium hexafluorophosphate concentration

would substantiate indirectly anion coadsorption mechanism for the other electrolytes.^{1f,g}

Experimental Section

All experimental methods and procedures employed in this investigation have been described previously.^{1b,d,e}

Discussion

A relationship between the modified Koutecky rate parameter,^{1d,3} λ , and the potential of the outer Helmholtz plane,¹² OHP potential, Ψ^0 , has previously derived

$$\lambda = \frac{k_f(K_h[L]^0)^x\sqrt{t}}{\sqrt{D}} \exp\left(-\frac{zF}{RT}\Psi^0\right) \quad (1)$$

where k_f is the forward rate constant of the complexation reaction at the electrode surface, K_h is a Henry's law constant, $[L]^0$ is the bulk ligand concentration, x is the stoichiometric coefficient for the reaction, z is the average bulk charge of the ion(s) taking part in the chemical reaction at the surface, and the other symbols have their usual significance. The dependence of the prewave current on the nickel(II) concentration showed that the

(1) For other papers of this series see: (a) H. B. Mark, Jr., and C. N. Reilley, *J. Electroanal. Chem.*, **4**, 189 (1962); (b) H. B. Mark, Jr., *J. Electroanal. Chem.*, **7**, 276 (1964); (c) H. B. Mark, Jr., L. R. McCoy, E. Kirowa-Eisner, and H. C. MacDonald, Jr., *J. Phys. Chem.*, **72**, 1083 (1968); (d) L. R. McCoy, H. B. Mark, Jr., and L. Gierst, *J. Phys. Chem.*, **72**, 4637 (1968); (e) H. B. Mark, Jr., and L. R. McCoy, *Rev. Polarogr.*, **14**, 122 (1968); (f) L. R. McCoy and H. B. Mark, Jr., *J. Phys. Chem.*, **73**, 953 (1969); (g) L. R. McCoy and H. B. Mark, Jr., *ibid.*, **73**, 2764 (1969).

(2) This research was supported in part by the National Science Foundation, Grant No. NSF GP-9307.

(3) J. Koutecky, *Collect. Czech. Chem. Commun.*, **18**, 597 (1953).

(4) L. Gierst, *Trans. Symp. Electrode Processes*, 109 (1959).

(5) J. Dandoy and L. Gierst, *J. Electroanal. Chem.*, **2**, 116 (1961).

(6) The possible formation in the bulk solution of 1:1 complexes of nickel(II) with the anion of the supporting electrolyte or OH⁻ was considered to explain the $z = +1$. However, this value of z was found to be independent of the nature of the supporting electrolyte anion and of pH changes between 6.0 and 7.5.^{1d,e,f,g} Also spectrophotometric studies did not show any significant differences on changing the anion of the supporting electrolyte.^{1b,g}

(7) The coadsorption was thought to arise from a π -electron interaction of the aromatic ring of the ligand with the electrode surface. This interaction results in an electron deficiency on the solution side of the adsorbed ligand. Thus an anion would tend to adsorb on the ring of the adsorbed OPDA.

(8) D. C. Grahame, *Chem. Rev.*, **41**, 441 (1947).

(9) L. G. Sillén and A. E. Martell, "Stability Constants of Metal Ion Complexes," The Chemical Society, Burlington House, London, 1964, p 262.

(10) F. C. Anson, private communication of unpublished results, 1969.

(11) R. Payne, *J. Amer. Chem. Soc.*, **89**, 489 (1967); K. S. Whiteley, Ph.D. Thesis, University of Birmingham, England, 1957; D. J. Barclay, *J. Electroanal. Chem.*, **19**, 318 (1968).

(12) The OHP is assumed here to be approximately equal to the reaction plane of the chemical complexation reaction. Thus, the OHP potential, Ψ^0 , is essentially equal to the reaction plane potential.^{1d}

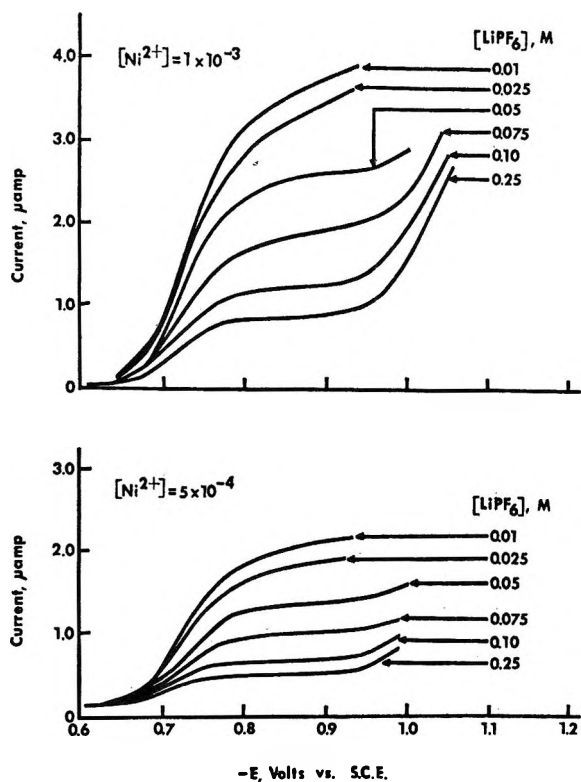


Figure 1. Dependence of prewave on the concentration of lithium hexafluorophosphate. [OPDA] = 2×10^{-4} M, pH 7.0.

reaction was first order with respect to this ion. The variation of the rate parameter as a function of the OPDA concentration showed that the reaction was first order with respect to this species also. The same results were obtained in the studies with other electrolytes; it was therefore thought that the overall reaction mechanism was the same for LiPF_6 as previously demonstrated for other electrolytes.^{1d,f,g}

In order to determine the value of z , it is simply necessary to maintain a constant bulk concentration of OPDA and nickel(II) and vary the potential of the OHP, Ψ^0 , by varying the concentration of LiPF_6 .^{1d,4} Under these conditions eq 1 reduces to

$$\log \lambda = \text{constant} - \frac{zF}{RT} \Psi^0 \quad (2)$$

As the value of Ψ^0 becomes more negative (a decrease in LiPF_6 concentration cathodic to the electrocapillary maximum),^{1d,r,8} eq 2 predicts that the rate parameter and, hence, the limiting current of the prewave will increase as is observed in Figure 1. The rate parameter, λ , can be determined experimentally from the polarographic data of Figure 1 according to the following relationship

$$i/i_d = F(\lambda) \quad (3)$$

where i is the limiting current of the prewave and i_d is the diffusion-limited current of nickel(II). Typical plots of $\log \lambda$ vs. Ψ^0 ¹³ are shown in Figure 2. The slope

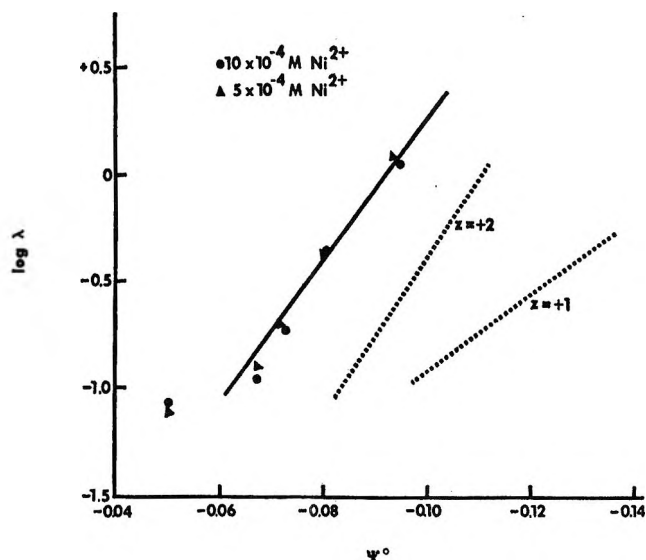


Figure 2. Dependence of the rate parameter on the OHP potential. Current measured at -0.8 V(sce).

of the line is in agreement with a value of $z = +2$ as one would expect for the reaction of the hexaaquanickel(II) ion with the neutral OPDA. This result also lends some support to the conclusion that the coadsorbed anion does act as a partner in the surface reaction as suggested previously for the other anions.⁹ This would account for the "anomalous" value for z of $+1$ found in the studies with other anions as the electrolyte.

(13) Actual Ψ^0 values for PF_6^- have not been determined. Anson, however, has found that the adsorption characteristics of PF_6^- are essentially identical with F^- . Thus Ψ^0 values for F^- as given by Russell's tables¹⁴ were used here.

(14) C. D. Russell, *J. Electroanal. Chem.*, **6**, 486 (1963).

The Empirical Shielding Parameter Q and Trisubstituted Benzenes

by G. Socrates

Department of Polymer Science, Brunel University, London, England (Received October 14, 1969)

Anomalous *ortho* proton and fluorine chemical shifts have been observed for chloro-, bromo-, and iodo-substituted benzenes.¹⁻⁴ These anomalies cannot be explained by the magnetic anisotropy of the halogens.⁵

(1) H. Spiesecke and W. G. Schneider, *J. Chem. Phys.*, **35**, 731 (1961).

(2) H. S. Gutowsky, D. W. McCall, B. R. McGarvey, and L. H. Mayer, *J. Amer. Chem. Soc.*, **74**, 4809 (1952).

(3) A. J. R. Bourns, D. G. Giles, and E. W. Randall, *Proc. Chem. Soc.*, 200 (1963).

(4) N. Boden, J. W. Emsley, J. Feeney, and L. H. Sutcliffe, *Mol. Phys.*, **8**, 133 (1964).

(5) J. S. Martin and B. P. Dailey, *J. Chem. Phys.*, **39**, 2722 (1963).

Table I: Observed Chemical Shifts, τ

	X	Q	H(3)	H(5)	H(6)	Me(2)	Me(4)	X
1	H	2.28	3.13	3.15	2.95	7.73	7.73	3.15
2	CH ₃	1.17	3.18	3.27	3.17	7.83	7.73	7.73
3	CH ₃ O	0.6	3.18	3.21	3.46	7.90	7.83	6.32
4	OH	0.38 ^a	3.20	3.28	3.53	7.86	7.82	4.61
5	CN	3.5	2.94	2.99	2.61	7.58	7.67	
6	Cl	2.55	3.07	3.18	2.88	7.75	7.79	
7	Br	3.16	3.05	3.23	2.68	7.72	7.81	
8	I	3.98	3.05	3.40	2.45	7.69	7.81	
9	NO ₂	4.0-6.3 ^b	2.94	2.94	2.19	7.53	7.68	
10	NH ₂	0.11	3.20	3.25	3.65	8.00	7.89	6.89

^a The value employed here was obtained from monosubstituted benzenes. ^b The Q value for the nitro group varies over the range given.

The presence of time-dependent electric fields arising from the substituent may account for the *ortho* effect observed in halogen compounds but this concept fails badly when the substituent is a proton.^{4,6,7} An increase in the paramagnetic term of the Ramsey Shielding equation⁸ should account for the *ortho* effect.⁹ A very good linear correlation is found between *ortho* shifts and the quantity $Q = P/Ir^3$ where P is the polarizability of the C-X bond, r is the length of the bond, and I is the first ionization potential of the substituent atom X.¹⁰⁻¹⁶

Experimental Section

The spectra were observed on a Varian 100-Hz high-resolution nuclear magnetic spectrometer. All samples were thoroughly degassed before recording the spectra.

Most of the compounds studied were available commercially. All the samples were purified by distillation under reduced pressure. 4-Chloro-1,3-dimethylbenzene was prepared from xylydine by forming the diazonium salt and then adding cuprous chloride and hydrochloric acid, boiling point 187°.

4-Bromo-1,3-dimethylbenzene was prepared by the direct bromination of *m*-xylene, boiling point 203°. 4-Iodo-1,3-dimethylbenzene was prepared from xylydine by forming the diazonium salt and then adding excess potassium iodide, boiling point 109° at 10 mm pressure.

Results and Discussion

The proton magnetic resonance spectra of the series of compounds, 1-X,2,4-dimethylbenzene, studied were observed in dilute carbon tetrachloride solution (5% v/v), tetramethylsilane being employed as an internal reference.

The ring proton resonances were analyzed using a computer assuming an ABC system. A simple non-iterative program was employed which from the input parameters set up and diagonalized the Hamiltonian matrix by successive approximations, hence calculating transition energies and line intensities. Preliminary spectral parameters were determined by employing the empirical substituent additivity rules^{5,17} and where

possible, homonuclear spin decoupling was also used. By the comparison of the observed and analyzed spectra, the chemical shifts of the aromatic protons could be estimated to be better than 0.01 ppm.

The chemical shifts for the 1-X,2,4-dimethylbenzenes are given in Table I. The shielding parameters Q for the various substituents, X, are also given in this table.

In Figure 1 the chemical shift of the aromatic proton H(6) adjacent to the substituent is plotted against the parameter Q .

An extremely good linear correlation is observed. The equation of the best straight line obtained by the method of least squares is

$$\tau_{H(6)} = -0.30Q + 3.66$$

The maximum deviation observed from this line is 0.02 ppm. In Figure 2 the chemical shift of the methyl group adjacent to the substituent is plotted against the parameter Q . A definite linear correlation exists although not as good as that obtained above. A similar correlation for the *para* methyl group chemical shift is not found to exist.

Therefore it would appear that the same mechanism determines the shielding of both the aromatic proton and the methyl group adjacent to the substituent. In

- (6) T. Schaefer, W. F. Reynolds, and T. Yonemoto, *Can. J. Chem.*, **41**, 2969 (1963).
- (7) V. M. S. Gill and W. A. Gibbons, *Mol. Phys.*, **8**, 199 (1964).
- (8) E. Pitcher, A. D. Buckingham, and F. G. A. Stone, *J. Chem. Phys.*, **36**, 124 (1962).
- (9) N. F. Ramsey, *Phys. Rev.*, **78**, 609 (1951).
- (10) F. Hruska, H. W. Hutton, and T. Schaefer, *Can. J. Chem.*, **43**, 2395 (1965).
- (11) T. Schaefer, F. Hruska, and H. M. Hutton, *ibid.*, **45**, 3143 (1967).
- (12) W. B. Smith and G. M. Cole, *J. Phys. Chem.*, **69**, 4413 (1965).
- (13) W. B. Smith and J. L. Roark, *J. Amer. Chem. Soc.*, **89**, 5018 (1967).
- (14) J. L. Roark and W. B. Smith, *J. Phys. Chem.*, **73**, 1043 (1969).
- (15) J. L. Roark and W. B. Smith, *ibid.*, **73**, 1046 (1969).
- (16) W. B. Smith and J. L. Roark, *ibid.*, **73**, 1049 (1969).
- (17) P. Diehl, *Helv. Chim. Acta*, **44**, 829 (1961).

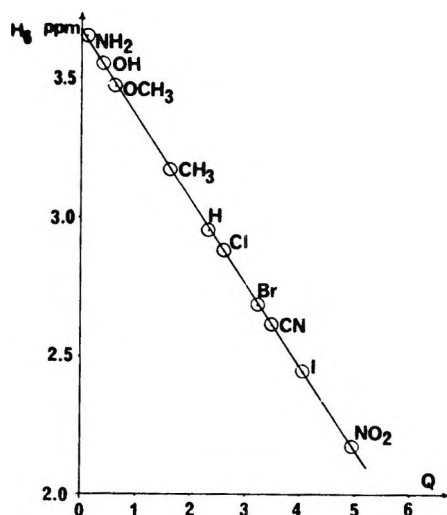


Figure 1. The chemical shift of H(6) on the τ scale is plotted against the parameter Q .

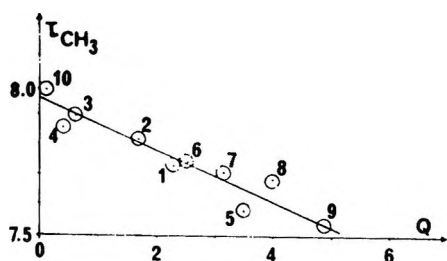


Figure 2. The chemical shift on the τ scale of the methyl group adjacent to the substituent X is plotted against the parameter Q .

conclusion, a very good correlation of the Q parameter with the chemical shift of the aromatic proton adjacent to the substituent does exist for 1-X,2,4-dimethylbenzenes.

Acknowledgment. The author wishes to thank the Department of Chemistry, University College, London, for the use of their Varian 100 Hz high-resolution nuclear magnetic resonance spectrometer.

Free-Radical Intermediates in the Reaction of the Hydroxyl Radical with Nitrogen Heterocyclic Compounds¹

by Hitoshi Taniguchi

Department of Chemistry, Faculty of Science, Kyoto University, Kyoto 606, Japan (Received February 9, 1970)

Many electron spin resonance (esr) studies have been carried out on the nitrogen heterocyclic radical ions in solution to clarify the origin of nitrogen nuclear hyperfine (hf) coupling.²⁻⁷ These radical ions have some-

what delocalized π -electron systems in which it is considered that the spin densities on the carbon atoms bonded to the nitrogen atom contribute much less to the observed isotropic component of the nitrogen hf coupling constant (a_N) than does the spin density on the nitrogen atom itself.

On the other hand, in a preceding paper⁸ concerning the free-radical intermediates from amino acid derivatives and related compounds with the hydroxyl radical, it was reported that the splitting due to the nitrogen hf coupling was hardly observed in most of the radicals studied. In these radicals the unpaired electron is more or less localized in the $2p_\pi$ orbital of the carbon atom directly bonded to the nitrogen.

In order to obtain further esr data with respect to the relation between a_N and the spin density distributions, radicals produced by the reaction of the hydroxyl radical with several nitrogen heterocyclic compounds and pyrimidine derivatives have been studied in this work using a continuous-flow method. The hydroxyl radical was generated chemically in a titanous (Ti^{3+}) chloride-hydrogen peroxide (H_2O_2) system. Nicolau, *et al.*,⁹ reported the intermediate radicals from pyrimidine derivatives formed in a Ti^{3+} - H_2O_2 system, which did not come to the author's attention until the present experiments were finished.

Experimental Section

The experimental arrangement and procedures for the observation of intermediate radicals in a Ti^{3+} - H_2O_2 system were essentially the same as described elsewhere.^{8,10} Esr spectra of the intermediate radicals were recorded between 5 and 13 msec after the reaction had started.¹¹ The modulation width used for the recording was varied from 0.5 to 1.6 G. The hf coupling constants were measured using manganous ion as a reference (splitting between the two central peaks, 86.9 G).

Uracil and 1,3-dimethyluracil were synthesized from malic acid, urea, and methyl sulfate according to the

(1) This work was presented in part at the 22nd Annual Meeting of the Chemical Society of Japan, Tokyo, April 1969.

(2) J. C. M. Henning, *J. Chem. Phys.*, **44**, 2139 (1966), and references cited therein.

(3) P. T. Cottrell and P. H. Rieger, *Mol. Phys.*, **12**, 149 (1967).

(4) C. L. Talcott and R. J. Myers, *ibid.*, **12**, 549 (1967).

(5) A. R. Buick, T. J. Kemp, G. T. Neal, and T. J. Stone, *J. Chem. Soc. A*, 1609 (1969).

(6) L. Lunazzi, A. Mangini, G. F. Pedulli, and F. Taddei, *ibid.*, **B**, 163 (1970).

(7) M. D. Sevilla, *J. Phys. Chem.*, **74**, 805 (1970).

(8) H. Taniguchi, H. Hatano, H. Hasegawa, and T. Maruyama, *ibid.*, **74**, 3063 (1970).

(9) C. Nicolau, M. McMillan, and R. O. C. Norman, *Biochim. Biophys. Acta*, **174**, 413 (1969).

(10) H. Taniguchi, K. Fukui, S. Ohnishi, H. Hatano, H. Hasegawa, and T. Maruyama, *J. Phys. Chem.*, **72**, 1926 (1968).

(11) The author is grateful to Japan Electron Optics Laboratory Co. for affording an opportunity to use an esr spectrometer.

Table I: Structures and Hyperfine Coupling Constants of the Intermediate Radicals^a

Substrate	Radical	Coupling constant, ^b G			
		C ₁ -H	C ₂ -H	N	Other
Pyrrolidine		21.8	35.1		
Ethyleneurea		13.4	38.7		
ε-Caprolactam		22.3	23.4		
1,3-Dimethyluracil		18.3			
Uracil		19.0 (18.1)	21.5 (21.2)	(0.8)	(0.8) ^c
Thymine			(15.1) (22.4) ^d		
		(18.7)			
Isosorotic acid		(17.8)			
Cytosine		(18.3)	(18.3)		

^a See ref 13 for the notations in column 3. ^b The values in parentheses were obtained by Nicolau, *et al.*⁹ ^c Coupling constant due to two protons. ^d Coupling constant due to methyl protons.

usual method.¹² *Anal.* Calcd for C₄H₄O₂N₂: C, 42.86; H, 3.60; N, 24.99. Found: C, 42.62; H, 3.47; N, 25.16. Calcd for C₆H₆O₂N₂: C, 51.42; H, 5.75; N, 19.99. Found: C, 51.63; H, 5.84; N, 19.84. Other materials were obtained from commercial sources and used without further purification.

The calculation of π -electron spin density was performed with a KDC-II (HITAC 5020) computer of Kyoto University.

Results and Discussion

An esr spectrum of the intermediate radical from pyrrolidine is reproduced in Figure 1. Esr spectra from four other substrates were also recorded with



Figure 1. Electron spin resonance spectrum of the intermediate radical from pyrrolidine.

sufficient signal-to-noise ratios to allow for their analyses. The structures and hf coupling constants assigned to the intermediate radicals of pyrrolidine,

(12) D. Davidson and O. Baudisch, *J. Amer. Chem. Soc.*, **48**, 2379 (1926).

ethyleneurea (2-imidazolidinone), ϵ -caprolactam, 1,3-dimethyluracil, and uracil are summarized in Table I; hf coupling data obtained by Nicolau, *et al.*,⁹ are also shown in parentheses.

(1) *Identification of the Intermediate Radicals.* Results in Table I indicate the general tendency that in the reaction between $Ti^{3+}-H_2O_2$ and the nitrogen heterocyclics studied, the hydroxyl radical abstracts the hydrogen atom preferentially from the C-H bond adjacent to the imino group or to the nitrogen atom of the heterocyclic ring, except in the case of uracil in which the hydroxyl radical is added to the double bond of the pyrimidine ring.

As for ϵ -caprolactam, a similar hf structure would be observed when the hydroxyl radical attacked the C-H bond adjacent to the carbonyl group. However, the spin density calculation shows that with the radical produced in this way the spin density on C_1 ¹³ becomes too small to explain the observed C_1 -H proton hf coupling. The assigned structure seems reasonable also in view of the above-mentioned general tendency of reaction of the hydroxyl radical with the other substrates studied.

The radical from uracil can be assigned to either structure I or II in Table I, produced as a result of the addition of the hydroxyl radical to the double bond, structure II appearing more probable according to the assignment of Nicolau, *et al.*,⁹ who observed small nitrogen hf splitting of 0.8 G. The 1:2:1 triplet spectrum from 1,3-dimethyluracil indicates, however, an equal coupling of the unpaired electron with two protons, leading to the assignment to structure I or II in Table I, produced as a result of the hydrogen abstraction from a methyl group. This difference in reactivity between uracil and 1,3-dimethyluracil may be analogous to the case of benzene and toluene in which, with the former, the addition of the hydroxyl radical occurs, whereas, with the latter, the abstraction of hydrogen from the methyl group takes place.¹⁴ At present structures I and II seem equally probable for 1,3-dimethyluracil, although the possibility cannot be completely neglected that a radical similar to that from uracil is formed but with an accidental coincidence of C_1 -H and C_2 -H¹³ proton couplings giving 1:2:1 triplet, as happens to be the case with the cytosine radical.

Morpholine, N-methyl-2-pyrrolidone, N-vinyl-2-pyrrolidone, piperazine hexahydrate, pyridine, α -picoline, β -picoline N,N-dimethylcyclohexylamine, and sodium diethylbarbiturate did not give any resolved esr spectra of their intermediate radicals.

The nitroxide radicals from pyrrolidine and morpholine were not detected in this study either, although Hudson and Hussain¹⁵ reported their formation by an alkaline hydrogen peroxide oxidation. The difference between the two results may come from the difference in pH which was 1.4-2.2 in our $Ti^{3+}-H_2O_2$ system. Such an example of the pH dependence was also ob-

served in the reaction of diethylamine with a $Ti^{3+}-H_2O_2$ system.^{10,16}

(2) *Calculations of π -Electron Spin Densities.* The π -electron spin densities were calculated with the LCAO-MO-SCF method developed by Yomosa,¹⁷ who applied the method successfully to the calculation of the π -electronic structure of the peptide group.¹⁸ This is essentially the Hückel MO method except that the value of Coulomb integral α_r for the atom r is successively refined through the formula

$$\alpha_r' = \alpha_r + \frac{2}{3}(X_{r+1} - X_r)Q_r\beta \quad (1)$$

where X_r is the electronegativity of the r atom with the net charge Q_r and X_{r+1} is that of the atom next to r in the periodic table. The starting values of Coulomb and resonance integrals used in the SCF calculation are listed in Table II. The starting value of Q_r was esti-

Table II: Parameters Used in Molecular Orbital Calculations

Group	Atom (X)	h_X^a	Bond (C-Y)	k_{CY}^b
C=C=O	C	0.2	C-C	0.9
	O	1.2	C=C	1.1
N=C=O	C	0.27	C-N	1.0
	O	1.2	C=O	2.0
C- $\begin{cases} CH_3 \\ CH_2 \end{cases}$	C	-0.1	C- $\begin{cases} CH_3 \\ CH_2 \end{cases}$	0.7
	$\begin{cases} CH_3 \\ CH_2 \end{cases}$	2.0		
$-\dot{N} <$	N	1.6		
$-N^+ \leftarrow$	N	2.0		

^a $h_X = (\alpha_X - \alpha_C)/\beta$ for Coulomb integral. The Coulomb integral, α_C , is taken to be that for carbon, and the resonance integral, β , is that for the carbon-carbon bond in benzene.

^b $k_{CY} = \beta_{CY}/\beta$ for resonance integral.

mated from the result of the Hückel MO calculation. The values of electronegativity were after those of Daudel, *et al.*¹⁹

The calculated values of π -electron spin densities on C_1 and N are shown in columns of ρ_{C_1} and ρ_N of Table III. The sum of spin densities on the carbon atoms bonded to the nitrogen atom in question, $\sum_i \rho_{C_i}$, is also shown.

(13) The designations C_1 and C_2 refer to the position relative to the carbon atom which bears the unpaired electron.

(14) W. T. Dixon and R. O. C. Norman, *J. Chem. Soc.*, 4857 (1964).

(15) A. Hudson and H. A. Hussain, *ibid.*, B, 251 (1968).

(16) R. E. Florin, F. Sicilio, and L. A. Wall, *J. Res. Nat. Bur. Stand., Sect. A*, 72, 49 (1968).

(17) S. Yomosa, *Biopolym. Symp.*, No. 1, 1 (1964).

(18) The author is indebted to Mr. M. Sakoda for the computer programs of the LCAO-MO-SCF calculations.

(19) R. Daudel, R. Lefebvre, and C. Moser, "Quantum Chemistry," Interscience, New York, N. Y., 1959, p 74.

Table III: Calculated Spin Densities and Theoretical Nitrogen Hyperfine Coupling Constants^a

Radical ^b	ρ_{C_1}	Q_{CH^H} , G	ρ_N	C_1N $\Sigma_i \rho_{C_i}$	a_N , G
Pyrrrolidine	0.7957	27.4	0.1304	0.8117	1.14
Ethyleneurea	0.7638	17.5	0.0951	0.7794	0.36
ϵ -Caprolactam	0.8016	27.8	0.1030	0.8386	0.41
1,3-Dimethyl- uracil					
I	0.7928	23.1	0.0605	0.8193	0.58
II	0.8383	21.8	0.0673	0.8638	0.52
Uracil					
I	0.8250	23.0	0.0097	0.0267	0.17
II	0.8055	23.6	0.1215	0.88	0.88
Thymine					
I	0.8150	27.5 ^c	0.0099	0.16	0.16
II	0.8055	23.2	0.1215	0.88	0.88
Isoorotic acid	0.8055	22.1	0.1215	0.88	0.88
Cytosine	0.7976	22.9	0.1133	0.8303	0.68

^a See text and ref 13 for the notations. ^b Radical structures are shown in Table I. ^c Q value of C_1-CH_3 group.

The spin density calculations by McLachlan's method²⁰ did not improve the result, probably because of the fairly localized π -electron systems treated.

(3) *Proton Coupling Constants.* The proportionality constants Q_{CH^H} in the McConnell relation²¹

$$a_{C_1-H} = Q_{CH^H} \rho_{C_1} \quad (2)$$

were estimated from the observed C_1-H coupling constants a_{C_1-H} and the calculated spin densities ρ_{C_1} , the result being shown in column 3 of Table III. The Q_{CH^H} values are in a reasonable range (22–28 G) except in the case of the ethyleneurea radical (17.5 G).

The small C_1-H coupling observed for the ethyleneurea radical may be ascribed to a somewhat nonplanar configuration of bonding orbitals around the C_1 carbon atom as suggested by Fessenden²² and recently confirmed by Dobbs, *et al.*,²³ for oxygen-containing radicals, *i.e.*, to the bending of the ring and the consequent s character of the orbital containing the unpaired electron.

(4) *Nitrogen Coupling Constants.* It is interesting to note that although the nitrogen atom is bonded to C_1 , the splitting due to the nitrogen atom was observed in neither of the radicals studied in this work nor in the preceding one.⁸ Since the observed line width was 2–3 G under the experimental conditions employed, the unresolved a_N is estimated to be about 1 G or less.

Kashiwagi and Kurita²⁴ observed the nitrogen hf splitting of 1.8 G in the free radical produced in an X-

irradiated single crystal of ϵ -caprolactam which is the same radical species as that in the present flow system. Since the conformation of a radical produced in a crystal by irradiation is generally restricted by the particular crystal field involved, their observation of 1.8-G splitting may presumably be ascribed to a somewhat restricted conformation of the ϵ -caprolactam radical in the host crystal.

The value of a_N depends not only on the spin density ρ_N at the nitrogen atom but also on the spin densities ρ_{C_i} at the carbon atoms bonded to the nitrogen atom² and can be estimated according to

$$a_N = |Q_N^N \rho_N + Q_{CN}^N \sum_i \rho_{C_i}| \quad (3)$$

When the numerical values of Q_N^N and Q_{CN}^N are taken to be 24.3 and -2.5 G, respectively, the calculated values of a_N become less than 1.1 G, which are too small to be detected under the experimental conditions employed, as shown in Table III.

The parameters, Q_N^N and Q_{CN}^N , obtained in this work, are comparable to those proposed for the radical anions of pyridine, pyrazine, and pyrimidine (27.3 and -1.7 G, respectively) based on the experimentally obtained spin densities.⁴ The small differences between the two sets of parameters might be ascribed to the excess charge effect on the hf interaction^{2,3,25} and the ambiguity in the spin density calculation.

The present result shows that in the nitrogen heterocyclic radical with the unpaired electron fairly localized on the carbon atom adjacent to the nitrogen, the nitrogen hf coupling constant a_N becomes vanishingly small, because the contribution to a_N from the π -electron spin density on the nitrogen atom is canceled by the negative contribution from the spin densities on the adjacent carbon atoms through the σ - π interaction.

Acknowledgment. The author wishes to thank Professor H. Hatano for his continuous interest and encouragement. He also expresses his gratitude to Dr. K. Akasaka for his helpful discussions and critical reading of the manuscript.

(20) A. D. McLachlan, *Mol. Phys.*, **3**, 233 (1960).

(21) H. M. McConnell, *J. Chem. Phys.*, **24**, 632, 764 (1956).

(22) R. W. Fessenden, *J. Phys. Chem.*, **71**, 74 (1967).

(23) A. J. Dobbs, B. C. Gilbert, and R. O. C. Norman, *Chem. Commun.*, 1353 (1969).

(24) M. Kashiwagi and Y. Kurita, *J. Chem. Phys.*, **40**, 1780 (1964).

(25) J. R. Bolton, *ibid.*, **43**, 309 (1965).

COMMUNICATIONS TO THE EDITOR

Prediction on the Mass Spectra of Normal Alkanes with the Molecular Orbital Theory¹

Sir: An important relationship on the scission probability of the skeletal bond of alkanes has been found between their mass spectra and charge density at the highest occupied molecular orbital (HO-MO).^{2,3} The agreement between theory and experiment is especially good if the mass spectra are measured with an ion source of low temperature and low ionizing voltage, *i.e.*, under such experimental conditions that the successive fragmentations are eliminated. Good examples are the cases of normal hexadecane and tridecane.^{3c}

However, there remains an unresolved problem for predicting the mass spectra because the theory cannot determine which one of the two complementary fragments would be given a positive charge at the scission of the parent ion. This situation is reflected by plotting the relative yield of the fragment ions of hexadecane $C_{16}H_{34}$ against the number of carbons C_i contained in them. As the open and small circles in Figure 1 show, the highest C_i in the measured curve does not coincide with the scission of the eighth bond, but rather it shifts to a C_i number higher than it. Since the scission probability $\phi_n(\nu)$ of the ν th bond of the normal alkane C_nH_{2n+2} is proportional to its charge density at the HO-MO of the parent ion, it can be given approximately by eq 1, from which the above asymmetric skewness of the curve cannot be derived, because $\sin(\nu\pi/n) = \sin[(n-\nu)\pi/n]$.

$$\phi_n(\nu) = \frac{2}{n} \sin^2 \left(\frac{\nu\pi}{n} \right) \quad (\nu = 1, 2, 3, \dots, n-1) \quad (1)$$

Now, if the fragmentation occurs at the parent ion by electron bombardment, Stevenson's rule⁴ on the ionization potential of radicals can be applied; *viz.*, the fragment with the higher C_i number would be charged more abundantly if the ionizing voltage is just above the ionization potential plus the bond dissociation energy required for the fragmentation. Then, Figure 1 seems to indicate that a quantitative relation may exist in determining the probability for each complementary fragment to be charged when the ionizing voltage is much higher than the above threshold energy, because both fragments can be charged in such an experimental condition.

To investigate this problem, the working hypothesis is proposed that the relative probability for a fragment to be given the positive charge is proportional to the

sum of the charge densities allotted to each group in the fragment. If this hypothesis is true, it follows that the fragment ion containing more carbon atoms becomes more abundant than the complementary one produced by the same scission.

This hypothesis can be investigated quantitatively by calculating the charge density of the HO-MO at each group. As the method of calculation, the LCGO approximation⁵ was adopted, regarding CH_3 and CH_2 groups as the same united atoms. Then, the charge density is given by the same formula as eq 1, only if ν be defined by the group number instead of the skeletal bond number of an alkane containing n carbon atoms. Therefore, the relative probability for a fragment ion containing m carbon atoms to be produced in the mass spectrum, $P_n(m)$, can be expressed by the following general equation

$$P_n(m) = 2\phi_n(m) \sum_{l=1}^m \frac{2}{n+1} \sin^2 \left(\frac{l\pi}{n+1} \right) = \frac{2}{n(n+1)} \sin^2 \frac{m\pi}{n} \times \left[2m+1 - \frac{\sin \left(\frac{2m+1}{n+1} \right) \pi}{\sin \left(\frac{\pi}{n+1} \right)} \right] \quad (2)$$

If eq 2 is utilized, new theoretical values shown by crosses in Figure 1 can be obtained, reproducing the observed values well. A similar tendency is identified in the case of n -tridecane, but not so clearly, probably because the ionizing voltage is still high.^{3c} A more favorable result was reported on normal triacontane $C_{30}H_{62}$,⁶ whose mass spectrum was measured at 17 V. The comparison of $P_n(m)$ between experiment and theory is shown in Figure 2. Even though errors in the experimental values are large because of very low heights of each peak, the shift of maximal yield of the curve from the central C_i number to the higher can be indicated qualitatively. Considering the degree of

(1) Report XXIII on molecular orbital theory for mass spectra.

(2) (a) K. Fueki and K. Hirota, *Nippon Kagaku Zasshi*, **81**, 212 (1960); (b) J. C. Lorquet, *Mol. Phys.*, **9**, 101 (1965); (c) K. Hirota and Y. Niwa, *J. Phys. Chem.*, **72**, 5 (1968).

(3) (a) Y. Niwa and K. Hirota, *Bull. Chem. Soc. Jap.*, **41**, 1746 (1968); (b) K. Hirota, Y. Niwa, and M. Yamamoto, *J. Phys. Chem.*, **73**, 464 (1969); (c) K. Hirota, Y. Niwa, and I. Fujita, *Z. Phys. Chem.*, (Frankfurt am Main), **67**, 244 (1969).

(4) D. P. Stevenson, *Discuss. Faraday Soc.*, **10**, 35 (1951).

(5) J. L. Franklin, *J. Chem. Phys.*, **22**, 1324 (1954).

(6) G. Remberg, E. Remberg, M. Spitteller-Friedmann, and G. Spitteller, *Org. Mass Spectrosc.*, **1**, 87 (1968).

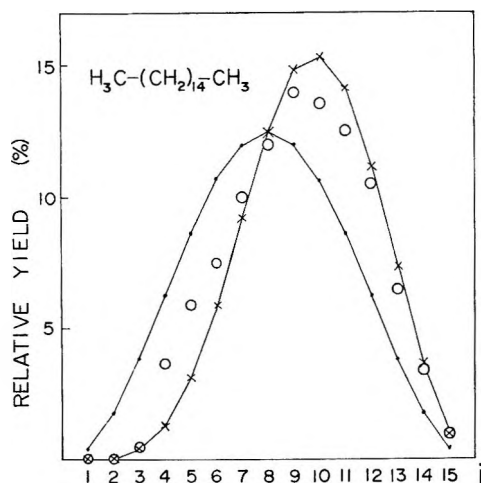


Figure 1. Relative yield of the fragment ions of normal hexadecane vs. their number of carbons: ionizing voltage 10 V and temperature of the ion source 105°: •, calculated value by eq 1; ×, calculated value by eq 2; O, measured value.

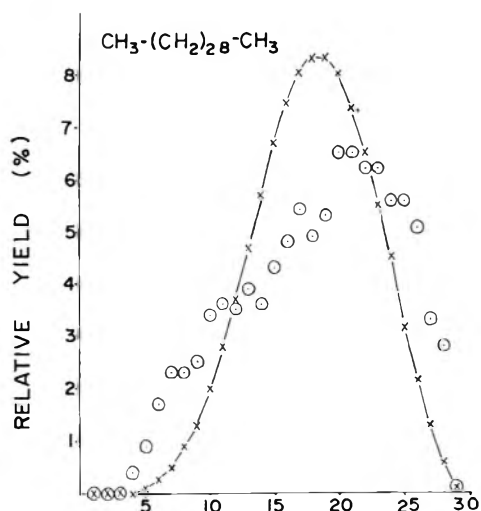


Figure 2. Relative yield of the fragment ions of normal triacontane vs. their number of carbons: ionizing voltage 17 V and temperature of the ion source 90°: ×, calculated value by eq 2; O, measured value.

approximation in the calculation, the above agreement is satisfactory.

The result thus obtained can be summarized by the statement that when rapid, competitive scission occurs at each bond of the parent ion, the two complementary fragments produced have a positive charge in the ratio of the relative probabilities given by the working hypothesis.

It may be a new problem to investigate the relationship between Stevenson's rule and the hypothesis introduced in this paper on other compounds than on normal alkanes.

DEPARTMENT OF CHEMISTRY
FACULTY OF SCIENCE
OSAKA UNIVERSITY
TOYONAKA, OSAKA 560, JAPAN

MITSUO SAITO
IWAO FUJITA
KOZO HIROTA

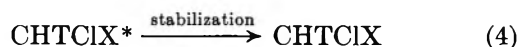
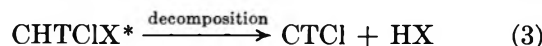
RECEIVED MARCH 2, 1970

A Kinetic Study of Monochlorocarbene Insertion into Silicon-Hydrogen Bonds

Sir: The carbene insertion reaction was thought to be a unique process for singlet methylene with the carbon-hydrogen bond, but recently both it and CCl_2 have been observed to insert into other types of single bonds.^{1,2} Singlet methylene inserts with ease into the Si-H bond of various methyl-substituted silanes.³⁻⁵ In fact, it was found to insert into the Si-H bond 7-9 times faster than in the C-H bond of methylsilane, indicating that the Si-H bond insertion is one of the fastest methylene reactions known.^{4,5} Also, the insertion of CCl_2 into Si-H and Si-C bonds of silacyclobutane has been performed recently.⁶

In the present work we wish to report the insertion of monochlorocarbene into the Si-H bond and a kinetic study on this insertion process. From our results it can be demonstrated that CHCl inserts into the Si-H bond more readily than it adds to the carbon-carbon double bond. The latter process was thought to be the most efficient carbene interaction.¹

Monochlorocarbene in the form of CTCl was produced by the hot atom excitation method.^{7,8} A recoil tritium atom with high kinetic energy may substitute for a hydrogen atom in CH_2Cl_2 or CH_2ClF to give an excited molecule which decomposed by HX elimination to yield CTCl .



Reactants which include He^3 , CH_2ClX , O_2 , silanes, and sometimes ethylene were sealed in 1720 Pyrex bulbs and were irradiated at a neutron flux of 10^{13} neutrons/(cm^2 sec) for 5 to 20 min. The products were analyzed with standard radio-gas chromatographic techniques.⁹

(1) W. Kirmse, "Carbene Chemistry," Academic Press, Inc., New York, N. Y., 1964.

(2) J. Hine, "Divalent Carbon," The Ronald Press Co., New York, N. Y., 1964.

(3) J. W. Simons and C. J. Mazac, *Can. J. Chem.*, **45**, 1717 (1967).

(4) C. J. Mazac and J. W. Simons, *J. Amer. Chem. Soc.*, **90**, 2484 (1968).

(5) W. L. Hase, W. G. Brieland, and J. W. Simons, *J. Phys. Chem.*, **73**, 4401 (1969).

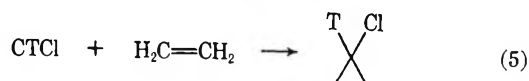
(6) D. Seyferth, R. Damrauer, and S. S. Washburne, *J. Amer. Chem. Soc.*, **89**, 1538 (1967).

(7) (a) Y.-N. Tang and F. S. Rowland, *ibid.*, **87**, 1625 (1965); (b) *ibid.*, **89**, 6420 (1967); (c) *ibid.*, **90**, 574 (1968).

(8) For the formation and reactions of CHCl in solution, see G. L. Closs and J. J. Coyle, *ibid.*, **87**, 4270 (1965).

(9) J. K. Lee, E. K. C. Lee, B. Musgrave, Y.-N. Tang, J. W. Root, and F. S. Rowland, *Anal. Chem.*, **34**, 741 (1962).

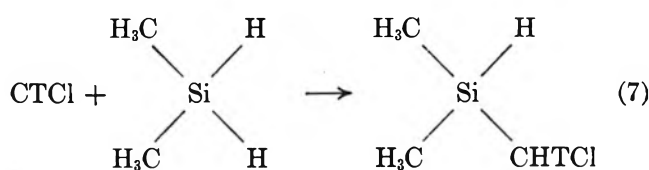
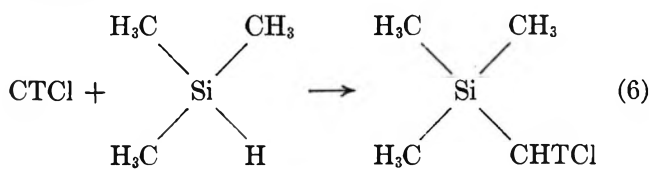
CTCl derived by the above method has been shown to add very efficiently to ethylene, giving cyclopropyl



chloride-*t*. At 33 to 60 cm total pressure the decomposition/stabilization ratio for CHTClX*, expressed in the form of *c*-C₃H₄TCl/CHTClX, was 0.30 ± 0.02 for unscavenged and 0.23 ± 0.03 for O₂-scavenged CH₂Cl₂ samples when measured in systems containing ethylene.^{7a,c} In the case of CH₂ClF, the corresponding ratio for O₂-scavenged samples is 0.10 ± 0.01.^{7a}

The difference in the two ratios of scavenged and unscavenged CH₂Cl₂ systems can be explained as follows. In the scavenged samples, about 1/4 of the CTCl is removed by O₂ in one form or another, either before or after its interaction with ethylene. The 0.30 value from the unscavenged systems probably represents essentially the total amount of CTCl formed because there is nothing else in the system that can effectively compete with ethylene for the CTCl, and also any diradicals formed will have a chance to undergo a ring-closure process instead of being scavenged by O₂.

In the present work, we have treated CTCl with (CH₃)₃SiH (TMS) and (CH₃)₂SiH₂ (DMS) and have measured the yields of the corresponding Si-H insertion products, trimethylchloromethylsilane-*t* (TMCMS) and dimethylchloromethylsilane-*t* (DMCMS).



As is seen in Table I, the TMCMS-*t*/CHTCl₂ and DMCMS-*t*/CHTCl₂ ratios from the well scavenged methylsilane systems are 0.31 ± 0.01, indicating that the same amount of CTCl as previously observed in the unscavenged ethylene-addition CH₂Cl₂ systems undergoes an insertion reaction into Si-H bonds. This coincidence in value again supports the supposition that a ratio of 0.31 ± 0.01 probably represents all the CTCl formed in the system.¹⁰ Evidently Si-H bonds are much more effective than ethylene in competing with O₂ for all the CHCl formed.

Actual experiments, designed to measure the relative reactivity of CTCl toward Si-H bond insertion *vs.* C=C bond addition, were carried out by directly mixing methylsilane and ethylene and letting them compete for the CTCl produced in the system. The results are recorded in Table II. The values represent the

specific reactivities per bond. The large error is due to overlapping peaks. Only TMCMS-*t* or DMCMS-*t* were measured directly in most of the analyses. The values for *c*-C₃H₄TCl were obtained by taking the difference between 0.31, the expected CTCl production, and the observed chloromethylsilane yield. From the data in Table II, one can see that on a per bond basis

Table I: Results of CTCl Insertion into Si-H Bonds in Monosilane and Methylsilanes^a

Reacting silane	CTCl source	Product ratio ^b
$\begin{array}{c} \text{X} \quad \text{Z} \\ \diagdown \quad \diagup \\ \text{Si} \\ \diagup \quad \diagdown \\ \text{Y} \quad \text{H} \end{array}$	CH ₂ Cl ₂	0.31 ± 0.03
		0.32 ± 0.02
		0.32 ± 0.01 ^c
(CH ₃) ₂ SiH ₂	CH ₂ ClF	0.14 ± 0.01
	CH ₂ Cl ₂	0.32 ± 0.03
SiH ₄	CH ₂ Cl ₂	0.30 ± 0.01
		<0.01
		<0.01

^a Typical samples consist of the following pressures (cm) of gases: He³ (2), O₂ (5), CH₂ClX (20), and methylsilanes (20).

^b Most of the error limits represent range of multiple runs.

^c This sample consists of 50 cm of TMS.

CTCl insertion into the tertiary Si-H bond in TMS is about six times more reactive than its addition to the C=C bond. This is in contrast to the general assumption that the carbon-carbon double-bond addition is probably the most efficient reaction for carbenes.^{1,11}

Table II: Relative Reactivity of CTCl toward Si-H Insertion and C=C Addition^a

Molecules	Relative reactivity per bond ^b
(CH ₃) ₃ SiH	6.2 ± 1.9
H ₂ C=CH ₂	(1.0)
(CH ₃) ₂ SiH ₂	1.0 ± 0.2
SiH ₄	<0.1

^a Typical samples consist of the following pressures (cm) of gases: He³ (2), O₂ (5), CH₂Cl₂ (20), ethylene (20), and methylsilanes (20). ^b Error limits represent range of multiple runs.

(10) TMCMS-*t*/CHTCl₂ ratios varying from 0.33 to 0.43 were observed for the unscavenged TMS systems. However, in this case, additional TMCMS-*t* may have been formed by the combination of CHTCl derived from excited CHTCl₂ with (CH₃)₃Si produced by radiation damage. In the CH₂Cl₂-C₂H₄ system, the corresponding combination of CHTCl with C₂H₄ or C₂H₆ will not give *c*-C₃H₄TCl, the carbene reaction product.

(11) For CH₂, the rate of C=C bond addition is approximately 10 times faster than that of C-H bond insertion. See, for example, J. N. Butler and G. B. Kistiakowsky, *J. Amer. Chem. Soc.*, **82**, 759 (1960); **83**, 1324 (1961).

This means, at least for monochlorocarbene, that the double-bond addition is far from as efficient as taking place on every collision.

The comparison also shows that the CTCl insertion into the tertiary Si-H bond is about six times easier than the insertion into the less sterically hindered secondary Si-H bond. This implies both the possible presence of a bond-strength effect or an inductive effect and the possible absence of steric hindrance as a major controlling factor in the carbene insertion reaction.

CTCl reactions with SiH₄ were also attempted, but there was no detectable amount of the expected insertion product, SiH₃CHTCl. The absence of insertion into the stronger Si-H bond in SiH₄ is consistent with the trend observed above for TMS and DMS. However, other complications such as secondary reaction of the resulting product are also possible.

Preliminary results on a comparison of the relative reactivities of TMS and ethylene at 60 and 0° indicates that the Si-H insertion increases by at least another fivefold relative to C=C addition when going toward 0°. This means that their difference in reactivity is primarily due to a lower energy of activation for the Si-H bond insertion process.

Acknowledgment. This research is kindly supported by the Robert A. Welch Foundation. We also appreciate the cooperation of Texas A&M Nuclear Science Center Reactor Personnel.

DEPARTMENT OF CHEMISTRY
TEXAS A&M UNIVERSITY
COLLEGE STATION, TEXAS 77843

Y.-N. TANG
S. H. DANIEL
N.-B. WONG

RECEIVED MARCH 25, 1970